THE UNIVERSITY
of EDINBURGH

Investigating Synaptopathy following Traumatic Brain Injury in a preclinical model

Aimun A.B. Jamjoom

Ph.D. Thesis

University of Edinburgh
Centre for Clinical Brain Sciences
2019

Declaration

I declare that this thesis and the work described herein is my own unless indicated otherwise and has not been submitted for any other degree.

Aimun Jamjoom
February 2019

Acknowledgements

The work presented in this thesis only came about by the support and encouragement of a number of people. Firstly, I would like to thank Professor Seth Grant for supporting me early in the process of applying for PhD funding when I was an untested entity and had no basic science experience. Then for guiding and advising me through my PhD and all along sharing his thoughts, insights and pearls of wisdom with me. I would also like to extend thanks to Professor David Webb for his early support and giving me the freedom to develop a project idea and the Wellcome Trust for the grant that allowed me to pursue it. Throughout the PhD, there also a number of important individuals who supervised and guided me including Dr Naboru Komiyama, Dr Jonathan Rhodes, Professor Peter Andrews and Professor Karen Horsburgh.

I would like to thank a number of people who helped me transition into the world of science and were hugely supportive in navigating its administrative labyrinth. This includes Kathryn Elsegood, Ann Ross and Elaine Marshall. All were very generous with their time and willingness to help. Alongside this, I need to pay special thanks to Melissa Cizeron who supervised me in my first few months and taught me all the key techniques and procedures needed to undertake my PhD experiments. There were many more lab membrs who gave me tips, feedback and advice along the way: Matt Broadhead, Dimitra Koukaroudi, Marcia Roy, Laura Tomas-Roca, Vlad Anton and YK Ko. I would also like to recognise the contributions of Evgeniia Rusina and Jude Milvidaite who worked on aspects on my project and put in many hours immunostaining slides or clicking on a screen to place regions of interest. I can't forget to mention Dr. Fei Zhu who provided early advice in my PhD and whose work (in the shape of the transgenic mice) I built upon. This is similarly the case with Dr. Ricky Qui who developed the machine learning approaches used in this thesis and whom I pestered a great deal for technical advice and support. In particular, I need to thank Sarah Lempiere, Jamie Rose and Cathy McLaughlin who provided me with all manner of support, advice and -very importantly – formed the ultimate lunch crew. I enjoyed our lunch chats, coffee and shared desserts.

My family also deserve huge thanks for the love, support and guidance that they have given me over the years. My grandparents: *Seedo* Othman, *Unna* Amina and Granny Roberta. But, in particular, *Seedo* Bakur for his unwavering support and encouragement in my academic development. His belief in the elevating power of

education and the importance of knowledge have been guiding principles in my life. These principles were instilled in me via my parents who deserve special thanks and recognition for living and breathing my education and career development with me from the very beginning. Along with my brother Bakur, they felt the pain of my failures and celebrated with me at my successes.

Finally, I need to pay special thanks to Christine - my wonderful wife, friend and mother of our beautiful new baby, Tala. Christine has lived through the ups and downs of applying for PhD funding and has been with me during the emotional rollercoaster of rejected fellowship applications, (un)successful data collection and failed experiments. She was always kind, gave me no-nonsense advice and was generous with our time together to let me work and focus on my research.

List of Figures

List of Tables

Abbreviations

Abbreviation	Full denotation
AD	Alzheimer's Disease
AJ	Aimun Jamjoom
AMPA	α-amino-3-hydroxy-5-methyl-4-isoxazolepropionic acid
AMPAR	α-amino-3-hydroxy-5-methyl-4-isoxazolepropionic acid receptor
ANOVA	Analysis of variance
AP	Action Potential
APP	Amyloid Precursor Protein
ATP	Adenosine triphosphate
AUDd	Dorsal auditory area
AUDp	Primary auditory area
AUDv	Ventral auditory area
BED	Bilateral entorhinal deafferentation
BLAa	Basolateral amygdalar nucleus, anterior part
BLAp	Basolateral amygdalar nucleus, posterior part
BLAv	Basolateral amygdalar nucleus, ventral part
BMAp	Basomedial amygdalar nucleus, posterior part
BP	Band Pass
CA	Cornu Ammonis
CAslm	Cornu ammonis, stratum lacunosum-moleculare
CAso	Cornu ammonis, stratum oriens
CAsp	Cornu ammonis, pyramidal layer
CAsr	Cornu ammonis, stratum radiatum
Ca2+	Calcium ion
CC	Corpus Callosum
CCI	Controlled Cortical Impact
CDC	Centre for Disease Control and Prevention
CN/NFAT	Calcineurin/Nuclear factor of activated T-cells
COApl	Cortical-amygdalar area
Cpd	Cerebral peduncle
CR3	Complement Receptor 3
CT	Computerized Tomography

CTE	Chronic Traumatic Encephalopathy
CZI	Carl Zeiss Image
DAI	Diffuse Axonal Injury
DAPI	4',6-diamidino-2-phenylindole
DG	Dentate Gyrus
DGmo	Dentate gyrus, molecular layer
DGpo	Dentate gyrus, polymorph layer
DGsg	Dentate gyrus, granule cell layer
DLG	Disc Large Homolog
DNA	Deoxyribonucleic acid
DTI	Diffusion Tensor Imaging
ECT	Ectorhinal cortex
ECT	Ectorhinal area
ED	Emergency Department
EDH	Extradural Haematoma
eGFP	Enhanced Green Flourescent Protein
EM	Electron Microscopy
EMCCD	Electron Multiplying Charge Coupled Device
ENTI	Entorhinal area
FPI	Fluid Percussion Injury
FT	Farb Teiler
GAP-43	Growth Associated Protein 43
GCS	Glasgow Coma Scale
GFAP	Glial fibrillary acidic protein
GluR2	Glutamate ionotropic receptor AMPA type subunit 2
H+E	Hematoxylin and eosin stain
Hyp	Hypothalamus
Iba-1	Ionized calcium binding adaptor molecule 1
ICD	International Classification of Diseases
IL6	Interleukin-6
KI	Knock-in
KO	Knock-out
LA	Lateral amygdalar nucleus
LDP	Long Term Depression

LED	Light-emitting diode
LFPI	Lateral Fluid Percussion Injury
LTP	Long Term Potentiation
MAGUK	Membrane-associated Guanylate Kinase
MEA	Medial amygdalar nucleus
mKO2	Kusabira Orange
MMP	Matrix metalloproteinases
MOp	Primary motor cortex
MOs	Secondary motor cortex
MRC CRASH	Medical Research Council CRASH trial
MRI	Magnetic Resonance Imaging
NA	Numerical Aperture
NADPH	Nicotinamide adenine dinucleotide phosphate
NFAT	Nuclear factor of activated T-cells
NFL	National Football League
NMDA	N-methyl-D-aspartate
NMDAR	N-methyl-D-aspartate receptor
OCT	Optimal cutting temperature compound
PAA	Piriform-amygdalar area
PBS	Phosphate Buffered Saline
PCR	Polymerase Chain Reaction
PCS	Postconcussion Syndrome
PERI	Perirhinal area
PET	Positron Emission Tomography
PFA	Paraformaldehyde
PIR	Piriform area
PKCalpha	Protein kinase C alpha
PSD	Postsynaptic Density
PSD93	Postsynaptic Density Protein 93
PSD95	Postsynaptic Density Protein 95
RAC	Ring Aperture Contrast
RGB	Red Green Blue scale
RNS	Reactive Nitrogen Species
ROI	Region of Interest

ROS	Reactive Oxygen Species
RSPd	Retrosplenial area, dorsal part
RT	Righting Time
RTA	Road Traffic Accident
SAP102	Synapse Associated Protein 102
SAP97	Synapse Associated Protein 97
SDH	Subdural Haematoma
SDM	Spinning Disc Microscopy
SDS-PAGE	Sodium dodecyl sulfate–polyacrylamide gel electrophoresis
SL	Sarah Lempriere
SSp-bfd	Primary somatosensory area, barrel field
SSp-tr	Primary somatosensory area, trunk
STAT3	Signal transducer and activator of transcription 3
SV2A	Synaptic vesicle glycoprotein 2A
TAE	Tris-Acetate-Ethylenediaminetetraacetic acid
TBI	Traumatic Brain Injury
TEa	Temporal association area
Th	Thalamus
TIFF	Tagged Image File Format
TNF	Tumour Necrosis Factor
TNF-alpha	Tumour Necrosis Factor alpha
TSPO	Translocator Protein
UK	United Kingdom
USA	United States of America
UV	Ultraviolet
WHO	World Health Organisation
WT	Wildtype

Abstract

There is growing evidence that neural network disruption has a major contribution to Traumatic Brain Injury (TBI) morbidity. Understanding more about the impact of TBI on synaptic structure and function may help elucidate post-injury neural network disturbance. In this thesis we aimed to achieve this by studying two postsynaptic density proteins: post-synaptic density protein 95 (PSD95) and Synapse Associated Protein 102 (SAP102). These proteins are major scaffold proteins that assemble neurotransmitter receptors, channels and enzymes into multi-protein signalling complexes. We aimed to pursue the hypothesis that TBI disrupts the levels and location of PSD95 and SAP102 and thereby impairs synapse function contributing to post-injury neural network disruption.

In this thesis, we aimed to investigate mild TBI as it constitutes over three quarters of cases, patients can suffer from a range of symptoms and a substantial number do not get back to their pre-injury function. To do this, we validated a model of mild TBI using the Lateral Fluid Percussion Injury (LFPI) device. In wildtype mice, we found that a single mild LFPI led to an increased righting time (a simple behavioural assay) in the injury cohort. Histopathological analysis showed evidence of dysmorphic cortical cells and traumatic axonal pathology in the corpus callosum. Coupled to this, there was a significant inflammatory response within the injury cohort with elevated numbers of astrocytes and microglia. Together, this data showed evidence of behavioural, axonal and inflammatory changes after a mild LFPI.

The project utilized mice that had enhanced green fluorescent protein (eGFP) fused with the C-terminus of the endogenous PSD-95 protein and kusabira orange (mKO2) fused to SAP102. Male PSD95-eGFP and mKO2-SAP102 mice aged 8-16 weeks were randomised to a mild LFPI or sham and followed up to 7 or 28 days. Using high resolution confocal microscopy and machine learning approaches, PSD95 and SAP102 synaptome maps for puncta density, size and intensity were created. We found a significant reduction in synaptic puncta density at 28 days post-injury. This was evident in brain regions distal to the injury site including the contralateral cortex and hippocampus. We also observed evidence of synapse density recovery in the ipsilateral cortex between 7 and 28 days indicating synaptic recovery following a traumatic insult. There were differential patterns of change between PSD95 and SAP102 with evidence of more pronounced PSD95 puncta loss and recovery

suggesting SAP102 is less vulnerable to TBI. We found evidence of a chronic inflammatory response with elevated numbers of microglia at 28 days. There was a negative association between puncta density and microglia numbers which may indicate a role for microglia in synapse removal post-TBI.

In conclusion, using a brain-wide unbiased synaptic mapping approach, we interrogated the impact of a mild traumatic injury on the postsynaptic density proteins PSD95 and SAP102. We observed a reorganization of the synaptome following injury which was progressive and involved brain regions distal from the injury site. Our study also highlighted the capacity for synaptic recovery post-injury and pointed towards a potential role of chronic inflammation on post-TBI synaptopathy.

Lay Summary

Synapses, the connections between neurons, are essential to all behaviours. Recent studies have shown that subtle damage to synapses may cause a range of brain diseases such as autism and schizophrenia. Traumatic Brain Injury (TBI) is a major health problem for which there are currently no known drug therapies. It can lead to significant long-term morbidity while even mild injuries, which constitute over three quarters of TBI cases, can cause a range of symptoms that negatively impact patients' lives. The focus of TBI research has primarily been at the level of the neuron and very little is known about the effects it has on synapses. In this thesis, we describe the use of a novel mouse model that has been engineered so that its synapses are fluorescent and therefore readily examined with a microscope. This permitted us to ask if TBI damages synapses and how they recover after injury. We used state-of-the-art microscopes that allowed us to survey the entire mouse brain. The data generated was then analysed with a machine learning approach which provided detailed information about synapse numbers, size and brightness. In our experiments, we found that an experimental TBI led to a delayed reduction in the number of synapses a month after the injury and that brain regions distant from the injury site lost synapses. In mice that sustained a TBI, we found that the cortex recovered synapses after the injury suggesting that the brain has the capacity to recover lost connections between neurons. We also found a reduction in synapses in brain regions with high numbers of infiltrating microglial cells (immune cells) suggesting that these cells may play a role in synapse loss after TBI. The next steps for this research is to understand the impact of TBI on different subtypes of synapses and then use imaging techniques to examine synapses in humans who have suffered a TBI.

Table of Content

CHAPTER 1

Introduction

1.1 TRAUMATIC BRAIN INJURY

Traumatic Brain Injury (TBI) is a temporary or permanent impairment of brain function due to an external mechanical force to the head. It is a leading cause of death and disability around the world. TBI can occur due to a wide range of mechanisms including falls, road traffic accidents (RTA), assaults and sports or military-related injuries. It encompasses a heterogeneous and broad set of pathologies that overlap and vary in their severity and patient outcomes.

1.1.1 Epidemiological patterns and trends

Traumatic brain injury is a critical public health problem. Estimates vary widely across countries which in part is due to the varying quality and robustness of the epidemiological data (Roozenbeek et al. 2013). There are several reasons for the lack of robust population-based data in TBI. The lack of a clear definition of TBI (particularly mild injuries) has led to variation in the literature. The International Classification of Disease (ICD) definition in emergency department (ED) admissions can lead to false negatives and positives (Bazarian et al. 2006). The second limitation is under-reporting, patients – particularly those with mild injuries – do not routinely present to ED which can lead to under-estimation of the true burden of TBI. Taking these limitations into account, it is estimated that 7.7 million people are living with TBI-related disabilities in the European Union (Tagliaferri et al. 2006). In the USA, the Centre for Disease Control and Prevention monitor TBI incidence and have standardized definitions. Between 2002-2006, there were 1.7 million TBIs in the USA leading to 1.4 million ED visits. This included 275000 hospitalizations and 52000 deaths (Faul et al. 2010). Incidence of TBI is rising globally due to increased use of motor vehicles in low and middle income countries (Maas et al. 2008). Differences in low and high-income country TBI injury patterns are present. Analysis of MRC CRASH trial data showed that patients from low and middle income countries were younger and more likely to be injured in a RTA (MRC CRASH Trial Collaborators et al. 2008). Though historically seen as a disease of the young there has been an upward shift in the median age of patients sustaining a TBI in developed countries (Roozenbeek et al. 2013). This is explained by greater life expectancy, improvement in road safety and motor vehicles which have seen a reduction in RTA-related TBIs. CDC data has shown that the leading cause of TBI was falls (35.2%) followed by RTAs (17.3%) (Faul et al. 2010). This demographic shift towards older patients with TBIs due to falls has led to a shift from diffuse injuries to contusional injuries. Elderly

patients with TBI pose a particular challenge due to the presence of multiple comorbidities and the use of anticoagulant medication. Mortality in TBI appears to have remained static since 1990 compared to a period of improvement between 1970-1990 (Stein et al. 2010). The static mortality since 1990 may be due to the epidemiological shift to an older patient population. Societal costs of TBI are significant – not only related to the medical care but also the associated economic impact of the ensuing disability. In Europe, TBI is among the top three causes of injury-related medical costs (Polinder et al. 2007). While in the USA, the annual economic burden of TBI is estimated at $60 billion (Maas et al. 2008).

1.1.2 Classification of TBI

Due to the broad and heterogonous nature of TBI, there are several ways to classify it. Traditionally, classification has centred around three main areas: penetrating injury, structural damage on computerized tomography and clinical severity as measured by the Glasgow Coma Scale **(Figure 1.1)**.

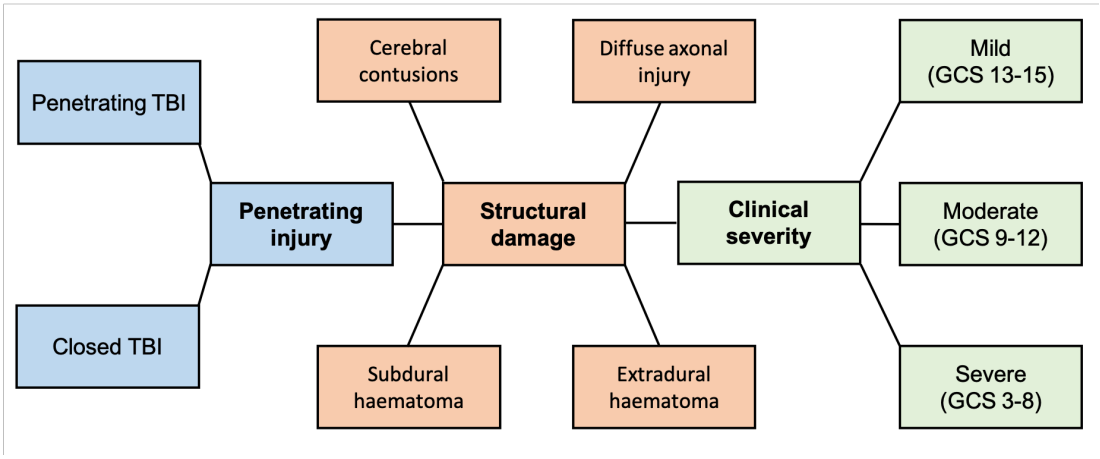

***Figure 1.1**: **Schematic of classification systems for TBI** demonstrating the three main classification systems: skull integrity, structural damage and clinical severity.*

1.1.2.1 Penetrating injury

Whether the skull is breached is an important classifying factor for TBI. Penetrating TBI occurs due to gunshot wounds, stabbings or blast projectiles. It is far less common than closed TBI, however patient outcomes are significantly worse. Within the civilian population, particularly in the USA, gunshot wounds are a major cause of penetrating head injuries. Aarabi and colleagues found that over a 24 month period, patient

mortality in the state of Maryland from gunshot wounds to the head was 91% (Aarabi et al. 2014).

1.1.2.2 Structural damage

Assessment for structural damage using neuroimaging has become a principle form of TBI classification **(Figure 1.2)**. The introduction of Computerized Tomography (CT) revolutionized the management of TBI as it provided a diagnostic tool to quickly differentiate between a range of intracranial injuries and guide management. Despite CT's limitations, which include its inability to identify subtle injuries and the fact it is momentary snapshot of an evolving process, it has been an integral part of classifying TBI and guiding its management.

1.1.2.2.1 Diffuse Axonal Injury

Diffuse axonal injury (DAI) is a form of intra-axial brain injury that involves widespread damage to white matter tracts **(Figure 1.2, A)**. It is a major cause of chronic disorders of consciousness after a severe TBI (Victoria E Johnson et al. 2013). However, there is growing evidence that a degree of axonal injury also occurs in even mild TBIs (Smith 2016). CT is not as sensitive as MRI in identifying DAI (Mittl et al. 1994). However, there is evidence that subtle early CT changes, including intraventricular haemorrhage, are associated with DAI (Mata-Mbemba et al. 2015).

1.1.2.2.2 Intracranial hemorrhage

Traumatic intracranial haemorrhages occur due to damage to blood vessels at the time of injury. The location and type of blood vessel determines the subtype of intracranial haemorrhage that is seen. Damage and rupture of intraparenchymal micro-vessels lead to intra-axial (within the brain substance) haemorrhage. While damage to bridging veins and arteries lead to extra-axial (out of the brain substance) haematomas.

1.1.2.2.3 Cerebral contusions

A cerebral contusion is defined as an intra-axial haemorrhagic lesion with necrotic tissue **(Figure 1.2, B)**. Contusions occur at the time of injury due to physical disruption of micro-vessels and the extrusion of blood into the brain substance (Kurland et al. 2012). They typically occur at the apex of the frontal and temporal lobes due to the relative motion of the brain compared to the bony cranium prominences. On CT,

contusions appear as hyperdense lesions within the parenchyma intermixed with normal (isodense) tissue. Contusive injury is associated with microvascular dysfunction due to vasoconstriction and thrombosis (Kurland et al. 2012). This can lead to worsening ischaemia, perilesional swelling and haemorrhagic progression. Contusions are typically seen in coup and contrecoup injuries. A coup injury occurs at the site of impact to the brain while contrecoup injuries occur at the site opposite to the area hit. The biomechanics of this process are due to the translation of the brain within the rigid skull leads to it colliding with the cranial vault after impact.

1.1.2.2.4 Subdural haematoma

Subdural haematoma (SDH) is a collection of blood situated underneath the dura mata but out of the brain substance **(Figure 1.2, C)**. The two main causes of subdural haematomas are accumulation of blood from a parenchymal laceration (usually high impact injury) or disruption of bridging vessels from cerebral acceleration-deceleration (usually lower impact injury) (M. Greenberg 2017). On CT, subdural haematomas appear as a hyperdense crescentic mass that, if large, can cause compression of the underlying brain.

1.1.2.2.5 Extradural haematoma

Extradural haematomas (EDH) are collections of blood outside of the dura mata **(Figure 1.2, D)**. They are not as common as subdural haematomas and are found in 1% of head trauma admissions (M. Greenberg 2017). They are commonly attributed to disruption of the middle meningeal artery by a temporoparietal skull fractures. Compared to SDH, EDH occur due to lower impact forces and patients typically present with a lucid period before their conscious level deteriorates. On CT, EDH appear as a biconvex hyperdense lesion adjacent to the skull.

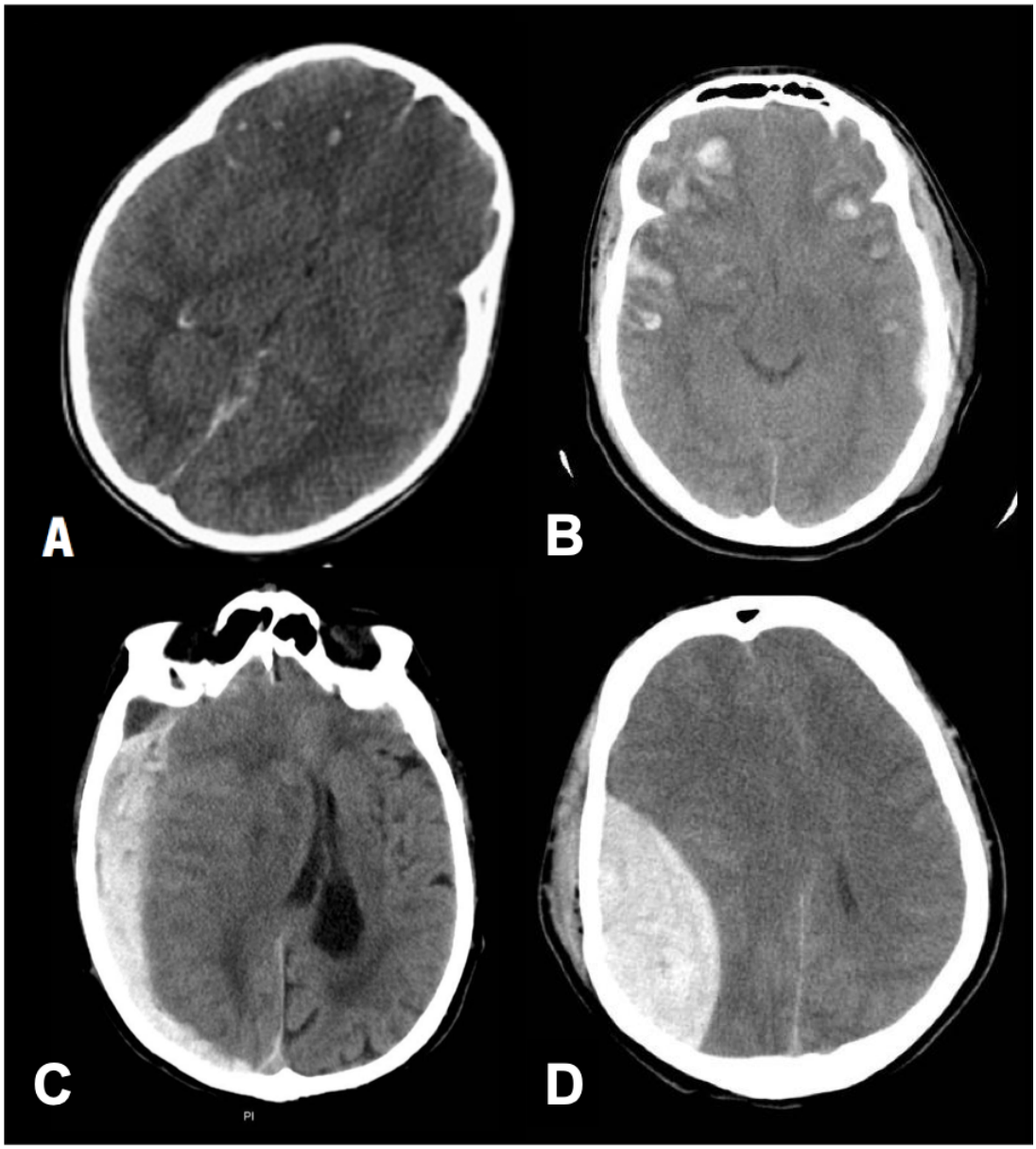

Figure 1.2: CT demonstrating TBI structural damage *findings of (A) diffuse Axonal Injury [image reproduced under creative common licence from* Ramalho and Castillo, (2015*)] (B) traumatic cerebral contusions [image reproduced under creative common licence courtesy of Dr Jeremy Jones, Radiopaedia.org, rID: 8079] (C) acute subdural haematoma [image reproduced under creative common licence courtesy of A.Prof Frank Gaillard, Radiopaedia.org, rID: 35891] (D) acute extradural haematoma [image reproduced under creative common licence courtesy of Dr Sandeep Bhutal, Radiopaedia.org, rID: 4458]*

1.1.2.3 Clinical Severity (Glasgow Coma Scale)

The severity of TBI is determined clinically by measuring the patient's conscious level using the Glasgow Coma Scale (GCS). The GCS is 15-point scale that looks at three areas: the patient's eyes, motor and verbal response **(Table 1.1)**. Patients can have a maximum aggregate score of 15 and a minimum of 3. The scale was first described by Teasdale and Jennett in 1974 and has been demonstrated as a strong predictor of mortality in TBI (Teasdale et al. 2014).

Eye opening		Verbal response		Motor response	
1	None	**1**	None	**1**	None
2	To stimulus	**2**	Sounds	**2**	Extension
3	To speech	**3**	Words	**3**	Abnormal flexion
4	Spontaneous	**4**	Confused	**4**	Normal flexion
		5	Orientated	**5**	Localizing
				6	Obeying commands

***Table 1.1**: **Glasgow Coma Scale** with breakdown of the three components: eye, verbal and motor response*

1.1.2.3.1 Moderate and Severe TBI

Based on the GCS, moderate TBI is considered a GCS 9-13 and severe TBI a GCS 3-8. Epidemiological studies have indicated that moderate and severe TBI compromise approximately a fifth cases with an equal distribution between the two severities (Bruns & Hauser 2003). Traumatic intracranial haemorrhages occur in 25–35% of patients with severe TBI and in 5–10% of moderate injuries (Maas et al. 2008). Outcome for patients following moderate and severe head injury can vary from death through to living independently. A multivariate analysis of 8686 patients' data drawn from 8 RCTs, demonstrated that the strongest predictors of patient outcome was: motor component of the GCS, pupillary response, age and CT characterization (Murray et al. 2007).

1.1.2.3.2 Mild Traumatic Brain Injury (mTBI)

Mild TBI is estimated to account for the majority (80%) of all cases of TBI (Bruns & Hauser 2003). Mild TBI and concussion are terms that are used interchangeably. Both

terms point towards a disruption of brain function following a mechanical force to the cranium. For the purposes of consistency, the term mild TBI will be used in this thesis. One of the challenges surrounding the research and management of mild TBI is unity around the definition of the disease. The WHO collaborating Centre for Neurotrauma Task Force on Mild Traumatic Brain Injury undertook a major review of literature and recommended the below definition in **Panel 1** (Carroll et al. 2004). Within this thesis, we define human mild TBI based upon the WHO taskforce definition.

Mild TBI is an acute brain injury resulting from mechanical energy to the head from external physical forces. Operational criteria for clinical identification include: (i) 1 or more of the following: confusion or disorientation, loss of consciousness for 30 minutes or less, post-traumatic amnesia for less than 24 hours, and/or other transient neurological abnormalities such as focal signs, seizure, and intracranial lesion not requiring surgery; (ii) Glasgow Coma Scale score of 13–15 after 30 minutes post-injury or later upon presentation for health care. These manifestations of mild TBI must not be due to drugs, alcohol, medications, caused by other injuries or treatment for other injuries (e.g. systemic injuries, facial injuries or intubation), caused by other problems (e.g. psychological trauma, language barrier or coexisting medical conditions) or caused by penetrating craniocerebral injury

Panel 1.1: WHO Taskforce recommended definition of mild TBI

Historically, mild TBI was deemed to be a benign process for which patients fully recovered. However, there is a growing body of evidence that mild TBI can lead to symptomology that can significantly affect patients' quality of life. A recent large prospective study of patients with mild TBI found that almost a half did not achieve a complete recovery at 6 months post-injury (van der Naalt et al. 2017). There are a number of sequelae for mild TBI including:

1.1.2.3.2.1 Post-concussional Syndrome

Post-concussional syndrome (PCS) is a constellation of symptoms that occur in patients following a mild TBI. These include somatic symptoms (headache, blurred vision, dizziness), cognitive symptoms (difficulty concentrating, memory problems) and emotional symptoms (irritability, low moods) that, in most cases, gradually resolve during the 12 weeks after the injury (Levin & Diaz-Arrastia 2015) **(Figure 1.3)**.

However, a proportion of patients have been found to develop persistent symptoms beyond 3 months. A prospective study of 107 patients found that 22% had persistent symptoms at 3 months (Hou et al. 2012). There is controversy surrounding PCS given the non-specific nature of the symptoms, particularly as these symptoms have also been identified in the general trauma population (King 2003; Meares et al. 2008). A number of studies have highlighted that a pre-morbid psychiatric history was a strong predictor of persistent PCS (Ponsford et al. 2011; Hou et al. 2012; Hellström et al. 2017). There is therefore a growing view that early phase PCS show association between neurological symptoms and cognitive function which, subsequently, in patients with persisting symptoms becomes less clear with a growing psychosocial basis (Williams et al. 2010). A large prospective cohort study of mild TBI patients found that the strongest predictive factors of 6-month outcome were indicators of emotional distress and coping strategies at 2 weeks post-injury (van der Naalt et al. 2017).

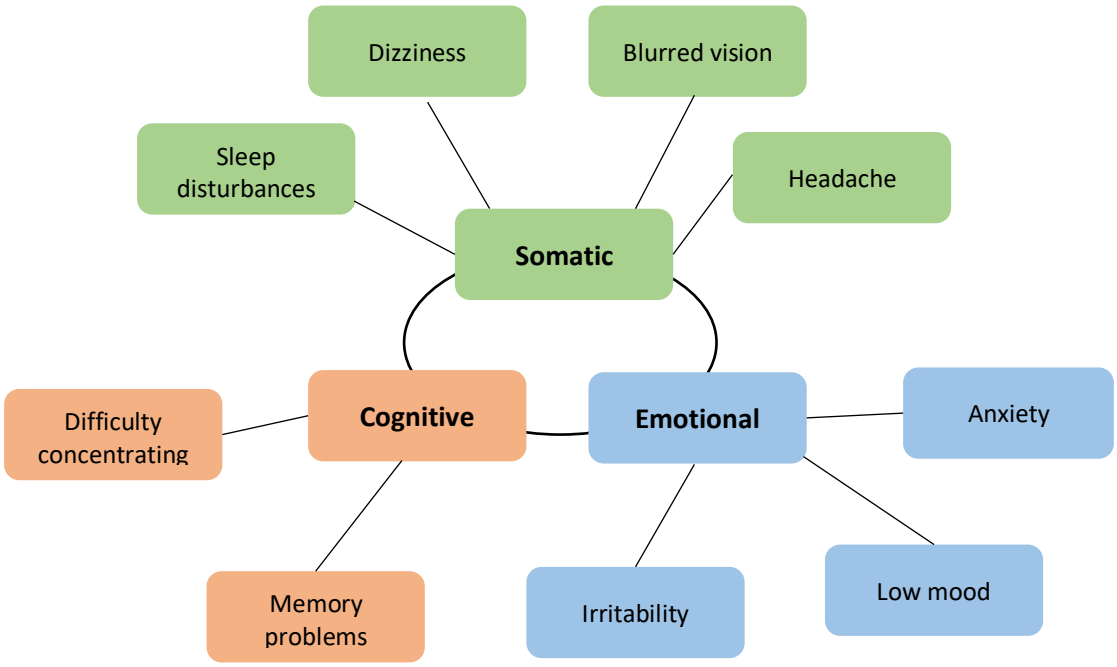

Figure 1.3: Schematic of constellation of post-concussional symptoms *demonstrating the main categories of symptoms patient experience: somatic, cognitive and emotional.*

1.1.2.3.2.2 Cognitive impairment

Several studies have attempted to map cognitive deficits in patients after a mild TBI. Karr and colleagues systematically reviewed the literature for meta-analyses of

neuropsychological outcomes after mild TBI (Karr et al. 2014). The review showed that a broad range of cognitive domains (executive function, memory, visuospatial skills) had been assessed in the context of mild TBI. The range of studies showed a wide variation in the effect sizes seen across the reported studies. However, mild TBI patients appeared to have worse performance in executive function, memory and attention assessments. The review found evidence that patients saw a resolution of deficits by 90 days while, interestingly, those with sport-related mild TBIs recovered quicker with cognitive domains reaching non-significance by 7 days post-injury.

1.1.2.3.2.3 Chronic Traumatic Encephalopathy

In 1928, the pathologist Dr. Harrison Martland published a seminal paper describing 'punch drunk syndrome'; a constellation of chronic motor and neuropsychiatric symptoms in former boxers (Martland 1928). The term dementia puglistica was ascribed to the progressive neuropsychiatric condition that emerged after repetitive mild TBIs and a number of case series indicated a neuropathological basis to the syndrome (Corsellis 1989; Roberts et al. 1990). However, interest in the condition was limited until evidence of similar findings in non-boxing contact sports such as in American Football and in military personnel (Omalu et al. 2011; McKee et al. 2009). The term Chronic Traumatic Encephalopathy (CTE) was introduced to describe the clinicopathological condition emerging from a wide range of physical exposures. Examined brains have demonstrated gross findings including brain atrophy, cavum septum pellucidum and ventricular enlargement (Douglas H. Smith et al. 2013). One of the most consistent neuropathological findings in CTE is the presence of neurofibrillary tangles (McKee et al. 2009). These tangles are typically located within the superficial layers of the cortex and have a propensity to be found deep within sulci. The consistency of tau findings in CTE cases has led to it being described as a tauopathy. In contrast, Amyloid beta –an important finding in Alzheimer's Disease- is a less consistent feature in CTE. A review of the literature, revealed that 66 (53%) of the 124 examined cases had evidence of amyloid pathology (Douglas H. Smith et al. 2013). A range of other pathological findings have included neuronal loss, white matter degeneration and inflammation (Omalu et al. 2011; Omalu et al. 2006; McKee et al. 2009).

1.1.3 Pathophysiology of Traumatic Brain Injury

The pathophysiology of TBI is a complex, dynamic and multifaceted process. To best understand it, TBI pathophysiology can be divided into primary and secondary injury phases **(Figure 1.4)**.

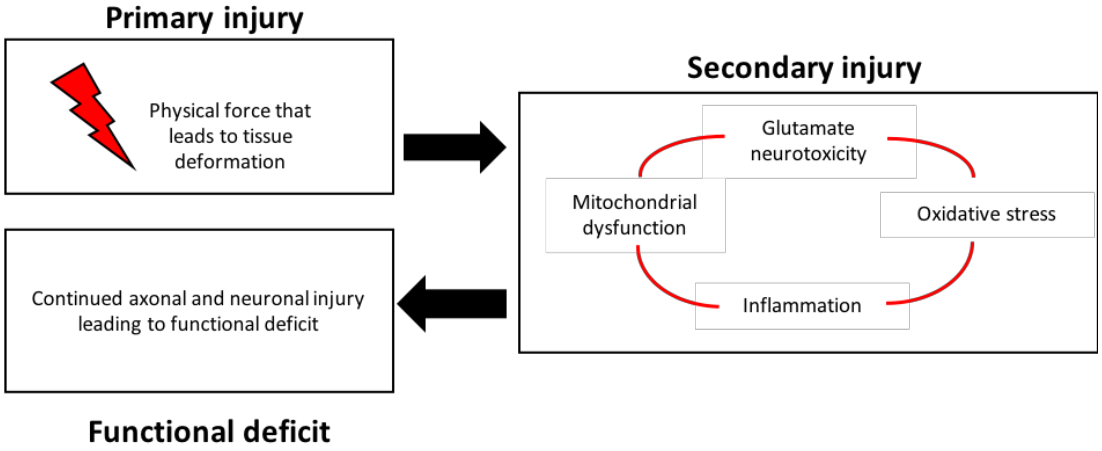

Figure 1.4: Schematic of primary and secondary injury processes following TBI. *A physical force to the head leads to tissue deformation during which neural, glial and vascular tissue is injured. Within minutes, this leads to the development of secondary injury pathways including glutamate neurotoxicity, oxidative stress, inflammation and mitochrondrial dysfunction. These pathways potentiate neuronal injury and contribute to functional deficit.*

1.1.3.1 Primary injury

Primary injury TBI is the tissue damage and disruption caused to the brain at the time of the external force application. Due to the broad and heterogeneous nature of external causes of TBI this can differ in the extent and severity of the damage. Taking this into account, the best approach to understanding primary injury is to consider the forces applied which can lead to focal and diffuse injuries. At the macroscopic level, focal forces to the skull can cause skull fractures and intracranial hemorrhages (intra-axial and extra-axial) due to disruption of blood vessels. While diffuse forces lead to shearing of white matter tracts. At the cellular level, diffuse forces particularly can lead to diffuse axonal injury and microhaemorrhages from disruption of small blood vessels. Ischaemic brain damage is usually superimposed on primary brain injury. This can be due to a multitude of causes including compression from extra-axial

haemorrhage, perilesional ischaemia around a contusion or due to focal microvascular disruption.

1.1.3.2 Secondary injury

Secondary injury results from ensuing pathophysiological mechanisms that begin within minutes of the primary injury and can last for months to years afterwards. The range and extent of these processes can vary according to the severity of the traumatic injury. Secondary injury pathways include:

1.1.3.2.1 Glutamate excitotoxicity

Following TBI, there is an increase in extraceullar excitatory amino acids including glutamate as cellular membranes rupture and cell content is released. Microdialysis studies in humans and preclinical models of TBI have demonstrated this early increase in glutamate (Folkersma et al. 2011; Chamoun et al. 2010). Surges in glutamate levels subsequently lead to ionic imbalances on the postsynaptic membranes. This includes the release of potassium (K+) for which levels correlate with injury severity (Katayama et al. 1990). In addition to perturbation in K+ levels, intracellular calcium (Ca^{2+}) accumulation has also been observed following TBI (Osteen et al. 2001; Fineman et al. 1993). Ca^{2+} overloading has been shown to lead to mitochondrial dysfunction and induce oxidative stress (Peng & Jou 2010; Xiong et al. 1997).

1.1.3.2.2 Oxidative stress

Free radicals are molecules with an unpaired electron which are highly reactive and can lead to cellular damage. They include both reactive oxygen (ROS) and reactive nitrogen (RNS) species. Free radicals are produced as part of normal metabolic activity and are managed by antioxidant systems. TBI disrupts this system leading to increases in free radicals that overwhelm the scavenging system and causes oxidative stress (O'Connell & Littleton-Kearney 2013). Mitochondria are an important source of free radicals. After TBI, Ca^{2+} accumulation leads to the activation of several enzymes that increase ROS and RNS production (Lewén et al. 2000). Several studies have attempted to quantify free radical changes or its consequences (lipid peroxidation and protein nitration) in preclinical TBI models. Hydroxyl radical, a ROS, was found to increase by 250% which was maintained above baseline for 90 minutes in a rat model of TBI (Marklund et al. 2001). Lipid peroxidation occurs when fatty acids

react with ROS leading to alterations in membrane permeability (Prins et al. 2013). Increases in markers of lipid peroxidation have been seen after preclinical models of TBI (Tyurin et al. 2000; Singh et al. 2006).

1.1.3.2.3 Mitochondrial dysfunction and energy crisis

Calcium accumulation and oxidative stress lead to mitochondrial dysfunction which in turns leads to reduced energy production. Preclinical studies have demonstrated reduction in ATP production and accumulation of mitochondrial calcium (Xiong et al. 1997; Sullivan et al. 1998). Imaging approaches have also been used to measure brain metabolic activity. The commonest modality has been Positron Emission Tomography (PET) using [^{18}F]Fluorodeoxyglucose. This method has been extensively utilized in mild TBI patients. A comprehensive review of the literature highlighted that, despite variation in the methodology and measurement approaches, a pattern of reduced glucose uptake or hypometabolism was clear in a variety of brain regions including the anterior cingulate, precuneus, anterior temporal lobe, superior parietal cortex and corpus callosum (Byrnes et al. 2014).

1.1.3.2.4 Inflammation

Following TBI, a complex and multifaceted inflammatory process develops which can be both beneficial and detrimental. Mechanical disruption of cells leads to the release of Damage Associated Molecular Patterns (DAMPs) which in turn leads to glial cells upregulating a range of cytokines including tumour necrosis factor (TNF) and interleukin-6 (IL-6) (Ransohoff & Brown 2012). A range of central and peripheral immune cells subsequently migrate to the trauma site. Initially, circulating neutrophils infiltrate followed by monocytes, dendritic cells and T lymphocytes (Clark et al. 1994; Jin et al. 2012). Microglia, resident immune cells, respond to injury by polarizing to two phenotypes as a response to differing cytokines (Colton 2009). The M1-like ‘proinflammatory’, though initially considered beneficial, can become harmful if prolonged (Wang et al. 2013; Loane et al. 2014). The M2-like ‘alternative’ phenotype are associated with the production of anti-inflammatory cytokines (Colton 2009). Several studies have charted the temporal profile of microglia phenotypes following experimental TBI (Jin et al. 2012; Wang et al. 2013). They have shown a bimodal response with a M2-like peak at 7 days followed by an M1-like peak at 3-4 weeks. There is growing evidence of chronic neuroinflammation following TBI years after the initial injury. Examination of autopsy brains following TBI showed activated microglia

up to 18 years after injury (Victoria E. Johnson et al. 2013). The development of Translocator Protein (TSPO) radioligands, a marker of activated glial response, has allowed the in-vivo investigation of inflammation after a TBI (Vivash & OBrien 2016). Two studies have used PET imaging to quantify inflammatory changes in-vivo post-TBI. Coughlin and colleagues undertook a case control study of NFL players who had experienced sport-related mild TBIs (Coughlin et al. 2017). The investigators observed a higher distribution of TSPO in 8 out of 12 brain regions within the NFL cohort. Similarly, Fujita and colleagues observed, in a mixed cohort of mild and moderate TBI, a global increase in TSPO signal across all brains in TBI patients (Fujita et al. 2017). Importantly, both these studies highlighted that inflammation was evident in patients months to years after the initial injury.

1.1.3.2.5 Axonal injury

Dynamic deformation of long white matter tracts at injury leads to disruption of axonal transport. This leads to progressive axonal dysfunction following the initial mechanical injury. Historically, traumatic axonal injury was determined using histological approaches such as haematoxylin and eosin (H+E) and silver staining (Douglas H Smith et al. 2013). However, the introduction of immunohistochemistry allowed for more specific targeting of axonally transported proteins. Amyloid Precursor Protein (APP) moves through the axonal cylinder by anterograde transport (Douglas H Smith et al. 2013). Mechanical perturbation of the axon leads to pooling of APP. Accumulation of this transported material leads to either varicosities along the length of the axonal or, in the event of complete disconnection, as a axonal bulb (Victoria E Johnson et al. 2013). Axons within a single specimen can be found in differing stages of degeneration and disconnection highlighting that it is an evolving pathology. The pathophysiology of this process is believed to be related to dysregulation of sodium channels leading to a calcium influx. This process leads to microtubular loss and energy failure secondary to microchondrial damage and ultimately impairs axonal transport (Wolf et al. 2001; Douglas H Smith et al. 2013). Preclinical histological studies have pointed towards evidence of diffuse axonal injury as an important pathological process in mild TBI (Spain et al. 2010; Mierzwa et al. 2015). However, histological confirmation of this in human beings is limited due to the low mortality rate after mild TBI. Advanced structural MRI modalities such as diffusion tensor imaging (DTI) provide detailed information on the ultrastructure of white matter tracts by measuring the random movement of water molecules through the brain tissues

(Alexander et al. 2007). Within this body of evidence, there is a great deal of variability in the imaging protocols however a meta-analysis of 13 studies of DTI following mild TBI demonstrated diffusion abnormalities within the corpus callosum, particularly its posterior arm (Aoki et al. 2012). A study assessing longitudinal DTI changes after a mild TBI revealed a dynamic pictures suggesting progressive axonal pathology that goes on for months post-injury (Veeramuthu et al. 2015). Importantly, a number of studies have demonstrated the predictive value of DTI changes on functional outcome following mild TBI (Yuh et al. 2014; Veeramuthu et al. 2015).

1.2 PRECLINICAL MODELS OF TRAUMATIC BRAIN INJURY

The heterogeneous nature of TBI has led to a wide array of preclinical animal models being developed over the years. Within the literature, there are two broad categories of TBI model: open and closed skull. Each of these models hold differing strengths and drawbacks in its ability to recapitulate aspects of the human disease **(Table 1.2)**. Although larger animals (such as pigs) have closer neuroanatomy to humans which makes them better to model the biomechanics of human TBI, rodents are mostly used for a range of reasons. These include their small size, short life span, lower housing costs and the ability to utilize genetically modified mouse models. This section will focus on a number of differing TBI models used in rodents.

1.2.1 Fluid Percussion Injury

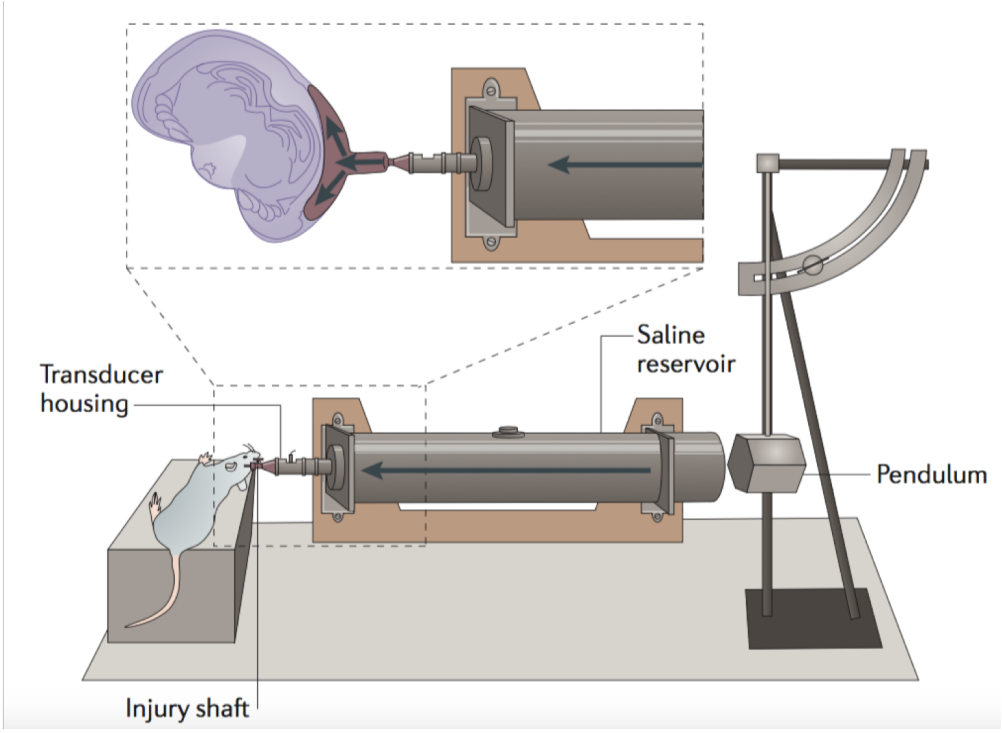

***Figure 1.5**: **Lateral fluid percussion injury model** demonstrating mouse attached to fluid reservoir. Pendulum is released to create a pressure pulse which is applied to the intact dura [image reproduced from Xiong et al (2013) with permission from Springer Nature]*

The Fluid Percussion Injury model is a well-established and widely used open skull TBI model **(Figure 1.5)**. It was initially developed in cats but then was modified for use in rodents (Thompson et al. 2005). Briefly, the mice undergo a craniectomy (removal of bone window) which can vary in location including: midline (centred over the sagittal suture), parasagittal (<3.5mm from the sagittal suture) or lateral (>3.5mm from the sagittal suture) (Xiong et al. 2013). The location of the craniectomy has been shown to be an important determinant of the extent and location of the brain lesion and functional motor outcome (Vink et al. 2001). In this thesis, we will focus on the lateral Fluid Percussion Injury (LFPI) model. The traumatic injury is inflicted by a fluid pressure pulse which is generated by release of a pendulum and is delivered to the surface of the intact dura causing brief deformation of the brain parenchyma. The severity of injury can be altered by the strength of the pressure wave by varying the height of the pendulum (Kabadi et al. 2010; McIntosh et al. 1989). Reflecting human TBI severity categories, the literature commonly refers to mild, moderate and severe

LFPI depending on the intensity of the pressure pulse. The LFPI model is considered to be a mixed focal and diffuse injury with histological findings akin to human disease including cortical contusion, white matter disruption and intraventricular haemorrhage (McIntosh et al. 1989; Xiong et al. 2013). There has been comprehensive cellular characterization of the LFPI with evidence of immediate (within minutes) neuronal injury which progresses to neuronal loss in the ipsilateral cortex and subcortical structures up to a week after the injury (Hicks et al. 1996). Mapping of inflammatory changes after LFPI have demonstrated a robust response including cytokine release and astroglial activation (Cao et al. 2012; Ambrosini et al. 2003; Vitarbo et al. 2004). Temporal-spatial axonal pathology has been characterized following LFPI which showed progressive cortical and subcortical axonal injury as indexed by accumulation of amyloid precursor protein (Pierce et al. 1996; Masumura et al. 2000). Importantly, evidence of progressive axonal injury was found in mild LFPI in the mouse (Spain et al. 2010). The behavioural sequelae of the LFPI have also been comprehensively investigated. This includes a transient loss of the righting reflex which has been used as a means to measure the severity of the injury (Carbonell et al. 1998; Schmidt & Grady 1995). A range of sensorimotor tests have been applied to rodents after LFPI (including beam balance, rota-rod and whisker test and acoustic startle) that demonstrated significant impairment in motor function in the injury groups (Hamm 2001; Sackheim et al. 2017; Learoyd & Lifshitz 2012; Saatman et al. 1997). Cognitive testing with the Morris Water Maze have shown post-injury impairment in spatial memory in LFPI rodents (Spain et al. 2010). Due to the technical difficulties of a craniotomy and hub application, the LFPI model suffers from a high exclusion rate. Alongside this, the biomechanics of the injury and need to open the skull means there is limited generalizability to the human disease. Saying that, LFPI reproduces many aspects of human TBI from its histopathology and functional and behavioural deficits. It allows for variation in injury severity and can be used in rodents which afford the ability to test hypotheses using genetically modified animals. These strengths make it a relevant and useful TBI model. Within this thesis, we aim to utilise the ability to vary the severity of LFPI to induce a milder injury. We define this as an injury leading to an elongated right reflex with evidence of axonal injury and inflammatory response but in the absence of gross disruption of brain architecture such as contusions.

1.2.2 Controlled Cortical Impact

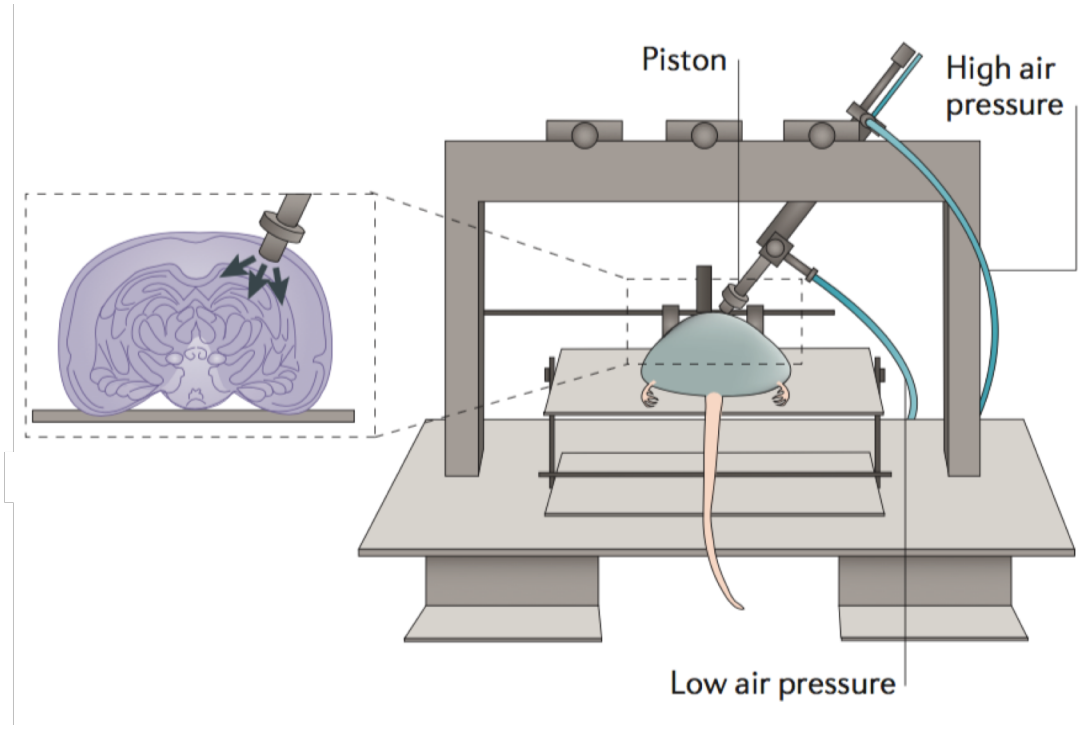

***Figure 1.6**: **Controlled Cortical Impact injury model** demonstrating the application of a rigid impact device into the mouse brain [image reproduced from Xiong et al (2013) with permission from Springer Nature]*

The Controlled Cortical Impact (CCI) model is a form of open skull TBI model **(Figure 1.6)**. Much like the LFPI model, it involves fashioning a craniectomy but then uses a rigid impact device to deform the cortical tissue (Dixon et al. 1991). The severity of the injury can be controlled by changing the depth, time and velocity of the impact device (Xiong et al. 2013). The ability to independently control these biomechanical parameters is an advantage over the LFPI. CCI leads to widespread cortical and subcortical neurodegeneration making it a mixed (focal and diffuse) injury model (Hall et al. 2005). The severity of cognitive deficit has been associated with the depth and speed of impact (Washington et al. 2012).

1.2.3 Weight Drop models

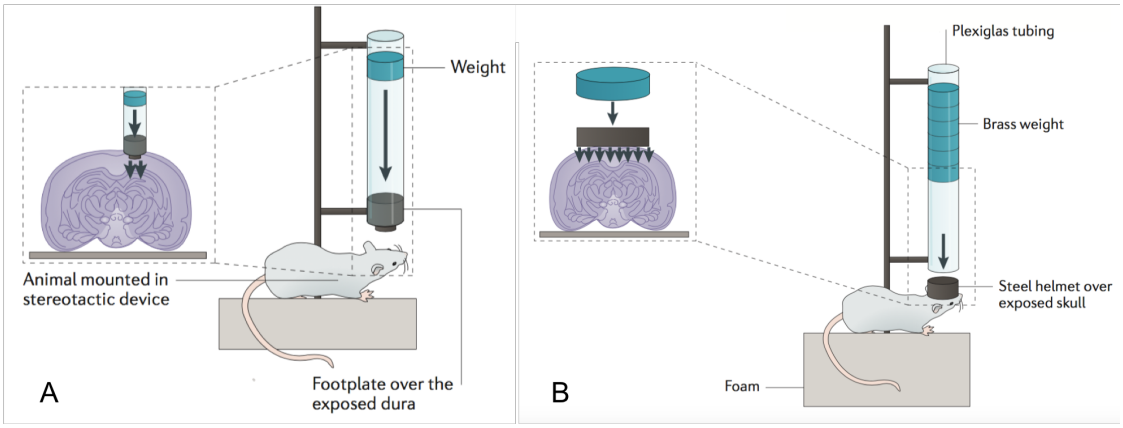

***Figure 1.7**: **Weight drop injury models** showing the Feeney weight device (A) and the Marmarou device (B) [image reproduced from Xiong et al (2013) with permission from Springer Nature]*

Weight drop models inflict a TBI by dropping a free-falling weight onto the rodent's head. The severity of the injury can be varied by altering the height in which the weight is dropped. There are several iterations of the weight drop model with differing procedures to the skull. The Feeney model delivers a weight to the intact dura after a craniotomy **(Figure 1.7, A)**. The model produces cortical contusion which progresses to haemorrhage into the white matter (Feeney et al. 1981). Alternatively, the Shohami model is a closed skull variation where the weight is dropped onto the intact unprotected skull (Shapira et al. 1988). The injury leads to a combination of cerebral contusion and diffuse axonal injury (Albert-Weissenberger et al. 2012; Xiong et al. 2013). In an attempt to model human diffuse axonal injury, Marmarou developed an impact acceleration model which involved attaching a stainless-steel disc to the exposed skull before releasing a guided weight to inflict the injury (Marmarou et al. 1994) **(Figure 1.7, B)**. The model is characterized by wide spread neuronal disruption and diffuse axonal injury throughout the corpus callosum, internal capsule and cerebellar peduncles (Abd-Elfattah Foda & Marmarou 1994). Weight drop models can recapitulate differing aspects of focal and diffuse human TBI. They are low cost however suffer from moderate reproducibility and high mortality rates (Xiong et al. 2013).

Model	Strength	Weakness	Focal	Diffuse
Fluid Percussion Injury	Reproducible, well characterized, varying injury severity	High exclusion rate, need for craniotomy	++	+
Controlled Cortical Impact	Reproducible, low mortality rate, varying injury severity	Need for craniotomy	++	+
Feeney weight drop	Similar biomechanics to human disease	Need for craniotomy, high mortality rate, Poor reproducibility	++	+
Shohami weight drop	Easy to operate, similar biomechanics to human disease	Poor reproducibility	+	++
Marmarou weight drop	Similar biomechanics to human disease	Poor reproducibility, high mortality rate	+	++

***Table 1.2**: **Comparative summary of different preclinical TBI models** [adapted from Xiong et al (2013)]*

1.3 THE EXCITATORY SYNAPSE

The mammalian brain is composed of a hugely complex network of neurons. How these neurons connect and communicate, referred to as the connectome, is increasingly seen as important to understanding the basis of cognition and behaviour (Oh et al. 2014). The synapse is the mode of communication between neurons. Information is transmitted via electrical impulse which is conducted down the neuron axon and then relayed to the dendritic tree of the next neuron. The junction between these two neurons is the synapse. Typically, the synapse is composed of a presynaptic axonal terminal and the dendritic postsynaptic density separated by the synaptic cleft. The existence of the synapse, a term coined by Sherrington in 1897, was a topic of debate for decades until electron microscopy (EM) studies confirmed their existence (De Robertis & Bennett 1955).

1.3.1 Synapse classification

1.3.1.1 Chemical versus electrical synapses

The electrical impulse travelling from one neuron to the next can be conducted by two means: direct electrical or indirect chemical transmission **(Figure 1.8)**. Electrical synapses allow for direct bidirectional cellular communication via gap junctions that consist of hemi-channels that permit the exchange of ions and small molecules **(Figure 1.8, B)**. Electrical synapses allow for rapid communication and are important during development and are believed to be necessary for the subsequent formation of chemical synapses (Pereda 2014). Conversely, chemical synapses propagate unidirectional communication between neurons indirectly by the release of neurotransmitters from presynaptic vesicles **(Figure 1.8, A)**. These neurotransmitters move across the synaptic cleft and bind to receptors on the postsynaptic density. This triggers a flow of charged molecules that, if sufficient, will leads to triggering of an action potential (AP) that propagates down the neuron. Though slower than electrical synapses, chemical synapses allow for greater modulation of signal propagation through changes in presynaptic vesicle and postsynaptic receptor numbers (Branco & Staras 2009).

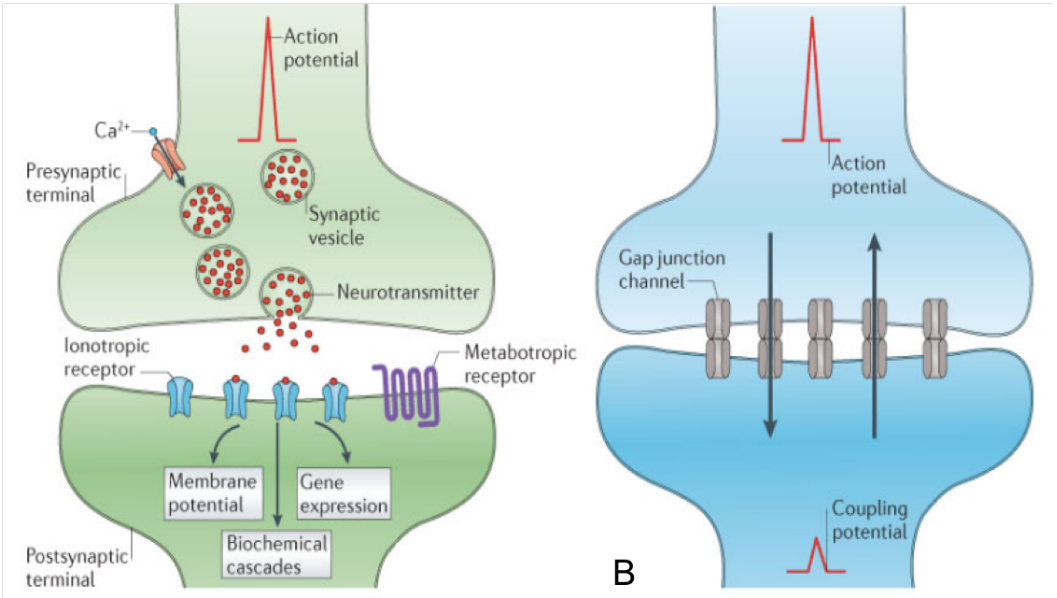

***Figure 1.8**: **Schematic representation of chemical and electrical synapses**. Image A demonstrates neurotransmitter release and inotropic receptors of chemical synapse. Image B demonstrates the hemi-channels of electrical synapses [image reproduced from Pereda et al (2014) with permission from Springer Nature]*

1.3.1.2 Excitatory versus inhibitory synapses

EM studies of chemical synapses by Gray led to observations that divided synapses into two types (Gray 1959). This classification was based upon the size and symmetry of the postsynaptic density and their location. Type 1 (axo-dendritic) typically have wide and pronounced postsynaptic thickening and are found on dendritic spines or shafts. Conversely, Type 2 (axo-somatic) synapses had smaller, less pronounced postsynaptic thickenings and were found on the soma. Subsequent immuno-labelling studies of different neurotransmitters led to classification of Type 1 synapse as 'excitatory' and Type 2 synapses as 'inhibitory' (Harris & Weinberg 2012). Gray's classification remains the most used to describe synapses however there is evidence that not all synapses fit neatly into these dichotomous categories (Klemann & Roubos 2011).

1.3.2 The excitatory postsynaptic density

The postsynaptic density (PSD) is made up of a network of proteins that interact to receive, process and convey synaptic inputs. Scaffolding proteins are a major component of the PSD of which the Disc Large Homolog (DLG) family is the most abundant in excitatory synapses.

1.3.2.1 The DLG protein family

The DLG family is part of the Membrane-associated Guanylate Kinase (MAGUK) protein superfamily. In invertebrates, a single Dlg protein is encoded by a single Dlg gene. Conversely, in vertebrates, the DLG family is composed of four proteins coded by four different genes: Synapse Associated Protein 97 (SAP97) is encoded by Dlg1; Postsynaptic Density Protein 93 (PSD93) is encoded by Dlg2; Synapse Associated Protein 102 (SAP102) is encoded by Dlg3 and Postsynaptic Density Protein 95 (PSD95) is encoded by Dlg4. In this thesis, we will focus on two DLG proteins: PSD95 and SAP102. DLG proteins are expressed at cell-cell interfaces in epithelial and neuronal cells. In mammals, PSD95 is brain specific while SAP102 is mainly expressed within the brain (Müller et al. 1996; Cho et al. 1992). Distribution patterns of PSD95 and SAP102 messenger ribonucleic acid (mRNA) and proteins have been characterized in the mouse brain (Fukaya et al. 1999; Fukaya & Watanabe 2000). mRNA distribution was high within the Cornu Ammonis (CA) and Dentate Gyrus (DG) hippocampal regions and neocortical layers (Fukaya et al. 1999). There was

moderate expression of PSD95 and SAP102 mRNA within the thalamus, cerebellum, hypothalamus and midbrain. Immunohistochemical examination of PSD95 and SAP102 protein expression found similar patterns to the mRNA findings (Fukaya & Watanabe 2000). The same study also examined subcellular expression of the two proteins. The authors found that PSD95 appeared as small puncta within the dendrite closely apposed to synaptophysin-positive nerve terminals. Within the forebrain, PSD95 is restricted to the PSD however, it has been identified presynaptically in Pinceau synapses (basket cells in the cerebellum that synapse onto Purkinje cells) (Hunt et al. 1996; Fukaya & Watanabe 2000; Laube et al. 1996). PSD95 has also been reported to be found within the juxtaparanodes, however its exact role in this structure remains to be fully elucidated (Rasband et al. 2002; Rasband & Trimmer 2001).

1.3.2.2 Structure and protein networks within PSD

The PSD usually lies within the distal end of the dendritic spine head. It measures 300-400nm wide and 30-50nm thick (Carlin et al. 1980). Due to its abundance in the brain, the PSD has undergone comprehensive biochemical analysis. Proteomic studies have revealed that the PSD contains approximately 1000 proteins and that these are relatively conserved between humans and mice (Bayés et al. 2012; Bayés et al. 2011). These proteins have a myriad of differing functions including: scaffolding, signalling, receptors and cytoskeletal elements (Sheng & Hoogenraad 2007). Of these proteins, PSD95 is one of the most highly abundant with approximately up to 300 PSD95 molecules per PSD (Cheng et al. 2006). PSD95 has been shown to form nanoclusters within the PSD (Broadhead et al. 2016). Within the PSD, SAP102 and PSD95 play a central role in organizing the differing proteins types (Kim & Sheng 2004).

1.3.2.3 PSD95 and SAP102 in receptor complexes

A number of differing studies have shown conflicting results in the role of PSD95 with the NMDA receptor (NMDAR). PSD95 knock down has been shown to both affect and not affect NMDAR transmission (Elias et al. 2006; Ehrlich et al. 2007). A recent study using Blue Native Page revealed that the NMDARs form 1.5MDa complexes with PSD95 and PSD93 (Frank et al. 2016). Interestingly, NMDARs were not present in the complexes when either PSD95 or PSD93 were knocked out suggesting that both are required to recruit the receptors into the complex. The same study showed that

SAP102 and SAP97 formed smaller (0.2-0.4MDa) complexes (Frank et al. 2016). The role of DLG proteins has also been studied in the context of the AMPA receptor (AMPAR). PSD95 indirectly binds to AMPAR via Stargazin (Nicoll et al. 2000). AMPAR function has been shown to mirror increases and decreases in PSD95 expression (Stein et al. 2003; Elias et al. 2008; Elias et al. 2006; Ehrlich et al. 2007). These observations are due to changes in the number of AMPAR clustering at the synaptic membrane (El-Husseini et al. 2000). Studies have also found that SAP102 may be involved in AMPAR transmission (Elias et al. 2006; Elias et al. 2008). However, KO SAP102 mice have been found to have normal AMPAR-mediated transmission (Cuthbert et al. 2007). Interestingly, double KO mice for PSD95 and PSD93 were found to have overexpression of SAP102 potentially indicating a compensatory role (Elias et al. 2006). This highlights that the DLG proteins may have an overlapping function in transmitting AMPARs to the synaptic membrane surface.

1.3.3 Function of PSD95 and SAP102

1.3.3.1 Synaptic plasticity

Synapses can strengthen or weaken over time in processes known as Long Term Potentiation (LTP) and Long Term Depression (LDP) respectively. The molecular mechanisms underlying LTP are believed to involve the activation of NMDAR which in turn increase the recruitment of AMPARs to the synaptic membrane. The role of the DLG proteins, particularly PSD95, have been extensively examined in the context of LTP. PSD95 KO mice have been found to have enhanced LTP (Migaud et al. 1998). While acute expression enhancement of PSD95 appears to dampen LTP (Ehrlich & Malinow 2004). In contrast, SAP102 KO mice show normal LTP when tested with high frequency stimulation protocols (Cuthbert et al. 2007). In the context of LDP, PSD95 overexpression induced potentiation with protocols that were typically insufficient to do so (Stein et al. 2003). While knock down of PSD95 impaired LDP (Ehrlich et al. 2007). Together, these data point towards a role of DLG proteins, particularly PSD95, in LTP and LDP.

1.3.3.2 Role in behaviour and cognition

Given the effect of manipulating PSD95 and SAP102 on synaptic plasticity, several studies have also assessed the impact of DLG mutations on the behavioural repertoire. Spatial learning, assessed using the Morris Water Maze, was severely impaired in mice with PSD95 KO (Migaud et al. 1998). While mice with SAP102 KO

showed impairments that could be overcome with additional training when compared to WT mice (Cuthbert et al. 2007). An elegant study using touchscreen cognitive testing comprehensively assessed the impact of PSD95 and SAP102 mutations on cognitive function (Nithianantharajah et al. 2013). The study assessed four domains of the cognitive repertoire: conditioning and simple learning, complex learning, cognitive flexibility and attention and response control. PSD95 KO showed marked simple learning deficits while SAP102 KO demonstrated comparable function to WT mice. In a visual discrimination test and extinction test assessing cognitive flexibility, SAP102 KO mice performed better than WT. Contrary to the SAP102 findings, PSD93 KO mice were found to have decreased function in these cognitive tests. These data indicate that PSD95 has a fundamental role in simple learning while SAP102 and PSD93 are important for forms of higher cognitive function.

1.3.3.3 Role in neurological disease

Mutations within genes encoding for PSD proteome have been found to be associated with up to 133 neurological and psychiatric diseases (Bayés et al. 2011). De novo mutations in schizophrenic patients were found to be over-represented in PSD genes (Fromer et al. 2014). A further proteomic study looking at PSD95 interaction networks found a significant correlation with schizophrenia susceptibility proteins within glutamate receptor clusters (Fernández et al. 2009). Coupled to this, a schizophrenic patient was found to have a deletion in DLG2 (PSD93) (Walsh et al. 2008). Interestingly, similar cognitive deficits were identified in humans and mice with PSD93 mutations (Nithianantharajah et al. 2013). Mutations within the gene that encodes SAP102 has also been associated with non-syndromic mental retardation (Zanni et al. 2010). Alongside evidence of the role of PSD mutations as the cause of a range of intrinsic brain disorders, synapses also appear to be part of the early pathophysiology of inflammatory and degenerative disorders such as multiple sclerosis and Alzheimer's disease (S. Hong et al. 2016; Wegner et al. 2006).

1.4 TRAUMATIC BRAIN INJURY AND THE SYNAPSE

The vital role of the synapse makes it an interesting area of study in the context of TBI. In this section, we will focus on examining the evidence looking at synaptopathy following TBI and the central role the synapse plays in TBI secondary injury.

1.4.1 The postsynaptic density as an intersection of TBI secondary injury

The postsynaptic density is a point where three major TBI secondary injury processes intersect and interact. These processes are: glutamate neurotoxicity, oxidative stress and inflammation:

1.4.1.1 Glutamate neurotoxicity

As previously discussed, TBI leads to a surge in glutamate which acts upon two main receptors within the postsynaptic density: NMDA and AMPA receptors **(Figure 1.9, A)**. NMDA receptors consist of 3 subunits (NR1, NR2 and NR3). Glutamate is an NMDA receptor agonist and binding leads to an influx of Ca^{2+} which is critical for signal transduction **(Figure 1.9, B)**. In TBI, elevated glutamate levels on the NMDA receptor leads to abnormal intracellular Ca^{2+} levels and contributes to neuronal death (Arundine et al. 2004; Arundine et al. 2003). AMPA receptors, which consist of 4 subunits (GLuR1-4), constitute one of the primary transducer at the excitatory synapse (Luo et al. 2011). AMPA receptor subunit composition is an important determinant of the receptor function (Ju et al. 2004). Several studies have shown that TBI-related glutamate increases can lead to changes in AMPA receptors that perpetuate glutamate toxicity by exacerbating Ca^{2+} overload. Particularly the release of intracellular calcium leads to the expression of AMPA receptors lacking subunit GluR2 which are highly permeable to calcium (Bell et al. 2009; Spaethling et al. 2008). This shift in AMPA receptor subtype is an important factor in exacerbating excitotoxic neuronal death. PSD95 connects to PKCalpha - the kinase that phosphorylates AMPA GluR2 – which promotes GluR2-deficient AMPA receptors and exacerbates TBI neurotoxicity. Perturbation of this relationship attenuates this toxicity (Bell et al. 2009) **(Figure 1.9, C)**.

1.4.1.2 Oxidative stress

The postsynaptic density plays an important role in the convergence of glutamate toxicity and oxidative stress. The activation of the NMDA receptor and the influx of Ca^{2+} leads to the generation of reactive oxygen and nitrogen species (Szydlowska & Tymianski 2010). PSD95 binds to the NMDA receptor and neuronal nitric oxidase. This relationship plays an important part in oxidative damage and it has been observed that its disruption led to reduced cell death in an in-vitro model of TBI (Arundine et al. 2004) **(Figure 1.9, F)**. PSD95 may not only have a role in mediating oxidative stress after TBI but also appears to be negatively impacted by it. A temporal

analysis of PSD95 found significant reductions in concentration of the protein at 24 hours post-injury following an earlier depletion of antioxidant systems and increase in oxidants (Ansari *et al.*, 2008 (1); Ansari *et al.*, 2008 (2)). Interestingly, a study by Yu using system biology approaches to analyse gene expression data from multiple TBI animal models highlighted nitric oxidase synthase 1 as a potential protein indicator of TBI (Yu et al. 2015).

1.4.1.3 Inflammation

Inflammation is a well described process following TBI. However, there is growing evidence that the inflammatory process acts through the synapse to further perpetuate TBI-secondary injury. Tumour Necrosis Factor alpha (TNF-alpha) is a proinflammatory cytokine that infiltrates the injury site and has been found to reduce expression of AMPA GluR2 (Beattie et al. 2002; Stellwagen et al. 2005) **(Figure 1.9, D)**. As described above, these changes in AMPA structure can worsen calcium overload and perpetuate cell death. More recently, Zhang and colleagues found in an in-vitro model of ischaemia and inflammation that microglial CR3 triggered long term depression by activation of NADPH oxidase and GluR2-mediate AMPA receptor internalisation (Zhang et al. 2014) **(Figure 1.9, E)**. Both these data point towards a role of inflammatory cells and cytokines impacting TBI-pathology through the synapse.

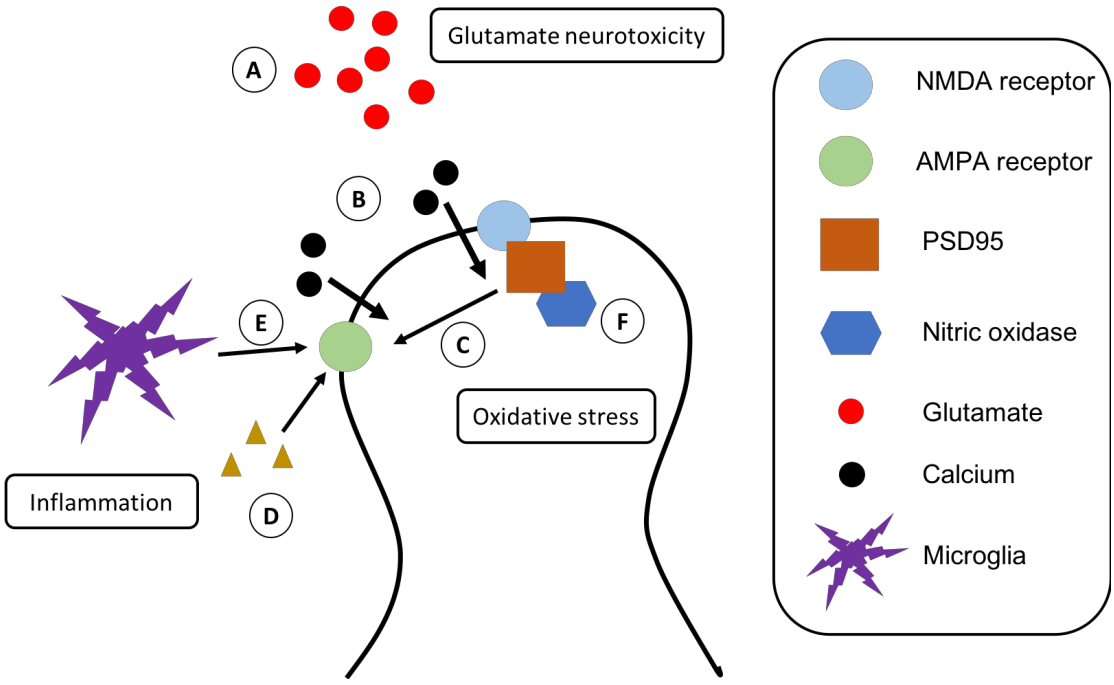

***Figure 1.9**: **TBI secondary injury and the postsynaptic density** demonstrating surge of glutamate following TBI (A) which leads to influx of Ca^{2+} into the cell at the NMDA and AMPA receptors (B). PSD95 which is bound to PKCalpha promotes a GluR2-deficient AMPA receptors and exacerbates TBI neurotoxicity (C). The release of TNF-alpha also acts upon the AMPA receptors and reduces expression of GluR2 which worsens neurotoxicity (D). Triggered by CR3, microglia lead to long term depression by activation of NADPH oxidase and GluR2-mediate AMPA receptor internalisation (E). PSD95 is bound to neuronal nitric oxidase plays a role in promoting oxidative stress after TB (F)I.*

1.4.2 Synaptic changes after TBI

Early evidence on the impact of TBI on synaptic plasticity and function came from electrophysiological studies examining LTP and LDP. Preclinical studies consistently showed impairments in LTP following LFPI (Miyazaki et al. 1992; Reeves et al. 1995; Sanders et al. 2000; Sick et al. 1998). These deficits in LTP, however, have been found to recovery over time (Norris & Scheff 2009). Conversely, LDP appeared not be affected in preclinical models of TBI (D'Ambrosio et al. 1998).

1.4.2.1 Synaptic loss following traumatic injury

Early clues on the impact of neuronal death on synapses came from electron microscopy ultrastructural studies that monitored synapse changes after denervation. Commonly used models included intraventricular injections of kainic acid or electro-ablation to injure neurons and subsequently analyze the impact on synaptic projections. Models using both of these approaches demonstrated a significant reduction in synaptic density between 3-4 days post-lesion (Marrone et al. 2004; Anderson et al. 1986). However, these approaches are limited in providing insights into TBI-related synaptopathy due to the differing mechanism. To overcome this, a number of studies have used biochemical and imaging approaches to quantify synaptic loss following various preclinical models of TBI **(Table 1.3)**. Using a moderate CCI model, Scheff used electronic microscopy to examine synaptic changes in the CA1 region of the hippocampus (Scheff et al. 2005). At 2 days post-injury, there was a 58% reduction in synapse numbers in the CA1 stratum radiatum in the injury group. A similar finding was found by Gao and colleagues who examined synaptic density in the dentate gyrus using immunohistochemistry against synaptophysin after a moderate CCI (Gao et al. 2011). At 3 days after the injury, the

density of synaptophysin-positive puncta was reduced by 30.77% compared to the sham mice. Biochemical approaches have also shown evidence of synaptic loss in TBI models. Using Western blotting in a CCI model, Wakade found a 46.6% reduction in hippocampal PSD95 in injury mice compared to sham 7 days after injury (Wakade et al. 2010). A similar study assessed a set of synaptic proteins (PSD95, Synapsin-I, SAP97 and GAP43) in the hippocampus at multiple time points post-CCI using Western blotting (Ansari *et al.*, 2008 (1)). The authors found significant reductions in PSD95 and Synapsin-I compared to sham from 48 hours which persisted up till 96 hours post-injury. System biological approaches have corroborated these findings. Yu et al analyzed high-throughput gene expression data from four different TBI animal models and found a suppressed network of proteins for which the proteins were associated with the synapse and centred around PSD95 (Yu et al. 2015). Though limited, there has been observations of synaptopathy in human cases of TBI. Castejon and colleagues undertook a small case series looking at human cortical tissue samples after TBI (Castejòn et al. 1995). Utilizing EM, the authors found evidence of swollen and shrunken presynaptic terminals and separation from the postsynaptic density. The authors also described dendritic swelling and evidence of synaptic phagocytosis by astroglial cells. This later observation opens questions regarding the underlying mechanism of synaptic loss. Axonal injury is an important part of TBI pathology. Canty and colleagues used two-photon microscopy and laser microsurgery to look at the effect of axotomy on synapses in-vivo at a single axon level (Canty, Teles-Grilo Ruivo, et al. 2013). The authors observed rapid reductions of synaptic density along the injured proximal axon within 6 hours.

1.4.2.1.1 The role of astroglia in synaptic damage and loss after TBI

A particularly important question is the role of astroglial cells in removing or ‘stripping’ synapses in disease. Several studies have made observations linking microglia to synapse removal in different disease models. Wake et al used two-photon microscopy and found that transient cerebral ischaemia led to more prolonged contact between microglia and presynaptic terminal, following which a number of boutons were noted to have disappeared (Wake et al. 2009). Similarly, Hong et al looked at a murine model of Alzheimer’s disease and observed early synapse loss that preceded plaque formation (S. Hong et al. 2016). The authors described microglia engulfment of synaptic elements which was not observed in mice with CR3 knock-out (a high affinity receptor expressed on macrophages) Subsequently, the authors observed a rescue

of synaptic loss using a microglia knockout model. They concluded that the complement cascade and microglia mediate early synaptic loss in Alzheimer's disease. An in-vitro study that aimed to model inflammation and ischaemia (two important pathologies in TBI) found evidence that the two processes act synergistically through microglial CR3 to induce LTD (Zhang et al. 2014). These data point toward a potential role of microglia in synaptic pruning however there is a lack of conclusive mechanistic evidence, particularly in the context of TBI. The role of astrocytes has also been examined in TBI. Furman and colleagues examined the effect of blockading the astrocytic calcineurin/NFAT signalling pathway on hippocampal synaptic function and protein levels (Furman et al. 2016). Using an adeno-associated virus delivery system to deliver VIVIT (an NFAT inhibitory peptide), the authors found a prevention of injury-induced synaptic strength loss in CA1 and an associated reduction in synaptic protein loss (PSD95 and GluR1). Interestingly, these observations occurred without a significant change in the number of astroglia between the treated and control rodents indicating that the synaptoprotective effects of VIVIT do not require an associated reduction in glial activation. Astrocytes have also been implicated in propagating synaptic damage by the release of D-serine. Perez et al found a shift from neuronal to astrocytic D-serine release after CCI (Perez et al. 2017). The authors found that astrocyte-specific elimination of D-serine rescued synaptic plasticity.

1.4.2.2 Synaptic recovery and circuit reorganization

Alongside observing the degree of synaptic loss after injury, a range of studies have also looked at synaptic recovery and reorganization. Denervation studies described post-injury synaptogenesis after the initial loss. This process of recovery has been observed from as early as 6-10 days after the injury and has been followed up to 30-60 days after the lesion injury (Marrone et al. 2004; Anderson et al. 1986). However, TBI involves a complex and interactive set of secondary injury processes which may impact synaptic recovery. A combination of deafferentation and central fluid percussion has been used to tease out the effect of TBI secondary injury on synaptic recovery. Reeves and colleagues found that a combination of CA1 deafferentation and central FPI led to persistent impairment of LTP and an associated reduction in NMDA receptor immunobinding compared to deafferentation alone (Reeves et al. 1997). Two studies examined reactive synaptogenesis using EM in preclinical models of TBI **(Table 1.3)**. Scheff and colleagues found a recovery of CA1 synapse density

at 10 days post injury which continued to day 30 and plateaued at 70% of control mice (Scheff et al. 2005). Semchenko used a rotatory head injury model in rats and found an increase in sensorimotor cortical synaptic density from day 7 to day 30 post-injury compared to control (Semchenko et al. 2006). Interestingly, another study by Canty using laser axotomy and two-photon microscopy observed regeneration in a subset of axons which then went on to form synaptic boutons to prelesional postsynaptic densities (Canty, Huang, et al. 2013).

1.4.2.2.1 The role of astrocytes in synaptic circuit remodeling after TBI

These observations point towards a degree of limited or maladaptive synaptic reorganization post-injury. The mechanisms underlying post-injury synaptogenesis have been investigated. Astrocytic Matrix Metalloproteinase-3 (MMP3), an enzyme involved with the breakdown of the extracellular matrix, has been implicated in maladaptive synaptic recovery after TBI (Huntley 2012). A study comparing deafferentation alone to deafferentation and FPI found persistent elevated increases in MMP3 for which there was significant colocalization to astrocytes in the combined injury group (Falo et al. 2006). Pharmacological inhibition of MMP3 led to increases in PSD thickening on EM and an improvement in spatial learning. Similarly, Nikolakopoulou found evidence of the involvement of astrocytic Ephrin-B1 in synaptic remodelling after a moderate CCI in mice (Nikolakopoulou et al. 2016). After injury, an upregulation of Ephrin-B1 was observed which coincided with a decrease in the presynaptic protein VGlut1. Ablation of Ephrin-B1 accelerated the recovery of VGlut1 puncta. The authors linked Ephrin-B1 to STAT3 phosphorylation which they implicated in synaptic remodelling. A similar conclusion was reached by Tyzack and colleagues who examined the role of astrocytic STAT3 in synaptic remodelling in a facial murine nerve axotomy model (Tyzack et al. 2014). The authors implicated astrocytic STAT3-regulated release of thrombospondin-1 in post-injury synaptic remodelling. The study found that KO of thrombosopondin-1 led to impaired synaptic recovery which mirrored findings in a model of cerebral ischaemia which showed deficits in synaptic density and functional recovery with KO of thombospondin-1/2 (Liauw et al. 2008). In TBI, there is evidence of thrombospondin upregulation in both in-vitro and in-vivo models (Tran et al. 2012). Plasma levels of thrombospondin-1 has also been found to be elevated in patients with TBI and may act as a prognostic biomarkers (Wang et al. 2016). Astrocytes may also play a role in post-injury circuit reorganisation by the secretion of Hevin, a synaptogenic protein (Singh et al. 2016).

Furnam and colleagues found an increase in Hevin levels in injury mice compared to sham which was further amplified by the blockade of the calcineurin/NFAT signalling pathway (Furman et al. 2016). These data together suggest that astrocytes may play a double-edged role in synaptic reorganization post-TBI releasing enzymes and proteins that have been observed to both promote and impair synaptic recovery.

Study	Model	Time-point(s)	Method	Synaptic protein	Finding
Scheff, 2005	CCI	2, 10, 15, 30 and 60 days	EM	n/a	Reduction in CA1sr synaptic density to 44% of control at day 2 post-injury followed by gradual increase to day 30 which then plateaued at 86% of control density
Semchenko, 2006	Rotatory head model	1, 3, 7, 14 and 30 days	EM	n/a	Reduction in sensorimotor synaptic density to 76.4% of control at day 1. This was followed by gradual decrease to 63.9% of control at day 7 followed by an increase to 81.9% of control by day 30.
Shojo, 2006	LFPI	2, 15 and 30 days	Immuno-histochemistry + Western blot	Cortical Synaptophysin	There was increased synaptophysin immunoreactivity in cortex ipsilateral to injury and in the subcortical white matter on ipsilateral side. There was no significant difference in synaptopysin over time when measured with Western Blot
Ansari, 2008 (1)	CCI	1, 3, 6, 12, 24,	Western Blot	Hippocampal	Hippocampal Synapsin-I and PSD95 significantly

		48, 72 and 96 hours		SAP97, PSD95 and GAP43	reduced from 48h. SAP97 reduced at 96h with no significant reduction in GAP43 compared to sham
Ansari, 2008 (2)	CCI	3, 6, 12, 24, 48, 72 and 96 hours	Western Blot	Cortical Synapsin-I, SAP97, PSD95 and GAP43	Cortical PSD95 and synapsin-I dropped from 24hrs and remained low up to 96 hr. SAP97 declined at 96 hr but GAP-43 failed to show any changes
Wakade, 2010	CCI	1, 2, 3 and 7 days	Western blot	Hippocampal PSD95	Delayed reduction of hippocampal PSD95 at 7 days post-injury
Gao, 2011	CCI	3 day	Immuno-histochemistry	Hippocampal Synaptophysin	Injury group had reduction in puncta density to 69.23% of sham mice
Nikolakopoulou, 2016	CCI	1, 3 and 7 days	Immuno-histochemistry	VGlut-1	Significant reduction in CA1sr VGlut-1 puncta from day 3 post-injury which persists at day 7 compared to sham
Meabon, 2016	Blast model	1, 30 days	Western Blot	Cerebrellar PSD95	No difference in PSD95 Western Blot optical density at 1 day between injury and sham but significant reduction between sham and blast mice at 30 days

Table 1.3: Summary of preclinical studies examining post-TBI synaptic changes

1.4.2.3 Synapse subtypes and TBI

As discussed in an earlier section, there is EM evidence of differing types of excitatory synapse. More recently, whole brain molecular synaptome mapping has shown there

to be huge heterogeneity in synaptic subtypes across the mouse brain (Zhu et al. 2018). This degree of molecular phenotyping has not been described in the context of TBI, however there is some evidence to suggest that brain injury leads to changes to different synapses. Investigators have observed differing responses from synaptic subtypes to denervation (Marrone et al. 2004). Conversely, Scheff's study which looked at CA1 synapses after CCI found no significant difference in synaptic size between the injury and sham groups over time (Scheff et al. 2005). A study using two-photon microscopy and laser microsurgery found that newly formed terminaux boutons were preferentially lost after axotomy compared to older more established boutons (Canty, Teles-Grilo Ruivo, et al. 2013). This data, though limited, points towards differing vulnerabilities and responses to TBI from synaptic subtypes.

1.5 SUMMARY AND RATIONALE

In this section, we have examined the impact of TBI on a population level and highlighted that even mild injuries can have a significant impact on patients' lives. The pathophysiology of TBI is a complex, interconnected process with a number of secondary injury pathways including glutamate neurotoxicity, oxidative stress and inflammation. The synapse appears to both play a role in and be directly affected by TBI. Preclinical studies looking at the impact of TBI on the synapse have shown early reduction in synaptic density in certain brain regions and there is evidence of maladaptive synapse reorganization thereafter. However, the approaches used in these studies were limited, both in the scope of the brain regions examined and the number of synaptic proteins. Therefore, our understanding of the impact of TBI on the synapse remains incomplete.

1.6 THESIS AIMS AND HYPOTHESIS

In this thesis, we aim to examine the whole-brain temporal spatial impact of a mild LFPI model on the synapse by studying two postsynaptic density proteins (PSD95 and SAP102). To overcome the limitations of the literature, we aim to utilize a knock-in model where two fluorescent proteins are tagged to PSD95 and SAP102. With the use of an in-house developed machine learning algorithm, we aim to create whole brain synaptome maps to examine the temporal spatial profile of PSD95 and SAP102 after a mild TBI. We hypothesize that a mild LFPI will induce a progressive, dynamic and differential alteration in PSD95 and SAP102 levels.

CHAPTER 2

Material and Methods

2.1 ANIMALS

All animal experimentation was undertaken in accordance with Home Office guidelines [Animal (Scientific Procedures) Act 1986] and was approved by The University of Edinburgh. Surgical experimental procedures were undertaken on the project license of Dr. Jonathan Rhodes (70/7984).

2.1.1 Wild type C57BL/6 mice

Adult male mice in experiment described in Chapter 3 were purchased from Charles River Laboratories. The mice were allowed to acclimatize in the animal unit for at least 7 days prior to experimentation. They were aged 8-12 weeks at the time of the surgical procedure. The mice were kept in a 12-hour light/dark cycle and given free access to food and water before and after the experimental procedure.

2.1.2 PSD95-eGFP and SAP102-mKO2 Knock-in (KI) mouse line

Both the PSD95-eGFP and SAP102-mKO2 mouse lines were generated by Dr. Fei Zhu under the supervision of Dr. Noboru Komiyama and Prof. Seth Grant. The mice used in the LFPI experiments were male homozygous for PSD95-eGFP and hemizygous for SAP102-mKO2 and aged between 8-16 weeks at the time of surgery. The mice were kept in a 12-hour light/dark cycle and given free access to food and water before and after the experimental procedure.

2.1.2.1 Generation of mouse line

The generation of the mouse line is fully described in Dr. Fei Zhu's PhD thesis. The gene targeting technique used for PSD95 and SAP102 has been described previously (Fernandez, 2009). Two mouse lines were generated, eGFP and mKO2 were inserted in-frame in the last coding exon of Dlg4 (PSD95) and Dlg3 (SAP102) respectively **(Figure 2.1)**. Briefly, a targeting vector was created which contained the homologous DNA sequence for Dlg3 or Dlg4 linked to the corresponding fluorescent protein. The final vector contained a 5' homology arm and a 3' homology arm which, respectively, was 6.3kb and 2.9kb for Dlg4 and 2kb and 5.7kb for Dlg3. The vector contained neomycin-resistance gene sequence and was flanked by loxP sites for future excision with Cre recombinase. Diptheria toxin A gene was inserted as a negative selection marker for random integration events. Sanger sequencing was used to confirm vector functions and PCR cloned fragments. Targeting vectors were separately electroporated into mouse embryonic stem cells (E14Tg2a). Cells with stable

integration of DNA were selected out with the use of G418 antibiotic – only cells expressing neomycin were selected through resistance to antibiotic. While cells with random integration would have diphtheria and therefore were less likely to survive. Subsequently, long range PCR was used to confirm correct targeting. From here, clones were then expanded and microinjected into a blastocyst and inserted into a recipient female. Male chimeras were then crossed with wild type mice from C57BL/6J strain and the resultant litters genotyped to confirm targeted allele transmission to the F1 generation. Heterozygous F1 generation mice were crossed with Cre-deleter mice to remove the loXP flanked neo cassette. Finally, the reporter line mouse lines, were established by breeding heterozygote mice with C57BL/6J wild type mice before interbreeding to create the homozygous mice.

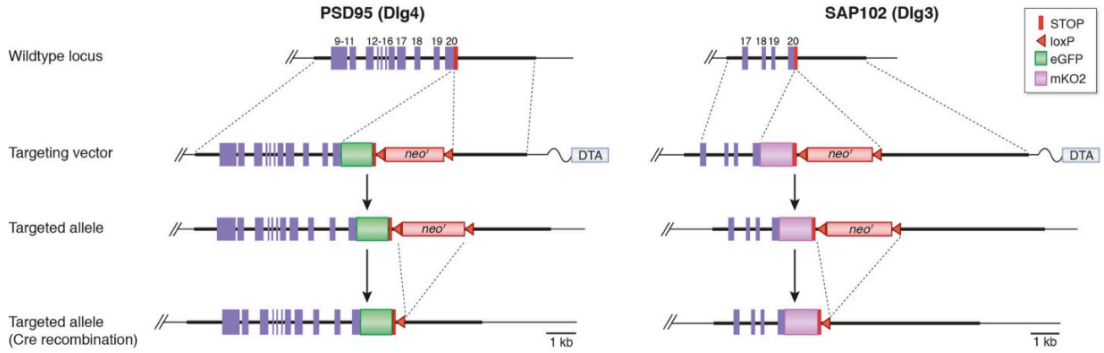

***Figure 2.1**: **Schematic representation of generation of PSD95-eGFP and SAP102-mKO2 mice.** The wildtype genomic locus of PSD95 (Dlg4) and SAP102 (Dlg3) are represented along with corresponding targeting vectors. These vectors contain DNA encoding for fluorescent proteins [eGFP = green bar and mKO2 = pink bar]. Alongside the fluorescence protein DNA, the targeting vector contained a neomycin positive selection cassette adjacent to a LoxP site and a Diptheria Toxin A (DTA) negative selection cassette. The target allele is shown before and after Cre recombination. Image reproduced from Zhu et al. (2018) under creative common licence.*

2.1.2.2 Characterization of mouse line

Biochemical, electrophysical and imaging techniques were used to comprehensively characterize the transgenic knock-in mouse model. These experiments were performed by Dr. Fei Zhu, Dr. Maksym Kopanitsa, Dr. Zhen Qui and Dr. Melissa Cizeron. A detailed description can be found in Dr. Zhu's and Dr. Cizeron's theses

and in a recently submitted manuscript. A summary of their findings is described below:

2.1.2.2.1 Biochemical characterization

Western blots were used to measure the overall expression of PSD95 and SAP102. This experiment was undertaken by Dr. Fei Zhu. Briefly, mouse forebrains were homogenised in deoxycholate buffer and centrifuged. Proteins were then run through sodium dodecyl sulphate (SDS)-PAGE gel. Following this, they were transferred to a nitrocellulose gel and labelled with either anti-PSD95 or anti-SAP102 antibodies. The results showed that PSD95-eGFP and SAP102-mKO2 levels were similar to those of the endogenous proteins **(Figure 2.2)**.

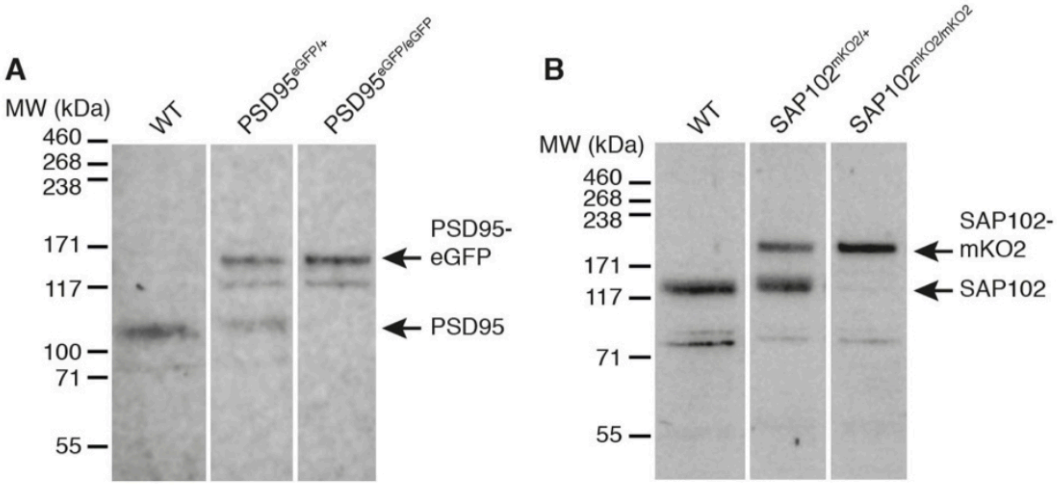

***Figure 2.2**: **Western blot of postsynaptic proteins** demonstrating analysis from wildtype, heterozygous and homozygous forebrain homogenates for PSD95-eGFP (A) and SAP102-mKO2 (B). Molecular weight in kDA. Image reproduced from Zhu et al. (2018) under creative common licence.*

2.1.2.2.2 Electrophysiological characterization

The functional impact of inserting the fluorescent proteins was assessed using electrophysiology. Dr. Maksym Kopanitsa undertook the experiments described below. Acute brain slices from the two mouse lines were collected and recordings from CA1 were taken as previously described (Kopanitsa et al. 2006). Input-output relationships, paired-pulse facilitation and theta burst stimulation were assessed. No significant differences were found between the knock-in and wildtype mice.

2.1.2.2.3 Imaging characterization

Spatial expression patterns of the two proteins (PSD95 and SAP102) were also assessed with a number of experiments. Firstly, low magnification images of the knock-in mouse lines were examined and the distribution patterns compared to those described in the literature. Alongside this, qualitative comparisons were made between knock-in expression patterns and those using antibody staining. These two experiments were undertaken by Dr. Fei Zhu and are described in her thesis. Following from this, Dr. Melissa Cizeron and Dr. Zhen Qui used high resolution confocal microscopy (SDM) and machine learning algorithms (details of the methodology can be found below and in Dr. Melissa Cizeron's thesis) to create whole brain synaptome maps of PSD95 and SAP102 expression at the single synapse resolution. Data on the density, intensity and size of the puncta was analysed. This demonstrated differential regional expression of the two proteins with unique patterns for the measured metrics **(Figure 2.3)**.

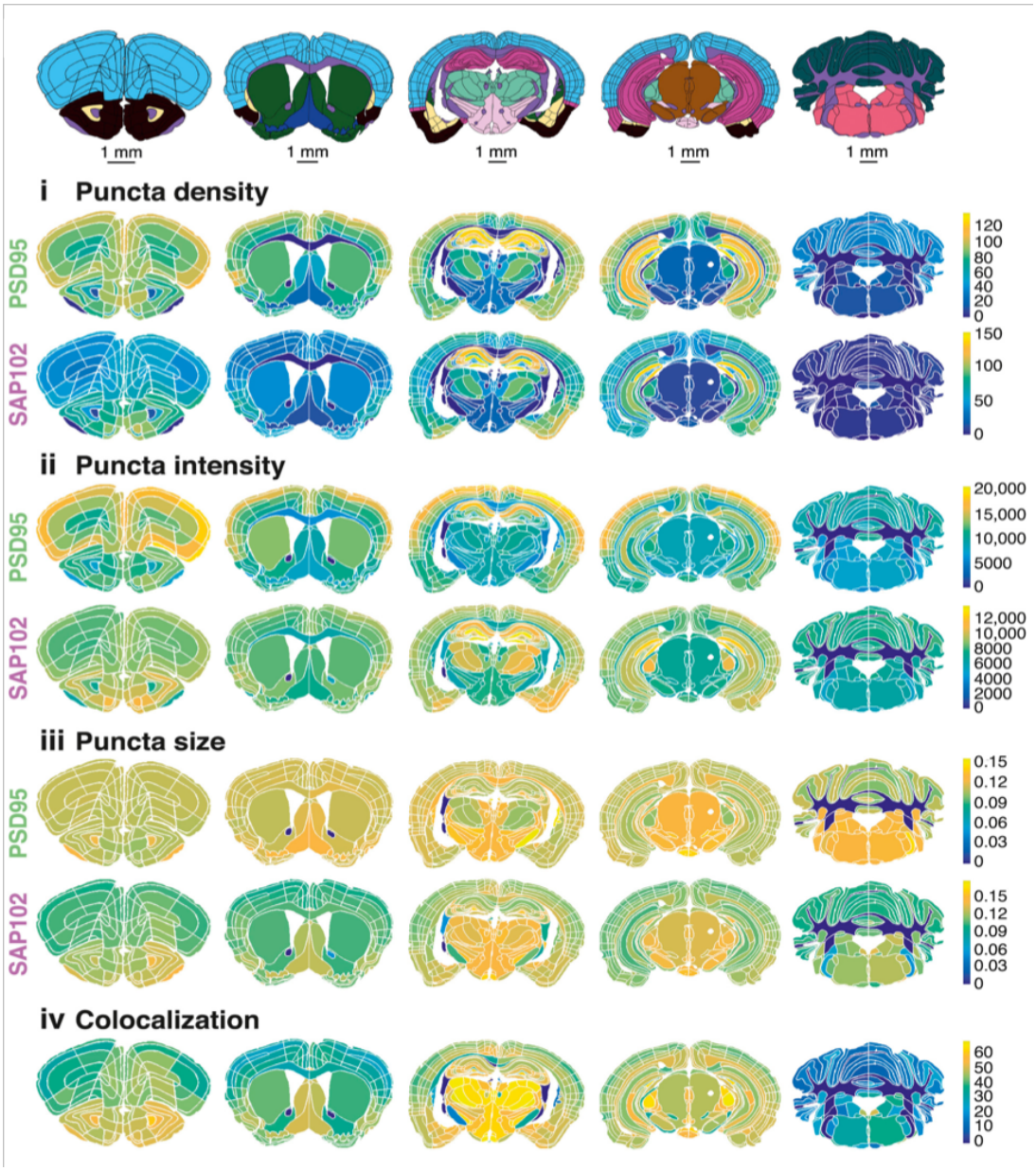

Figure 2.3: ***PSD95 and SAP102 synaptome maps*** *demonstrating (i) puncta density (puncta per 100 μm^2) (ii) puncta intensity (16-bit grey scale) (iii) puncta size (μm^2) and (iv) colocalisation (%) for PSD95 (above) and SAP102 (below). Image reproduced from Zhu et al. (2018) under creative common licence.*

2.2 GENOTYPING

All genotyping was undertaken by either Mr. David Fricker or Ms. Rand Dahan.

2.2.1 Tissue collection

Every mouse had two samples of tissue collected for genotyping at two time-points. The first sample was an ear clipping taken at 3 weeks of age. This sample was used to provide an initial genotyping screen to allow mouse selection for experimentation. The second tissue sample included two tail samples approximately 2-3mm in length taken at the time of transcardial perfusion. A second round of analysis was undertaken using this sample to confirm the mouse was the correct genotype. If there was evidence of discrepancy, then a further analysis was done on the final sample if required. Therefore, all mice had at least two rounds of genotyping.

2.2.2 Polymerase Chain Reaction (PCR) protocol

DNA was extracted from tail or ear samples using MyTaq Extract-PCR kit (Bioline). A 2µl sample of extracted DNA was mixed with 0.5µl of the specific primers **(Table 2.1)**. For PSD95-eGFP allele, MyTaq HS (Bioline) was used. The DNA and primers were mixed with 4µl of 5X PCR buffer, 0.15µl Taq enzyme and 12.85µl of double distilled water to make a volume of 20µl. For the SAP102-mKO2 allele, two separate mixtures were created with the associated primers as outlined in **Table 2.1**. The DNA and primers were mixed with 2.5µl of 5X PCR buffer, 0.15µl Taq enzyme, 0.5 µl of 10mM deoxynucleotide triphosphate (dNTPs) and 18.35µl of double distilled water to make a volume of 20µl.

Allele	Name	Sequence
PSD95-eGFP	95GFPExF_N1	GTCACATGTCTTTGTGACCTTG
	95GFPUTRR_N1	GATACATGCAGAGAGGAGTGTC
	95GFP_FN2	CATCAAGGTGAACTTCAAGATC
SAP102-mKO2 *(mutant reaction)*	SAP102 mKOF3-1	GCCAGATGAAGACCACCTACAAG
	SAP102 UTR_R1	GGGACAAGAACAGTAGTCATTTG
SAP102-mKO2 *(WT reaction)*	SAP102 ExonF2	CATCACAGGAGGGTCGTTACTAG
	SAP102 UTR_R1	GGGACAAGAACAGTAGTCATTTG

Table 2.1**: **PSD95 and SAP102 primer sequences used for PCR protocol

Allele	PCR cycle conditions		
PSD95-eGFP	95°C	1mins	
	95°C	15secs	35 cycles
	55°C	15min	
	72°C	45sec	
	72°C	5mins (optional)	
	4°C	Forever	
SAP102-mKO2	95°C	15 mins	
	94°C	45 sec	35 cycles
	55°C	45 sec	
	72°C	1 min	
	72°C	10 mins	

Table 2.2**: **Cycling conditions used for PSD95 and SAP102 reactions

The mixtures were then placed in the PCR machine with reaction specific cycling condition as described in **Table 2.2**. A 2% agarose gel in Tris-Acetate-EDTA (TAE) containing 0.5% ethidium bromide was used to separate the PCR products. These were then visualized by UV transillumination (UVP GelDoc-It TS2 Imager). **Table 2.3** highlights the amplification products observed for the PSD95 and SAP102 reactions.

Allele		Amplification product size
PSD95-eGFP	Wildtype	330bp
	Mutant	514bp
SAP102-mKO2	Wildtype	280bp
Wildtype reaction	Mutant	1.1kb
SAP102-mKO2	Wildtype	No band
Mutant reaction	Mutant	280bp

Table 2.3**: **PSD95 and SAP102 amplification products

2.3 LATERAL FLUID PERCUSSION INJURY MODEL

The mice were anaesthetized with 5% isoflurane (Merial, UK) in 100% O2 prior to surgery for 2 minutes. The mice were then weighed and placed in stereotaxic frame (Model 900, David Kopf Instruments). A nose cone was used to maintain anaesthesia **(Figure 2.4, A)**. During surgery, the mice's' body temperature was maintained at 37±0.5^{o}c using a heat pad and rectal thermometer probe (Homoeothermic blanket control unit, Harvard Apparatus). A razor was then used to shave a small patch of hair from the top of the mouse's head and eye ointment (Xailin) was applied to the eyes. A midline scalp incision was fashioned and the skin flaps reflected using skin clips. A plastic guide was glued onto the skull using 3M Vetbond and a lateral 2mm circular craniectomy was then trephined (Miltex) midway between the bregma and lambda. Care was taken to not injure underlying dura. An injury hub was created by cutting off the female end of Luer-Loc needle hub. This was secured over the craniectomy site using glue (Loctite Power Flex Gel) and dental cement (Simplex Red, Associated Dental Products) **(Figure 2.4, B)**. The mice were then removed from the stereotatic frame and the depth of anaesthesia reduced till they responded to tail pinch. The mice were then replaced in the anaesthetic box for 1 minute. Once complete, the injury hub was filled with normal saline and attached to the fluid percussion device (Custom Design and Fabrication, Virginia Commonwealth University) **(Figure 2.4, C)**. When they showed response to tail stimulus (to standardize anaesthesia levels) had a mild to moderate injury (1.1-1.5 atm) was inflicted. This was determined by oscilloscope attached to the fluid percussion device **(Figure 2.4, D)**. Sham mice had the exact same procedure except the release of the pendulum to inflict the percussion injury.

Following this, the mice were disconnected from the fluid percussion device and placed on their back to measure their righting time - a marker of the neurological severity of the injury. A righted animal was defined as having moved all four limbs onto the surface it was lying on. The righting reflex has been found to correlate with injury severity (Hamm 2001). Importantly, the righting reflex can be effected by anaesthesia necessitating a consistent experimental protocol (Eakin et al. 2015). Clear exclusion criteria were defined **(Table 2.4)**. Following righting, the mice were then re-anesthetized and had the hub removed and the skin incision sutured using 5-0 Vicryl (Ethicon). A 2mg/kg dose of Bupivicaine (AstraZeneca) was applied to the wound to manage pain. Mice were then placed in a heated recovery chamber kept at 30^{o}C (Lyon Electric Company) for 30 minutes prior to being returned to a cage. A range of time-points for recovery were used including: 24 hours, 7 days and 28 days. Mice were initially monitored daily for the 5 days postoperatively. Following this, they were assessed once a week till the end of the experiment.

2.3.1 Randomization protocol

Mice were randomized to the following four cohorts: 7 day injury, 7 day sham, 28 day injury and 28 day sham. When a group of mice became eligible for randomization, each mouse would be allocated a number from 1 – n. A random sequence generator (www.random.org) was used to produce the sequence 1 - n in random order. Using this random order, the mice would be sequentially allocated to the four cohorts in the following order: 7 day injury, 7 day sham, 28 day injury and 28 day sham. In the event that there were not enough mice to be randomized to all four cohorts, then the unfilled groups would be rolled over to the following experiment.

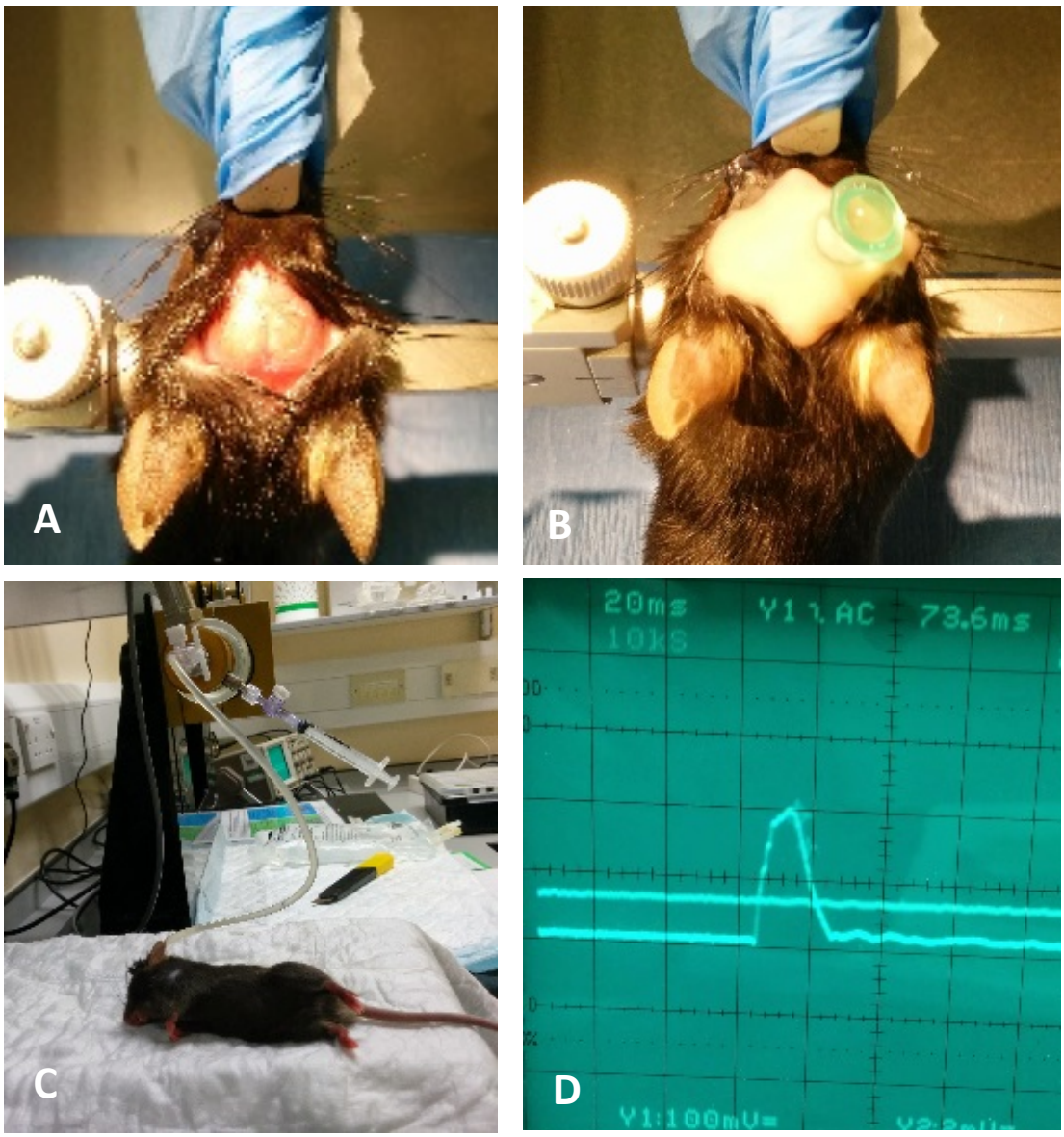

***Figure 2.4**: **Lateral fluid percussion injury procedure** demonstrating the major steps including craniectomy with dura intact (A) followed by hub fixation with dental cement (B) and subsequently attaching the mouse to the FPI device (C) and the oscilloscope readout (D)*

Exclusion Criteria
Dural tear during craniectomy
Dural rupture occurring following application of fluid pulse or removal of hub
Post-injury paralysis lasting greater than 30 minutes

Table 2.4**: **Exclusion criteria for fluid percussion injury experiments

2.4 TISSUE COLLECTION AND PROCESSING

2.4.1 Transcardial perfusion and brain fixation

Mice were administered a terminal dose of intraperitoneal injection of 0.1ml 20% phenobarbital sodium (Euthatal – Merial Animal Health Ltd). Once the mice were fully anaesthetized (not responding to tail pinch), they were pinned to a cork board and underwent a thoracotomy. The heart was fully exposed and a small knick was made in the right atrium. Subsequently, 10mls of phosphate buffered solution (PBS - Fisher Scientific) was injected slowly into the left ventricle. This was followed by 10mls of 4% paraformaldehyde (PFA - prepared by diluting 16% Alfa Aesar in 1:4 PBS). Following this, the mice were decapitated and the brain dissected free from the skull. It was subsequently post-fixed in 5mls of 4% PFA for 3-4 hours and then placed in a 30% sucrose solution (prepared by diluting VWR Chemicals sucrose in PBS) for 48 hours. The brains were then placed in a solution of 50:50 30% sucrose and Optimum Cutting Temperature medium (OCT - VWR International) for 1 hour before being embedded in a mould (Sigma-Aldrich) in OCT. This was achieved by immersing the moulds in a beak of isopentane (Sigma-Aldrich) which was then placed in liquid nitrogen. Once frozen, the brains were kept at -80^{o}c till they were sectioned.

2.4.2 Blinding

After brains were removed and were being fixed in sucrose solution they were blinded by a member of the Grant lab (Sarah Lempriere - SL). SL applied a blinding code to each mouse and kept a central register of the mice and blinding codes which was inaccessible to the primary investigator (AJ). The blinding was unmasked after the generation of the raw subregional puncta data to allow for subgroup analysis.

2.4.3 Cryosectioning protocol

A NX70 Thermo Cryostat was used to cut coronal sections 18 microns in depth. A small drop of PBS was placed on a Superfrost Plus glass slide (Thermo Scientific) before sections were collected. A total of two sections were placed on each slide. Slides were left to dry at 4^{o}c overnight following which they were stored at -80^{o}c till further analysis. Sections were kept away from light as much as possible to minimize loss of fluorescence.

2.5 HISTOLOGY

2.5.1 Haematoxylin and Eosin (H+E) staining

Slides containing sections from the level corresponding to approximately -1.94mm from bregma according to Frankilin and Paxinos were selected for haematoxylin and eosin staining. Selected slides were washed in a 1% PBS bath for 5 minutes. After this, slides were hydrated through graduated ethanol concentrations followed by rinsing in running water for 5 minutes. The slides were then placed in filtered Shandon ready-made Harris Haematoxylin Acidified [ThermoFisher Scientific (#6765003)] for 3 minutes followed by rinsing in running water. The haematoxylin was then differentiated in 1% acid alcohol for 10 seconds. After rinsing, the slides were then placed in Scott's Tap Water substitute (1 litre distilled water, 20g $MgSO_4$, 3.5g $NaHCO_3$) for 2 minutes. From there, the slides were placed in Shandon EosinY Alcoholic [ThermoFisher Scientific (#6766007)]. Following rinsing in running water, the slides were dehydrated through increasing graduated alcohol concentrations. The slides were finally cover-slipped using DPX [Sigma (06522)]. All stages were performed at room temperature (RT).

2.5.2 Immunohistochemistry

2.5.2.1 Amyloid Precursor Protein (APP) immunostaining

Sections were defrosted and the OCT was washed away by agitating in 1% PBS for 5 minutes. After this, slides were hydrated through graduated ethanol concentrations. The Leica Novolink Max Polymer Detection system (406040647) was used. In summary, a peroxidase block was applied for 30 minutes. Following this, the sections underwent antigen retrieval in citric acid (1.05g in 500mls TBX at pH 6) in a pressure cooker up to 125^{o}C. Subsequently, the sections were then treated with a protein block for 15 minutes. This was followed by application of 1:1000 anti-amyloid precursor protein A4 clone 22C11 (Millipore MAB348) antibody for 30 minutes. Subsequently, the post primary solution was applied for 30 minutes followed by a polymer for a further 30 minutes. Dab (1:200) was applied to the sections for 1 minute. The sections were then counterstained with Haematoxylin for 60 seconds followed by Scott's Tap Water for 2 minutes. Following this, the sections were dehydrated through increasing concentrations of ethanol prior to immersion in xylene. Finally, the sections were cover slipped using DPX [Sigma (06522)]. All stages were performed at RT unless stated otherwise. For Chapter 4, block was for 30 minutes and primary antibody incubation was for 90 minutes.

2.5.2.2 Astroglial immunostaining

Sections were washed of OCT in a 1% PBS bath for 5 minutes. After this, the sections were incubated with blocking solution (Triton 0.2%, Bovine Serum Albumin 5%) at RT followed by an overnight incubation of the sections with the primary antibody solutions at 4°C: Rabbit GFAP antibody (Abcam ab7260) (1:500) and Goat Iba-1 Polyclonal IgG antibody (Abcam ab5076) (1:150). After washing, secondary antibodies were applied: Donkey anti-rabbit Alexa Flour 546 IgG H&L (Abcam ab10040) (1:300) and donkey anti-goat Alexa Flour 647 IgG H&L (Abcam ab150079) (1:300) for 1 hour at RT. The secondary antibodies were then washed off with three 10-minute washes. DAPI (1:1000) was applied during the penultimate wash at RT. The slides were then cover-slipped using Mowiol. Evgenia Rusina assisted in the immunohistochemistry. For Chapter 4 there was a change in protocol: 10% BSA solution was applied for 1 hours, we decreased the concentration of Goat Iba-1 Polyclonal IgG antibody (Abcam ab5076) and left it to incubate at RT for 90 minutes followed by TBS only washes and then incubation with donkey anti-goat Alexa Flour 647 IgG H&L (Abcam ab150079) (1:500) for 1 hour followed by three 5 minute TBS only washes.

2.5.2.3 Synaptic vesicle glycoprotein 2A staining

Evgenia Rusina performed this immunohistochemistry protocol under AJ's supervision. The OCT was washed away from the sections by agitating in a 1% PBS bath for 5 minutes. A blocking solution (Bovine Serum Albumin 5%, Triton 0,5%) was applied for 1 hour. Following this, the sections were incubated with Rabbit anti-SV2A (Abcam ab32942) (1:1000) for 1 hour. Subsequently, sections were washed with five 5-minute washes. After that, the secondary antibody Goat Anti-Rabbit Alexa Fluor 647 (Abcam ab150079) (1:2000). Then five more 5-minute washes were performed with the application of DAPI (1:1000) with the third washing. Finally, the sections were cover-slipped using Mowiol [Sigma (4-88)]. All stages were performed at RT.

2.5.2.4 4',6-diamidino-2-phenylindole (DAPI) staining

DAPI staining was applied to all sections except those stained with APP. Sections were incubated in 1:1000 4',6-diamidino-2-phenylindole (Sigma) diluted in PBS. For sections with no other immunostaining, the slides were left to defrost then washed in a PBS bath for 5 minutes. Following this, DAPI was applied to the section for 15 minutes followed by a 5-minute PBS bath. For sections undergoing other

immunostaining, the DAPI solution was applied as an alternative to the penultimate washing solution after the secondary antibody incubation.

2.5.3 Mowiol preparation

Mounting solution was prepared by dissolving 96g of glycerol (Sigma-Aldrich) and 38.4g Mowiol (Calbiochem) in 192ml 0.2M Tris buffer at 8.5pH and 95ml MilliQ water. The mixture was then heated up to 50^{o}c till clear. Following centrifuge at 8500rpm for 15 minutes, the supernatant was collected and 2.5% 1,4-Diazabicyclo[2.2.2]octane (Sigma-Aldrich) added. Mowiol was stored at -20^{o}c until used.

2.5.4 Coverslip mounting

For all sections (expect those stained for APP and H+E), 12µl of Mowiol was applied to each section and then covered using 1.5 thickness coverslips (VWR International). For APP and H+E staining, 20µl DPX (Sigma) was applied to each section and then covered using 1.5 thickness coverslips (VWR International). Efforts were made to remove air bubbles.

2.6 IMAGING TECHNIQUES

2.6.1 Wide field fluorescence microscopy

The Zeiss Axioscan.Z1 was used for wide field microscopy of mouse brain sections. It allowed for high throughput automated scanning of up to 100 slides. Both fluorescence (DAPI, GFAP, Iba-1, SV2A) and bright field (APP, H+E) microscopy was used for the experiments in this thesis. Images were acquired at 20X using a Zeiss Plan-Apochromat lens with a numerical aperture (NA) of 0.8. Excitation light was emitted using a Light Emitting Diode (LED) with a range of 400-700nm. This light was then filtered with a band pass (BP) filter and split using Farb Teiler (FT) before being projected onto the sample. Emission light was also split using FT and filtered with the BP filter before being detected by a high sensitivity camera (Hamamatsu Orca-flash 4.0 monocome camera). For image acquisition, Ring Aperture Contrast (RAC) at 2.5X objective lens was used to obtain an overview of the slide. Following this, an automated two-step focusing process took place: coarse focusing at 10X followed by fine focusing at 20X. Sequential images were then acquired and stitched automatically. Different settings were applied as described in **Table 2.5**.

Chapter	Stain	Excitation wavelength (nm)	Emission wavelength (nm)	LED strength (%)	Exposure time (ms)
Chapter 3	**DAPI**	395	445	100	2
	GFAP	578	603	100	350
	Iba-1	650	668	100	360
Chapter 4	**DAPI**	395	445	100	1.3
	Iba-1	650	668	100	375
	SV2A	650	668	25	72

***Table 2.5**: **Zeiss Axioscan.Z1 settings for wide field fluorescence microscopy** showing the different parameters for excitation and emission wavelength along with LED strength and exposure time.*

2.6.2 Spinning disc confocal microscopy

The data presented in this thesis was acquired using the Andor Revolution XDi system using a Dual Nipkow disk (CSU-W1) which combines two pinholes 25 and 50 µm. The Andor Revolution XDi system has 4 lasers: 405nm, 488nm, 561nm, 640nm. For experiments in this thesis, we used 488nm (eGFP) and 561nm (mKO2). Light from the lasers was directed onto the sample using a dichroic mirror and quad filter. A 2x post-magnification lens was placed in front of camera to increase sampling rate. The system also contained the Borealis Perfect Illumination Delivery which improves the uniformity of the field illumination. Images were acquired using the Olympus UplanSAPO 100x oil immersion lens (N.A 1.4) and detection was achieved using the Andor iXon Ultra monochrome back-illuminated EMCCD. Acquired images were images were 512 x 512 pixel and 16-bit depth. For whole brain acquisition, images underwent mosaic tilling across a grid defined by the user. Within this grid, focus points were placed by the user which allowed for adaptive focusing throughout the imaged sample. No z-stacking was taken in images in this thesis.

2.7 IMAGE ANALYSIS

2.7.1 Semi-quantitative analysis of Amyloid Precursor Protein

Slides were blinded and then examined using Olympus BX-51 microscope set at 20x. A semi-quantitative approach was taken to determine the number of APP-positive varicosities within the corpus callosum. An APP-positive varicosity was defined as a dark aggregate of staining lying within the corpus callosum as shown in **Figure 2.5**. A total number of varicosities were counted for both the ipsilateral and contralateral corpus callosum.

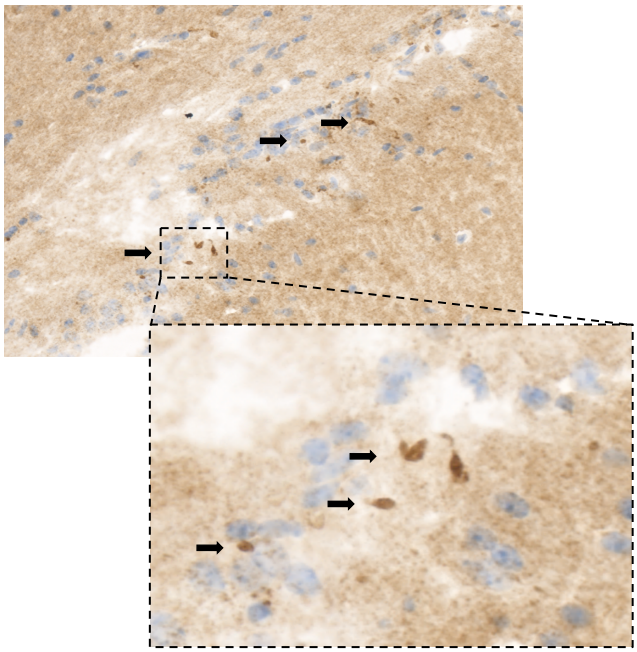

Figure 2.5: Amyloid precursor protein aggregates *in the corpus callosum as indicated with black arrows.*

2.7.2 Semi-automated quantification of cellular immunostains

Images acquired by the Zeiss Axioscan.Z1 were converted from Carl Zeiss Image (CZI) format into Tagged Image File Format (TIFF) using the ZEN software. Multichannel image were split into their respective channels during the conversion process. The TIFF images were then converted into 8-bit images and a threshold was applied with the parameters defined in **Table 2.6** and then converted into binary images **(Figure 2.6)**. ImageJ was then used to apply regions of interest across the mouse brain. Finally, a semi-automated particle analysis script was applied to count the number of immunostain positive cells with the defined parameters.

Chapter	Stain	Threshold	Particle size
Chapter 3	GFAP	0-9	0.008-0.2
	Iba-1	0-17	0.005-0.1
Chapter 4	Iba-1	0-17	0.005-0.2

Table 2.6: ImageJ parameters used for Iba-1 and GFAP particle analysis *demonstrating the thresholding and particle sizes*

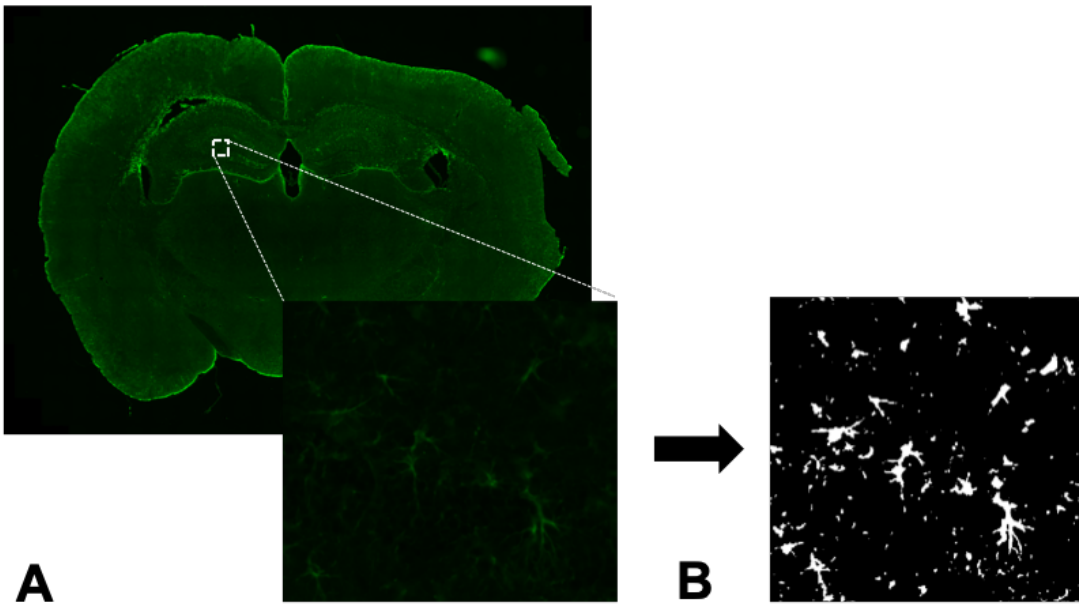

Figure 2.6: GFAP analysis using ImageJ *demonstrating conversion of TIFF image (A) into binary image (B) prior to particle analysis*

2.7.3 SV2A field intensity analysis

Evgenia Rusina performed the image analysis under my supervision. Carl Zeiss Image (CZI) formatted images were analyzed using ZEN software. Regions of interest (ROI) corresponding to major brain regions were applied and the raw fluorescence intensity value measured. To adjust for variation in immunostaining, the fluorescence intensity value of the corpus callosum was deducted and then divided by the intensity value of the whole brain to produce a final normalized SV2A intensity value.

2.7.4 Automated synaptic puncta analysis

2.7.4.1 Mouse brain regions of interest delineation

Images generated from the SDM were stitched to create a montage image to allow delineation. The code to do this was written by Dr. Zhen Qui **(Appendix 1)**. The code downsized each image by factor of 16 and stitched tiles side by side using the image metadata **(Figure 2.7)**. This whole brain montage image was then saved as a TIFF file. Montages were generated for both channels: 488 and 561. Subsequently, the polygon selection function in ImageJ was used to delineate regions based upon Allen Institute mouse brain atlas. These delineations, which were saved as a ZIP file, would be subsequently incorporated in binary function into the automated puncta analysis process and used to calculate median values for each metric per region which were then plotted. Evgenia Rusina and Jude Milvidaite assisted in generating the mouse brain delineations in Chapter 4.

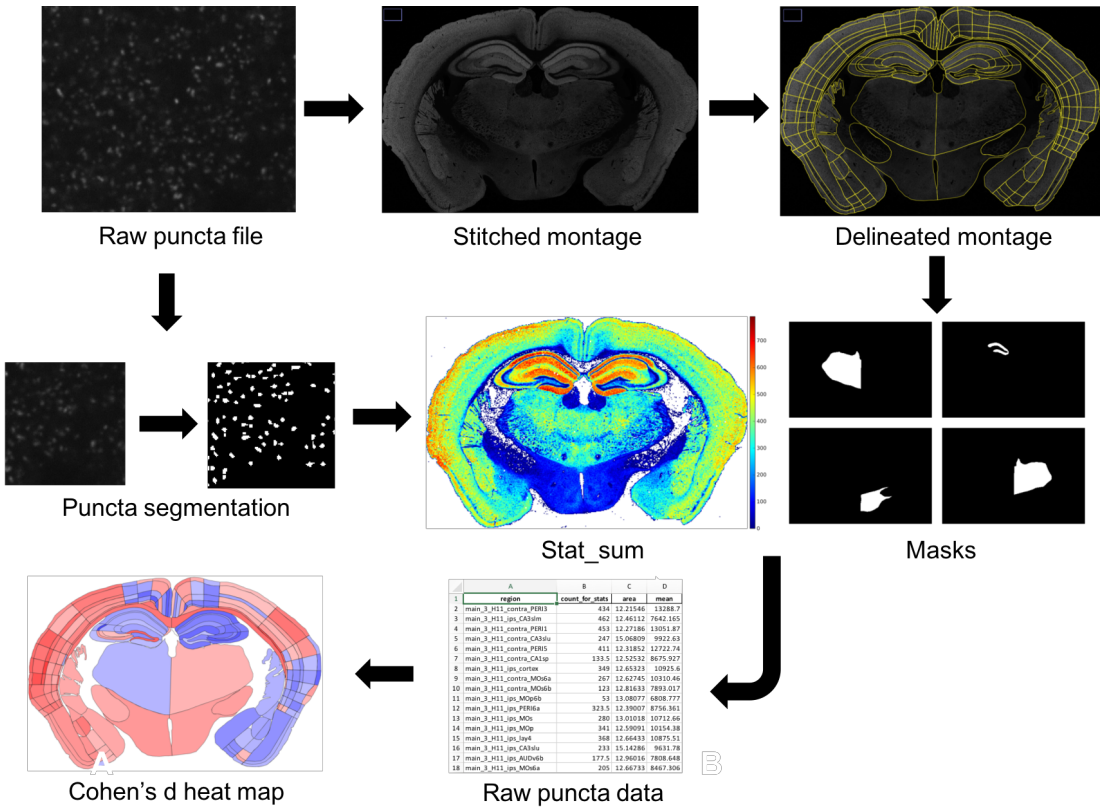

Figure 2.7: Pipeline for image analysis of PSD95 and SAP102 synaptome *demonstrating the conversion of raw puncta data into a stitched montage which subsequently was delineated using ImageJ. The raw data then underwent object segmentation and stat_sum image generation. Masks created from the delineated file were then applied to the stat_sum image and raw puncta data generated in an Excel*

file. This data was then processed (as described below) to generate spatial heat maps for PSD95 and SAP102 puncta density, size and intensity.

2.7.4.2 Puncta detection and segmentation using Ensemble

A novel detection method using supervised machine learning techniques was developed in-house by Dr. Zhen Qui using Matlab and Python. To generate a 'ground truth' of puncta detection, a series of randomly selected image subsets were analysed by independent researchers. Using the 'cell counter' plugin for ImageJ, synaptic puncta were manually counted for each protein (PSD95 and SAP102). This training set was then used to train the machine learning algorithm. The Ensemble method has a proven performance in generalization error prediction (Breiman 2001) making it a strong candidate for puncta classification from diverse intensities. Once a punctum was detected, it was then segmented by generating a ROI around the object. From this ROI, three parameters were then calculated: puncta intensity, density and area. The puncta density was calculated by averaging the number of puncta per tile. The puncta intensity was calculated by averaging the intensity of pixels within the punctum. While the puncta area was calculated as the number of pixels within the punctum which was then converted into μm^2 as detailed below.

2.7.4.3 Generation of LFPI synaptome maps

Below we describe the image analysis pipeline used to generate the synaptome maps for the LFPI experiment:

2.7.4.3.1 Stage 1: Object segmentation

In stage 1, we used the Ensemble detection and segmentation method as described above. To do this, each tile (which was constituted of 512 x 512 pixels) was divided into 4 images. The puncta within these images were detected and the segmentation parameters described above calculated. This data was saved as a text file with the coordinates of the puncta and associated measurements.

2.7.4.3.2 Stage 2: Generation of 'Stat_Sum' image

The data within the text files was then converted into a 3D array containing three coordinates: x, y and z. The x and y values represented coordinates of the pixels. The z value represented a subset in which each value corresponded to a particular puncta parameter. So, different puncta parameters, such as puncta size, is represented at

different z levels. The mean value for each puncta parameter per sub-tile was calculated by dividing the sum of the pixel z value and then divided by the number of puncta per sub-tile.

2.7.4.3.3 Stage 3: Binary mask generation and regional quantification

The ROI delineation ZIP files were then converted into binary masks. For each brain, there were 222 sub-regions delineated which translated into an equivalent number of masks which were applied to the 'Stat_Sum' image. For each puncta metric, the median value was calculated for each mask which was then complied into a Microsoft Excel sheet for further processing as described below.

2.7.4.3.4 Stage 4: LFPI Cohen's *d* heatmap generation

To graphically represent the sub-regional differences between the injury and sham mice, we calculated the Cohen's *d* effect size (described in statistical analysis section) comparing the two cohorts. These values were then mapped onto a 2D coronal image of a mouse brain by converting the Cohen's *d* value into a colour spectrum value (described below) before using the 'flood fill' tool in ImageJ to colour the sub-regions.

2.8 STATISTICAL ANALYSIS

2.8.1 Raw puncta metric calculations

The Ensemble method generated raw puncta metrics that required adjustment to reflect their biological basis. No adjustment was made for the puncta intensity which was kept as a raw grey scale value. Pixel dimensions were 84nm x 84nm giving it a surface area of 0.007056μm^2. To calculate the puncta area in μm^2 we multiplied this value by the raw number of pixel per puncta provided by Ensemble. For density, Ensemble provided the mean number of puncta per a quarter tile. Each full tile was composed of 512x512 pixels therefore giving it a surface area of 1849μm^2. Therefore, to calculate the puncta density /μm^2 we used the following equation with x representing the raw Ensemble puncta density:

$$d = \left(\frac{x}{1849}\right) \times 400$$

2.8.2 Two-group comparisons

Two-group comparisons were undertaken using Graphpad Prism 7. Normality was tested for using the Shapiro-Wilk Normality test. For unpaired non-parametric data the Mann Whitney U test was used while for parametric data the Student's unpaired t-test was utilized. The Chi-square test was used for categorical data.

2.8.3 Correlation

To look for linear relationships between two variables, a Pearson coefficient was calculated using Graphpad Prism 7. The Pearson coefficient varies from -1 to 1 which related to perfect negative and positive relationships. The significance of the linear relationship was calculated using a two-tailed test.

2.8.4 Multiple group comparison

For analysis of multiple groups, we used Analysis of Variance (ANOVA) with post-hoc multiple comparison with Bonferroni correction. However, for the sub-region analysis of the synaptic puncta, we opted to undertake post-hoc multiple t-tests to compare the injury and sham cohorts. Due to the number of comparisons (>200) the use of statistical correction would be too conservative and lead to false negatives. However, not using any correction does increase the likelihood of false positives. To address this, we took a two-tiered approach to interpret the significant findings from the multiple t-tests. Firstly, we only discussed significant results that clustered anatomically together as this was more likely to represent a true biological effect. We defined clustering as three or more sub-regions within two or more adjacent brain regions. For isolated sub-regions, we then applied a higher significance threshold to it ensure that false positives were not discussed. A form of correction is to divide the usual p-value threshold ($p>0.05$) by the number of comparisons. In our study, this would be 0.05 divided by 222 giving isolated sub-regions a p-value threshold of 0.0002.

2.8.5 Cohen's *d* effect size

Cohen's *d* measures the difference in effect size between two groups. It is calculated as the difference between two means divided by their pooled standard deviation. In the case of this thesis, a comparison between the injury cohort mean (x_1) would have the sham cohort mean (x_2) deducted from it and then divided by the pooled standard deviation (s):

$$d = \frac{x_1 - x_2}{s}$$

The pooled standard deviation (s) is calculated with the below equation where n_1 and n_2 are the numbers for the respective groups. While s_1 and s_2 are the standard deviations for the corresponding groups:

$$s = \sqrt{\frac{(n_1 - 1)s_1^2 + (n_2 - 1)s_2^2}{(n_1 + n_2 - 2)}}$$

If the mean value of the injury cohort for a sub-region was less than that of the sham cohort the Cohen's *d* effect size would be negative. While if the injury cohort had a larger mean then the Cohen's *d* effect size would be positive.

2.8.6 Colour scheme calculation for heat-map

To graphically represent the Cohen's *d* effect sizes, each sub-regional value was converted into a triad of values for conversion into an RGB scale (values of 0-255 for each of the three colours: red, green and blue). For negative Cohen's *d* effect sizes the colour blue was picked and for positive values the colour red. To calculate the RGB values, the following equation was used with x representing the Cohen's *d* effect size:

$$Positive\ Cohen's\ d = \left(0.75 - \frac{x}{2}\right) \times 255$$

$$Negative\ Cohen's\ d = \left(0.75 + \frac{x}{2}\right) \times 255$$

For negative Cohen's *d* effect size the blue value was set at 255 and the results of the above calculation applied to red and green. While for positive results, the red scale was set at 255 and then results of the equation applied to blue and green. These RGB values were then translated into the ImageJ 'colour picker' function following which the 'flood fill' tool was used to apply the appropriate colour to the sub-region.

CHAPTER 3

Characterization of mild fluid percussion injury model in wildtype mice

3.1 INTRODUCTION

The fluid percussion Injury model is an open skull model that causes a mixed – focal and diffuse – injury. The model was first established in cats and was subsequently modified to be used in mice by Carbonell (Carbonell et al. 1998). A major benefit of using the model in mice is the ability to utilize genetically modified animals to answer focused mechanistic questions. However, the surgical preparation of the model with mice comes with several technical challenges. A flexible cranium and fragile dura pose difficulties in maintaining an intact dura and minimizing brain injury in sham mice (which undergo the full surgical procedure except for application of the fluid pulse). This coupled to known factors, such as craniectomy location, can lead to variation in injury morphology which highlights the importance of robust characterization of the model by a new user (Vink et al. 2001). A major benefit of the LFPI is its ability to vary the intensity of the fluid percussion pulse to reflect differing severities of human TBI. Mild TBI accounts for over 80% of head injuries and can lead to post-concussional symptoms that affect patients' quality of life (Bruns & Hauser 2003; Levin & Diaz-Arrastia 2015). Several studies have aimed to characterize a mild LFPI in murine models. Hylin and colleagues applied LFPIs of 1.0 and 1.5 atm to rats and found limited cognitive changes in 1.0 atm cohort but evidence of significant impairment in the 1.5 atm cohort associated with a robust neuroinflammatory response and evidence of water matter changes shown with Diffusion Tensor Imaging (Hylin et al. 2013). A study by Spain looking at mild LFPI (0.9±0.1 atm) in mice found moderate neuronal damage in the cortex in both the injury and sham mice but minimal neuronal injury within the hippocampus (Spain et al. 2010). The same study found evidence of progressive diffuse axonal pathology in the injury group in sites distal to the percussion site. The aim of this chapter is to establish an experimental protocol for a mild LFPI in wildtype C57BL/6 mice. We define this as an injury leading to an elongated right reflex with evidence of axonal injury and inflammatory response but in the absence of gross disruption of brain architecture such as contusions.

3.2 SUMMARY OF METHODS AND EXPERIMENTAL PIPELINE

To characterize the LFPI model, 40 male C57BL/6 mice aged between 8-12 weeks were included in the study. They were randomly allocated to either injury or sham LFPI groups as detailed in Chapter 2. Briefly, the mice were anaesthetized with isoflourane and were attached to a stereotactic frame. A circular craniectomy was fashioned and a hub secured using glue and dental cement. The mice were then

attached to the fluid percussion device and either underwent a mild fluid pulse (1.1-1.2) or sham (no release of pendulum) procedure **(Figure 3.1, A)**. Following this, the righting time was measured and then the mice were kept in a warm (30°C) chamber till they recovered. After the LFPI procedure, the mice were allowed to survive to 24 hours and then underwent transcardial perfusion and the brains were harvested. After post-fixation in a 30% sucrose solution, the brains were embedded in OCT and then cryosectioned into 18μm coronal sections **(Figure 3.1, B)**. Sections corresponding to approximately -1.94mm from bregma were selected and underwent H+E staining alongside immunostaining for APP, Iba-1 and GFAP as detailed in Chapter 2. For the analysis, brains were blinded. The Iba-1 and GFAP immunofluorescence staining was performed on a single section and then imaged using a wide field fluorescence microscope **(Figure 3.1, D)**. The multichannel images were split and ImageJ was used to count positive cells within delineated anatomical regions of interest. For H+E and APP staining, a semi-quantitative approach was taken using a light microscope in which damaged neurons were qualitatively examined and APP positive aggregates within the corpus callosum were counted **(Figure 3.1, C and E)**.

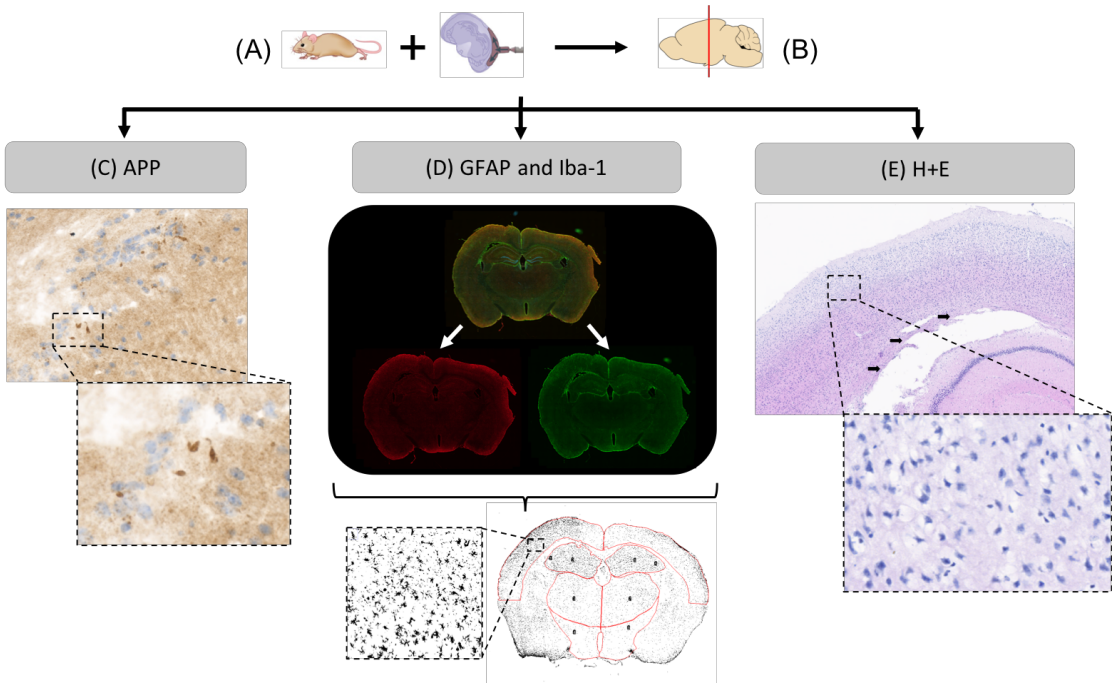

***Figure 3.1**: **Schematic of mild LFPI characterization experiment methodology.** Forty mice were randomised to injury or sham LFPI procedures (A). The injury cohort underwent a 1.1-1.2 atm fluid percussion injury. After 24 hours, the mice underwent transcardial perfusion and the brains were harvested following which they were*

cryosectioned into 18μm sections (B). Brains sections were stained with APP and the number of aggregates in the ipsilateral corpus callosum were quantified (C). GFAP and Iba1 immunofluorescence was performed and widefield microscopy used to image the sections (D). The GFAP and Iba1 channels were then split and ImageJ used to quantify positive cells within 8 major brain regions. H+E staining was performed and qualitative analysis of corpus callosum fracturing (black arrows) and neuronal injury was performed (E)

3.3 EXPERIMENTAL RESULTS

A total of twenty-six mice (15 injury and 11 sham) were included in the final analysis **(Figure 3.2)**. Fourteen mice were excluded for the following reasons: 11 dural ruptures (dural breach at time of fluid percussion), 2 dural tears (dural breach when performing craniectomy) and 1 post-injury paralysis. This gave the experiment an attrition rate of 35%. The below flow diagram highlights the animal exclusion:

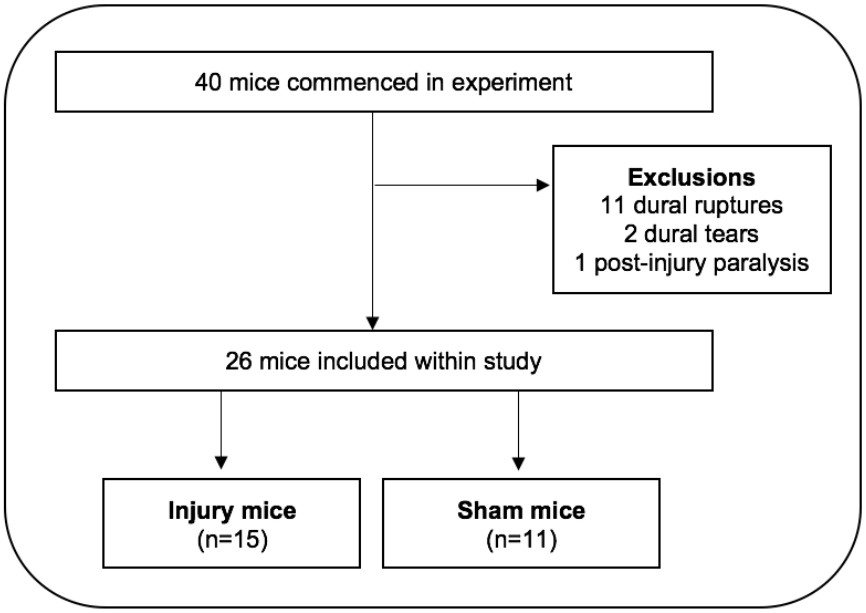

***Figure 3.2**: **Flow diagram demonstrating mouse exclusion.** A total of 14 mice were exclude: 11 dural ruptures (tears due to application of fluid pulse to dura), 2 dural tears (dural injury as craniectomy is elevated) and 1 post-injury paralysis (lasting greater than 30 minutes)*

There was no significant difference between the injury (25.4g ± 0.7) and sham (25.1g ± 0.4) mice weights (p=0.77; student t-test). The injury mice were exposed to a percussion amplitude of 1.18±0.03atm.

3.3.1 Injury cohort exhibited increased righting times

Following application of the fluid percussion pulse or sham procedure, the mice were detached from the LFPI device and placed on their back to check their right time (RT) – a simple behavioural assay to assess acute brain function disruption **(Figure 3.3, A)**. In our experiment, injury mice had a statistically significant higher RT (431.4 ± 178.2 seconds) compared to sham mice (40.3 ± 57.5 seconds) (p<0.0001; Mann Whitney U test) **(Figure 3.3, B)**.

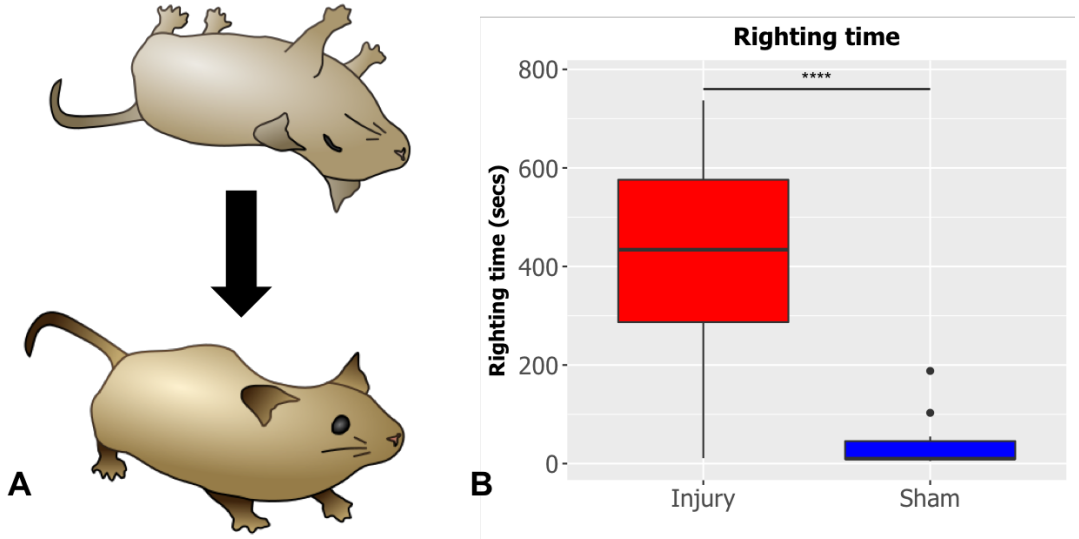

Figure 3.3**: **Mouse righting time following LFPI experiment**. A mouse was considered righted once it had placed all four paws on the floor (A). In the experiment, we found significantly elevated RT for injury mice (n=15) compared to sham mice (n=11) (B). The mouse images were taken from Wikimedia Commons. [* = p<0.0001].*

3.3.2 Dysmorphic neurons and fractured corpus callosum found in injury cohort

Haematoxlyin and Eosin (H+E) staining was used to examine for evidence of tissue damage and cellular injury **(Figure 3.4)**. For H+E, we analysed 7 mice in the injury cohort and 6 mice in the sham cohort. This revealed no significant cortical disruption or contusion across both the injury and sham groups. However, more mice in injury group (85%) had evidence of ipsilateral corpus callosal fracturing compared to the

sham mice (16.7%) (p=0.01; Chi-squared test). Closer inspection of neuronal morphology showed that the injury group mice had evidence of neuronal cell injury in all the mice in cortical layers 1 and 2/3. Just under half (42.8%) of injury mice had evidence of neuronal injury extending down to cortical layer 6a. Conversely, only half of the sham mice had injured neurons in cortical layer 1 and a third had injured neurons extending into cortical layer 2/3. There was no evidence of visible neuronal cell death in the hippocampus across both cohorts.

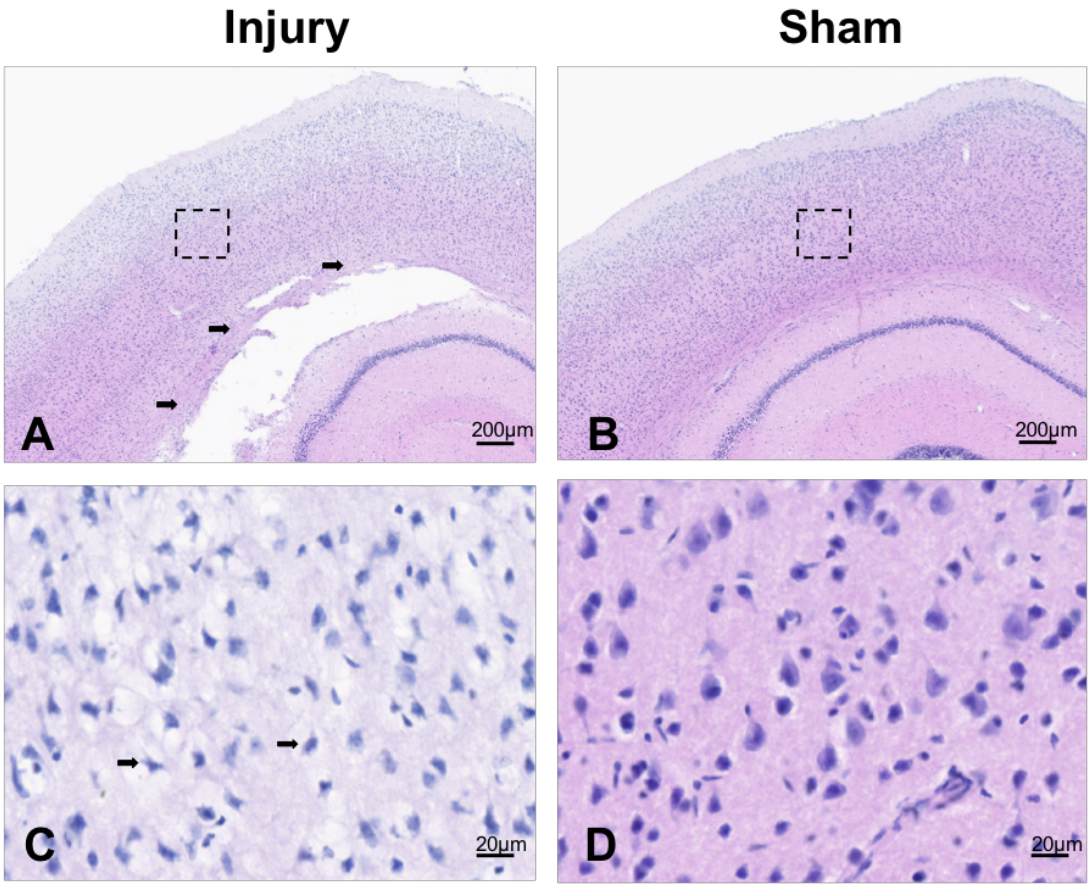

Figure 3.4: Hamatoxylin and Eosin analysis of LFPI experiment. *Injury cohort (n=7) demonstrated corpus callosal fracturing (A – black arrows) which is not evident in sham (n=6) example (B). Magnification of selected region highlights dysmorphic injured neurons in injury mice (C – black arrows). Scale bars in A and B (200 µm) in C and C (20 µm)*

3.3.3 Injury cohort demonstrated evidence of traumatic axonal pathology

To measure the degree of traumatic axonal pathology, we examined the brain tissue with Amyloid Precursor Protein (APP). Injured axons appeared as dark aggregates

(Figure 3.5, A) which were semi-quantitatively counted. Using two-way ANOVA, we observed statistically significant differences between the injury and sham cohorts ($F(1,42)=36.94$; $p<0.0001$) and between the ipsilateral and contralateral corpus callosum ($F(1,42)=34.89$; $p<0.0001$). In post-hoc Bonferroni multiple comparison, the ipsilateral corpus callosum in the injury cohort had significantly higher numbers of APP positive aggregates (74.1 ± 38.6) compared to both the contralateral corpus callosum in the injury mice (1.8 ± 2.1) ($p<0.0001$) and the ipsilateral corpus callosum in the sham mice (0.8 ± 1.0) ($p<0.0001$) **(Figure 3.5, B)**. There was no significant difference between the number of APP positive puncta in the corpus callosum in the sham mice ($p>0.9999$).

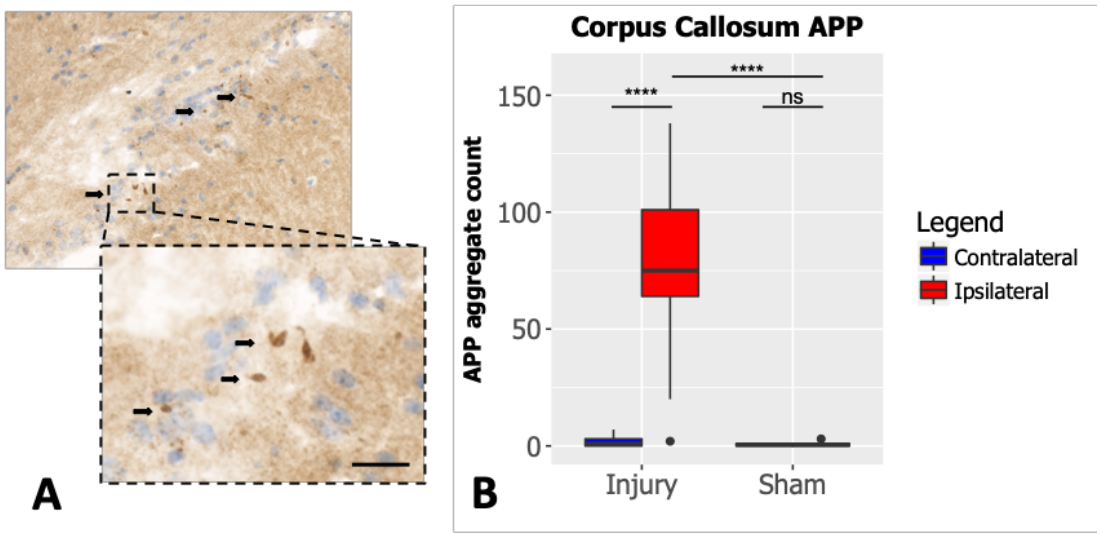

Figure 3.5**: **Amyloid precursor protein analysis in LFPI experiment.** Image A demonstrates APP positive aggregates in ipsilateral corpus callosum in injury mice (black arrows) and bar chart highlights differences in aggregate numbers between injury and sham mice (B). Scale bar = 20 μm. [* = p<0.0001]*

3.3.4 Inflammatory changes following mild LFPI

3.3.4.1 Microglia indexed with Iba-1

We aimed to examine the inflammatory response following LFPI by staining for microglia using the antibody Iba-1 **(Figure 3.6, A)**. Using two-way ANOVA, we found statistically significant differences between the ipsilateral and contralateral cortical Iba-1 numbers ($F(1,48)=23.5$; $p<0.0001$) but not between the injury and sham mice ($F(1,48)=2.95$; $p=0.092$). Post-hoc Bonferroni correction multiple comparisons revealed elevated Iba-1 numbers in the ipsilateral cortex in the injury mice (2767 ±

1352) compared to the contralateral cortex (1230 ± 642.1) which reached statistical significance (p=0.0002) **(Figure 3.6, B)**. There was no statistically significant difference in the number of Iba-1 cells in the ipsilateral cortex between the injury (2767 ± 1352) and sham mice (2030 ± 791.3) (p=0.287). In the hippocampus, we observed statistically significant difference between the injury and sham cohorts (F(1,48)=16.29; p=0.0002) but not between the ipsilateral and contralateral hemispheres (F(1,48)=3.97; p=0.0521). Post-hoc Bonferroni test revealed significantly elevated numbers of Iba-1 cells within the injury ipsilateral hippocampus (1168 ± 575.3) compared to the ipsilateral hippocampus in the sham mice (458.0 ± 275; p=0.0006) **(Figure 3.6, C)**. There was no difference in the number of Iba-1 positive cells across the groups in the thalamus and hypothalamus.

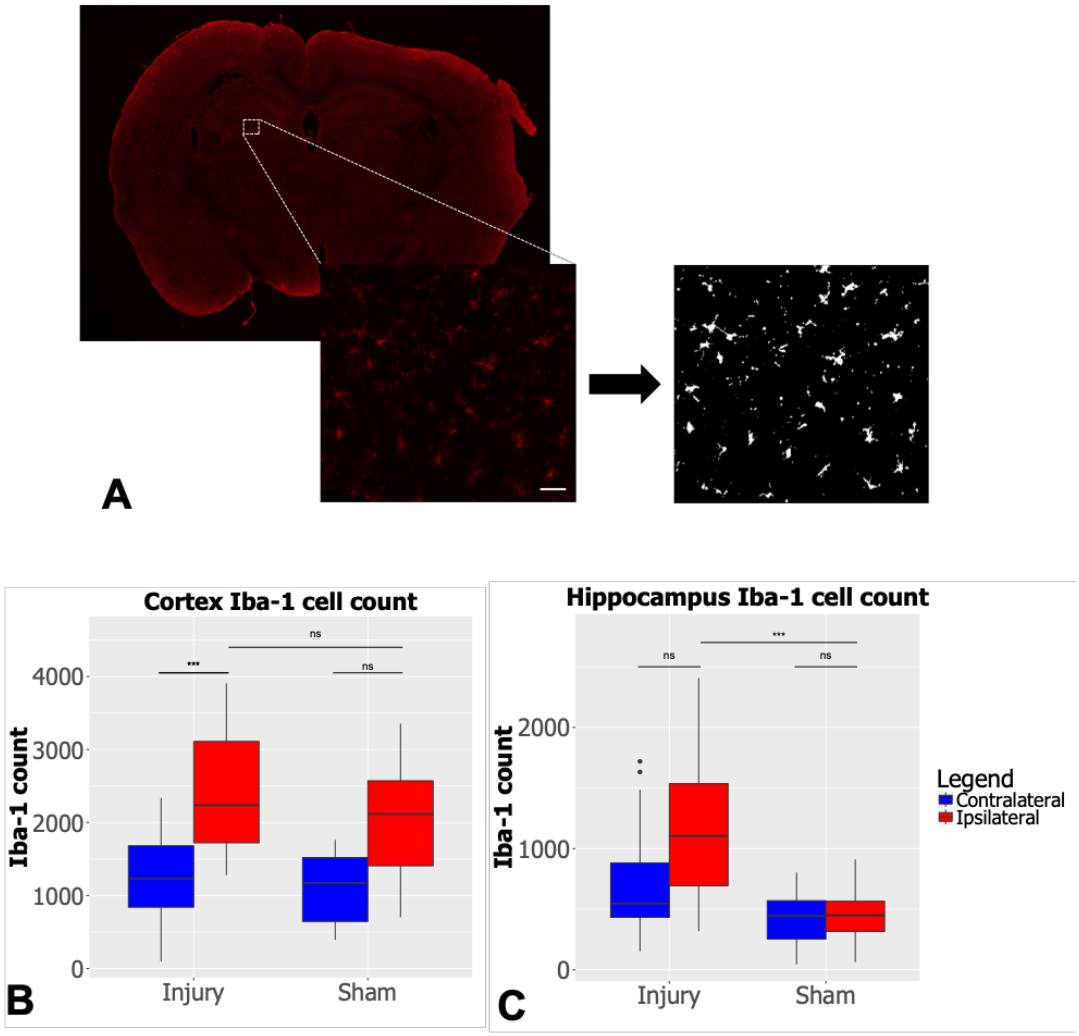

***Figure 3.6**: **Iba-1 immunostaining and quantification in LFPI experiment**. Iba1 immunofluorescence was imaged using wide-field microscopy and ImageJ utilised for*

*particle analysis (A). Quantification demonstrated elevated Iba1 positive cells in the ipsilateral cortex in both injury and sham mice (B). However, significantly elevated Iba1 positive cells in the ipsilateral hippocampus in the injury cohort (C). Scale bar = 100μm. [**** p≤0.0001; *** p≤0.001; ** p≤0.01; * p≤0.05; ns p>0.05]*

3.3.4.2 Astrocytes indexed with GFAP

Similar to Iba1, we aimed to examine astrocytic changes following LFPI. To do this, we used immunofluorescence staining for GFAP **(Figure 3.7, A)**. Analysis using two-way ANOVA revealed statistically significant differences between GFAP numbers within the cortex in the injury and sham mice ($F(1,48)=8.07$; $p=0.006$) and the ipsilateral and contralateral hemispheres ($F(1,48)=65.39$; $p<0.0001$). Post-hoc Bonferroni revealed an elevated number of GFAP positive cells in the ipsilateral cortex in the injury mice (1390 ± 424.5) compared to the contralateral cortex in the injury mice (505.6 ± 212.8; $p<0.0001$) and the ipsilateral cortex in the sham mice (963.4 ± 326.6, $p=0.07$) **(Figure 3.7, B)**. In the hippocampus, there was significant difference between the injury and sham cohorts ($F(1,48)=9.08$; $p=0.004$) but not between the ipsilateral and contralateral hippocampi ($F(1,48)=0.397$; $p=0.5$). Multiple comparisons with post-hoc Bonferroni test revealed significantly higher numbers of GFAP positive cells in the ipsilateral hippocampus in the injury mice (1195 ± 484.2) compared to the ipsilateral hippocampus in the sham mice (638.8 ± 415.2) ($p=0.025$) **(Figure 3.7, C)**. There was no difference in the numbers of GFAP positive cells across the cohorts in the thalamus and hypothalamus.

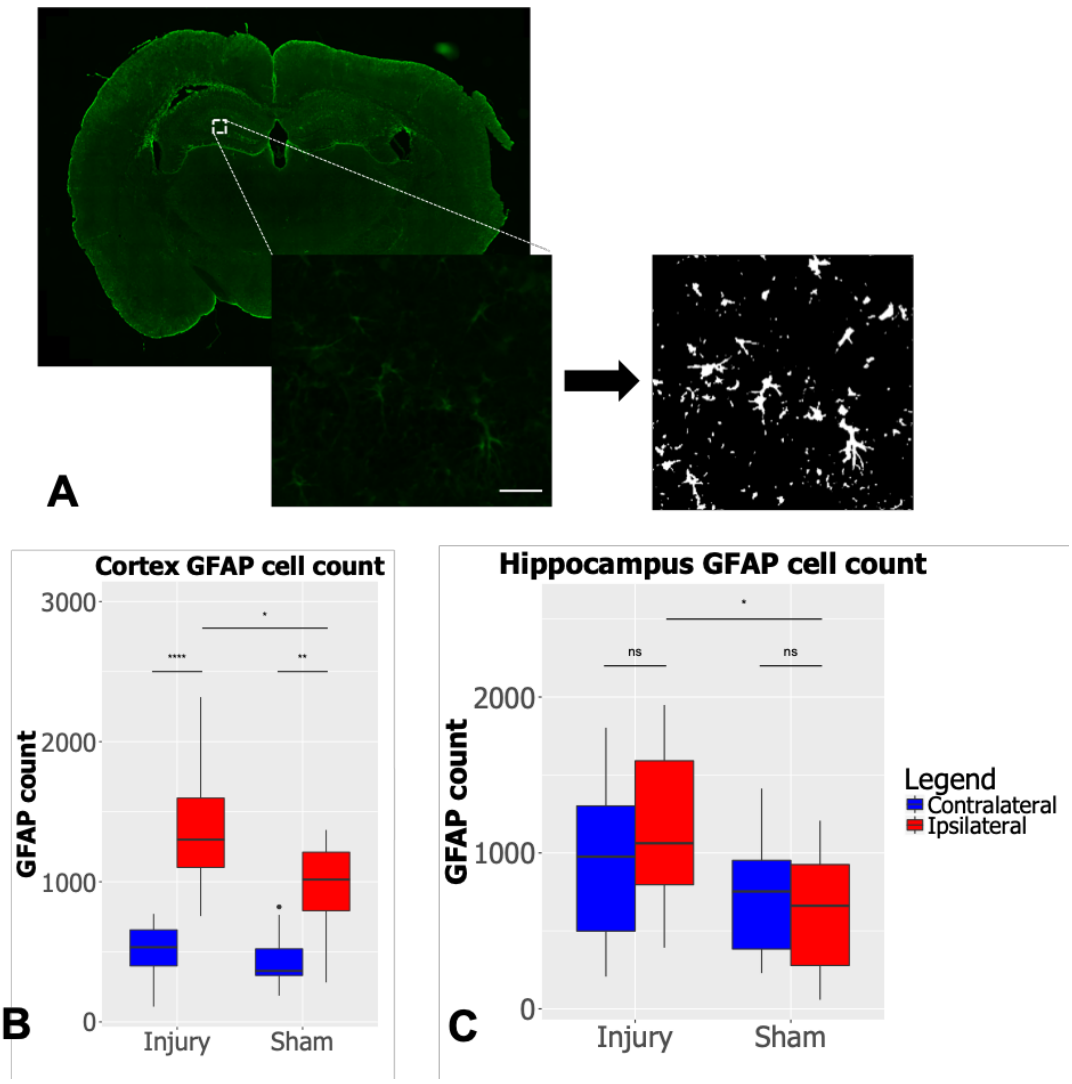

Figure 3.7**: **GFAP immunostaining and quantification in LFPI experiment.** GFAP immunofluorescence was imaged using wide-field microscopy and ImageJ utilised for particle analysis (A). Quantification demonstrated significantly elevated GFAP positive cells in the ipsilateral cortex in injury compared to sham mice (B). Similarly, we observed significantly elevated GFAP positive cells in the ipsilateral hippocampus in the injury cohort (C). Scale bar = 100μm. [* $p \leq 0.0001$; *** $p \leq 0.001$; ** $p \leq 0.01$; * $p \leq 0.05$; ns $p > 0.05$]*

3.4 CHAPTER DISCUSSION AND CONCLUSION

Mild TBI account for over 80% of all head injuries and lead to a myriad of post-concussional symptoms which can significantly affect patients (Bruns & Hauser 2003; Levin & Diaz-Arrastia 2015). In this chapter, we describe the characterization of a mild LFPI model which demonstrated axonal and inflammatory pathology with minimal neuronal cell death. One of the defining parameters of mild TBI is a period of loss of

consciousness or disorientation. In our study, we used the righting time which is a simple behavioural assay to assess for evidence of brain function disruption. We found that injury mice had significantly extended righting times compared to sham mice. The presence of structural injury (such as contusion or extra-axial collections) is not common in mild TBI. A study found that only 14% of patients with GCS 14 and above had positive findings on CT (Smits et al. 2007). This was evident in our model which failed to have any mice exhibiting significant contusion or cortical disruption. Furthermore, H+E examination revealed neuronal injury but no significant neuronal cell death. This has been found in other studies characterising mild LFPI (Spain et al. 2010; Hylin et al. 2013). Axonal injury is believed to be a major pathological finding in mild TBI. This has been demonstrated histopathologically in a limited number of mild TBI cases (Bumbergs et al. 1995). However, more recently, diffusion MRI has been utilised to study white matter tract changes after mild TBI as a proxy of axonal integrity. A meta-analysis of studies on the subject concluded that there is evidence of white matter tract abnormalities within the corpus callosum of mild TBI patients (Aoki et al. 2012). Animal models have been particularly important in investigating axonal pathology after a mild injury. This has been demonstrated in a number of differing models across different animals including mice, rats and pigs (Spain et al. 2010; Hylin et al. 2013; Browne et al. 2011). Immunohistochemical examination for APP accumulation is currently the gold standard for studying axonal pathology in both human and preclinical TBI (Hill et al. 2016). APP is transported through axons and mechanical disruption leads impaired transport and subsequent accumulation of the protein (Tang-Schomer et al. 2012). In our study, we found evidence of pronounced APP expression in the ipsilateral corpus callosum in the injury group at 24 hours. Alongside the APP findings, we also observed astroglial activation using Iba1 and GFAP to index microglia and astrocytes respectively. Within the cortex, the sham mice had evidence of significant astroglial activation in the ipsilateral compared to the contralateral cortex. This finding was important in highlighting the sham procedure was sufficient to induce an inflammatory response. However, this finding was not evident within the hippocampus and significant differences were noted between the injury and sham cohorts. This reflects findings from human mild TBI studies which has found inflammatory changes using molecular imaging techniques (Coughlin et al. 2017). Several preclinical studies have demonstrated astroglial activation following a single mild TBI (Shultz et al. 2011; Shultz et al. 2012; Lafrenaye et al. 2015). In this chapter, we have described the characterization of a mild TBI model utilizing the LFPI

device. The model demonstrated axonal and astroglial pathology without overt neuronal cell death. These characteristics mirror those seen in human mild TBI and are consistent with preclinical findings in the literature. We therefore believe this model is suitable for examining the impact of mild traumatic injury on synaptic pathology.

CHAPTER 4

Mapping changes in the Synaptome map following a mild lateral fluid percussion injury using a knock-in transgenic mouse model

4.1 INTRODUCTION

Traumatic Brain Injury (TBI) is a critical public health problem, of which, mild TBI is the most common injury. A large prospective cohort study found that almost half (44%) of patients with a mild TBI had an incomplete functional recovery at 6 months (van der Naalt et al. 2017). As described in Chapter 1, a combination of preclinical and human imaging studies has provided insights into the neuronal, axonal and inflammatory impact of mild TBI. However, there is limited understanding of the effect of mild TBI on the synapse. The synapse plays an important role in a range of cognitive processes and has been implicated in a number of neurological disorders including schizophrenia and Alzheimer's disease (Nithianantharajah et al. 2013; Fromer et al. 2014; S. Hong et al. 2016). In TBI, the synapse is an area of confluence for a range of secondary injury processes including inflammation, glutamate neurotoxicity and oxidative stress. A number of studies have attempted to examine the impact of TBI on the synapse using immunohistochemistry, western blot and electron microscopy (Scheff et al. 2005; Gao et al. 2011; Wakade et al. 2010). Collectively, these data point towards an early loss of synapses (or synaptic proteins) followed by a period of reorganization. However, the approaches used in the experiments either provided limited spatial information, focused on single sub-regions or utilized antibodies against synaptic proteins which suffer from issues around non-specificity. To overcome these methodological limitations, we aimed to utilize a strain of transgenic mouse with eGFP and mKO2 knocked into PSD95 and SAP102 respectively. With the use of an in-house developed machine learning algorithm, we aimed to create whole brain synaptome maps to examine the temporal-spatial profile of PSD95 and SAP102 after a mild TBI. Using the LFPI, an established model of TBI, we first characterized the neuronal, axonal and inflammatory impact of a mild injury (1-1.5atm) in wildtype mice as described in Chapter 3. This demonstrated evidence of significant axonal and inflammatory pathology in the injury group without pronounced disruption of the brain architecture. In this chapter, we describe using this LFPI procedure to examine the impact of a single mild LFPI injury in the eGFP-PSD95 mKO2-SAP102 mice across two time-points: 7 and 28 days. We opted for these time-points for a number of reasons. Firstly, there is evidence of delayed degeneration of synapses at 7 days followed by synaptic recovery that peaks at 28 days (Wakade et al. 2010; Scheff et al. 2005). We conducted a pilot study that followed mice up to 24 hours and 7 days after injury which demonstrated more pronounced synapse loss in the injury cohort compared to sham at 7 days compared to 24 hours **(Appendix 2)**.

Based on this data, we opted to make 7 days our first time-point. Coupled to this, there is growing literature on the neurodegenerative and chronic inflammatory sequalae of TBI and we were interested to look at the longer-term impact of TBI on the synapse (Wilson et al. 2017). We therefore opted to follow the mice up to 28 days for this reason and to provide temporal data on synapse change.

In this chapter, we first describe the early behavioural impact of the injury using the righting time. Secondly, we compare the areas of the major brain regions between the injury and sham mice to assess for differences in architecture that may bias observations seen in the synaptome map. Thirdly, using previously described markers, we examined the axonal and inflammatory effects between the injury and sham groups as a means to validate the observations seen at the synaptic level. Fourthly, due to the asymmetrical nature of the LFPI, we then compared the synaptic metrics (density, area and intensity) for 6 major brain regions of the left and right hemispheres in a group of naïve eGFP-PSD95 mKO2-SAP102 mice. Following this, we examined the two synaptic proteins, starting with PSD95. For each protein, we first calculated the synaptic metrics of the whole ipsilateral cortex. From here, we then examined the synaptic density of the sub-regions of the cortex. Having focused on the cortex, we then calculated the Cohen's *d* effect size differences for 222 sub-regions between the injury and sham map and plotted them on a spatial map. A similar approach was used to examine temporal changes after an injury group between 7 and 28 days. From there, we then examined the relationship between PSD95 and SAP102 and how it changed following LFPI. Finally, we assessed the association between PSD95 and SAP102 and the presynaptic protein, SV2A, and the microglial marker Iba-1.

4.2 SUMMARY OF METHODS AND EXPERIMENTAL PIPELINE

In order to examine the impact of LFPI on the synaptome, male PSD95-eGFP and SAP102-mKO2 knock-in mice aged between 8-16 weeks were randomised to four groups: injury or sham at 7 and 28 days **(Figure 4.1, A)**. Briefly, the mice were anaesthetised with 5% isoflurane and underwent a right circular craniectomy to which a hub was attached. The mice were then attached to the LFPI device and either had a mild LFPI pulse (1-1.5 atm) applied or a sham (no pulse). Mice were then recovered and followed up to 7 or 28 days. A fifth group of non-randomised naïve mice were included within the study as a control. Mice were sacrificed by transcardial perfusion

and their brains were collected. Brains were subsequently cryosectioned and coronal 18μm sections approximately corresponding to approximately -1.94mm from bregma according to Franklin and Paxinos were selected **(Figure 4.1, B)**. The Andor Revolution XDi system was used to image the sections for which each tile corresponded to 512x512 pixels (84nm/pixel). Direct fluorescence from PSD95-eGFP was imaged using the 488nm laser line (30% laser intensity; 48ms exposure time; 250 EMCCD gain) and SAP102-mKO2 was imaged using the 561nm laser line (50% laser intensity; 100ms exposure time; 250 EMCCD gain) **(Figure 4.1, C)**. A rectangular montage was created and 222 brain sub-regions based on the Allen Mouse Brain Atlas were delineated using ImageJ **(Figure 4.1, D and E)**. A key for the sub-region nomenclature can be found in **Figure 4.2**. The Ensemble method was then utilised to detect individual puncta and generate three metrics for each of the two proteins: puncta density (number of puncta per unit area), puncta area (size of the puncta) and puncta intensity (mean grey value of the puncta) **(Figure 4.1, F)**. Median puncta metrics were then calculated for the individual brain sub-regions and represented visually in spatial heatmaps **(Figure 4.1, G)**.

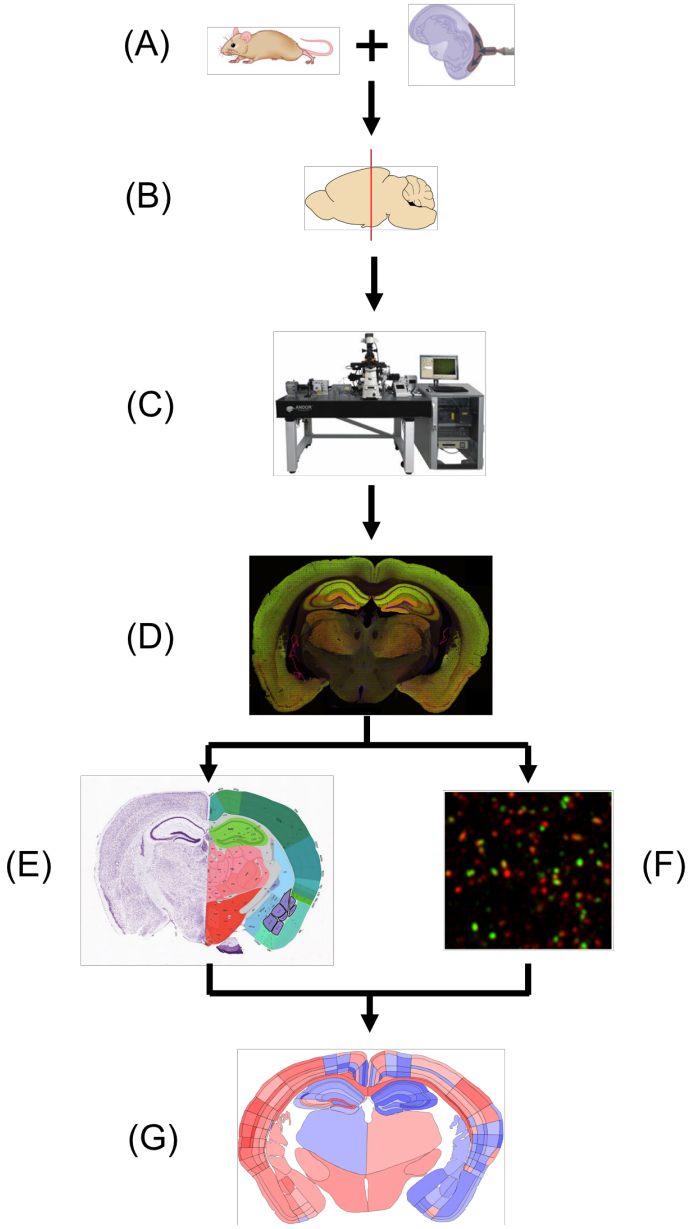

***Figure 4.1**: **Schematic of mild LFPI PSD95-eGFP SAP102-mKO2 mice experiment methodology**: a mild LFPI or sham was applied to double knock-in PSD95-eGFP mKO2-SAP102 mice (A) after follow-up to 7 or 28 days the mice were culled and their brain cryosectioned to 18μm sections (B) following which they were imaged with the Andor Revolution XDi system (C). Single coronal stitched image created per mouse (D) and ImageJ used to delineate 222 sub-regions of interest based on Allen Institute Mouse Brain Atlas (E) following which Ensemble method (F) used to detect puncta and quantify puncta density, area and intensity which were plotted onto regional heat maps (G)*

Abv	Name	Abv	Name
RSPv	Retrosplenial area, ventral part	CP	Caudoputamen
RSPd	Retrosplenial area, dorsal part	Cpd	Cerebral peduncle
MOs	Secondary motor cortex	Hyp	Hypothalamus
MOp	Primary motor cortex	Th	Thalamus
SSp-tr	Primary somatosensory area, trunk	CA1so	Cornu ammonis 1, stratum oriens
SSp-bfd	Primary somatosensory area, barrel field	CA1sp	Cornu ammonis 1, pyramidal layer
AUDd	Dorsal auditory area	CA1sr	Cornu ammonis 1, stratum radiatum
AUDp	Primary auditory area	CA1slm	Cornu ammonis 1, stratum lacunosum-moleculare
AUDv	Ventral auditory area	CA2so	Cornu ammonis 2, stratum oriens
TEa	Temporal association area	CA2sp	Cornu ammonis 2, pyramidal layer
ECT	Ectorhinal area	CA2sr	Cornu ammonis 2, stratum radiatum
PERI	Perirhinal area	CA2slm	Cornu ammonis 2, stratum lacunosum-moleculare
ENTI	Entorhinal area	CA3so	Cornu ammonis 3, stratum oriens
PIR	Piriform area	CA3sp	Cornu ammonis 3, pyramidal layer
PAA	Piriform-amygdalar area	CA3sr	Cornu ammonis 3, stratum radiatum
COApl	Cortical-amygdalar area	CA3slm	Cornu ammonis 3, stratum lacunosum-moleculare
BLAv	Basolateral amygdalar nucleus, ventral part	CA3slu	Cornu ammonis 3, stratum lucidum
BMAp	Basomedial amygdalar nucleus, posterior part	DGmo	Dentate gyrus, molecular layer
BLAp	Basolateral amygdalar nucleus, posterior part	DGsg	Dentate gyrus, granule cell layer
BLAa	Basolateral amygdalar nucleus, anterior part	DGpo	Dentate gyrus, polymorph layer
MEA	Medial amygdalar nucleus		

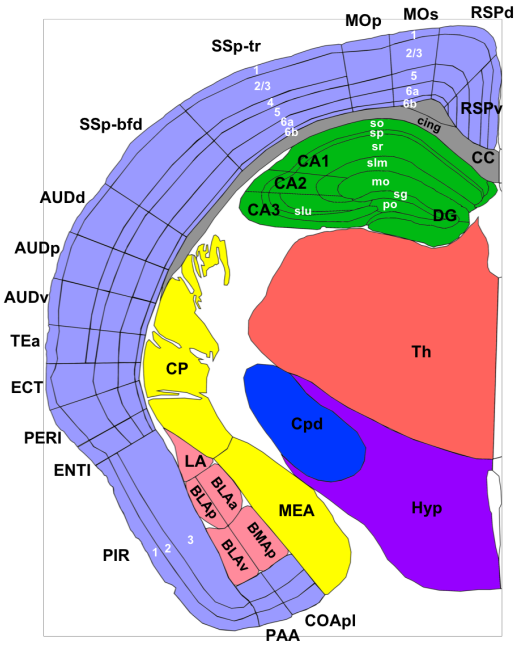

***Figure 4.2**: **Delineation map sub-regions of coronal section of mouse brain** made in accordance with Allen Mouse Brain Atlas. Each hemisphere include 111 sub-regions for which the complete names for abbreviations are demonstrated in the attached table.*

4.3 EXPERIMENTAL RESULTS

A pilot study of 6 mice was performed to provide data to power this experiment **(Appendix 2)**. These calculations indicated that a total of 9 should be randomized to each cohort, therefore a total of 64 mice were randomized into this experiment. Of these mice, 20 had to be excluded for the following reasons: 9 mice developed dural ruptures, 6 mice were found to have an incorrect genotype on reanalysis, 4 sustained dural tears and 1 mouse died two days post-operatively. **Figure 4.3** shows the final cohort numbers.

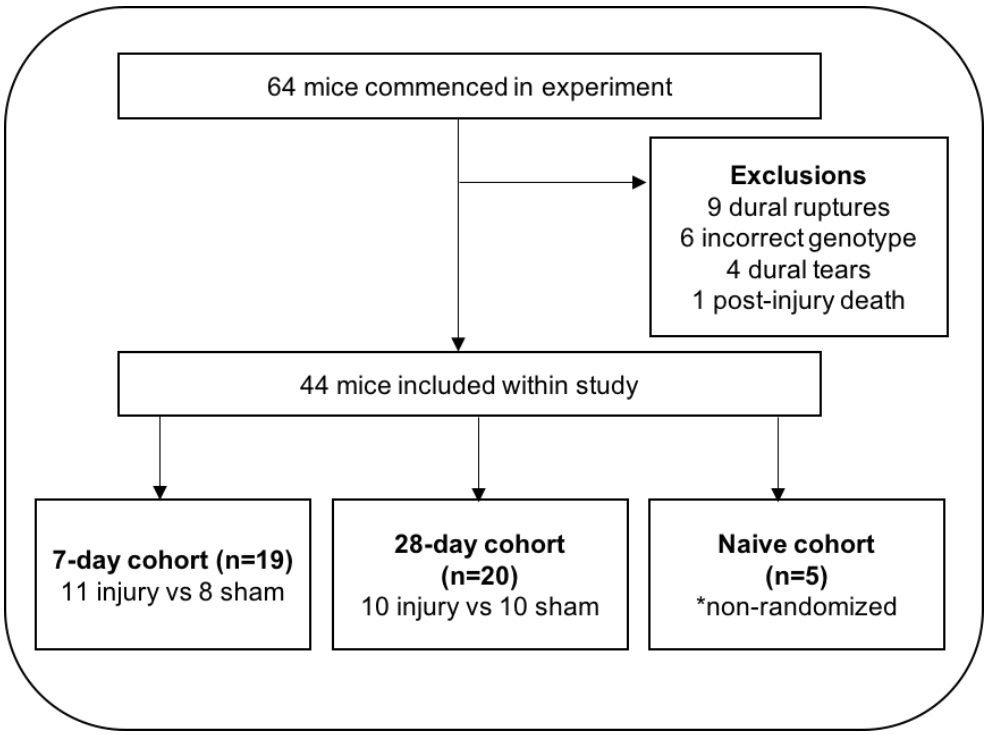

***Figure 4.3**: **Flow diagram of mouse cohorts in study** demonstrating mouse numbers in different cohorts*

The mean mouse weight was 26.5±3.2g. A comparison of the cohorts' weight showed that there was no significant variation across the groups. The mean fluid percussion intensity was 1.26±0.1atm. There was no significant difference in the intensity of the fluid percussion wave between the 7-day (1.27±0.07atm) and 28-day (1.24±0.14atm) cohorts (p=0.5; student t-test) **(Figure 4.3)**. From this data, we conclude that there was no significant differences in the mice randomized to the different cohorts and that the intensity of the percussion pulse did not differ across the time-points.

4.3.1 Injury mice exhibit increased righting times

To examine whether the fluid percussion led to an early alteration in brain function we measured the righting time (RT) of the mice. The injury cohort had an RT of 562.4±271 seconds compared to the sham cohort for an RT of 79±118.6 seconds was observed ($p<0.0001$; student t test) **(Figure 4.4)**. Using this simple behavioural assay, we conclude that application of the fluid pulse led to early alteration in brain function. This observation is limited by the fact it was an unblinded test and that it only provides information on brain function immediately post-injury.

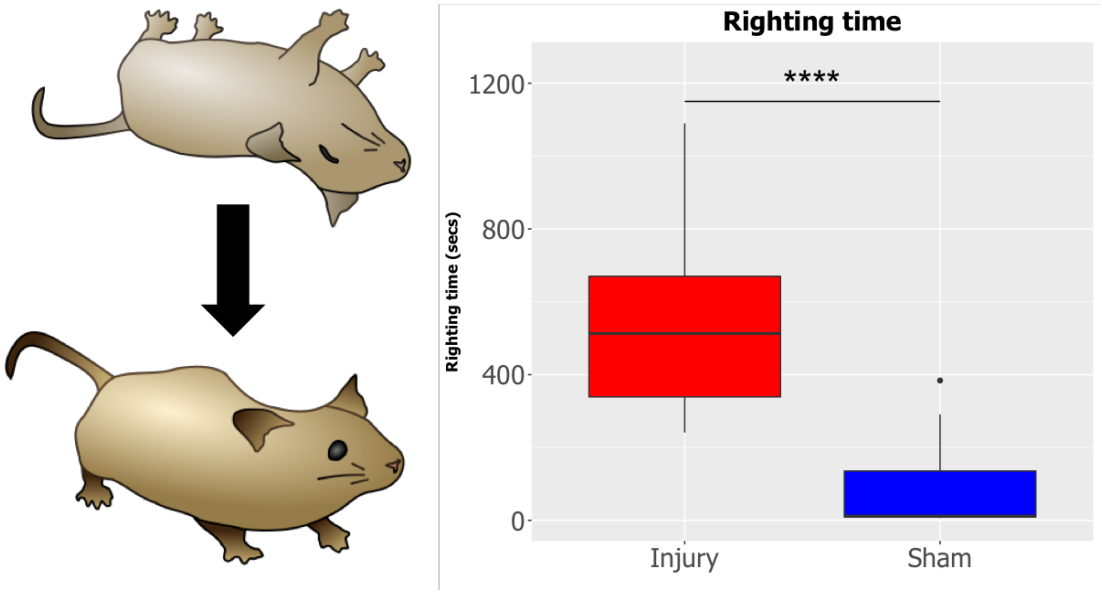

Figure 4.4**: **Comparison of righting times between injury and sham mice** which demonstrates significant increase in RT in the injury group compared to the sham group. Boxplot represents median and interquartile range. Mouse images taken from Wikimedia Commons. [* p≤0.0001; *** p≤0.001; ** p≤0.01; * p≤0.05; ns p>0.05]*

4.3.2 No difference in regional architecture between injury and sham mice

TBI can lead to cerebral oedema and atrophy which can distort the regional architecture of the brain. To examine whether this was present in our experimental groups, we used area analysis to ascertain whether there were differences between the injury and sham groups in 6 major brain regions: cortex, corpus callosum, hippocampus, thalamus, striatum and hypothalamus **(Figure 4.5)**. Two-way ANOVA was used to compare injury and sham groups for each region (ipsilateral and contralateral) across the two time-points. No significant differences were observed across any of the regions at either 7 days or 28 days. Therefore, we conclude that there are no major differences in gross brain architecture between the injury and sham groups. However, this conclusion must be caveated by the fact that our analyses are of 2-dimensional area measurements and not full volumetric values and we only looked at major regions and not individual sub-regions.

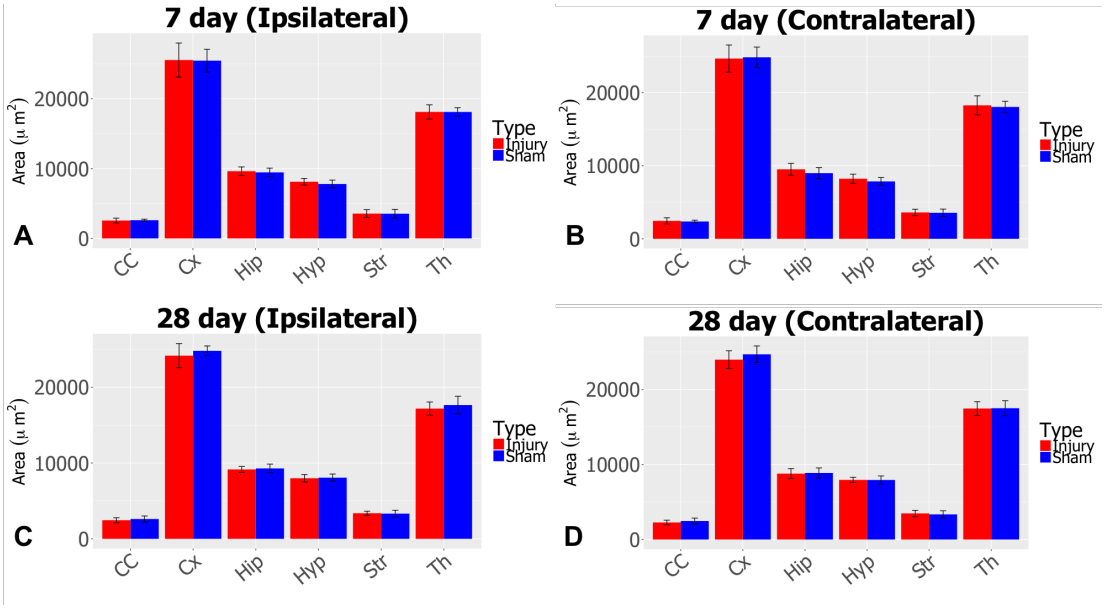

Figure 4.5: Comparison of regional area between injury and sham mice*. No significant differences (p>0.05) were observed between the injury (red) and sham (blue) mice in 6 major brain regions (CC: corpus callosum; Cx: cortex; Hip: hippocampus; Hyp: hypothalamus; Str: striatum; Th: thalamus) across the ipsilateral and contralateral hemispheres for both 7 and 28 days (A-D). Graphs shown are bar charts with standard deviations.*

4.3.3 Axonal injury observed in corpus callosum of injury mice

Axonal pathology is a pathological hallmark of TBI. To assess whether this was the case in our experiment, Amyloid Precursor protein (APP) was used to examine the degree of axonal pathology in the ipsilateral corpus callosum **(Figure 4.6, A)**. Using two-way ANOVA, there was statistically significant difference the injury and sham cohorts ($F(1,35)=15.71$; $p=0.0003$) but not between 7 and 28 days ($F(1,35)=2.21$; $p=0.146$). In a post-hoc Bonferroni test, the injury cohort was found to have significantly elevated numbers of corpus callosal APP aggregates at 7 days (44.7 ± 25.4) compared to the sham mice ($11.5\pm18.$; $p=0.006$). At 28 days, the injury cohort had 27.6 ± 22.2 aggregates compared to the sham mice which were found to have 9.3 ± 10.7 but this did not reach statistical significance ($p=0.3$) **(Figure 4.6, B)**. These data provide evidence of significant axonal pathology in our injury cohorts which peaks at 7 days. We conclude that, in the absence of major structural differences between the injury and sham groups, axonal injury was induced by application of the percussion pulse. This observation is made only within the corpus callosum which limits its generalisability to other brain regions.

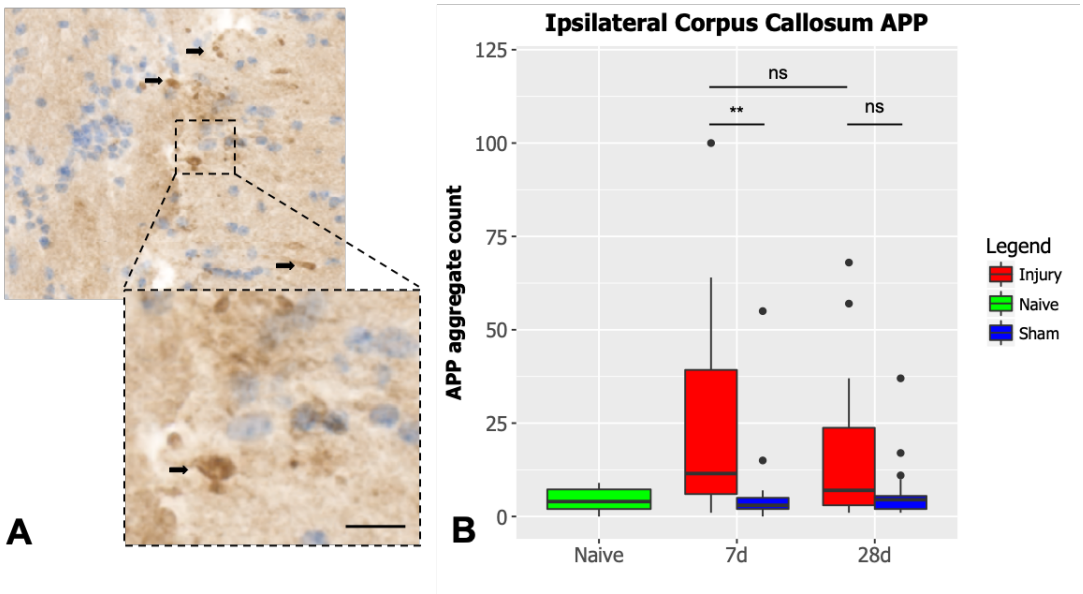

Figure 4.6: Comparison of APP aggregates in the ipsilateral corpus callosum*. This demonstrated APP aggregates in the corpus callosum of injury mice (A) and graph highlighting differences in ipsilateral corpus callosum aggregate counts between injury, sham and naïve mice across the two time points (B). Boxplot denote the median and interquartile range. Scale bar = 20μm. [**** p≤0.0001; *** p≤0.001; ** p≤0.01; * p≤0.05; ns p>0.05]*

4.3.4 Injury cohort exhibited progressive inflammatory response

Post-traumatic inflammation is a major secondary injury process after TBI. To examine inflammatory changes in our experimental group we stained for Iba-1, a marker of microglial activity **(Figure 4.7 A)**. With two-way ANOVA, we observed that comparison of injury and sham mice had a statistically significant effect in the ipsilateral cortical (F(1,31)=14.57;p=0.0006), contralateral cortical (F(1,31)=6.99; p=0.01) and ipsilateral hippocampal (F(1,31)=9.43; p=0.004) and contralateral hippocampal (F(1,31)=5.95; p0.02) Iba-1 count. Utilising post-hoc Bonferroni test, we found that at 7 days, the number of Iba-1 positive cells were increased in the injury cohort's ipsilateral cortex (1011±386) compared to the sham mice (563.8±251.4; p=0.041) **(Figure 4.7, B)**. The number of Iba-1 cells had remained elevated at 28 days in the injury cohort's ipsilateral cortex (837.5±398) compared to the sham cohort (434.9±223.5, p=0.09), but this did not reach statistical significance. Within the ipsilateral hippocampus there was a statistically significant difference in Iba-1 cell count between the injury and sham mice at 7days (p=0.02) **(Figure 4.7, C)**. Within

the contralateral hemisphere, there was no significant different in Iba-1 cell count at 7 days in the cortex between the injury and sham mice ($p>0.999$) **(Figure 4.7, D)**. However, by 28 days the number of Iba-1 positive cells were significantly higher in the injury group (1017±473.3) compared to the sham group which had a mean of 397.6±226.4 cells ($p=0.0036$). In the contralateral hippocampus there was no difference in Iba-1 cell count between injury and sham at 7 days ($p=0.627$) and 28 days ($p=0.13$) **(Figure 4.7, E)**. However, there was a statistically significant temporal increase in the number of Iba-1 cells from 7 to 28 days ($p=0.038$). There were no significant differences in the number of Iba-1 positive cells between the injury and sham groups and across the two time-points in the thalamus and hypothalamus. From this data, we can conclude that in the injury group there was increased microglial numbers in the ipsilateral cortex and hippocampus from day 7 post-injury which persisted to 28 days post-injury. Interestingly, we observed a delayed increase in microglia numbers in the contralateral cortex and hippocampus in the injury group. This points towards a progressive inflammatory process that extends well beyond the initial injury.

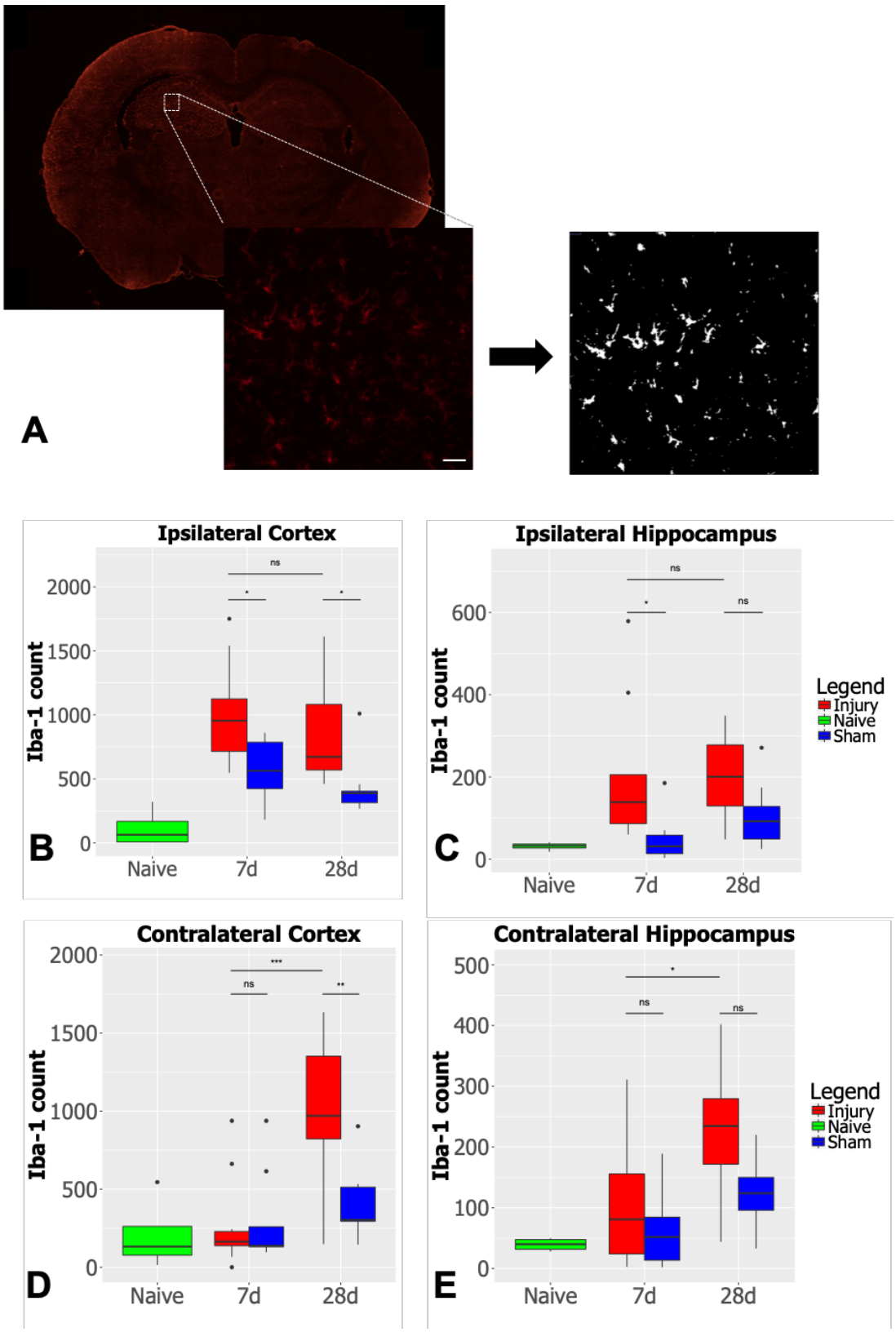

Figure 4.7: Comparison of Iba-1 positive cells between injury and sham mice. *Image demonstrates Iba-1 immunohistochemistry and image J conversion (A) and a comparison of Iba-1 positive cell numbers across the ipsilateral and contralateral*

*cortex and hippocampus (B-E). Boxplots denote median and interquartile range. Scale bar = 100μm. [**** p≤0.0001; *** p≤0.001; ** p≤0.01; * p≤0.05; ns p>0.05]*

4.3.5 No left-right asymmetry detected in the PSD95 and SAP102 synaptome maps

Due to the unilateral nature of the fluid percussion model, it was important to ensure that there was no inherent asymmetry between the left and right hemispheres in our naïve cohort that may bias observations seen between the ipsilateral and contralateral hemispheres in both the sham and injury mice **(Appendix 3)**. To do this, we compared 6 major brain regions (cortex, hippocampus, thalamus, hypothalamus, striatum and corpus callosum) between the left and right hemispheres in our naïve cohort. The synaptic density, area and intensity for both PSD95 and SAP102 were compared. Using two-way ANOVA, we found no significant differences in any of the synaptic metrics across both proteins **(Figure 4.8)**.

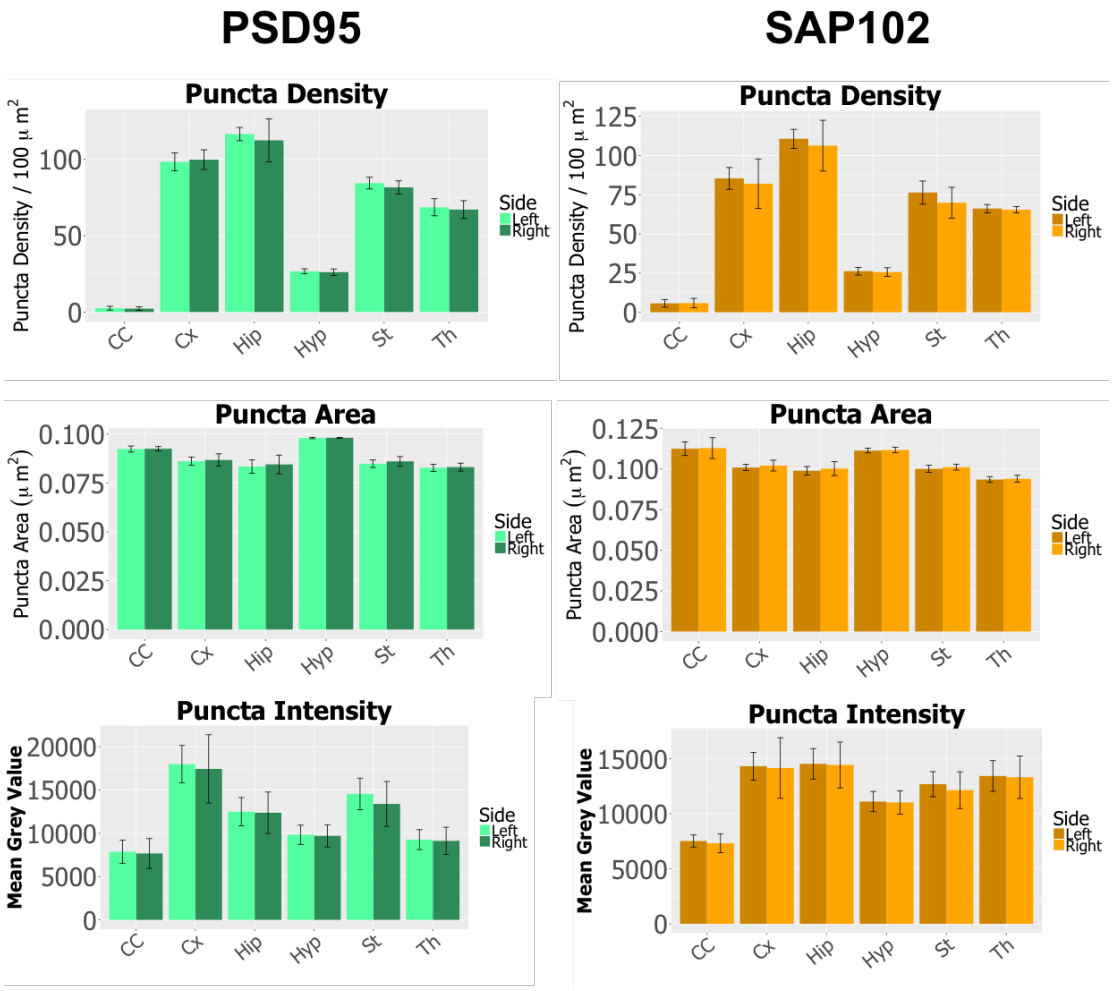

Figure 4.8: Left-Right comparison of major brain regions in naïve mice. *No significant difference (p>0.05) between right and left hemispheres for major brain regions (CC: corpus callosum; Cx: cortex; Hip: hippocampus; Hyp: hypothalamus; St: striatum; Th: thalamus) for puncta density, area and intensity in both PSD95 and SAP102.*

4.3.6 Reorganization of PSD-95 synaptome map following injury

4.3.6.1 Comparison of PSD95 puncta metrics in ipsilateral cortex

Due to the focal nature of the LFPI model, we first examined the impact of the LFPI on the ipsilateral cortex. A gross examination of the whole ipsilateral cortex was undertaken looking at PSD95 puncta density, area and intensity in the three mice cohorts (naïve, sham and injury) and across the 2 time-points (7 and 28 days). Two-way ANOVA revealed that mouse cohort had a statistically significant effect on the overall puncta density effect ($F(2,43)=11.14$; $p=0.0001$). Multiple comparisons with Bonferroni correction revealed that at 7 days there was a significant drop in cortical PSD95 density in both the injury (86.4 ± 7.2 per $100\mu m^2$; $p=0.001$) and sham (87.9 ± 7.9 per $100\mu m^2$; $p=0.006$) mice compared to the naïve cohort (99.7 ± 7.2 per $100\mu m^2$) **(Figure 4.9, A)**. However, there was no significant difference in cortical PSD95 density between the injury and sham mice at 7 days ($p>0.999$). At 28 days, the PSD95 density in the injury group (90.13 ± 4.8 per $100\mu m^2$) remained significantly reduced compared to the naïve cohort ($p=0.026$) which was no longer the case with the sham cohort (93.31 ± 4.4 per $100\mu m^2$; $p=0.219$). There were no significant differences between the cohorts for both PSD95 puncta area and intensity **(Figure 4.9, B and C)**. This data indicates a drop in ipsilateral cortical PSD95 density in both the sham and injury groups compared to the naïve cohort with no differences observed in puncta area and intensity.

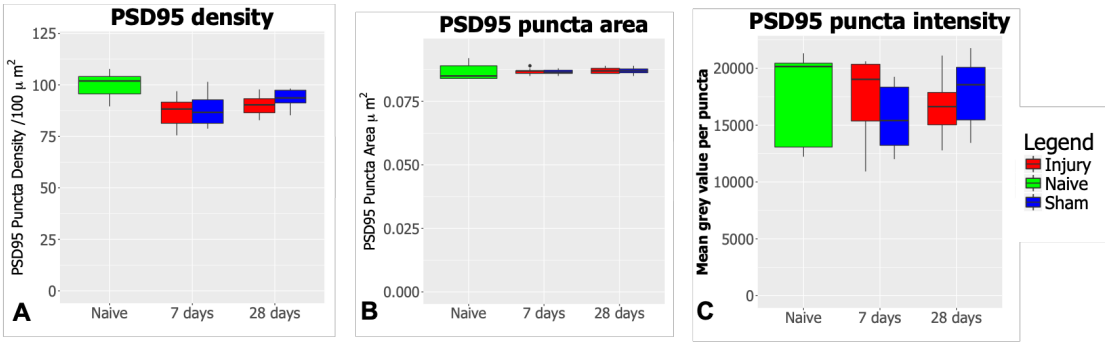

***Figure 4.9**: **Comparison of PSD95 metrics in the ipsilateral cortex** between the three cohorts (injury, sham and naïve) for PSD95 density (A), puncta area (B) and puncta intensity (C)*

4.3.6.2 Comparison of PSD95 density in ipsilateral cortical regions

Given the observed differences in gross ipsilateral cortical PSD95 density, we then aimed to compare regional PSD95 density in the ipsilateral cortex in more detail. The cortex was subdivided into its major regions including: retrosplenial, motor, somatosensory, auditory, temporal association, ectorhinal, perihinal and entorhinal areas **(Figure 4.10, A)**. These were plotted from medial to lateral to demonstrate regional alterations in PSD95 density **(Figure 4.10, B and C)**. Using two-way ANOVA, we observed significant variation between the cohorts (injury, sham and naïve) at 7 days ($F(2,273)=20.56$; $p<0.0001$) and 28 days ($F(2,286)=28.5$; $p<0.0001$). With multiple testing with Bonferroni correction, we observed significant decreases in PSD95 density in both the sham and injury mice compared to the naïve mice within the primary motor area (MOp) and trunk somatosensory area (SSp-tr). The injury cohort demonstrated further significant decreases in PSD95 density compared to the naïve cohort in the secondary motor area (MOs) [82.55±7.5 vs 70.86±7.9 per 100μm^2; $p=0.04$] and the barrel field somatosensory area (SSp-bfd) [99.08±9.6 vs 86.56±9.3 per 100μm^2; $p=0.02$]. At 28 days, there remained a significant reduction in PSD95 density in both the injury and sham groups compared to the naïve group in MOp and SSp-tr. The injury cohort demonstrated persisting reduction in PSD95 density in SSp-bfd compared to the naïve cohort [99.08±9.6 vs 89.32±5.8 per 100μm^2; $p=0.008$]. Alongside this, the injury cohort had significantly reduced PSD95 density in the dorsal auditory area (AUDd) compared to the naïve cohort [102.74±7.3 vs 93.59±4.7 per 100μm^2; $p=0.01$]. There were no significant differences between the injury and sham groups across both time-points. These data indicate that the motor and somatosensory areas of the mouse cortex were most affected by the LFPI procedure

which are situated underneath the craniotomy site. Interestingly, the results highlight that the process of the removal of the bone flap led to a comparable reduction in PSD95 density in the sham mice. However, it appears that the application of the LFPI pulse led to significant reduction in PSD95 puncta density distal to the craniotomy site (SSp-bdf and AUDd) in the injury group compared to the naïve mice which was not present in the sham cohort.

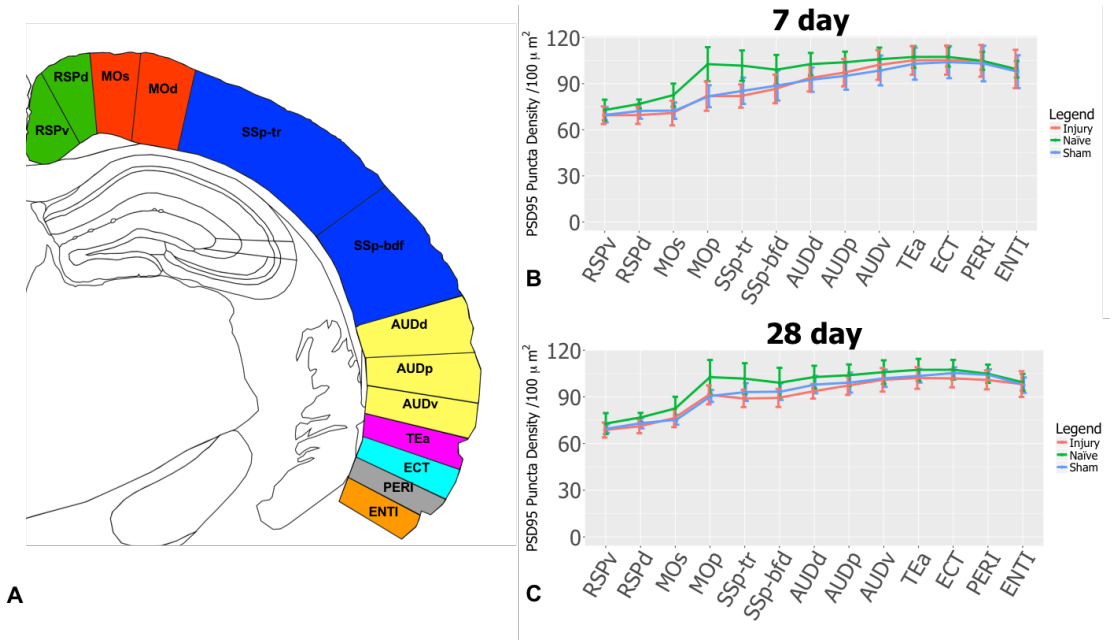

Figure 4.10: Comparison of cortical sub-regional PSD95 density. *Representation of the cortical regions (A) with line graph of cortex regional PSD95 density at 7 days (B) and 28 days (C). Abbreviations: RSPv: Retrospenial area ventral part; RSPd: Retrospenial area dorsal part; MOs: Secondary motor area; MOp: Primary motor area; SSp-tr: Somatosensory area trunk; SSp-bfd: Somatosensory area barrel field; AUDd: Doral auditory area; AUDp: Primary auditory area; AUDv: Ventral auditory area; TEa: Temporal association area; ECT: Ectorhinal area; PERI: Perirhinal area; ENTI: Entorhinal area.*

4.3.6.3 Sub-regional changes in the PSD-95 synaptome map following LFPI

To investigate the impact of the LFPI model at the sub-regional level across the whole synaptome, we then subdivided the brain into 222 sub-regions (111 sub-regions in ipsilateral and contralateral hemispheres to the fluid percussion injury) and a Cohen's *d* value was measured comparing injury with sham for PSD95 puncta density, area and intensity **(Appendix 4)**. These effect sizes were then plotted on a spatial heat

map of a coronal mouse brain section **(Figure 4.11)**. Two-way ANOVA was used to examine the effect of experimental cohort (injury vs sham) on the three PSD95 metrics. Post-hoc unpaired student t-tests were then utilized to examine the significance of differences seen at the sub-regional level. Two-way ANOVA showed that there was a significant difference observed between the injury and sham cohort for both PSD95 puncta density at 7 days ($F(1,3370)=35.09$; $p<0.0001$) and 28 days ($F(1,3986)=165.1$; $p<0.0001$) and intensity across both 7 days ($F(1,3770)=140$; $p<0.0001$) and 28 days ($F(1,3986)=300.3$; $p<0.0001$). Conversely, there was no significant difference ($p>0.05$) between injury and sham for PSD95 puncta area. Using post-hoc t-tests, at 7 days there was evidence of significant sub-regional clustering for PSD95 puncta density, size or intensity. There were a number of isolated sub-regions with $p<0.05$ however none of these reached the threshold of $p<0.0002$ and are therefore not considered within the discussion of the results **(Figure 4.11)**. These findings indicate that there was significant difference in the synaptome between injury and sham at 7 days. At 28 days, we observed a reduction in PSD95 puncta density Cohen's *d* effect size in the injury compared to the sham cohort **(Figure 4.11, A)**. This was most pronounced within the contralateral hippocampus with differences within clustering sub-regions in the CA1, CA3 and the dentate gyrus all reaching statistical significance ($p<0.05$). We also observed reductions in Cohen's *d* effect size in the injury group in the isocortex bilaterally. This included significant differences within the ipsilateral somatosensory barrel-field (SSp-bfd) and dorsal auditory areas (AUDd) alongside the contralateral trunk somatosensory trunk (SSp-tr) and primary auditory areas (AUDp). Conversely, there was a less clear pattern of change in PSD95 puncta area **(Figure 4.11, B)**. However, there was no evidence of sub-region clustering or isolated sub-regions with $p<0.0002$. The PSD95 puncta intensity revealed a uniform global reduction in Cohen's *d* effect size in the injury group compared to the sham, however none of these were considered significant based on our interpretation thresholds **(Figure 4.11, C)**.

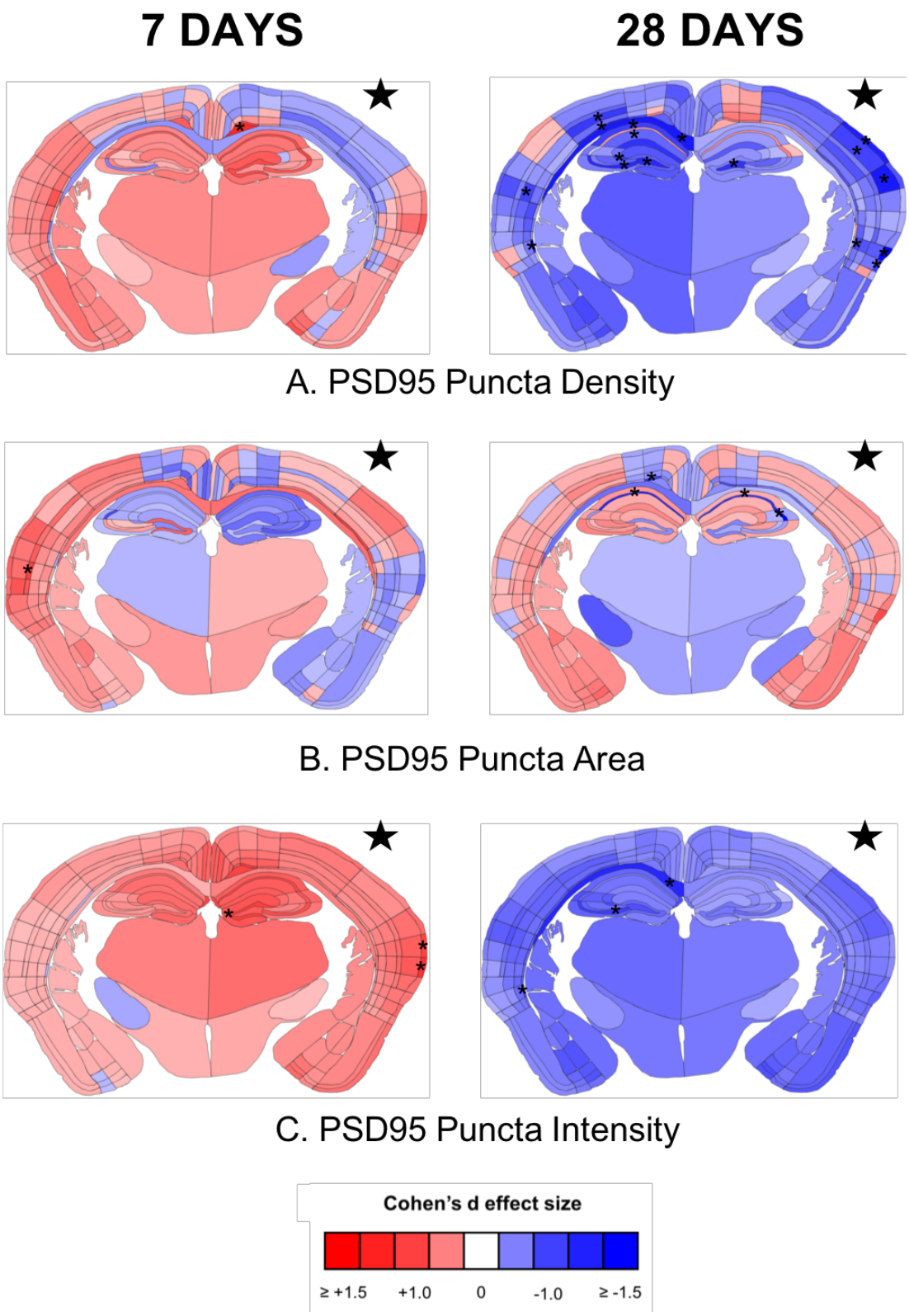

Figure 4.11: Sub-regional PSD95 synaptome map comparing injury and sham mice *across 7 days and 28 days looking at PSD95 puncta density (A), PSD95 puncta*

*area (B) and PSD95 puncta intensity (C). Large black star identifies side of fluid percussion. [* = p<0.05].*

To examine the relationship between the PSD95 synapse metric changes seen after injury, we calculated the Pearson correlation co-efficient between the Cohen's *d* effect sizes for each of the metrics across both time points. There was a negative relationship between PSD95 density and area at 7 days (r=-0.249; p=0.0002) that became more pronounced at 28 days (r=-0.538; p<0.0001) **(Figure 4.12, A)**. Similarly, a negative relationship was observed between PSD95 area and intensity at both 7 days (r=0.618; p<0.0001) and 28 days (r=-416; p<0.0001) **(Figure 4.12, B)**. Conversely, PSD95 density and puncta intensity revealed significant positive correlation across both time-points: 7 days (r=0.233; p=0.0005) and 28 days (r=0.574; p<0.0001) **(Figure 4.12, C)**. Collectively, this data indicates that the LFPI leads to progressive alteration in the synaptome up to a month after a single mild injury. In particular, it demonstrated a marked global reduction in both PSD95 puncta density in the injury compared to the sham group at 28 days centred around the contralateral hippocampus and isocortex bilaterally.

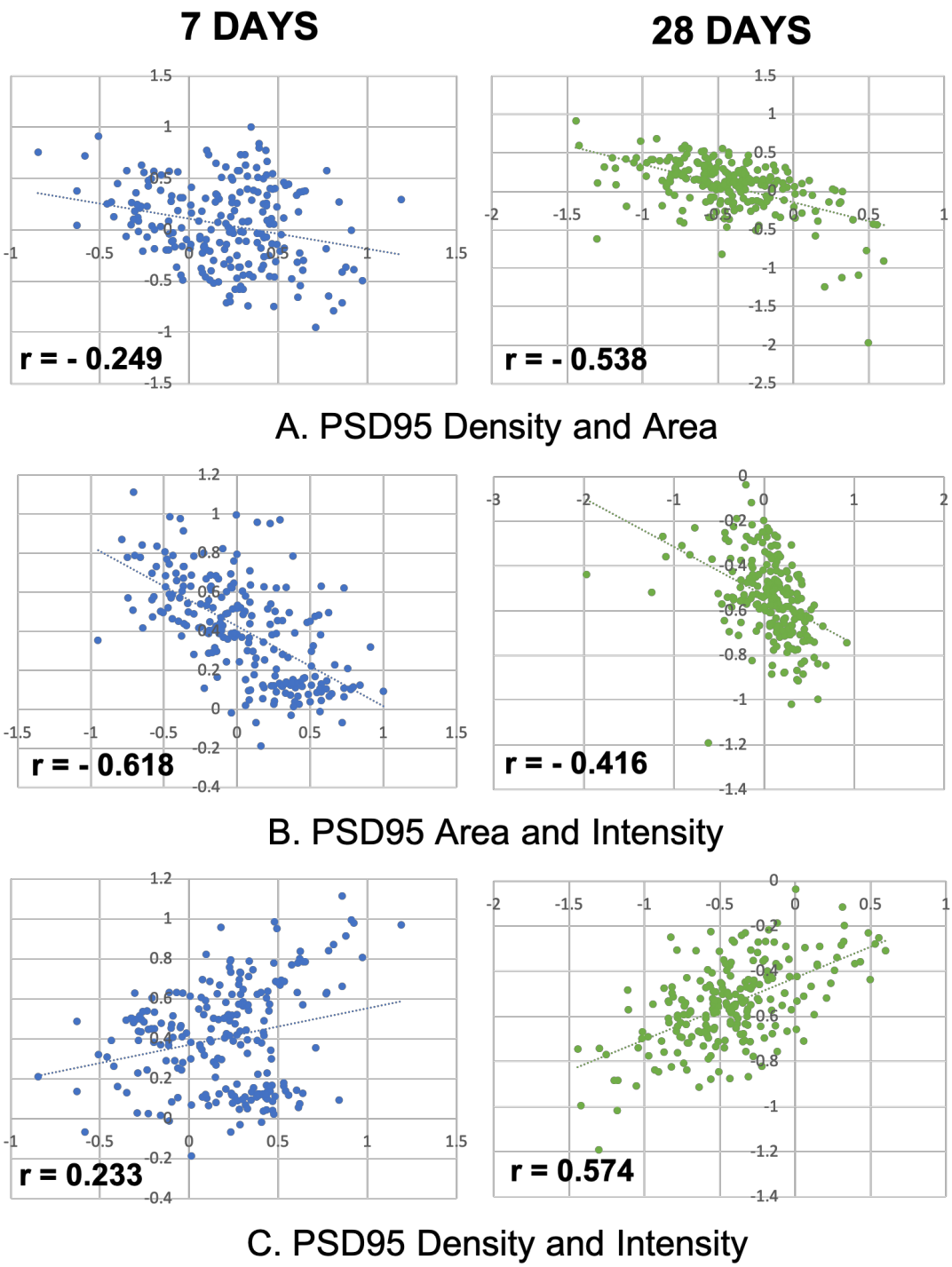

Figure 4.12: Correlation between PSD95 metrics Cohen's d effect size. *Scatterplots of Cohen d effect sizes for 222 brain sub-regions comparing PSD95 density and area (A); PSD95 area and intensity (B) and PSD density and intensity (C)*

4.3.6.4 Temporal changes in PSD95 synaptome map in injury cohort

To better understand the temporal changes in PSD95 in the injury groups, we mapped Cohen's *d* effect sizes of the 28-day against the 7-day injury groups across the 222 brain regions **(Figure 4.13)**. The same statistical approach as described earlier was used: two-way ANOVA to examine the impact of time-points (7 days vs 28 days) followed by unpaired student t-tests for sub-region analysis. Comparison of the temporal cohorts with two-ANOVA showed significant difference between the two cohorts ($p<0.0001$) for all three PSD95 metrics. On comparison of the 222 sub-regions using post-hoc multiple t-tests, we observed a substantial increase in PSD95 puncta density Cohen's *d* effect size in the ipsilateral cortex at 28 days compared to 7 days **(Figure 4.13, A)**. This was centred around the primary motor (MOp) and somatosensory trunk (SSp-tr) areas. However, despite this increase, PSD95 puncta density within the ipsilateral motor and somatosensory cortical regions did not return to naïve mice levels. We observed an increase of 6% from 83% of naïve density at 7 days up to 89% by 28 days. The differences observed in the superficial (layer 1 and 2/3) of the MOp and deeper layers of SSp-tr (layers 4, 5 and 6a) reached statistical significance ($p<0.05$). This contrasted against relative PSD95 puncta density reduction in the contralateral cortex of which the ventral retrosplenial area (RSPv), barrel-field somatosensory (SSp-bfd) and auditory areas all demonstrated significant reductions in Cohen's *d* effect size at 28 days compared to 7 days. A similar pattern was observed for PSD95 puncta intensity which revealed small increases in Cohen's *d* effect size in the ipsilateral cortex mainly within the superficial layers of MOp and SSp-tr **(Figure 4.13, C)**. However, none of these observations were statistically significant ($p>0.05$). There was a reduction in Cohen's *d* effect size in other brain regions distal to the injury site. Sub-regions within the ectorhinal (ECT), perirhinal (PERI) and ventral auditory (AUDv) areas showed statistically significant reductions in the 28 day versus the 7 day injury cohort. Conversely, PSD95 puncta area demonstrated very pronounced statistically significant changes in the ipsilateral isocortex and subcortical plate. In the isocortex, we observed statistically significant increases in PSD95 puncta areas in the 28 days cohort within the isocortex distal to the fluid percussion site **(Figure 4.13, B)**. In particular, the piriform (PIR), entorhinal (ENT), perirhinal (PERI), ectorhinal (ECT) and temporal association (TEa) areas saw statistically significant changes in Cohen's *d* effect size. We also observed similar increases in PSD95 puncta area Cohen's *d* effect size in the ipsilateral cortical sub-plate with statistically significant findings within the lateral amygdalar nucleus (LA)

and both anterior and posterior parts of the basolateral amygdalar nucleus (BLAp and BLAa). To examine the relationship between the PSD95 metrics, we calculated the Pearson correlation co-efficient for the Cohen's d effect sizes across the 222 brain sub-regions. This demonstrated a significantly positive relationship between PSD95 density and puncta intensity (r=0.471; p<0.0001). While PSD95 puncta area and density (r=-0.345; p<0.0001) and mean (p=-0.479; p<0.0001) showed significantly negative correlations. This data indicates that following LFPI, there is a focal increase in PSD95 density and puncta intensity at the site of injury between 7 and 28 days. While there is evidence of relative reductions in both metrics at regions distal to the injury site. This indicates that the synaptome map following injury is a dynamic entity with evidence of both synapse loss and recovery occurring in tandem.

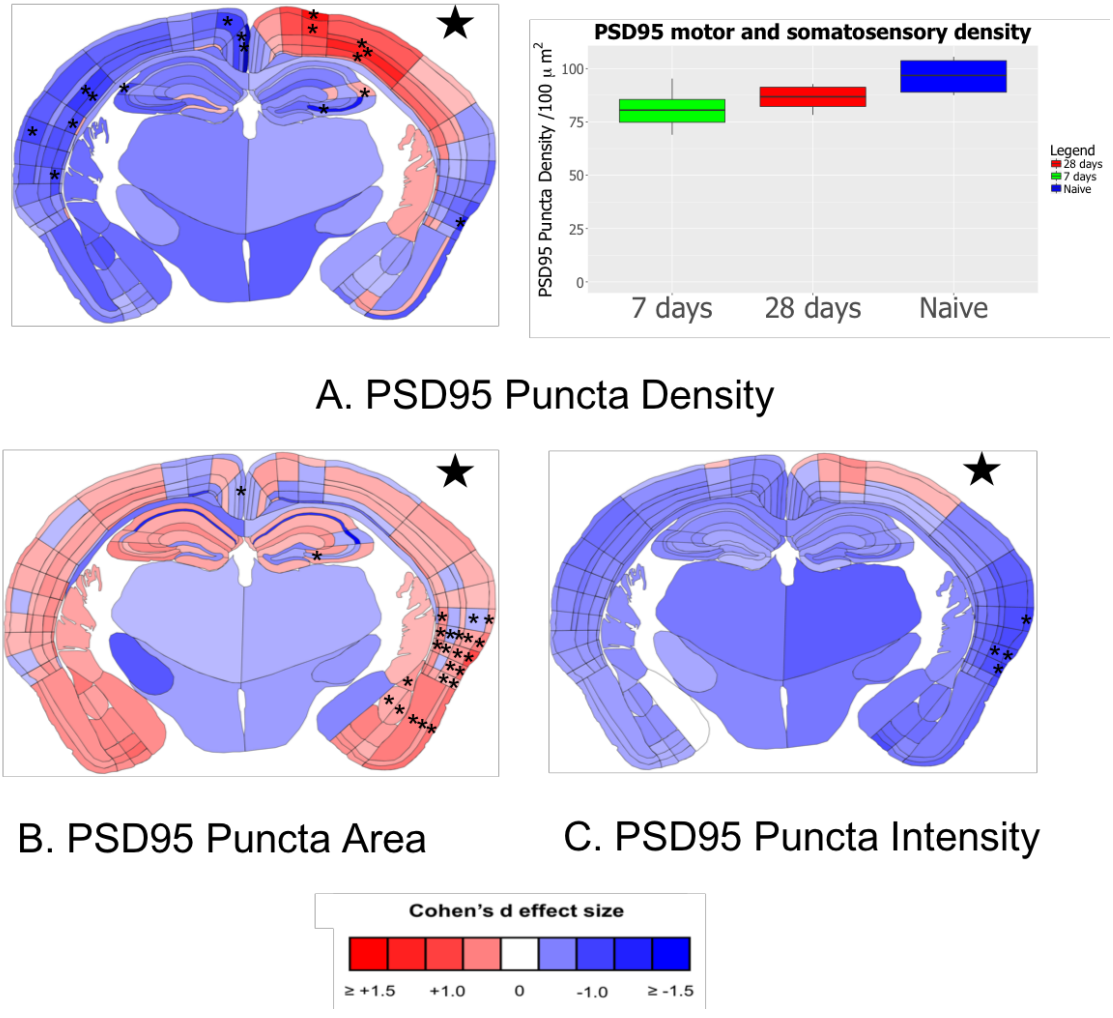

Figure 4.13: Subregional PSD95 synaptome map comparing 7 and 28 days in injury group *looking at PSD95 puncta density including a boxplot graph of ipsilateral motor and somatosensory PSD95 at 7 days, 28 days and naïve mice (A), PSD95*

*puncta area (B) and PSD95 puncta intensity (C). Large black star identifies side of fluid percussion. [* = p<0.05].*

4.3.7 Reorganization of SAP102 synaptome map following injury

4.3.7.1 Comparison of SAP102 puncta metrics in ipsilateral cortex

Similar to PSD95, we first examined the impact of the LFPI on the synaptic metrics of the whole ipsilateral cortex. Using two-way ANOVA, we found that the mouse cohorts had a statistically significant impact on the overall effect of puncta intensity ($F(2,43)=3.96$; $p=0.026$) but not puncta density ($F(2,43)=2.38$; $p=0.1$) or size ($F(2,43)=1.33$; $p=0.27$). Using multiple comparisons with Bonferroni correction, at 7 days, neither the injury (71.5±12.4 per 100μm^2; $p=0.377$) nor sham (68.7±12.4 per 100μm^2; $p=0.203$) mice saw significant differences in their SAP102 puncta density compared to naïve mice (82.0±17.7 per 100μm^2) **(Figure 4.14, A)**. A similar pattern was seen at 28 days in both the injury (72.8±9.3 per 100μm^2; $p=0.544$) and sham mice (76.7±9.1 per 100μm^2; $p>0.999$) compared to the naïve mice. There were no significant differences between the cohorts for both SAP102 puncta area or mean intensity in multiple comparison analysis **(Figure 4.14, B and C)**. These data indicate that, compared to PSD95, SAP102 appears to less vulnerable to loss following a traumatic insult.

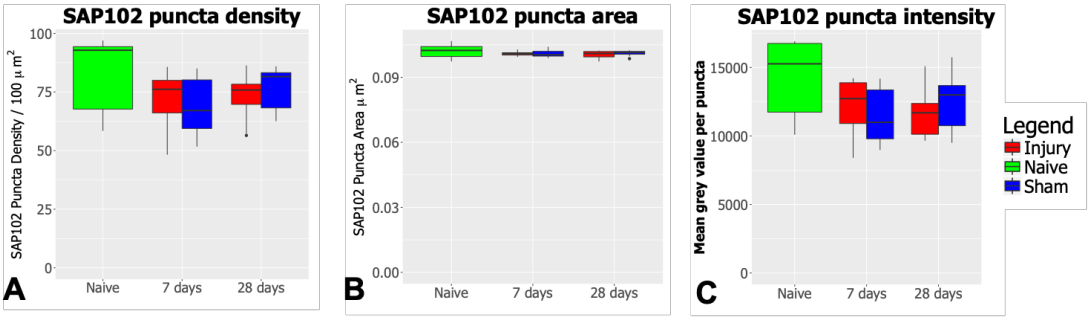

Figure 4.14: Comparison of SAP102 metrics in the ipsilateral cortex *between the three cohorts (injury, sham and naïve) for PSD95 density (A), puncta area (B) and puncta intensity (C)*

4.3.7.2 Comparison of SAP102 density in ipsilateral cortical regions

To further examine for cortical regional changes in SAP102 puncta density, we subdivided the ipsilateral cortex into 13 sub-regions. Using two-way ANOVA, we observed a significant effect of the mouse cohorts on puncta density at 7 days

(F(2,273)=12.5; p<0.0001) and 28 days (F(2,286)=12.27; p<0.0001). With multiple correction with Bonferroni corrections, we observed a reduction in SAP102 puncta density in the primary motor area between both the injury (67.9±12.9 100μm^2) and sham (63.6±11.1 100μm^2) cohorts compared to the naïve mice (80.7±20.0 100μm^2) at 7 days, however these observations did not reach statistical significance (p>0.05) **(Figure 4.15, B)**. There were no reductions in SAP102 puncta density in the somatosensory areas in both the injury and sham mice. Throughout the cortical regions, there were no statistically significant differences observed between the three cohorts across both time-points. This highlights SAP102's limited response to LFPI. The reasons for these observations may either be that SAP102 has greater biological resistance to traumatic insult compared to PSD95 or our observations are limited by detection bias. This latter explanation is plausible particularly given the greater standard deviations seen within our SAP102 density measurements compared to PSD95.

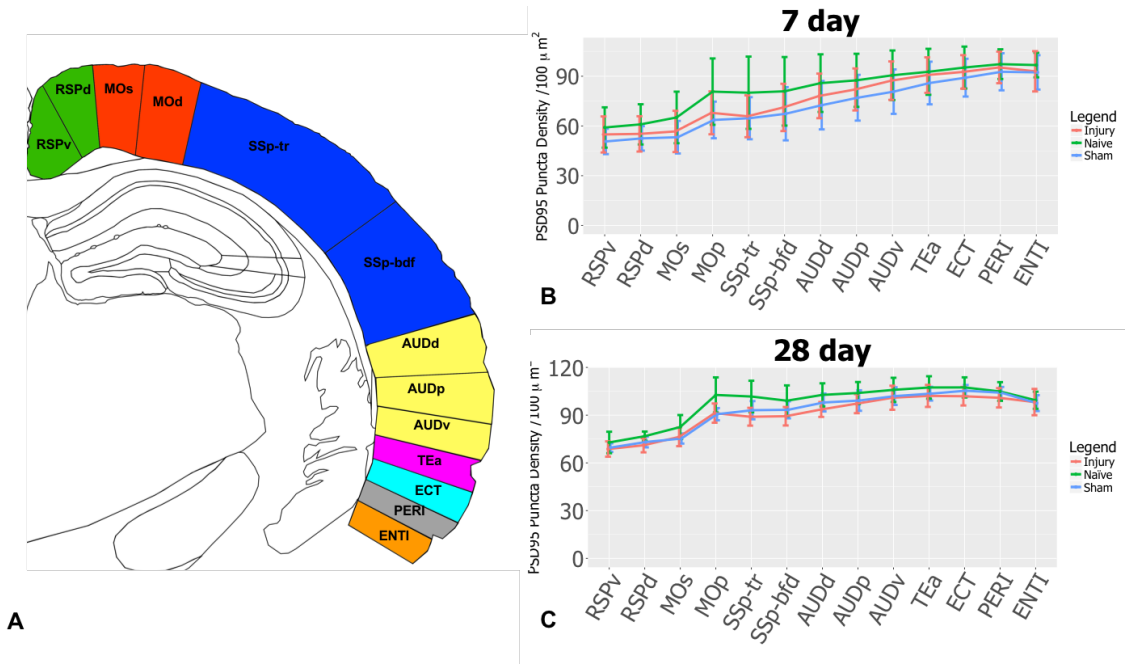

Figure 4.15: Comparison of cortical subregional SAP102 density. *Representation of the cortical regions (A) with line graph of cortex regional SAP102 density at 7 days (B) and 28 days (C). Abbreviations: RSPv: Retrospenial area ventral part; RSPd: Retrospenial area dorsal part; MOs: Secondary motor area; MOp: Primary motor area; SSp-tr: Somatosensory area trunk; SSp-bfd: Somatosensory area barrel field; AUDd: Doral auditory area; AUDp: Primary auditory area; AUDv: Ventral auditory*

area; TEa: Temporal association area; ECT: Ectorhinal area; PERI: Perirhinal area; ENTl: Entorhinal area

4.3.7.3 Sub-regional changes in the SAP102 synaptome map following LFPI

As with PSD95, we subdivided the brain into 222 sub-regions and a Cohen's *d* effect size was measured comparing injury with sham for SAP102 puncta density, area and intensity **(Appendix 5)**. These effect sizes were then plotted on a spatial heat map of a coronal mouse brain section **(Figure 4.16)**. Two-way ANOVA was used to examine the effect of injury type (injury vs sham) followed by unpaired student t-tests to more closely examine the significance of sub-regions. The two-way ANOVAs observed significant differences ($p<0.0001$) across the injury and sham cohorts across all three SAP102 metrics across both time-points: puncta density at 7 days ($F(1,3770)=44.46$; $p<0.0001$) and 28 days ($F(1,3986)=149.5$; $p<0.0001$); puncta size at 7 days ($F(1,3770)=28.50$;$p<0.0001$) and 28 days ($F(1,3986)=44.75$; $p<0.0001$); puncta intensity at 7 days ($F(1,3770)=68.44$; $p<0.0001$) and 28 days ($F(1,3986)=232.2$; $p<0.0001$). Within the post-hoc multiple t-tests no individual comparison met the $p<0.0002$ threshold and therefore isolated sub-regions are not discussed. At 7 days, there was an increase in Cohen's *d* effect size of SAP102 puncta area in the contralateral primary and ventral auditory areas. Otherwise, there were no other significant difference observed for SAP102 synaptic parameters **(Figure 4.16)**. Much like PSD95, at 28 days, we observed a reduction in SAP102 puncta density Cohen's *d* effect size in the injury group contralateral hippocampus including the polymoreph layer of the dentate gyrus **(Figure 4.16, A)**. SAP102 puncta area exhibited reductions in Cohen's d effect size within the isocortex bilaterally **(Figure 4.16, B)**. There was clustering of statistically significant observations centred around the deeper layers (layer 5, 6a and 6b) of the secondary motor area (MOs) and ventral and dorsal retrosplenial areas (RSPd and RSPv) within the ipsilateral isocortex. Similar reductions were observed within the deep layers of MOp and MOs in the contralateral isocortex. SAP102 intensity did not demonstrate any significant findings.

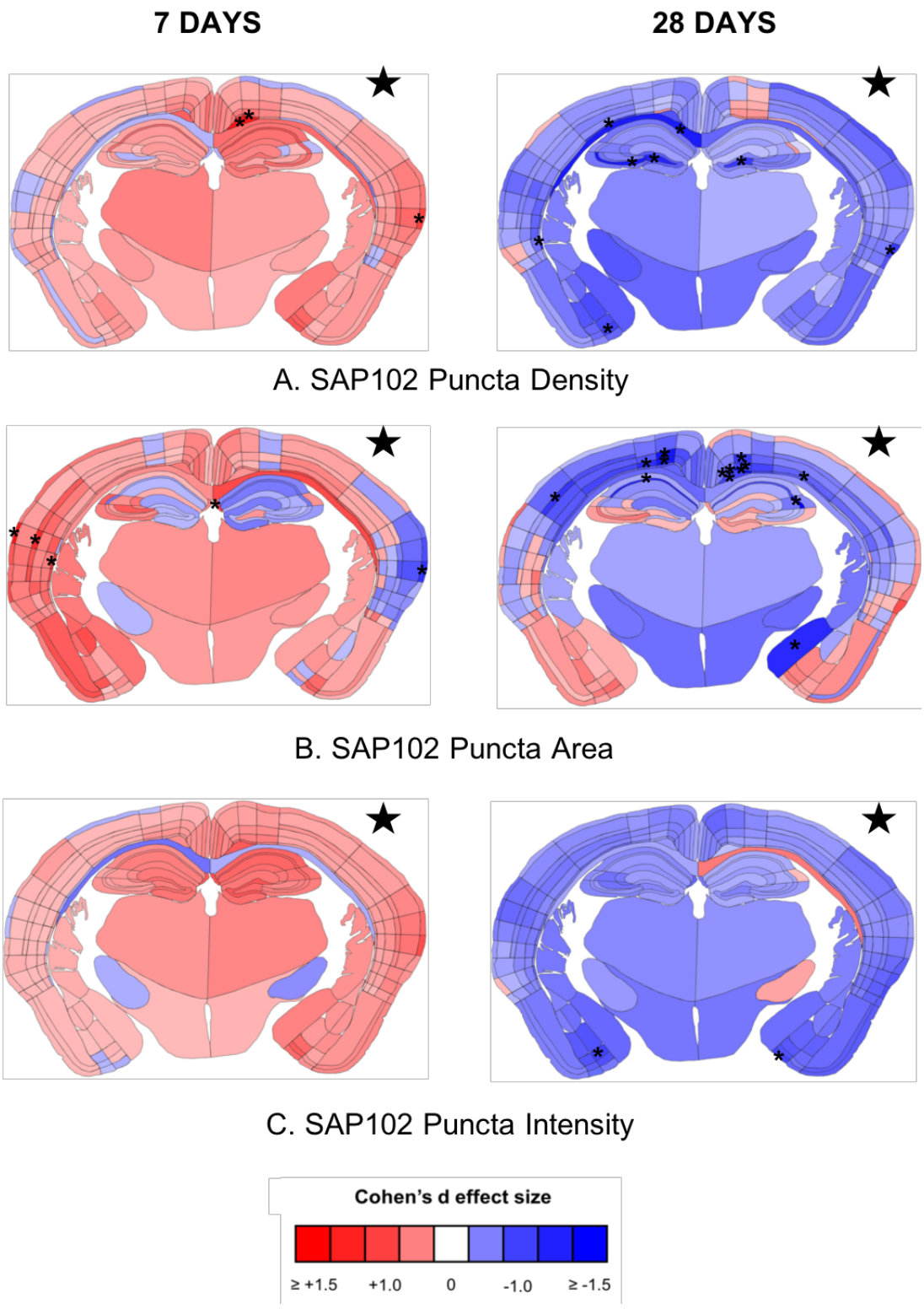

***Figure 4.16**: **Sub-regional SAP102 synaptome map comparing injury and sham mice** across 7 days and 28 days looking at SAP102 puncta density (A), SAP102 puncta area (B) and SAP102 puncta intensity (C). Large black star identifies side of fluid percussion. [* = p<0.05].*

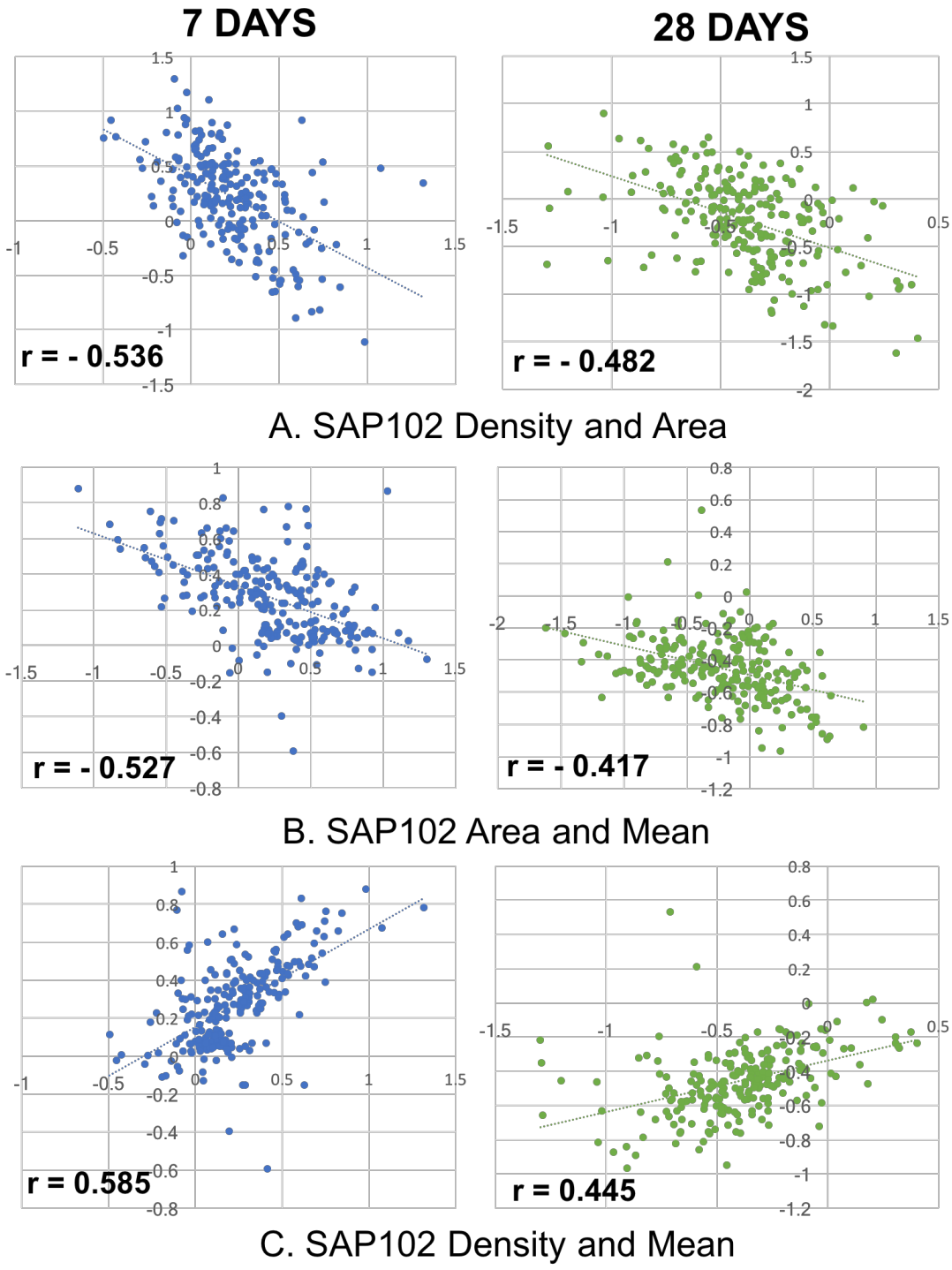

Figure 4.17: Correlation between SAP102 metrics Cohen's d effect sizes *Scatterplots of Cohen d effect sizes for 222 brain sub-regions comparing SAP102 density and area (A); SAP102 area and mean (B) and SAP102 density and mean (C)*

To examine the relationship between the SAP102 puncta metric changes seen after injury, we calculated the Pearson correlation co-efficient between the Cohen's *d* effect sizes for each of the metrics across both time points **(Figure 4.17)**. Similar to PSD95, there was a negative relationship between SAP102 puncta density and size after injury. The Pearson R correlation coefficient was -0.536 ($p<0.0001$) at 7 days and -0.482 ($p<0.0001$) at 28 days. Similarly, SAP102 puncta size and intensity had a significantly negative relationship at both 7 days ($r=-0.527$; <0.0001) and 28 days ($r=-0.418$; <0.0001). However, the SAP102 puncta density and intensity had a positive relationship with a correlation coefficient of 0.585 ($p<0.0001$) at 7 days and a coefficient of 0.445 ($p<0.0001$). Together these data show that SAP102, much like PSD95, showed progressive region-specific decline in puncta density and intensity at 28 days following injury. These findings along with the correlation analysis show that TBI leads to loss of synapse numbers but also the amount of SAP102 protein within the remaining synapses at 28 days post-injury.

4.3.7.4 Temporal changes in SAP102 synaptome map in injury cohort

To better understand the temporal changes in SAP102 in the injury groups, we mapped the Cohen's *d* effect sizes of the 28-day against the 7-day injury groups across the 222 brain regions **(Figure 4.18)**. Two-way ANOVAs demonstrated significant differences ($p<0.0001$) between the time-points for all three SAP102 puncta metrics. Unlike PSD95, SAP102 puncta density Cohen's *d* effect size increased modestly in the cortex underlying the fluid percussion site with only layer 1 of the primary motor cortex (MOp) reaching statistical significance ($R=1.1$; $p=0.02$) **(Figure 4.18, A)**. Even though the difference between the injury and sham were modest, they mirrored PSD95 density changes in the ipsilateral motor and somatosensory cortex compared to naïve mice. For SAP102, at 7 days the injury density was 85% of naïve increasing up to 89% by 28 days. Areas distal to the percussion site [ectorhinal (ECT), perirhinal (PERI) and entorhinal (ENT) areas] in the ipsilateral cortex saw statistically significant relative reductions in SAP102 puncta density Cohen's *d* effect size **(Figure 4.18, C)**. Alongside this, there was a global reduction in effect size in other brain regions of which the ipsilateral cortical areas distal to the percussion site were statistically significantly affected (ECT, PERI, ENT and TEa areas). Conversely, these same regions showed statistically significant increases in SAP102 puncta area **(Figure 4.18, B)**. To better examine the relationship between the SAP102 puncta metrics, we calculated the Pearson correlation co-

efficient for the Cohen's d effect sizes across the 222 brain sub-regions. This demonstrated a significantly positive relationship between SAP102 puncta density and intensity (r=0.605; p<0.0001). We observed negative relationships between SAP102 puncta area and the two metrics: intensity (r=-0.052; p<0.0001) and density (r=-0.537; p<0.0001). This data indicates that following LFPI, there are progressive changes occurring within the ipsilateral cortical hemisphere. Regions at the percussion site demonstrated increases in SAP102 puncta density as more distal regions saw reductions in puncta density and intensity coupled with a modest increase in puncta size between 7 to 28 days.

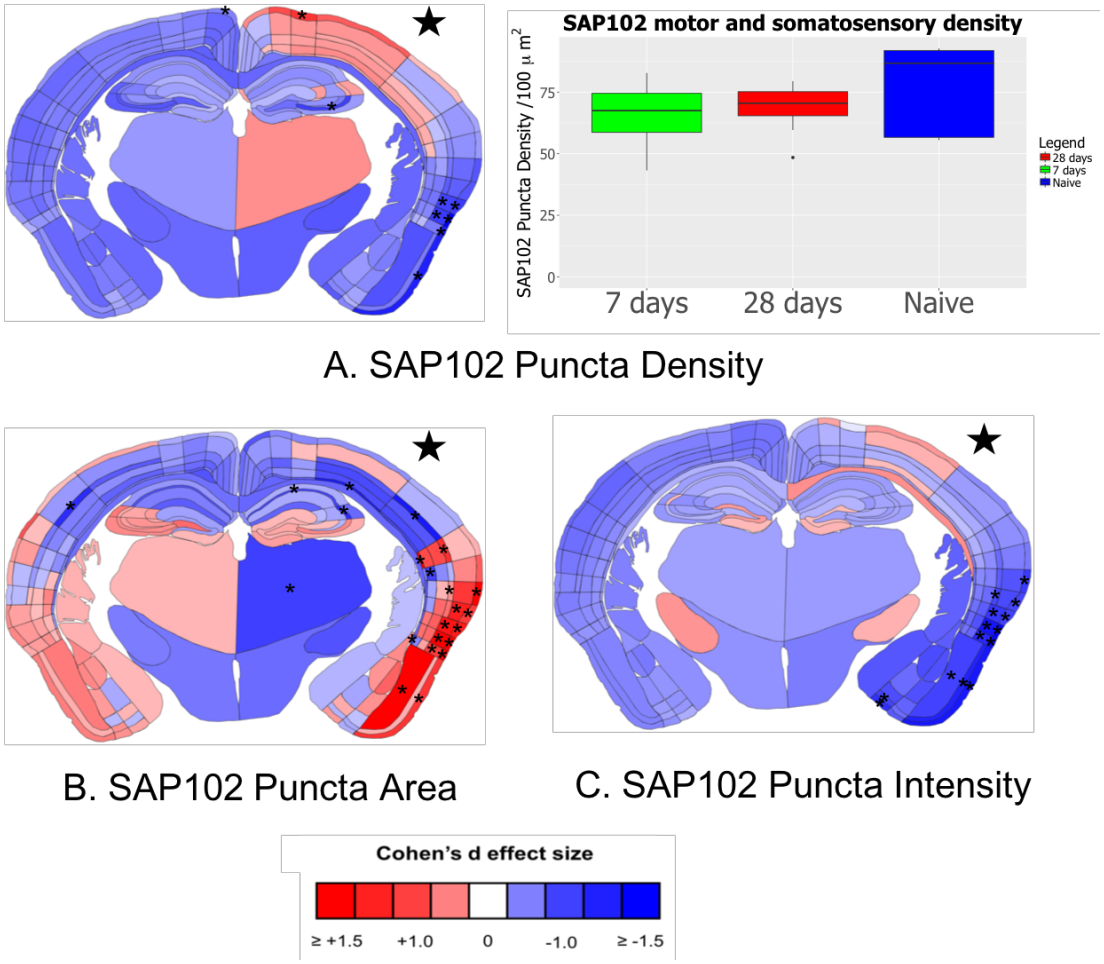

Figure 4.18: Subregional SAP102 synaptome map comparing 7 and 28 days in injury group *looking at SAP102 puncta density including a boxplot graph of ipsilateral motor and somatosensory PSD95 at 7 days, 28 days and naïve mice (A), SAP102 puncta area (B) and SAP102 puncta intensity (C). Large black star identifies side of fluid percussion. [* = p<0.05]*

4.3.8 Correlation between PSD95 and SAP102 following LFPI

Next, we aimed to examine the relationship between changes observed in PSD95 and SAP102. To determine this, we first assessed the relationship between SAP102 and PSD95 in the naïve mice cohort (n=5). We correlated the mean values of PSD95 and SAP102 across 222 sub-regions **(Figure 4.19, A1-3)**. We found very strong statistically significant positive correlation between PSD95 and SAP102 density ($r=0.963$; $p<0.0001$) and area ($r=0.937$; $p<0.0001$). We also observed a positive correlation between PSD95 and SAP102 for puncta intensity albeit less strong ($r=0.474$; $p<0.0001$). We then aimed to examine the relationship between the changes seen after LFPI between PSD95 and SAP102. To do this, we correlated the Cohen's *d* effect sizes for PSD95 and SAP102 puncta parameters across the 7 and 28-day time-points **(Figure 4.19, B)**. We found that at 7 days there was a strongly positive correlation between PSD95 and SAP102 intensity ($r=0.9054$; $p<0.0001$). There were also statistically significant positive relationships between density ($r=0.5912$; $p<0.0001$) and size ($r=0.627$; $p<0.0001$). At 28 days, density was found to have a very strong positive correlation ($r=0.8463$; $p<0.0001$) compared to size ($r=0.6803$; $p<0.0001$) and intensity ($r=0.6645$; $p<0.0001$). These findings point towards a positive relationship between PSD95 and SAP102 following an LFPI. Interestingly, there were differences in the strength of correlation between the time-points. At 7 days, puncta intensity showed strong correlation ($r=0.905$) which may reflect a close relationship between the changes of the amount of PSD95 and SAP102 protein within the synapse after injury. The relationship for puncta density at 7 days was not as strong ($r=0.5912$) suggesting differential susceptibility to PSD95 and SAP102 dominant synapses. However, by 28 days there was a stronger correlation of PSD95 and SAP102 density ($r=0.8463$) reflecting that the degree of puncta loss for the two proteins had become more aligned.

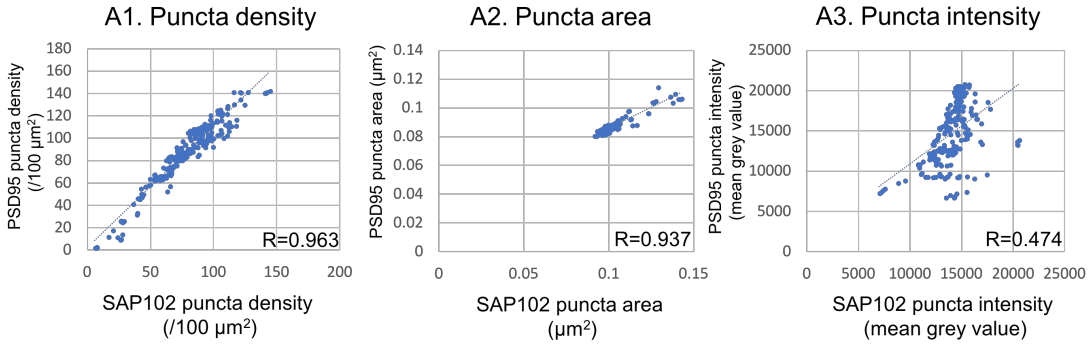

B	Synapse parameters		
	Density	Size	Intensity
7 days	0.5912****	0.627****	0.9054****
28 days	0.8463****	0.6803****	0.6645****

Figure 4.19: Correlation between PSD95 and SAP102 puncta parameters. *Correlation between PSD95 and SAP102 puncta parameters in 222 sub-regions in naïve mice (n=5) for puncta density (A1), puncta area (A2) and puncta intensity (A3). Alongside this, we examined the relation between the Pearson correlation coefficient following LFPI for the three parameters across 7 and 28 days (B) [**** = p<0.0001]*

4.3.9 Impact of LFPI on the presynaptic protein SV2A

To further examine the synaptic effects of LFPI on the synapse, we investigated the presynaptic protein SV2A. Given our observation of reduction in PSD95 and SAP102 density at 28 days, we opted to investigate SV2A at this time-point. Using a different brain section to the one imaged with the SDM, the protein was tagged with an immunohistochemistry protocol and then imaged using wide field florescence microcopy **(Figure 4.20, A)**. Twelve brain regions (ipsilateral and contralateral cortex, hippocampus, thalamus, hypothalamus, subcortical plate and striatum) were delineated using ImageJ and a raw florescence intensity measured for SV2A. To help address for variation in SV2A intensity across brains, we normalized the value by deducting the SV2A intensity of the corpus callosum from the regional value and then dividing this by the SV2A intensity value of the whole mouse brain. A two-way ANOVA showed a significant difference between the injury and sham groups (p=0.0005). There were significant reductions in SV2A value in the injury cohort compared to sham in the contralateral cortex (p=0.036), hippocampus (p=0.02) and thalamus (p=0.017). We also observed a significant increase in SV2A in the ipsilateral cortex in the injury group compared to the sham group (p=0.011). To better understand the

relationship between the changes in SV2A and the postsynaptic proteins PSD95 and SAP102, we correlated the synapse metrics of the postsynaptic proteins and the normalized intensity value of SV2A in 12 mice (injury n=7; sham n=5). We opted to examine this relationship in the contralateral hippocampus as it provided insight into the relationship between pre- and post-synaptic proteins downstream from axonal injury. We found that there were strong positive correlations between SV2A and both PSD95 density (r=0.779; p=0.003) and SAP102 (r=0.711; p=0.009) **(Figure 4.20, B and C)**. A similar positive, statistically significant relationship was observed between SV2A and PSD95 puncta intensity (r=0.787; p=0.002) and SAP102 puncta intensity (r=0.713; p=0.009). Interestingly, SV2A was negatively correlated with PSD95 puncta area with a Pearson correlation coefficient of -0.648 (p=0.02). SAP102 puncta area was also negatively correlated with SV2A (r=-0.567) but this did not reach statistical significance (p>0.05). This data shows that following LFPI, the presynaptic protein SV2A mirrors changes observed in PSD95 and SAP102. We found evidence of significant reductions in SV2A normalized intensity in the contralateral cortex, hippocampus and thalamus which we had also seen in the more detailed high-resolution mapping of PSD95 and SAP102. When we looked more closely at this relationship within the contralateral hippocampus we found statistically significant relationships between SV2A and both PSD95 and SAP102 density and intensity. This is supportive evidence of synaptic loss distal to the injury site at 28 days post-LFPI. Interestingly, PSD95 puncta size was negatively correlated with SV2A suggesting that loss of presynaptic bouton may occur more within smaller synapses.

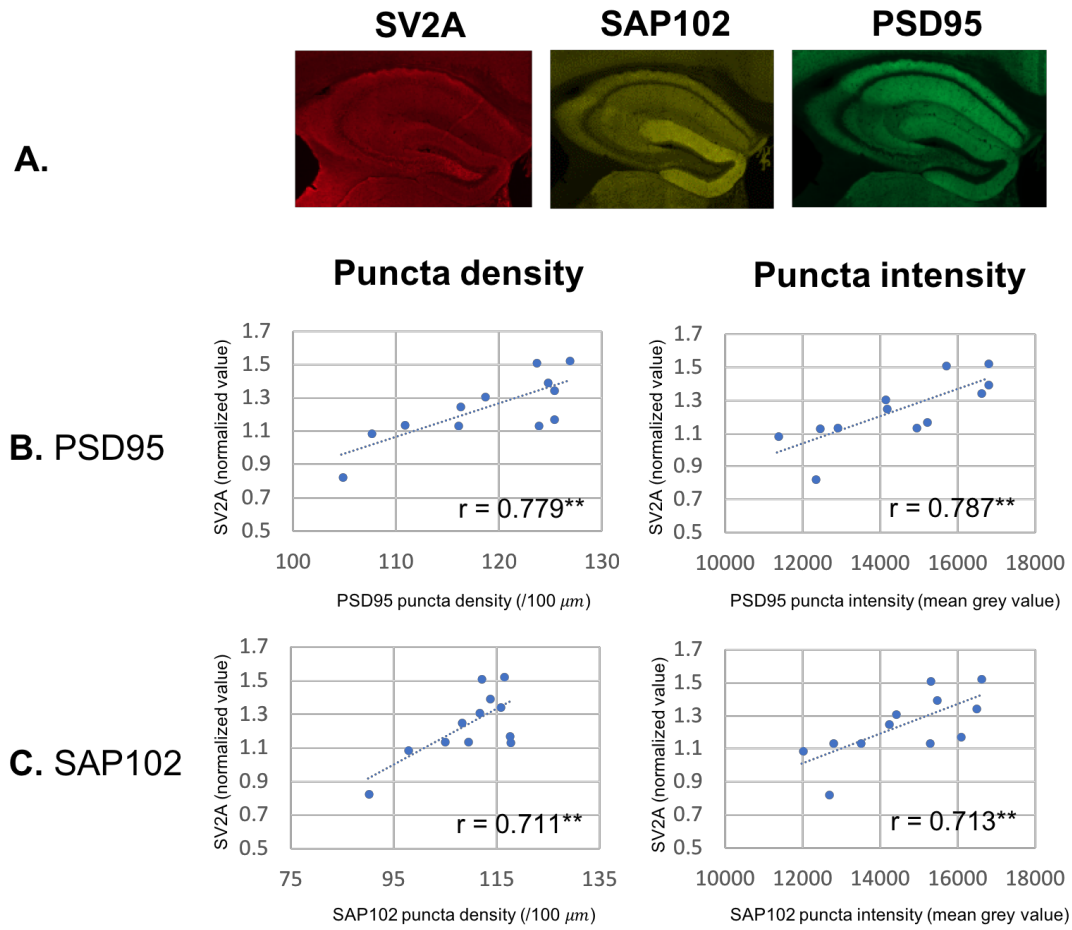

Figure 4.20: Correlation between PSD95 and SAP102 puncta parameters and SV2A*. Wide field fluorescence image of three synaptic proteins imaged with difference fluorescence wavelengths: SV2A (far red), SAP102 (red) and PSD95 (green) (A). Correlation between PSD95 (B) and SAP102 (C) puncta density and intensity (injury n=7; sham n=5) in the contralateral hippocampus and normalised SV2A value [** p≤0.01]*

4.3.10 Correlation of PSD95 and SAP102 metrics with Iba-1

Finally, we aimed to examine the relationship between the three puncta metrics and Iba1. There is evidence that microglia play a role in removing the synapse in both health and disease (Soyon Hong et al. 2016). To determine the relationship between PSD95, SAP102 and Iba-1 we looked at the Pearson correlation coefficient between each of the proteins' three metrics and the number of Iba-1 positive cells. As we were interested in the role of microglia in synaptic loss in the chronic phase of TBI we focused our analysis on the contralateral cortex and hippocampus at 28 days in a cohort of 17 mice. This revealed a statistically significant negative correlation between

Iba-1 cell count and both PSD95 (r = -0.609; p=0.0001) and SAP102 (r = -0.671; p<0.0001) puncta density **(Figure 4.21)**. Interestingly, this was reflected with a statistically significant positive correlation between both PSD95 and SAP102 puncta area. SAP102 puncta intensity and Iba-1 count had a significant negative correlation (r = -0.545; p=0.0009). The observations made in the synaptome map and Iba-1 cell counting indicate that at 28 days the contralateral hemisphere undergoes a significant increase in microglia numbers alongside a reduction in both PSD95 and SAP102 puncta density. This relationship is significantly correlated in our dataset. Studies within Alzheimer mice models have observed the phagocytic role of microglia in early synapse loss (S. Hong et al. 2016). This data shows a negative association between synapse and microglia numbers which fits with these observations however does not conclude direction causation. Similarly, the positive correlation between Iba-1 and puncta size could be explained by the phagocytosis of smaller synapses by the microglia.

	Synapse parameters		
	Density	**Size**	**Intensity**
PSD95	-0.609***	0.674****	0.167 (ns)
SAP102	-0.671****	0.491**	-0.545***

Figure 4.21: Correlation between PSD95 and SAP102 puncta parameters and Iba-1*. Correlation between PSD95 and SAP102 puncta parameters in the contralateral hippocampus and cortex across 17 mice (both sham and injury) [**** p≤0.0001; *** p≤0.001; ** p≤0.01; * p≤0.05; ns p>0.05]*

4.4 CHAPTER DISCUSSION AND CONCLUSION

In this chapter, we investigated the impact of a fluid percussion injury on two post-synaptic density proteins, PSD95 and SAP102, using a transgenic knock-in reporter mouse model. Utilizing a machine learning approach, we were able to interrogate synaptic changes across a whole coronal mouse brain section and produced synaptome maps for both proteins' puncta density, area and intensity. This provided highly detailed spatial and temporal insights into alterations in the synaptic proteins PSD95 and SAP102 after a traumatic injury. Our main findings were a progressive alteration in the synaptome of the injury mice. This reorganisation was most pronounced at 28 days post-injury when we observed reductions in both PSD95 and

SAP102 puncta density and intensity. These changes were centred around the hippocampus and cortex contralateral to the side of the injury. Our unbiased, whole brain approach, highlighted a reduction in both synapse numbers and the number PSD95 and SAP102 molecules within the remaining synapses in regions distal to the injury site. Coupled to this, we also observed a significant increase in PSD95 puncta density in the injury cohort from 7 to 28 days. Underpinning these observations, we found no significant differences in the area of the major brain regions between the injury and sham mice and evidence of elevated aggregates of APP in the ipsilateral cortex that peaked at 7 days. Alongside this, we observed progressive inflammatory changes, as index with Iba-1, within the cortex and hippocampus. Collectively, these data confirm histopathological findings in keeping with mild TBI and provide a firm basis to examine changes in the PSD95 and SAP102 synaptome. Interestingly, our data showed a negative correlation between Iba-1 positive cell numbers and both PSD95 and SAP102 density within the contralateral hippocampus. This correlation, though not evidence of direct causation, fits with other data that have implicated the microglia in synaptic pruning in disease processes (S. Hong et al. 2016). Overall, we conclude that we validated a model of mild LFPI in a cohort of transgenic knockin reporter mice. This model has allowed us to interrogate the impact of a mild traumatic injury on the postsynaptic density proteins PSD95 and SAP102. We observed a reorganization of the synaptome following injury which was progressive and involved brain regions distal from the injury site and also showed evidence of synaptic recovery. We will discuss these findings and their implications in greater detail in Chapter 5 however they highlight that TBI leads to synatopathy long after the initial insult but with evidence of synaptogenesis.

CHAPTER 5

Discussion and Conclusions

5.1 SUMMARY OF FINDINGS

5.1.1 Wildtype characterization of mild LFPI

To examine the impact of TBI on the synapse, we first had to develop and validate a protocol for a mild fluid percussion injury model. In a cohort of twenty-six mice (15 injury and 11 sham) we examined the impact of a mild lateral percussion pulse (1.18±0.03atm) on righting time, neuronal morphology, axonal injury and inflammatory response. We found evidence of a significantly elevated righting time in the injury cohort (431.4±178.2 vs 40.3±57.5 seconds; $p<0.0001$). Coupled to this, H+E staining demonstrated altered neuronal morphology in the ipsilateral cortex to the percussion pulse in the injury group. We also observed significantly more APP-positive aggregates in the ipsilateral corpus callosum in the injury mice compared to the sham (74.1±38.6 vs 1.8±2.1; $p<0.0001$). We then examined inflammatory response after the LFPI and found increased numbers of microglia and astrocytes, as indexed with Iba-1 and GFAP respectively, in the ipsilateral compared to the contralateral cortex in both the injury and sham mice. This highlighted that even the act of performing the craniectomy on the sham mice led to an inflammatory response. The application of the percussion pulse, did however, lead to a significantly elevated number of both microglia and astrocytes in the ipsilateral hippocampus in the injury cohort compared to the sham. Taken together, these findings validated a model of mild LFPI in mice that led to elevated righting time, altered cortical neuronal morphology and axonal pathology in the injury cohort. It also demonstrated that the act of removing the cranial bone in the sham mice led to a degree of cortical injury and inflammatory response.

5.1.2 Behavioural, axonal and inflammatory changes in knock-in cohort

To internally validate our knock-in reporter cohort of mice we examined differences in the behavioural, axonal and inflammatory response between the injury and sham groups. Much like in the wildtype characterization experiment, we found significantly elevated righting time in the injury cohort compared to the sham (562.4±271 vs 79±118.6 seconds; $p<0.0001$). We examined later time-points in the knock-in cohort, however, found elevated corpus callosum APP-positive aggregates in the injury group compared to the sham. These findings were significantly elevated at 7 days (44.7±25.4 vs 11.5±18.; $p=0.0018$) and remained elevated in the injury group at 28 days, however the difference was no longer statistically significant (27.6±22.2 vs 9.3±10.7; $p=0.07$). To investigate inflammatory response, we immunostained for microglia and found evidence of elevated iba-1 positive cells at 7 days (1011±386 vs

563.8±251.4; p=0.012) and 28 days (837.5±398 vs 434.9±223.5, p=0.001). Interestingly, within the contralateral hemisphere to the LFPI there was no significant differences in iba-1 cell counts at 7 days been the injury and sham cohort. However, at 28 days injury group had significantly elevated microglia in both the cortex (1017±473.3 vs 397.6±226.4; p=0.01) and hippocampus (227.5±114.9 vs 125±55; p=0.03). These findings highlight that post-LFPI inflammation is a progressive process with increased microglial numbers in brain regions distal to the percussion site a month after ictus. Overall, these observations of elevated righting time, axonal injury and increased microglial activity internally validate the knock-in cohort as a precursor to investigating the changes in PSD95 and SAP102.

5.1.3 Temporal and spatial changes in PSD95 following LFPI

After validating the behavioural and cellular changes in the injury cohort, we then investigated the impact of a mild percussion pulse on the postsynaptic protein PSD95. Utilizing a knock-in reporter mouse model, confocal microscopy and machine learning approaches we quantified PSD95 puncta density, size and intensity. There was no difference in PSD95 density within the ipsilateral cortex in the injury cohort compared to the sham. A closer investigation of the cortical sub-regions found no statistically significant differences between the injury and sham cohorts across both time-points and all cortical sub-regions. However, when compared to naïve mice (no surgery), both the injury and sham cohorts exhibited significantly reduced PSD95 in the ipsilateral motor and somatosensory regions. These findings highlight that the craniectomy in the sham group led to a pronounced reduction in PSD95 density in the ipsilateral cortex which was comparable to the injury cohort (which experienced both a craniectomy and percussion pulse). To further investigate the effect of the percussion pulse on PSD95 distal brain regions, we created whole brain synaptome maps for PSD95 puncta density, size and intensity across the two time-points (7 and 28 days). Cohen's *d* effect sizes were calculated and spatial heat maps constructed. At 7 days, there was no significant differences in the synaptic parameters between the injury and sham mice. Conversely, at 28 days, we observed a pronounced and statistically significant reduction in PSD95 puncta density spanning regions of the cortex bilaterally (somatosensory and auditory regions) and the contralateral hippocampus (CA1, CA3 and dentate gyrus). These findings show that synaptic loss after a traumatic insult is a progressive process that continues to occur up to a month after the initial injury. Coupled to this, synapse loss happens in regions distal to the

injury site. We then examined the temporal profile of PSD95 in the injury cohort between 7 and 28 days. This demonstrated that PSD95 puncta density increased from 7 to 28 days within the ipsilateral motor and somatosensory regions. This process of recovery occurred in tandem with reductions in density in the contralateral cortex and in the ipsilateral cortex distal to the percussion site. This highlights that the PSD95 synaptome is a dynamic entity with both sub-regional recovery and loss happening in tandem. Coupled to this finding, we observed a significant increase in PSD95 puncta size in the ipsilateral cortex and cortical sub-plate distal to the percussion site. Alongside this, there was a significant reduction in PSD95 puncta intensity within a similar distribution in the ipsilateral cortex. These findings point towards a temporal increase in PSD95 puncta size along with a reduction in density and intensity. Together, this data suggests a preferential loss of smaller synapses over time and a shift to larger puncta but with an associated reduction in PSD95 protein within each synapse.

5.1.4 Temporal spatial changes in SAP102 following LFPI

The SAP102 synaptome demonstrated less observed changes to LFPI compared to PSD95. There was no significant reduction in SAP102 density between the injury cohort and both the sham and naïve mice within the ipsilateral cortex, as a whole and divided into its sub-regions. Much like PSD95, there was limited statistical significance between injury and sham miceat 7 days. By 28 days, a similar pattern of puncta density was observed in SAP102 compared to PSD95. Significant puncta density loss was seen in contralateral hippocampus. Interestingly, SAP102 demonstrated reductions in puncta size in a constellation of deep cortical layers in the ipsilateral motor and retrosplenial areas. This was mirrored in the contralateral cortex within the deep layers of the motor areas. There was a much more muted temporal recovery of SAP102 in the ipsilateral cortex compared PSD95. There was however, a much more pronounced, pattern of increasing puncta size coupled to reduced puncta intensity within the ipsilateral cortex distal to the fluid percussion site. These data, coupled to the significant positive correlation between PSD95 and SAP102 Cohen's *d* effect sizes, suggest that the broad patterns of protein loss and recovery are similar between the two proteins. However, SAP102 demonstrated less pronounced density loss compared to PSD95 and an equally limited recovery of SAP102 puncta between 7 and 28 days in the injury cohort. This may suggest that SAP102 is less susceptible to traumatic injury when compared to PSD95 or that our ability to measure it was more

limited possibly related to the intensity fluorescence from the mKO2 protein which was hemizygous compared to PSD95 which was homozygous.

5.1.5 Relationship between SV2A and Iba-1 with post-synaptic density proteins

To examine the relationship between PSD95 and SAP102 and the presynaptic terminal, we stained a series of brain section with SV2A. Within the 28-day cohort, we found evidence of SV2A reduction in the contralateral cortex, hippocampus and thalamus. Interestingly, when we correlated SV2A and the PSD95 and SAP102 puncta metrics within the contralateral hippocampus, we found significant positive correlations between SV2A and both postsynaptic protein puncta density and intensity. This finding suggests that both the pre- and post-synaptic terminals of the synapse are lost together. When then examined the relationship between Iba-1 and the two synaptic proteins in the contralateral cortex and hippocampus. We found a significant negative relationship between PSD95 and SAP102 density and Iba-1 positive cell count. This association suggests that infiltrating microglia may play a role in synaptic pruning post-TBI. Coupled to this, there was a significant positive correlation between the synaptic puncta area and number of Iba-1 cells. This suggests that as the number of microglia increases there is a shift towards larger synapses. This could be explained by microglial preferential pruning of smaller synapses. Together, this data provides a useful presynaptic control that reflect findings we observed in the postsynaptic proteins. It also provides correlative relationships between PSD95 and SAP102 and microglia.

5.2 DISCUSSION OF FINDINGS

In this thesis, we have described the impact of a LFPI on the synaptome maps of two postsynaptic proteins: PSD95 and SAP102. Our findings highlight that the synaptome is susceptible to traumatic injury showing temporal spatial patterns of loss up to 28 days after injury and in sub-regions distal to the injury site. Our findings also highlighted synaptic recovery and reorganization between 7 and 28 days in the cortex ipsilateral to the injury.

5.2.1 Delayed synapse loss occurs at 28 days after injury

Our most striking finding was a significant drop in PSD95 and SAP102 puncta density at 28 days. This was centred around the contralateral hippocampus and the cortex bilaterally. Other studies have looked primarily at early time-points (<7 days), however

a number have examined later follow-up times. Scheff and collagues used EM to examine the impact of a moderate CCI on the synapses of the ipsilateral CA1 stratum radiatum (Scheff et al. 2005). The investigators found a comparative reduction in puncta density in the injury group compared to the sham group at 30 days. However, they saw an early and dramatic reduction in puncta density at day 2 post-injury which slowly recovered at 30 days before plateauing. Semchenko observed a similar pattern using a rotatory head model in rats with a reduction in synaptic density measured with EM at 7 days followed by an increase in density up to 30 days (Semchenko et al. 2006). On the other hand, using a blast model of TBI, Meabon found similar levels of cerebellar PSD95 in the injury and sham cohorts at day 1 followed by a significant reduction in PSD95 levels in the injury group at 30 days (Meabon et al. 2016). These differing observations are a product of substantially different TBI models, both in terms of the mechanism and severity of the injury and different techniques of synapse quantification and sub-regional analysis. However, they do collectively point towards a relative reduction in synapses at 30 days after a mechanical trauma which fits with our observations. An important finding in our study was that there was a delay in synaptic density changes between the injury and sham mice. At 7 days, the puncta density between the sham and injury groups showed little significant difference. When compared to the naïve sham, there was evidence of reduction in puncta density of the ipsilateral cortex in both the injury and sham mice suggesting that the act of craniectomy alone was enough of an insult to alter synapse numbers. It also suggests that the act of applying the fluid pulse to the injury cohort set in motion a pathological process that led to progressive loss of synapses that became evident at 28 days. Other studies have observed delayed drops in synapse numbers or protein concentrations at differing time-points. Ansari and colleagues examined the impact of CCI on a number of synaptic proteins using western blot (Ansari *et al.*, 2008 (1)). The investigators found a delayed reduction in PSD95 and Synapsin-I that occurred at 48 hours while SAP97 reduced at 96 hours compared to sham. Wakade found a similar finding with a delayed drop in PSD95 at 7 days following CCI (Wakade et al. 2010). These studies found that synaptic proteins reduced at earlier time-points compared to our observations. Part of the reason for this is the regions examined were ipsilateral to the injury site and the severity of the traumatic injuries were higher. It is important to note that compared to the naïve sham mice we observed significant reductions in PSD95 density in the ipsilateral cortex at 7 days indicating that our findings are not a significant outlier compared to the literature. Collectively, these data suggest that

synapse loss is not immediate and can take time to develop highlighting a potential window for intervention.

5.2.2 The impact of traumatic axonal pathology on the synapse

We also examined post-traumatic axonal pathology in our experimental cohort to help understand its relationship with our observations in the synapse. Though our methodology was limited to the ipsilateral corpus callosum it helped provide important data into the state of axonal pathology in our cohort. We found elevated levels of APP aggregates at both 7 and 28 days, though this difference was not significant at the latter time-point. The application of an external force onto the brain leads to deformation of axons. Microtubular failure secondary to calcium influx leads to impairment of axonal transport (Douglas H Smith et al. 2013). APP, which is transported through the axon, then starts to accumulate leading to the visualised varicosities. In severe cases, primary axotomy occurs and Wallerian degeneration occur within the distal axon. Using a cortical lesion model, Gilingwater et al found evidence of degenerating synapse terminals in the striatum at day 2 post-lesion in wildtype mice which peaked at day 3 and had resolved by day 10 (Gillingwater et al. 2006). Interestingly, when they examined Wallerian Degeneration slow mice model (a spontaneous dominant mutation in mice that delays axon degeneration), they found delayed and less pronounced synaptic degeneration within the striatum. Their findings indicate that axonal pathology is intimately linked with the synapse and that protection against axon degeneration delays and limits synapse loss. Diffusion MRI studies in humans have demonstrated white matter tract degeneration post-injury which bring into question the extent of synapse loss downstream (Aoki et al. 2012). One of the strengths of our study, was the whole brain unbiased approach which highlighted that the contralateral hippocampus and in particular the dentate gyrus is vulnerable to synapse loss after injury. The loss of synapse density in the dentate gyrus had been demonstrated earlier by Gao et al after a moderate CCI (Gao et al. 2011). Our observation of a reduction in puncta density in the contralateral hippocampus and cortex is likely caused by axonal injury within the corpus callosum and hippocampal commissure which project onto the contralateral hemisphere (Zhou et al. 2013).

5.2.3 Synapse reorganization and recovery after traumatic injury

A further key finding was evidence of an increase in the density of synapses between 7 and 28 days within the ipsilateral cortex. There were significant increases within the

somatorsensory and motor regions which underlie the fluid precussion site. It is important to note that though the injury did demonstrate an increase in synaptic density at 28 compared to 7 days, it still had a lower density compared to naïve mice in the primary motor, somatosensory and dorsal auditory areas. Post-deafferentation synaptogenesis has been well documented in the past (Anderson et al. 1986). More recently, Scheff and colleagues also observed synapse recovery in the stratum radiatum of CA1 after a moderate CCI (Scheff et al. 2005). This recovery occurred from day 2 before plateauing at day 30 post-injury. Much like our finding, Scheff observed that the synapse density did not reach control levels despite following up to 60 days in his experiment. Investigators have also found similar patterns of recovery in GABAergic synapses. Erb and Povlishock examined the dorsal lateral vestibular nucleus in cats after a fluid percussion injury (Erb & Povlishock 1991). Using EM and light microscopy, they found a reduction in GABAergic puncta up until day 30 followed by a period of recovery up to 12 months after the injury. A number of studies have looked at the subject of synaptic recovery after TBI and attempted to tease out the impact of TBI secondary injury processes on synaptogenesis. To do this, hippocampal synaptic recovery was compared between bilateral entorhinal deafferentation (BED) alone and BED combined with a fluid percussion injury (FPI). Early findings from this approach found that the synaptic recovery observed in the BED model did not occur in the combined injury model (Phillips et al. 1994). This suboptimal synaptic recovery was termed ‘maladptaive synaptic plasticity’. A focus of research has been Matrix Metalloproteinases (MMPs) which are endopeptidases that affect cellular behaviour by processing various extracellular matrix molecules (Huntley 2012). Importantly, MMPs have been shown to play a role in mediating synaptic plasticity (Huntley 2012). However, a series of studies comparing BED with the combined BED and FPI model, demonstrated persistent elevates levels of a number of MMPs in the combined model suggesting that aberrant MMP elevation contributed to maladaptive synaptic recovery (Warren et al. 2012; Kim et al. 2005; Falo et al. 2006). Importantly, these studies found evidence of colocalization between MMPs and astrocytes and posited that reactive astrocytes may selectively induce MMPs. We found evidence of robust astrocyte activation at 24 hours when characterizing our wildtype cohort of mice. Astrocytes have been implicated in post-TBI impaired synaptic recovery through a number of other mechanisms. Furman et al examined the role of astrocytic calcineurin-dependent transcription factor Nuclear Factor of Activated T cells (CN/NFAT) (Furman et al. 2016). The investigators found blockade of the CN/NFAT pathway

using an adeno-associated virus led to a significant increase in the synaptogenic molecule Hevin. Similarly, Nikolakopoulou investigated another astrocyte-associated pathway involving Ephrin-B1 in a moderate CCI in mice (Nikolakopoulou et al. 2016). Following injury, the investigators observed an upregulation of Ephrin-B1 levels in hippocampal astrocytes which coincided with a decrease in the presynaptic protein VGlut1. The ablation of Ephrin-B1 accelerated the recovery of VGlut1 puncta. Finally, the authors then presented evidence that Ephrin-B1 may play a role in post-TBI synaptic recovery through STAT3 phosphorylation. This pathway has was also investigated by Tyzack et al in an axotomy model which concluded that astrocytic STAT3-regulated thrombospondin-1 contributed to post-injury synaptic remodelling (Tyzack et al. 2014). Thrombospondins are large astrocyte-secreted oligometric extracellular matrix proteins that have been found to promote synaptogenesis (Christopherson et al. 2005). Thrombospondins have been found to be elevated in both TBI patients and in preclinical models (Tran et al. 2012; Wang et al. 2016). Tran and colleagues found in an in-vitro model of TBI that thrombospondin-1 expression was significantly attenuated by a P2 receptor antagonist (Tran et al. 2012). Interestingly, addition of ATP (which is released upon traumatic damage of brain tissue), led primary culture of astrocytes to phosphorylate STAT3 (Washburn & Neary 2006). Together these data point towards a common pathway through STAT3 that regulates astrocytic thrombospondin release. From our findings and the literature, it is clear that synaptic recovery occurs following a traumatic insult to the brain. However, this process of remodelling is not complete particularly when compared to pure deafferentation models which do not include secondary brain injury processes. The astrocyte plays an important role in synaptogenesis and synaptic function in health and development (Allen & Eroglu 2017). However, a traumatic insult leads to astrocyte upregulation which appears to have a double-edged sword effect on synaptic recovery.

5.2.4 Microglia and synaptopathy after traumatic injury

Microglia are highly motile and are constantly surveying their surroundings (Nimmerjahn et al. 2005). There is also evidence that they selectively remove synaptic components in development (Paolicelli et al. 2011). The process in which microglia interact with synapses has been debated with suggestions that the phagocytosis. However, a recent study by Weinhard et al used a combination of imaging techniques to interrogate microglial-synapses interactions (Weinhard et al. 2018). They found that

microglia partial eliminate or trogocytosise (nibbling) presynaptic boutons and axons. We observed a significant increase in the number of Iba-1 positive cells in the injury compared to the sham cohort. It is important to note that craniectomy alone led to an inflammatory response in the sham cohort. However, we found a significant and temporally progressive inflammatory reaction that spread to the contralateral hemisphere at 28 days post-injury. Post-TBI inflammation has been well documented in human subjects. Both the examination of autopsy tissue and the use of in-vivo molecular imaging approaches have demonstrated evidence of chronic inflammation (Coughlin et al. 2017; Fujita et al. 2017; Victoria E. Johnson et al. 2013). In animal models, recent investigation has focused on understanding the differing phenotypes of microglia and their temporal profile. Macrophage polarization states have been applied to microglia with a distinction between 'pro-inflammatory' M1-like microglia and 'anti-inflammatory' M2-like microglia (Mosser & Edwards 2008). Jin and colleagues found a bimodal response of microglia with a M2-like peak at 7 days followed by an M1-like peak at 3 weeks (Jin et al. 2012). This reflected similar findings in a spinal cord injury model (Kigerl et al. 2009). A number of studies have suggested that chronic M1 microglia impair recovery and leads to neurodegenerative cascades (Block et al. 2007; Horn et al. 2008). However, this dichotomous distinction between M1 and M2-like microglia has been criticized as over-simplistic and that, in reality, a number of complex, overlapping polarization states are likely to be present (Jassam et al. 2017). Nonetheless, our finding of persistent microglial activation is in keeping with evidence pointing towards chronic inflammation. Interestingly, when we correlated the density of PSD95 and SAP102 with microglia numbers in the contralateral hemisphere, we found a significant negative correlation. Though this finding is an association and does not provide evidence of causation, it may suggest that as microglia numbers increased they contributed to the removal or stripping of synapses. The question of whether microglia have a role in synapse removal in disease states has been examined. In a preclinical model of Alzheimer's disease, Hong and colleagues suggested that an inappropriately activated complement pathway led to excessive microglial pruning of synapses (S. Hong et al. 2016). Wake et al used two-photon microscopy and found prolonged contact between microglia and presynaptic bouton in a model of transient cerebral ischaemia led to synapse loss (Wake et al. 2009). How microglia contribute to synaptopathy was looked at by Zhang and colleagues in an in-vitro model of inflammation and ischaemia, two important process after TBI (Zhang et al. 2014). The authors found that inducing hypoxia and

an inflammatory stimulus (lipopolysaccharide) triggered microglial-CR3 activated LTD.

5.2.5 Differential patterns PSD95 and SAP102 puncta response to LFPI

In this thesis, we investigated two synaptic proteins: PSD95 and SAP102. This allowed for comparison of the response of the proteins to a traumatic insult. We observed broadly similar responses to LFPI which was reflected by the positive correlation between the PSD95 and SAP102 Cohen's *d* effect size changes across all three puncta parameters for both time-points. The strength of this positive correlation, however, varied with only moderate positive correlations for puncta size (r=~0.6) at both time-points. When comparing the synaptome maps of puncta size, a divergence in response between PSD95 and SAP102 was notable at 28 days with a significant shift towards smaller SAP102 puncta centred around the motor and retrosplenial regions in both cortices. Scheff et al found no difference in synapse size in the CA1 after a CCI using EM during periods of denervation and synapse recovery (Scheff et al. 2005). Scheff and colleagues also studied CA1 synapses from patients with mild Alzheimer's Disease (AD) (Scheff et al. 2007). Using EM, the group observed a shift towards larger synapses in the AD cohort compared to patients with no cognitive impairment. This may be due to loss of smaller synapses during the neurodegenerative process. In our data set, we observed a temporal shift towards significantly larger puncta size (both PSD95 and SAP102) in the injury cohorts between 7 and 28 days within the ipsilateral cortex distal to the fluid percussion site. This pronounced observation may reflect a similar process of smaller synapse loss. We also noted moderate correlation of puncta density changes between the two proteins at 7 days (r=0.59). Comparing the heat maps, this is likely due to a reduction in PSD95 effect size in the ipsilateral cortex compared to SAP102, which did not demonstrate a similar reduction. This finding, along with the greater reductions in PSD95 density at 28 days, may suggest that PSD95 is more susceptible to loss following traumatic insult compared to SAP102. Coupled to this, we found that between 7 and 28 days, PSD95 puncta density showed a more pronounced recovery compared to SAP102 puncta. Within our lab, an in-house technique to subtype synapses using PSD95 and SAP102 synaptome imaging data identified 37 synaptic subtypes (Zhu *et al.*, 2018). This approach revealed a wealth of information about the synaptic diversity and that each subtype had a unique distribution across the mouse. Based on our data and prior experiments that revealed differences in synaptic protein

loss after TBI using Western Blotting (Mubeen A Ansari et al. 2008), we would expect the application of synaptic subtyping techniques would reveal differential responses to traumatic injury across the differing synapse types.

5.3 METHODOLOGICAL CONSIDERATIONS

5.3.1 The lateral fluid percussion injury model

The LFPI is a well-established and comprehensively characterized model of TBI (Thompson et al. 2005). Its strengths are its reproducibility, the ability to apply the model to mice and that the severity of the injury can be easily modified. The latter two strengths were very important for our study which aims to look at a milder injury severity and also centred on the use of a knock-in transgenic mouse model. However, from our experience the LFPI suffers from two major drawbacks. Firstly, it has a high attrition rate which in our main experiment sat at just over a fifth of randomized mice. This was an improvement compared to our wildtype characterization experiment which had an attrition rate of 35%. The main cause for mouse exclusion was dural rupture occurs after the application of the percussion pulse which is an inherent complication of the model. This high attrition rate can be very costly particularly in the context of expensive genetically modified animals. The second major weakness of the model is that the sham mice undergo a degree of brain injury during the process of bone flap removal. Despite very careful and meticulous technique, we found that we were inducing an inflammatory response in the sham mice and found that there was also a reduction in synapse density in their ipsilateral cortex. One of the major differentiator between injury and sham was the presence of APP aggregates in the corpus callosum which demonstrated that the application of the fluid pulse led to axonal injury. The similarity of synapse loss in the ipsilateral cortex of the sham mice without axonal pathology is an interesting finding, however it also likely masked the extent of the synaptic changes in the injury group when we looked at the Cohen *d* effect sizes between the cohorts.

5.3.2 Experimental design

We aimed to use robust methodological approaches to ensure our experiment was less susceptible to bias. Prior to commencing our main experiment, we undertook a pilot study of 6 mice followed up to 7 days to generate data for a power calculation. Using PSD95 density data from the ipsilateral cortex, we calculated that we required 9 mice per cohort to power the experiment. A criticism of this approach was that we

did not look at SAP102 and only concentrated on the ipsilateral cortex and puncta density. For the main experiment, we randomized the mice in the four cohorts: injury and sham across 7 and 28 days. As mice only become eligible for inclusion in the study once they were aged between 8-16 weeks, we would randomize small groups of mice across the four groups. Our randomization technique used a random number generator to ensure that no bias was introduced into the process. Our naïve cohort, however, was not randomized and was analyzed after the completion of the main experiment. This is important to note as it limits our ability to compare the naïve cohort to other groups. Alongside this, we only used the righting reflex as a behavioural test in these experiments. The righting reflex is a simple test and can only provide information in the acute phase of the injury. There are more robust means of examining the longer term effects of TBI on motor and cognitive function in mice such as the rota rod, Morris Water Maze and cognitive touch screen testing (Xiong et al. 2013; Bussey et al. 2012). This means we were unable to correlate functional changes to the observations we were making at the level of the synapse. Finally, we ensured that the primary investigator (AJ) was blinded to the mice cohort during from the tissue processing stage. A research number was applied to the mouse and a central register of the mice numbers was held by another member of the lab (SL). For logistic and technical reasons, we were unable to blind AJ to the mouse cohort from the point of injury. This may have led to bias in measuring the mouse righting time however, we felt that the main focus of the experiment was the synaptic analysis for which AJ was completely blinded during the stages of tissue processing and image analysis.

5.3.3 Unbiased imaging approach

Prior studies looking at synaptopathy following TBI either focused on specific brain regions or homogenised brains losing all spatial information. Both these two approaches tend to neglect brain regions and mean that any subtle synaptic changes are likely to be missed. As we have detailed in this thesis, TBI leads to global brain changes and therefore an approach that characterized synapses at the whole brain level is vital to better understanding post-TBI synaptopathy. We believe the high throughput and high-resolution approach we have described here is a major step in addressing the technical limitation of previous studies.

5.4 FUTURE DIRECTIONS

5.4.1 More detailed statistical analysis

We have captured a huge amount of data from the LFPI synaptome maps. In this thesis, we described a statistical analysis approach comparing the injury and sham cohorts using multiple t-tests. This approach is crude and at risk of generating false positives, particularly as there are >200 brain sub-regions and we set our p value at <0.05. An alternative approach would have been to utilise a two-way ANOVA with multiple comparison analysis, however our concern with this approach was that it would be too conservative due to the high number of sub-regions and miss potentially significant findings. We deemed our approach an appropriate middle ground that focused on sub-region clustering and then set a higher p-value threshold for isolated sub-regions. One more advanced technique to address these limitations is Bayesian inference approaches. Within the Seth Grant lab, Dr. Nathan Skene developed a Bayesian model to analyse Dr. Melissa Cizeron's synaptome dataset. This model could be modified to analyse the LFPI synaptome data

5.4.2 Colocalization and synapse subtyping

In this thesis, we described the analysis of three raw puncta parameters: size, density and intensity. Using this base raw data, there are further forms of analysis which can be applied to our dataset to gain deeper insights into post-TBI synaptopathy. In the first instance, the degree of colocalization between PSD95 and SAP102 can be examined to better understand how the relationship between the two proteins is affected by a traumatic insult. To further investigate synapse subtypes, Dr. Zhen Qui, in the Seth Grant lab, devised an advanced machine learning technique called the Weighted Clustering Ensemble method that used PSD95 and SAP102 synaptome data to classify individual synapses in an unsupervised manner. This technique identified 37 synaptic subtypes: 11 subtypes of PSD95-only Types, 7 subtypes of SAP102-only Types, and 19 subtypes of colocalized Types (Zhu et al. 2018). We plan on applying this approach to look at more granular detail on synaptic subtype changes following TBI.

5.4.3 SV2A molecular imaging

Recently, a novel PET ligand has been developed that targets SV2A and has been shown to measure synaptic density in-vivo (Finnema et al. 2016). During the last year of my PhD, we set up a collaboration with UCB Pharma (the company that developed

the ligand) and acquired the SV2A precursor in Edinburgh. A focus of future investigation will be the use of this ligand to translate our synapse preclinical findings in the LFPI model into humans. In the first instance, we aim to use autoradiography to assess the efficacy of the ligand on tissue sections from LFPI experiments. From there, we would aim to examine the ligand in-vivo in humans who had sustained a TBI.

5.5 CONCLUSIONS

In this thesis, we utilized the combination of a knock-in transgenic mouse model, high throughput imaging techniques and machine learning approaches to characterize whole synaptome reorganisation of the postsynaptic density proteins PSD95 and SAP102 following a mild traumatic fluid percussion injury. Our results demonstrated that synapse loss is a progressive process that happens up to a month post-injury. However, we also observed evidence of synapse recovery in the ipsilateral cortex between 7 and 28 suggesting that post-TBI synaptopathy is a dynamic process with both loss and recovery happening in tandem. Despite broadly similar patterns of change, we observed nuanced differences between SAP102 and PSD95 suggesting differences in synaptic subtypes responses to trauma. Finally, we observed a negative correlation between microglia numbers and synapse density suggesting a potential role for microglia in post-TBI synaptopathy. Collectively, this thesis provides one of the most comprehensive insights into synaptopathy following a TBI and lays groundwork for more detailed statistical and imaging analysis of the dataset and the use of molecular imaging techniques to translate our findings into humans.

REFERENCES

Aarabi, B. et al., 2014. Predictors of outcome in civilian gunshot wounds to the head. *J Neurosurg*, 120(120), pp.1138–1146.

Abd-Elfattah Foda, M.A. & Marmarou, A., 1994. A new model of diffuse brain injury in rats. *Journal of Neurosurgery*, 80(2), pp.301–313.

Albert-Weissenberger, C. et al., 2012. An experimental protocol for mimicking pathomechanisms of traumatic brain injury in mice. *Experimental & Translational Stroke Medicine*, 4(1), p.1.

Alexander, A.L. et al., 2007. Diffusion tensor imaging of the brain. *Neurotherapeutics : the journal of the American Society for Experimental NeuroTherapeutics*, 4(3), pp.316–29.

Allen, N.J. & Eroglu, C., 2017. Cell Biology of Astrocyte-Synapse Interactions. *Neuron*, 96, pp.697–708.

Ambrosini, E. et al., 2003. Astrocytes are the major intracerebral source of macrophage inflammatory protein-3?/CCL20 in relapsing experimental autoimmune encephalomyelitis and in vitro. *Glia*, 41(3), pp.290–300.

Anderson, K.J., Scheff, S.W. & DeKosky, S.T., 1986. Reactive synaptogenesis in hippocampal area CA1 of aged and young adult rats. *The Journal of Comparative Neurology*, 252(3), pp.374–384.

Ansari, M.A., Roberts, K.N. & Scheff, S.W., 2008. A Time Course of Contusion-Induced Oxidative Stress and Synaptic Proteins in Cortex in a Rat Model of TBI. *Journal of Neurotrauma*, 25(5), pp.513–526.

Ansari, M.A., Roberts, K.N. & Scheff, S.W., 2008. Oxidative stress and modification of synaptic proteins in hippocampus after traumatic brain injury. *Free radical biology & medicine*, 45(4), pp.443–52.

Aoki, Y. et al., 2012. Diffusion tensor imaging studies of mild traumatic brain injury: a meta-analysis. *Journal of Neurology, Neurosurgery & Psychiatry*, 83(9), pp.870–876.

Arundine, M. et al., 2003. Enhanced Vulnerability to NMDA Toxicity in Sublethal Traumatic Neuronal Injury *In Vitro*. *Journal of Neurotrauma*, 20(12), pp.1377–1395.

Arundine, M. et al., 2004. Vulnerability of central neurons to secondary insults after in vitro mechanical stretch. *The Journal of neuroscience : the official journal of the Society for Neuroscience*, 24(37), pp.8106–23.

Bayés, A. et al., 2011. Characterization of the proteome, diseases and evolution of the human postsynaptic density. *Nature neuroscience*, 14(1), pp.19–21.

Bayés, A. et al., 2012. Comparative study of human and mouse postsynaptic proteomes finds high compositional conservation and abundance differences for key synaptic proteins. *PloS one*, 7(10), p.e46683.

Bazarian, J.J. et al., 2006. Accuracy of Mild Traumatic Brain Injury Case Ascertainment Using ICD-9 Codes. *Academic Emergency Medicine*, 13(1), pp.31–38.

Beattie, E.C. et al., 2002. Control of Synaptic Strength by Glial TNFalpha. *Science*, 295(5563), pp.2282–2285.

Bell, J.D. et al., 2009. PICK1-mediated GluR2 endocytosis contributes to cellular injury after neuronal trauma. *Cell Death and Differentiation*, 16(12), pp.1665–1680.

Block, M.L., Zecca, L. & Hong, J.-S., 2007. Microglia-mediated neurotoxicity: uncovering the molecular mechanisms. *Nature Reviews Neuroscience*, 8(1), pp.57–69.

Branco, T. & Staras, K., 2009. The probability of neurotransmitter release: variability and feedback control at single synapses. *Nature Reviews Neuroscience*, 10(5), pp.373–383.

Breiman, L., 2001. Random Forests. *Machine Learning*, 45(1), pp.5–32.

Broadhead, M.J. et al., 2016. PSD95 nanoclusters are postsynaptic building blocks in hippocampus circuits. *Scientific Reports*, 6(1), p.24626.

Browne, K.D. et al., 2011. Mild Traumatic Brain Injury and Diffuse Axonal Injury in Swine. *Journal of Neurotrauma*, 28(9), pp.1747–1755.

Bruns, J. & Hauser, W.A., 2003. The epidemiology of traumatic brain injury: a review. *Epilepsia*, 44 Suppl 1(2), pp.2–10.

Bumbergs, P.C. et al., 1995. Topography of Axonal Injury as Defined by Amyloid Precursor Protein and the Sector Scoring Method in Mild and Severe Closed Head Injury. *Journal of Neurotrauma*, 12(4), pp.565–572.

Bussey, T.J. et al., 2012. New translational assays for preclinical modelling of cognition in schizophrenia: the touchscreen testing method for mice and rats. *Neuropharmacology*, 62(3), pp.1191–203.

Byrnes, K.R. et al., 2014. FDG-PET imaging in mild traumatic brain injury: a critical review. *Frontiers in neuroenergetics*, 5, p.13.

Canty, A.J., Huang, L., et al., 2013. In-vivo single neuron axotomy triggers axon regeneration to restore synaptic density in specific cortical circuits. *Nature communications*, 4, p.2038.

Canty, A.J., Teles-Grilo Ruivo, L.M., et al., 2013. Synaptic elimination and protection after minimal injury depend on cell type and their prelesion structural dynamics in the adult cerebral cortex. *The Journal of neuroscience : the official journal of the Society for Neuroscience*, 33(25), pp.10374–10383.

Cao, T. et al., 2012. Morphological and genetic activation of microglia after diffuse traumatic brain injury in the rat. *Neuroscience*, 225, pp.65–75.

Carbonell, W.S. et al., 1998. Adaptation of the Fluid Percussion Injury Model to the Mouse. *Journal of Neurotrauma*, 15(3), pp.217–229.

Carlin, R.K. et al., 1980. Isolation and characterization of postsynaptic densities from various brain regions: enrichment of different types of postsynaptic densities. *The Journal of cell biology*, 86(3), pp.831–45.

Carroll, L. et al., 2004. Methodological issues and research recommendations for mild traumatic brain injury: the who collaborating centre task force on mild traumatic brain injury. *Journal of Rehabilitation Medicine*, 36, pp.113–125.

Castejòn, O.J., Valero, C. & Dìaz, M., 1995. Synaptic degenerative changes in human traumatic brain edema. An electron microscopic study of cerebral cortical biopsies. *Journal of neurosurgical sciences*, 39(1), pp.47–65.

Chamoun, R. et al., 2010. Role of extracellular glutamate measured by cerebral microdialysis in severe traumatic brain injury. *Journal of Neurosurgery*, 113(3), pp.564–570.

Cheng, D. et al., 2006. Relative and Absolute Quantification of Postsynaptic Density Proteome Isolated from Rat Forebrain and Cerebellum. *Molecular & Cellular Proteomics*, 5(6), pp.1158–1170.

Cho, K.O., Hunt, C.A. & Kennedy, M.B., 1992. The rat brain postsynaptic density fraction contains a homolog of the Drosophila discs-large tumor suppressor protein. *Neuron*, 9(5), pp.929–42.

Christopherson, K.S. et al., 2005. Thrombospondins Are Astrocyte-Secreted Proteins that Promote CNS Synaptogenesis. *Cell*, 120(3), pp.421–433.

Clark, R.S.B. et al., 1994. Neutrophil Accumulation After Traumatic Brain Injury in Rats: Comparison of Weight Drop and Controlled Cortical Impact Models. *Journal of Neurotrauma*, 11(5), pp.499–506.

Colton, C.A., 2009. Heterogeneity of Microglial Activation in the Innate Immune Response in the Brain. *Journal of Neuroimmune Pharmacology*, 4(4), pp.399–418.

Corsellis, J., 1989. Boxing and the brain. *BMJ : British Medical Journal*, 298(6669), pp.318–319.

Coughlin, J.M. et al., 2017. Imaging of Glial Cell Activation and White Matter Integrity in Brains of Active and Recently Retired National Football League Players. *JAMA Neurology*, 74(1), p.67.

Cuthbert, P.C. et al., 2007. Synapse-Associated Protein 102/dlgh3 Couples the NMDA Receptor to Specific Plasticity Pathways and Learning Strategies. *Journal of Neuroscience*, 27(10), pp.2673–2682.

D'Ambrosio, R. et al., 1998. Selective loss of hippocampal long-term potentiation, but not depression, following fluid percussion injury. *Brain research*, 786(1–2), pp.64–79.

Dixon, C.E. et al., 1991. A controlled cortical impact model of traumatic brain injury in the rat. *Journal of neuroscience methods*, 39(3), pp.253–62.

Dolorfo, C.L. & Amaral, D.G., 1998. Entorhinal cortex of the rat: Topographic organization of the cells of origin of the perforant path projection to the dentate gyrus. *The Journal of Comparative Neurology*, 398(1), pp.25–48.

Eakin, K., Rowe, R.K. & Lifshitz, J., 2015. *Modeling Fluid Percussion Injury: Relevance to Human Traumatic Brain Injury*, CRC Press/Taylor & Francis.

Ehrlich, I. et al., 2007. PSD-95 is required for activity-driven synapse stabilization. *Proceedings of the National Academy of Sciences of the United States of America*, 104(10), pp.4176–81.

Ehrlich, I. & Malinow, R., 2004. Postsynaptic Density 95 controls AMPA Receptor Incorporation during Long-Term Potentiation and Experience-Driven Synaptic Plasticity. *Journal of Neuroscience*, 24(4), pp.916–927.

El-Husseini, A.E. et al., 2000. PSD-95 involvement in maturation of excitatory synapses. *Science (New York, N.Y.)*, 290(5495), pp.1364–8.

Elias, G.M. et al., 2008. Differential trafficking of AMPA and NMDA receptors by SAP102 and PSD-95 underlies synapse development. *Proceedings of the National Academy of Sciences*, 105(52), pp.20953–20958.

Elias, G.M. et al., 2006. Synapse-Specific and Developmentally Regulated Targeting of AMPA Receptors by a Family of MAGUK Scaffolding Proteins. *Neuron*, 52(2), pp.307–320.

Erb, D.E. & Povlishock, J.T., 1991. Neuroplasticity following traumatic brain injury: a study of GABAergic terminal loss and recovery in the cat dorsal lateral vestibular nucleus. *Experimental brain research*, 83(2), pp.253–67.

Falo, M.C. et al., 2006. Matrix metalloproteinase-3 expression profile differentiates adaptive and maladaptive synaptic plasticity induced by traumatic brain injury. *Journal of Neuroscience Research*, 84(4), pp.768–781.

Faul, M. et al., 2010. Traumatic brain injury in the United States: national estimates of prevalence and incidence, 2002-2006. *Injury Prevention*, 16(Supplement 1), pp.A268–A268.

Feeney, D.M. et al., 1981. Responses to cortical injury: I. Methodology and local effects of contusions in the rat. *Brain research*, 211(1), pp.67–77.

Fernández, E. et al., 2009. Targeted tandem affinity purification of PSD-95 recovers core postsynaptic complexes and schizophrenia susceptibility proteins. *Molecular systems biology*, 5, p.269.

Fineman, I. et al., 1993. Concussive brain injury is associated with a prolonged accumulation of calcium: a 45Ca autoradiographic study. *Brain research*, 624(1–2), pp.94–102.

Finnema, S.J. et al., 2016. Imaging synaptic density in the living human brain. *Science*

translational medicine, 8(348), p.348ra96.

Folkersma, H. et al., 2011. Increased cerebral (R)-[(11)C]PK11195 uptake and glutamate release in a rat model of traumatic brain injury: a longitudinal pilot study. *Journal of neuroinflammation*, 8(1), p.67.

Frank, R.A.W. et al., 2016. NMDA receptors are selectively partitioned into complexes and supercomplexes during synapse maturation. *Nature Communications*, 7, p.11264.

Fromer, M. et al., 2014. De novo mutations in schizophrenia implicate synaptic networks. *Nature*, 506(7487), pp.179–184.

Fujita, M. et al., 2017. *PET imaging of translocator protein detects inflammation after traumatic brain injury in the areas with no MRI change*, Society of Nuclear Medicine.

Fukaya, M. et al., 1999. Distinct spatiotemporal expression of mRNAs for the PSD-95/SAP90 protein family in the mouse brain. *Neuroscience research*, 33(2), pp.111–8.

Fukaya, M. & Watanabe, M., 2000. Improved immunohistochemical detection of postsynaptically located PSD-95/SAP90 protein family by protease section pretreatment: a study in the adult mouse brain. *The Journal of comparative neurology*, 426(4), pp.572–86.

Furman, J.L. et al., 2016. Blockade of Astrocytic Calcineurin / NFAT Signaling Helps to Normalize Hippocampal Synaptic Function and Plasticity in a Rat Model of Traumatic Brain Injury. , 36(5), pp.1502–1515.

Gao, X. et al., 2011. Moderate traumatic brain injury causes acute dendritic and synaptic degeneration in the hippocampal dentate gyrus. *PloS one*, 6(9), p.e24566.

Gillingwater, T.H. et al., 2006. Delayed synaptic degeneration in the CNS of Wlds mice after cortical lesion. *Brain*, 129(6), pp.1546–1556.

Gray, E.G., 1959. Axo-somatic and axo-dendritic synapses of the cerebral cortex: an electron microscope study. *Journal of anatomy*, 93(Pt 4), pp.420–33.

Hall, E.D. et al., 2005. Spatial and Temporal Characteristics of Neurodegeneration after Controlled Cortical Impact in Mice: More than a Focal Brain Injury. *Journal of Neurotrauma*, 22(2), pp.252–265.

Hamm, R.J., 2001. Neurobehavioral assessment of outcome following traumatic brain injury in rats: an evaluation of selected measures. *Journal of neurotrauma*, 18(11), pp.1207–16.

Harris, K.M. & Weinberg, R.J., 2012. Ultrastructure of Synapses in the Mammalian Brain. *Cold Spring Harbor Perspectives in Biology*, 4(5), pp.a005587–a005587.

Hellström, T. et al., 2017. Predicting Outcome 12 Months after Mild Traumatic Brain Injury in Patients Admitted to a Neurosurgery Service. *Frontiers in Neurology*, 8, p.125.

Hicks, R. et al., 1996. Temporal and spatial characterization of neuronal injury following lateral fluid-percussion brain injury in the rat. *Acta Neuropathologica*, 91(3), pp.236–246.

Hill, C.S., Coleman, M.P. & Menon, D.K., 2016. Traumatic Axonal Injury: Mechanisms and Translational Opportunities. *Trends in Neurosciences*, 39(5), pp.311–324.

Hong, S. et al., 2016. Complement and microglia mediate early synapse loss in Alzheimer mouse models. *Science*, 352(6286), pp.712–716.

Hong, S., Dissing-Olesen, L. & Stevens, B., 2016. New insights on the role of microglia in synaptic pruning in health and disease. *Current opinion in neurobiology*, 36, pp.128–34.

Horn, K.P. et al., 2008. Another Barrier to Regeneration in the CNS: Activated Macrophages Induce Extensive Retraction of Dystrophic Axons through Direct Physical Interactions. *Journal of Neuroscience*, 28(38), pp.9330–9341.

Hou, R. et al., 2012. When a minor head injury results in enduring symptoms: a prospective investigation of risk factors for postconcussional syndrome after mild traumatic brain injury. *Journal of Neurology, Neurosurgery & Psychiatry*, 83(2), pp.217–223.

Hunt, C.A., Schenker, L.J. & Kennedy, M.B., 1996. PSD-95 is associated with the postsynaptic density and not with the presynaptic membrane at forebrain synapses. *The Journal of neuroscience : the official journal of the Society for Neuroscience*, 16(4), pp.1380–8.

Huntley, G.W., 2012. Synaptic circuit remodelling by matrix metalloproteinases in health and disease. *Nature reviews. Neuroscience*, 13(11), pp.743–57.

Hylin, M.J. et al., 2013. Behavioral and histopathological alterations resulting from mild fluid percussion injury. *Journal of neurotrauma*, 30(9), pp.702–15.

Jassam, Y.N. et al., 2017. Neuroimmunology of Traumatic Brain Injury: Time for a Paradigm Shift. *Neuron*, 95(6), pp.1246–1265.

Jin, X. et al., 2012. Temporal Changes in Cell Marker Expression and Cellular Infiltration in a Controlled Cortical Impact Model in Adult Male C57BL/6 Mice S. Nataf, ed. *PLoS ONE*, 7(7), p.e41892.

Johnson, V.E. et al., 2013. Inflammation and white matter degeneration persist for years after a single traumatic brain injury. *Brain*, 136(1), pp.28–42.

Johnson, V.E., Stewart, W. & Smith, D.H., 2013. Axonal pathology in traumatic brain injury. *Experimental neurology*, 246, pp.35–43.

Ju, W. et al., 2004. Activity-dependent regulation of dendritic synthesis and trafficking

of AMPA receptors. *Nature Neuroscience*, 7(3), pp.244–253.

Kabadi, S. V et al., 2010. Fluid-percussion–induced traumatic brain injury model in rats. *Nature Protocols*, 5(9), pp.1552–1563.

Karr, J.E., Areshenkoff, C.N. & Garcia-Barrera, M.A., 2014. The Neuropsychological Outcomes of Concussion: A Systematic Review of Meta-Analyses on the Cognitive Sequelae of Mild Traumatic Brain Injury.

Katayama, Y. et al., 1990. Massive increases in extracellular potassium and the indiscriminate release of glutamate following concussive brain injury. *Journal of Neurosurgery*, 73(6), pp.889–900.

Kigerl, K.A. et al., 2009. Identification of two distinct macrophage subsets with divergent effects causing either neurotoxicity or regeneration in the injured mouse spinal cord. *The Journal of neuroscience : the official journal of the Society for Neuroscience*, 29(43), pp.13435–44.

Kim, E. & Sheng, M., 2004. PDZ domain proteins of synapses. *Nature Reviews Neuroscience*, 5(10), pp.771–781.

Kim, H.J. et al., 2005. Elevation of hippocampal MMP-3 expression and activity during trauma-induced synaptogenesis. *Experimental Neurology*, 192(1), pp.60–72.

King, N.S., 2003. Post-concussion syndrome: Clarity amid the controversy? *British Journal of Psychiatry*, 183(OCT.), pp.276–278.

Klemann, C.J.H.M. & Roubos, E.W., 2011. The gray area between synapse structure and function-Gray's synapse types I and II revisited. *Synapse*, 65(11), pp.1222–1230.

Kopanitsa, M. V, Afinowi, N.O. & Grant, S.G., 2006. Recording long-term potentiation of synaptic transmission by three-dimensional multi-electrode arrays. *BMC Neuroscience*, 7(1), p.61.

Kurland, D. et al., 2012. Hemorrhagic Progression of a Contusion after Traumatic Brain Injury: A Review. *Journal of Neurotrauma*, 29(1), pp.19–31.

Lafrenaye, A.D. et al., 2015. Microglia processes associate with diffusely injured axons following mild traumatic brain injury in the micro pig. *Journal of Neuroinflammation*, 12(1), p.186.

Laube, G. et al., 1996. Ultrastructural localization of Shaker-related potassium channel subunits and synapse-associated protein 90 to septate-like junctions in rat cerebellar Pinceaux. *Brain research. Molecular brain research*, 42(1), pp.51–61.

Learoyd, A.E. & Lifshitz, J., 2012. Comparison of rat sensory behavioral tasks to detect somatosensory morbidity after diffuse brain-injury. *Behavioural Brain Research*, 226(1), pp.197–204.

Levin, H.S. & Diaz-Arrastia, R.R., 2015. Diagnosis, prognosis, and clinical management of mild traumatic brain injury. *The Lancet Neurology*, 14(5),

pp.506–517.

Lewén, A., Matz, P. & Chan, P.H., 2000. Free radical pathways in CNS injury. *Journal of neurotrauma*, 17(10), pp.871–90.

Liauw, J. et al., 2008. Thrombospondins 1 and 2 are necessary for synaptic plasticity and functional recovery after stroke. *Journal of cerebral blood flow and metabolism : official journal of the International Society of Cerebral Blood Flow and Metabolism*, 28(10), pp.1722–1732.

Loane, D.J. et al., 2014. Progressive Neurodegeneration After Experimental Brain Trauma. *Journal of Neuropathology & Experimental Neurology*, 73(1), pp.14–29.

Luo, P. et al., 2011. The role of glutamate receptors in traumatic brain injury: implications for postsynaptic density in pathophysiology. *Brain research bulletin*, 85(6), pp.313–20.

M. Greenberg, 2017. *Handbook of Neurosurgery*.

Maas, A.I., Stocchetti, N. & Bullock, R., 2008. Moderate and severe traumatic brain injury in adults. *The Lancet Neurology*, 7(8), pp.728–741.

Marklund, N. et al., 2001. Monitoring of Reactive Oxygen Species Production after Traumatic Brain Injury in Rats with Microdialysis and the 4-Hydroxybenzoic Acid Trapping Method. *Journal of Neurotrauma*, 18(11), pp.1217–1227.

Marmarou, A. et al., 1994. A new model of diffuse brain injury in rats. *Journal of Neurosurgery*, 80(2), pp.291–300.

Marrone, D.F., LeBoutillier, J.C. & Petit, T.L., 2004. Comparative analyses of synaptic densities during reactive synaptogenesis in the rat dentate gyrus. *Brain Research*, 996(1), pp.19–30.

Martland, H.S., 1928. Punch drunk. *Journal of the American Medical Association*, 91(15), p.1103.

Masumura, M. et al., 2000. Altered Expression of Amyloid Precursor Proteins After Traumatic Brain Injury in Rats: In Situ Hybridization and Immunohistochemical Study. *Journal of Neurotrauma*, 17(2), pp.123–134.

Mata-Mbemba, D. et al., 2015. Intraventricular Hemorrhage on Initial Computed Tomography as Marker of Diffuse Axonal Injury after Traumatic Brain Injury. *Journal of Neurotrauma*, 32(5), pp.359–365.

McIntosh, T.K. et al., 1989. Traumatic brain injury in the rat: Characterization of a lateral fluid-percussion model. *Neuroscience*, 28(1), pp.233–244.

McKee, A.C. et al., 2009. Chronic Traumatic Encephalopathy in Athletes: Progressive Tauopathy After Repetitive Head Injury. *Journal of Neuropathology & Experimental Neurology*, 68(7), pp.709–735.

Meabon, J.S. et al., 2016. Repetitive blast exposure in mice and combat veterans causes persistent cerebellar dysfunction. *Science translational medicine*, 8(321), p.321ra6.

Meares, S. et al., 2008. Mild traumatic brain injury does not predict acute postconcussion syndrome. *Journal of Neurology, Neurosurgery & Psychiatry*, 79(3), pp.300–306.

Mierzwa, A.J. et al., 2015. Components of Myelin Damage and Repair in the Progression of White Matter Pathology After Mild Traumatic Brain Injury. *Journal of Neuropathology & Experimental Neurology*, 74(3), pp.218–232.

Migaud, M. et al., 1998. Enhanced long-term potentiation and impaired learning in mice with mutant postsynaptic density-95 protein. *Nature*, 396(6710), pp.433–9.

Mittl, R.L. et al., 1994. Prevalence of MR evidence of diffuse axonal injury in patients with mild head injury and normal head CT findings. *AJNR. American journal of neuroradiology*, 15(8), pp.1583–9.

Miyazaki, S. et al., 1992. Enduring suppression of hippocampal long-term potentiation following traumatic brain injury in rat. *Brain research*, 585(1–2), pp.335–9.

Mosser, D.M. & Edwards, J.P., 2008. Exploring the full spectrum of macrophage activation. *Nature Reviews Immunology*, 8(12), pp.958–969.

MRC CRASH Trial Collaborators et al., 2008. Predicting outcome after traumatic brain injury: practical prognostic models based on large cohort of international patients. *BMJ (Clinical research ed.)*, 336(7641), pp.425–9.

Müller, B.M. et al., 1996. SAP102, a novel postsynaptic protein that interacts with NMDA receptor complexes in vivo. *Neuron*, 17(2), pp.255–65.

Murray, G.D. et al., 2007. Multivariable Prognostic Analysis in Traumatic Brain Injury: Results from The IMPACT Study. *Journal of Neurotrauma*, 24(2), pp.329–337.

van der Naalt, J. et al., 2017. Early predictors of outcome after mild traumatic brain injury (UPFRONT): an observational cohort study. *The Lancet Neurology*, 16(7), pp.532–540.

Nicoll, R.A. et al., 2000. Stargazin regulates synaptic targeting of AMPA receptors by two distinct mechanisms. *Nature*, 408(6815), pp.936–943.

Nikolakopoulou, A.M. et al., 2016. Astrocytic Ephrin-B1 Regulates Synapse Remodeling Following Traumatic Brain Injury. *ASN neuro*, 8(1), pp.1–18.

Nimmerjahn, A., Kirchhoff, F. & Helmchen, F., 2005. Resting Microglial Cells Are Highly Dynamic Surveillants of Brain Parenchyma in Vivo. *Science*, 308(5726), pp.1314–1318.

Nithianantharajah, J. et al., 2013. Synaptic scaffold evolution generated components of vertebrate cognitive complexity. *Nature neuroscience*, 16(1), pp.16–24.

Norris, C.M. & Scheff, S.W., 2009. Recovery of Afferent Function and Synaptic Strength in Hippocampal CA1 following Traumatic Brain Injury. *Journal of Neurotrauma*, 26(12), pp.2269–2278.

O'Connell, K.M. & Littleton-Kearney, M.T., 2013. The Role of Free Radicals in Traumatic Brain Injury. *Biological Research For Nursing*, 15(3), pp.253–263.

Oh, S.W. et al., 2014. A mesoscale connectome of the mouse brain. *Nature*, 508(7495), pp.207–214.

Omalu, B. et al., 2011. Chronic traumatic encephalopathy in an Iraqi war veteran with posttraumatic stress disorder who committed suicide. *Neurosurgical Focus*, 31(5), p.E3.

Omalu, B.I. et al., 2006. Chronic traumatic encephalopathy in a national football leagure player. *Neurosurgery*, 59(5), pp.1086–1093.

Osteen, C.L. et al., 2001. Age-Dependency of ^{45} Calcium Accumulation Following Lateral Fluid Percussion: Acute and Delayed Patterns. *Journal of Neurotrauma*, 18(2), pp.141–162.

Paolicelli, R.C. et al., 2011. Synaptic Pruning by Microglia Is Necessary for Normal Brain Development. *Science*, 333(6048), pp.1456–1458.

Peng, T.-I. & Jou, M.-J., 2010. Oxidative stress caused by mitochondrial calcium overload. *Annals of the New York Academy of Sciences*, 1201(1), pp.183–188.

Pereda, A.E., 2014. Electrical synapses and their functional interactions with chemical synapses. *Nature Reviews Neuroscience*, 15(4), pp.250–263.

Perez, E.J. et al., 2017. Enhanced astrocytic d-serine underlies synaptic damage after traumatic brain injury. *Journal of Clinical Investigation*, 127(8), pp.3114–3125.

Phillips, L.L. et al., 1994. Combined Fluid Percussion Brain Injury and Entorhinal Cortical Lesion: A Model for Assessing the Interaction Between Neuroexcitation and Deafferentation. *Journal of Neurotrauma*, 11(6), pp.641–656.

Pierce, J.E. et al., 1996. Immunohistochemical characterization of alterations in the distribution of amyloid precursor proteins and beta-amyloid peptide after experimental brain injury in the rat. *The Journal of neuroscience : the official journal of the Society for Neuroscience*, 16(3), pp.1083–90.

Polinder, S. et al., 2007. Assessing the burden of injury in six European countries. *Bulletin of the World Health Organization*, 85(1), pp.27–34.

Ponsford, J. et al., 2011. Long-term outcomes after uncomplicated mild traumatic brain injury: a comparison with trauma controls. *Journal of neurotrauma*, 28(6), pp.937–46.

Prins, M. et al., 2013. The pathophysiology of traumatic brain injury at a glance. *Disease models & mechanisms*, 6(6), pp.1307–15.

Ramalho, J. & Castillo, M., 2015. Dementia resulting from traumatic brain injury. *Dementia & neuropsychologia*, 9(4), pp.356–368.

Ransohoff, R.M. & Brown, M.A., 2012. Innate immunity in the central nervous system.

Journal of Clinical Investigation, 122(4), pp.1164–1171.

Rasband, M.N. et al., 2002. Clustering of neuronal potassium channels is independent of their interaction with PSD-95. *The Journal of cell biology*, 159(4), pp.663–72.

Rasband, M.N. & Trimmer, J.S., 2001. Developmental Clustering of Ion Channels at and near the Node of Ranvier. *Developmental Biology*, 236(1), pp.5–16.

Reeves, T.M. et al., 1997. The effect of combined fluid percussion and entorhinal cortical lesions on long-term potentiation. *Neuroscience*, 77(2), pp.431–44.

Reeves, T.M., Lyeth, B.G. & Povlishock, J.T., 1995. Long-term potentiation deficits and excitability changes following traumatic brain injury. *Experimental brain research*, 106(2), pp.248–56.

De Robertis, E.D. & Bennett, H.S., 1955. Some features of the submicroscopic morphology of synapses in frog and earthworm. *The Journal of biophysical and biochemical cytology*, 1(1), pp.47–58.

Roberts, G.W., Allsop, D. & Bruton, C., 1990. The occult aftermath of boxing. *Journal of Neurology, Neurosurgery, and Psychiatry*, 53(5), p.373.

Roozenbeek, B., R Maas, A.I. & Menon, D.K., 2013. Changing patterns in the epidemiology of traumatic brain injury. *Nature Publishing Group*, 9.

Saatman, K.E. et al., 1997. Insulin-like Growth Factor-1 (IGF-1) Improves both Neurological Motor and Cognitive Outcome Following Experimental Brain Injury. *Experimental Neurology*, 147(2), pp.418–427.

Sackheim, A.M. et al., 2017. Traumatic brain injury impairs sensorimotor function in mice. *Journal of Surgical Research*, 213, pp.100–109.

Sanders, M.J. et al., 2000. Chronic failure in the maintenance of long-term potentiation following fluid percussion injury in the rat. *Brain research*, 861(1), pp.69–76.

Scheff, S.W. et al., 2007. Synaptic alterations in CA1 in mild Alzheimer disease and mild cognitive impairment. *Neurology*, 68(18), pp.1501–8.

Scheff, S.W. et al., 2005. Synaptogenesis in the hippocampal CA1 field following traumatic brain injury. *Journal of neurotrauma*, 22(7), pp.719–32.

Schmidt, R.H. & Grady, M.S., 1995. Loss of forebrain cholinergic neurons following fluid-percussion injury: implications for cognitive impairment in closed head injury. *Journal of Neurosurgery*, 83(3), pp.496–502.

Semchenko, V. V. et al., 2006. Synaptic plasticity of the neocortex of white rats with diffuse-focal brain injuries. *Neuroscience and Behavioral Physiology*, 36(6), pp.613–618.

Shapira, Y. et al., 1988. Experimental closed head injury in rats: mechanical, pathophysiologic, and neurologic properties. *Critical care medicine*, 16(3),

pp.258–65.

Sheng, M. & Hoogenraad, C.C., 2007. The Postsynaptic Architecture of Excitatory Synapses: A More Quantitative View. *Annual Review of Biochemistry*, 76(1), pp.823–847.

Shultz, S.R. et al., 2011. A single mild fluid percussion injury induces short-term behavioral and neuropathological changes in the Long–Evans rat: Support for an animal model of concussion. *Behavioural Brain Research*, 224(2), pp.326–335.

Shultz, S.R. et al., 2012. Sub-concussive brain injury in the Long-Evans rat induces acute neuroinflammation in the absence of behavioral impairments. *Behavioural Brain Research*, 229(1), pp.145–152.

Sick, T.J., Pérez-Pinzón, M.A. & Feng, Z.Z., 1998. Impaired expression of long-term potentiation in hippocampal slices 4 and 48 h following mild fluid-percussion brain injury in vivo. *Brain research*, 785(2), pp.287–92.

Singh, I.N. et al., 2006. Time Course of Post-Traumatic Mitochondrial Oxidative Damage and Dysfunction in a Mouse Model of Focal Traumatic Brain Injury: Implications for Neuroprotective Therapy. *Journal of Cerebral Blood Flow & Metabolism*, 26(11), pp.1407–1418.

Singh, S.K. et al., 2016. Astrocytes Assemble Thalamocortical Synapses by Bridging NRX1α and NL1 via Hevin. *Cell*, 164(1–2), pp.183–196.

Smith, D.H., 2016. Neuromechanics and Pathophysiology of Diffuse Axonal Injury in Concussion. *Bridge (Washington, D.C. : 1969)*, 46(1), pp.79–84.

Smith, D.H., Hicks, R. & Povlishock, J.T., 2013. Therapy Development for Diffuse Axonal Injury.

Smith, D.H., Johnson, V.E. & Stewart, W., 2013. Chronic neuropathologies of single and repetitive TBI: substrates of dementia? *Nature Reviews Neurology*, 9(4), pp.211–221.

Smits, M. et al., 2007. Predicting intracranial traumatic findings on computed tomography in patients with minor head injury: the CHIP prediction rule. *Annals of internal medicine*, 146(6), pp.397–405.

Spaethling, J.M. et al., 2008. Calcium-Permeable AMPA Receptors Appear in Cortical Neurons after Traumatic Mechanical Injury and Contribute to Neuronal Fate. *Journal of Neurotrauma*, 25(10), pp.1207–1216.

Spain, A. et al., 2010. Mild Fluid Percussion Injury in Mice Produces Evolving Selective Axonal Pathology and Cognitive Deficits Relevant to Human Brain Injury. *Journal of Neurotrauma*, 27(8), pp.1429–1438.

Stein, S.C. et al., 2010. 150 Years of Treating Severe Traumatic Brain Injury: A Systematic Review of Progress in Mortality. *Journal of Neurotrauma*, 27(7), pp.1343–1353.

Stein, V. et al., 2003. Postsynaptic density-95 mimics and occludes hippocampal long-term potentiation and enhances long-term depression. *The Journal of neuroscience : the official journal of the Society for Neuroscience*, 23(13), pp.5503–6.

Stellwagen, D. et al., 2005. Differential Regulation of AMPA Receptor and GABA Receptor Trafficking by Tumor Necrosis Factor-. *Journal of Neuroscience*, 25(12), pp.3219–3228.

Sullivan, P.G. et al., 1998. Traumatic Brain Injury Alters Synaptic Homeostasis: Implications for Impaired Mitochondrial and Transport Function. *Journal of Neurotrauma*, 15(10), pp.789–798.

Szydlowska, K. & Tymianski, M., 2010. Calcium, ischemia and excitotoxicity. *Cell Calcium*, 47(2), pp.122–129.

Tagliaferri, F. et al., 2006. A systematic review of brain injury epidemiology in Europe. *Acta Neurochirurgica*, 148(3), pp.255–268.

Tang-Schomer, M.D. et al., 2012. Partial interruption of axonal transport due to microtubule breakage accounts for the formation of periodic varicosities after traumatic axonal injury. *Experimental Neurology*, 233(1), pp.364–372.

Teasdale, G. et al., 2014. The Glasgow Coma Scale at 40 years: Standing the test of time. *The Lancet Neurology*, 13(8), pp.844–854.

Thompson, H.J. et al., 2005. Lateral fluid percussion brain injury: a 15-year review and evaluation. *Journal of neurotrauma*, 22(1), pp.42–75.

Tran, M.D. et al., 2012. Trauma-induced expression of astrocytic thrombospondin-1 is regulated by P2 receptors coupled to protein kinase cascades. *NeuroReport*, 23(12), pp.721–726.

Tyurin, V.A. et al., 2000. Oxidative stress following traumatic brain injury in rats: quantitation of biomarkers and detection of free radical intermediates. *Journal of neurochemistry*, 75(5), pp.2178–89.

Tyzack, G.E. et al., 2014. Astrocyte response to motor neuron injury promotes structural synaptic plasticity via STAT3-regulated TSP-1 expression. *Nature communications*, 5, p.4294.

Veeramuthu, V. et al., 2015. Diffusion Tensor Imaging Parameters in Mild Traumatic Brain Injury and Its Correlation with Early Neuropsychological Impairment: A Longitudinal Study. *Journal of neurotrauma*, 32(19), pp.1497–509.

Vink, R. et al., 2001. Small Shifts in Craniotomy Position in the Lateral Fluid Percussion Injury Model Are Associated with Differential Lesion Development. *Journal of Neurotrauma*, 18(8), pp.839–847.

Vitarbo, E.A. et al., 2004. Tumor necrosis factor alpha expression and protein levels after fluid percussion injury in rats: the effect of injury severity and brain temperature. *Neurosurgery*, 55(2), pp.416-24; discussion 424–5.

Vivash, L. & OBrien, T.J., 2016. Imaging Microglial Activation with TSPO PET: Lighting Up Neurologic Diseases? *Journal of Nuclear Medicine*, 57(2), pp.165–168.

Wakade, C. et al., 2010. Delayed reduction in hippocampal postsynaptic density protein-95 expression temporally correlates with cognitive dysfunction following controlled cortical impact in mice. *Journal of neurosurgery*, 113(6), pp.1195–201.

Wake, H. et al., 2009. Resting Microglia Directly Monitor the Functional State of Synapses In Vivo and Determine the Fate of Ischemic Terminals. *Journal of Neuroscience*, 29(13).

Walsh, T. et al., 2008. Rare Structural Variants Disrupt Multiple Genes in Neurodevelopmental Pathways in Schizophrenia. *Science*, 320(5875), pp.539–543.

Wang, G. et al., 2013. Microglia/macrophage polarization dynamics in white matter after traumatic brain injury. *Journal of cerebral blood flow and metabolism : official journal of the International Society of Cerebral Blood Flow and Metabolism*, 33(12), pp.1864–74.

Wang, J.-L. et al., 2016. Plasma thrombospondin-1 and clinical outcomes in traumatic brain injury. *Acta Neurologica Scandinavica*, 134(3), pp.189–196.

Warren, K.M., Reeves, T.M. & Phillips, L.L., 2012. MT5-MMP, ADAM-10, and N-cadherin act in concert to facilitate synapse reorganization after traumatic brain injury. *Journal of neurotrauma*, 29(10), pp.1922–1940.

Washburn, K.B. & Neary, J.T., 2006. P2 purinergic receptors signal to STAT3 in astrocytes: Difference in STAT3 responses to P2Y and P2X receptor activation. *Neuroscience*, 142(2), pp.411–423.

Washington, P.M. et al., 2012. The effect of injury severity on behavior: a phenotypic study of cognitive and emotional deficits after mild, moderate, and severe controlled cortical impact injury in mice. *Journal of neurotrauma*, 29(13), pp.2283–96.

Wegner, C. et al., 2006. Neocortical neuronal, synaptic, and glial loss in multiple sclerosis. *Neurology*, 67(6), pp.960–7.

Weinhard, L. et al., 2018. Microglia remodel synapses by presynaptic trogocytosis and spine head filopodia induction. *Nature Communications 2018 9:1*, 9(1), p.1228.

Williams, W.H. et al., 2010. 1 Jin X, Ishii H, Bai Z, et al. Temporal Changes in Cell Marker Expression and Cellular Infiltration in a Controlled Cortical Impact Model in Adult Male C57BL/6 Mice. PLoS One 2012;7:e41892. doi:10.1371/journal.pone.0041892r. *Journal of neurology, neurosurgery, and psychiatry*, 81(10), pp.1116–22.

Wilson, L. et al., 2017. The chronic and evolving neurological consequences of traumatic brain injury. *The Lancet. Neurology*, 16(10), pp.813–825.

Wolf, J.A. et al., 2001. Traumatic axonal injury induces calcium influx modulated by tetrodotoxin-sensitive sodium channels. *The Journal of neuroscience : the official journal of the Society for Neuroscience*, 21(6), pp.1923–30.

Xiong, Y. et al., 1997. Mitochondrial Dysfunction and Calcium Perturbation Induced by Traumatic Brain Injury. *Journal of Neurotrauma*, 14(1), pp.23–34.

Xiong, Y., Mahmood, A. & Chopp, M., 2013. Animal models of traumatic brain injury. *Nature reviews. Neuroscience*, 14(2), pp.128–42.

Yu, C. et al., 2015. A systems biology strategy to identify molecular mechanisms of action and protein indicators of traumatic brain injury. *Journal of neuroscience research*, 93(2), pp.199–214.

Yuh, E.L. et al., 2014. Diffusion tensor imaging for outcome prediction in mild traumatic brain injury: a TRACK-TBI study. *Journal of neurotrauma*, 31(17), pp.1457–77.

Zanni, G. et al., 2010. A novel mutation in the DLG3 gene encoding the synapse-associated protein 102 (SAP102) causes non-syndromic mental retardation. *neurogenetics*, 11(2), pp.251–255.

Zhang, J. et al., 2014. Microglial CR3 Activation Triggers Long-Term Synaptic Depression in the Hippocampus via NADPH Oxidase. *Neuron*, 82(1), pp.195–207.

Zhou, J. et al., 2013. Axon position within the corpus callosum determines contralateral cortical projection. *Proceedings of the National Academy of Sciences*, 110(29), pp.E2714–E2723.

Zhu, F. et al., 2018. Architecture of the Mouse Brain Synaptome. *Neuron*, 99(4), p.781–799.e10.

APPENDIX

Appendix 1: Matlab script used to generate montage images (written by Dr. Zhen Qiu)

```
function stitching_Melissa
% SPECIFY THE INPUT DIRECTORY
root_dir = 'X:\microscopy\2014-04_SAP102KO_PSD95EGFP_Mapping\';
% SPECIFY THE OUTPUT DIRECTORY
out_dir = 'X:\users\Melissa\Montages\';
% SPECIFY THE MOUSE ID
Mouse_id = {'GHB29'};
% SPECIFY THE SECTION ID
Section_id = {'HC'};
d = dir(root_dir);
isub = [d(:).isdir]; %# returns logical vector
name_Folds = {d(isub).name}';
name_Folds(ismember(name_Folds,{'.','..'})) = [];
% temp_path = '/data/project/HBP/Jess/temp/';
down_sampling_factor = 16;
split_char ='\';% for windows
%% divide the folder name
Mouse_list = cell(length(name_Folds)-2,1);
Section_list = cell(length(name_Folds)-2,1);
parfor i = 1:length(name_Folds) - 2
   temp_folder_name_split = strsplit(name_Folds{i},'_');
   Mouse_list(i) = temp_folder_name_split(1);
   Section_list(i) = temp_folder_name_split(2);
end
%% select the mouse in the Mouse_id and Section_id.

n = 1;
for i = 1:length(Mouse_id)
   for j = 1:length(Section_id)
%        i,j
      temp_mouse_index                                                                    =
intersect(strmatch(Mouse_id{i},Mouse_list),strmatch(Section_id{j},Section_list));
      if ~isempty(temp_mouse_index)
         select_mouse_path{n} = [root_dir,name_Folds{temp_mouse_index(end)}];
         n = n +1;
      end
   end
end
if size(select_mouse_path,1) == 1
   select_mouse_path = select_mouse_path';
end

%% Then reorder the imported data based on the digitsfor i = 1:length(dir1)
row_num = zeros(length(select_mouse_path),1);
col_num = zeros(length(select_mouse_path),1);
for i = 1:length(select_mouse_path)
   disp(select_mouse_path{i});
   %% first get the number of rows and columns from the meta_data
```

```
   dir_meta = dir([select_mouse_path{i},split_char,'*.txt']);
   if ~isempty(dir_meta)
      fid = fopen([select_mouse_path{i},split_char,dir_meta(1).name]);
      montage_meta = textscan(fid,'%s',10, 'headerlines', 89);%% Number specifies
the line before the number of raws and columns in the metadata file
      col_num(i) = str2num(montage_meta{1}{6});
      row_num(i) = str2num(montage_meta{1}{8});
      fclose(fid);
      %% then get the image name and re-order the name
%        tic
      dir_image{i} = dir([select_mouse_path{i},split_char,'*.tif']);
%        t = toc;
      temp_digits = zeros(length(dir_image{i}),1);
      parfor j = 1:length(dir_image{i})
         temp_file_name = strsplit(dir_image{i}(j).name(1:end-4),'_');
         temp_digits(j) = str2num(temp_file_name{end}(2:end));
      end
      digits{i} = temp_digits;
      [~,ind] = sort(temp_digits);

      %% then load the data and save the downsample image in the memory

      pctRunOnAll warning off;
      % montage = cell(row_num,1);
      iminfo = imfinfo([select_mouse_path{i},split_char,dir_image{i}(ind(1)).name]);
%        pctRunOnAll warning off
%        im = uint16(rand(iminfo.Height/4,iminfo.Width/4,length(dir1))*100);
      im                                                                    =
zeros(iminfo(1).Height/down_sampling_factor,iminfo(1).Width/down_sampling_facto
r,length(temp_digits));
      tic
      parfor j = 1:length(temp_digits)
%             tic
         %    for j = 1:col_num;
%           j
         %    montage{i} = [montage{i},imread(dir1(ind).name)];
         im(:,:,j)                                                          =
imresize(imread([select_mouse_path{i},split_char,dir_image{i}(ind(j)).name]),1/down
_sampling_factor,'nearest');
         %       disp(dir1(ind(i).name));
         %    ind = ind +1;
         %    end
         %    montage{i} = imresize(montage{i} ,1/down_sampling_factor);
%             t = toc
      end
      t = toc
      montage = cell(row_num(i),1);
      ind = 1;
      for m = 1:row_num(i)
         for n = 1:col_num(i)
            %       i,j
            %       im(:,:,index) = normaliz(im(:,:,index));
            %       ind = (i-1)*col_num+j;
```

```
            mont = [montage{m},(im(:,:,ind))];
            ind = ind +1;
        end
    end
    montage_output = cell2mat(montage);
    temp_name = strsplit(select_mouse_path{i},split_char);

    imwrite(uint16(montage_output),[out_dir,'Montage_',temp_name{end},'.tif']);
%                                                                   temp_montage        =
reshape(im,[row_num*512/down_sampling_factor,col_num*512/down_sampling_fac
tor]);

    %     filename{end} = sprintf('m%.5d',digits);
    %         filename = [strjoin(filename,'_'),'.tif'];
    %     end
    %     movefile(dir1(i).name,[temp_path,filename]);
    %     end
  end
end
```

Appendix 2: Pilot LFPI experiment of PSD95-eGFP mKO2-SAP102 KI mice at 24 hours and 7 days

A total of male 12 eGFP-PSD95 mKO2-SAP102 mice aged 8-12 weeks were included within the pilot study: 24 hours (3 injury and 3 sham); 7 days (4 injury and 2 sham). The injury mice were exposed to a percussion amplitude of 1.19±0.03atm. Injury mice had a significantly higher righting time (RT) (295 secs) compared to sham mice (89 secs) (p=0.027). Mice were sacrificed at 24 hours and 7 days and their brains were processed as described in the methods section. Imaging of a whole brain mid-hippocampal coronal section was undertaken using the SDM. Analysis of the density of synaptic puncta per tile within the cortices revealed no significant different between injury or sham **[Figure 1]**.

Analysis of the density of PSD-95 positive puncta per tile within the cortices revealed no significant different between injury or sham. In the ipsilateral cortex at 24 hours, the density of PSD-95 puncta in the injury group was 335±4.5 compared to sham at 329±8.6 (p=0.4). By 7 days, the density of the injury group had dropped to 289±16.1 compared to sham (323±5) however this did not reach significant (p=0.13) **(Figure 1)**. Analysis of SAP102 revealed a reduction in SAP102 puncta in the ipsilateral cortex of the injury group (249±4.9) compared to the sham group (263±4.7) (p=0.1). At 7 days, the ipsilateral cortex in the injury group had a SAP102 density of 253±15.8 compared to the sham cohort 266±1 (p=0.533). There was no significant differences between the two cohorts across the two time points in the contralateral cortex.

Using this data, we performed power calculations for 24 hours and 7 days. We attempted a number of different a prior calculations **(Table 1)**. Based upon this, we opted for a priori calculation with alpha error=0.05 and power=0.95 which showed that we needed a sample size of 71 at 24 hours and 9 at 7 days. Based on these findings, we decided to proceed with 7 and 28 days as our primary time-points. Therefore, with four cohorts and an approximated attrition rate of 30%, we calculated a minimum of 47 mice to be randomised.

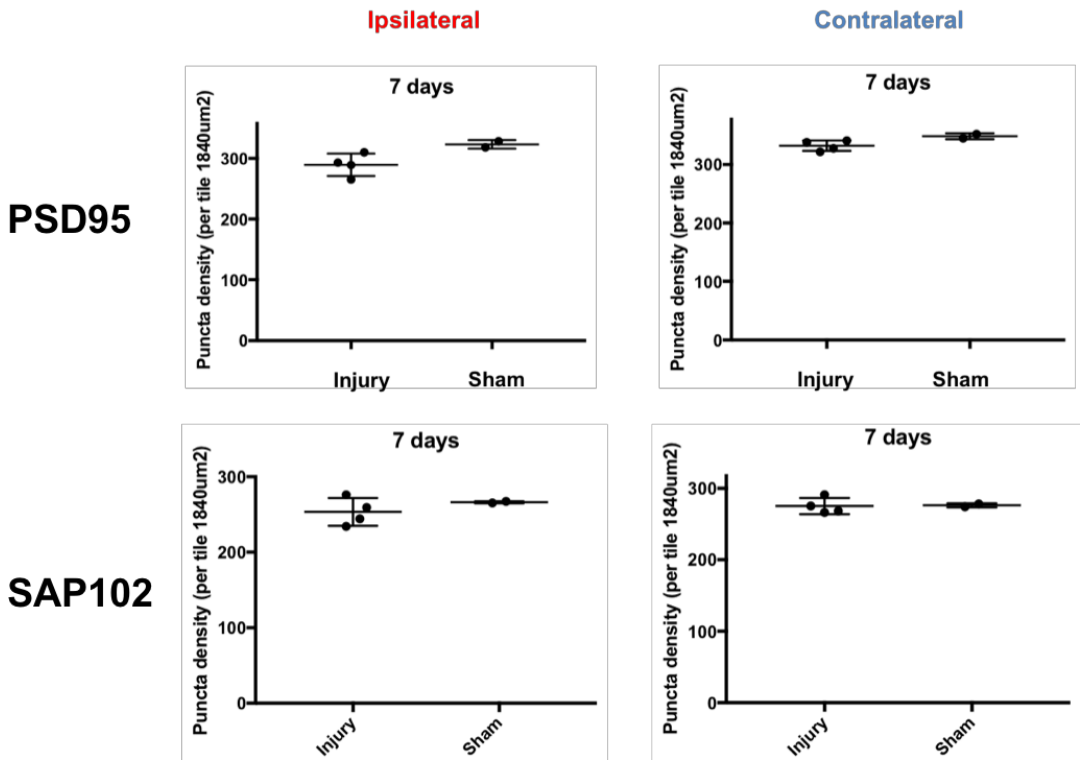

Figure 1: *Scatter plot demonstrating cortical PSD-95 and SAP102 cortex puncta density*

Alpha error	Power	Sample size
0.05	0.95	9
0.05	0.9	7
0.05	0.85	6
0.05	0.8	5
0.01	0.95	13
0.01	0.9	10
0.01	0.85	9
0.01	0.8	8

Table 1: *A priori calculations for 7 day cohort*

Appendix 3: Raw PSD95 and SAP102 data from naïve mice

Table 1: PSD95 puncta parameters for naïve mice

	Density		Size		Intensity	
Region	Average	SD	Average	SD	Average	SD
contra_amgmed	290.00	36.80	12.71	0.15	11538.43	955.99
contra_AUDd	455.80	32.09	12.24	0.25	18646.75	1748.31
contra_AUDd1	565.50	27.75	12.08	0.35	19940.67	1895.11
contra_AUDd3	494.20	29.81	12.36	0.27	20663.18	1867.96
contra_AUDd4	486.60	35.02	11.97	0.22	18689.27	2034.83
contra_AUDd5	419.90	33.02	12.30	0.25	17244.06	1896.09
contra_AUDd6a	403.40	20.48	12.12	0.26	16241.72	2141.20
contra_AUDd6b	307.10	39.53	12.40	0.38	12589.13	2395.71
contra_AUDp	469.70	32.37	12.18	0.23	18862.29	1697.40
contra_AUDp1	566.20	16.57	12.00	0.19	20407.82	968.62
contra_AUDp3	504.80	30.64	12.29	0.23	20637.98	1584.23
contra_AUDp4	498.60	23.96	11.95	0.23	19031.62	1916.66
contra_AUDp5	437.70	41.50	12.21	0.27	17475.57	1990.58
contra_AUDp6a	411.10	21.42	12.10	0.27	16379.57	2105.71
contra_AUDp6b	300.10	51.62	12.35	0.35	12880.48	2504.32
contra_AUDv	482.20	30.76	12.11	0.25	18784.89	1767.59
contra_AUDv1	568.10	31.89	11.98	0.30	19957.26	1775.18
contra_AUDv3	511.70	26.72	12.18	0.20	20308.89	1533.74
contra_AUDv4	517.20	34.80	11.93	0.25	19075.87	1887.65
contra_AUDv5	460.20	38.50	12.11	0.27	17756.28	2050.29
contra_AUDv6a	408.30	22.97	12.13	0.26	16621.04	2161.69
contra_AUDv6b	294.10	40.39	12.48	0.40	12504.69	2461.27
contra_BLAa	443.10	26.25	11.97	0.39	14649.98	1851.75
contra_BLAp	457.10	32.82	12.18	0.33	17087.92	1961.48
contra_BLAv	372.50	42.22	12.25	0.21	12831.57	1847.02
contra_BMAp	348.50	35.26	12.31	0.22	12407.22	1442.40
contra_CA1slm	502.10	16.90	12.11	0.44	13306.25	1872.96
contra_CA1so	654.90	45.90	11.52	0.46	14844.00	1797.70
contra_CA1sp	147.40	13.71	12.51	0.20	9409.77	1146.33
contra_CA1sr	655.50	50.03	11.63	0.46	16532.64	1968.97
contra_CA2slm	530.00	12.66	11.45	0.40	9453.96	1165.36
contra_CA2so	513.80	12.02	11.44	0.41	9608.00	1060.54

contra_CA2sp	65.50	26.62	14.79	0.96	7090.51	696.60
contra_CA2sr	478.50	22.88	11.76	0.51	9394.61	1025.47
contra_CA3slm	540.00	28.85	11.85	0.44	9724.69	1203.54
contra_CA3slu	264.20	19.07	14.76	0.50	11932.09	1449.86
contra_CA3so	462.40	28.46	12.07	0.53	9341.14	864.33
contra_CA3sp	121.20	29.16	15.34	0.68	9305.54	1124.85
contra_CA3sr	514.80	25.63	12.21	0.55	10845.94	1184.28
contra_CC	11.60	5.78	13.09	0.22	7861.25	1351.30
contra_cing	82.70	37.28	13.20	0.41	8887.29	1908.10
contra_COApl	359.80	23.64	12.43	0.23	12794.32	1407.97
contra_COApl1	388.60	22.15	12.23	0.21	13212.16	1093.95
contra_COApl2	346.50	37.83	12.54	0.30	12503.99	1649.23
contra_COApl3	345.10	14.46	12.49	0.15	12764.00	1557.23
contra_cortex	454.60	27.21	12.21	0.29	17983.41	2162.02
contra_CP	390.20	17.65	12.02	0.27	14554.62	1817.83
contra_cpd	14.00	9.14	13.69	0.39	7482.86	1030.89
contra_DG	657.20	42.64	11.59	0.52	13688.57	1625.69
contra_DGinf	656.40	39.63	11.62	0.51	13352.37	1747.04
contra_DGpo	220.90	18.10	14.75	0.43	9737.74	1145.91
contra_DGsg	45.90	11.83	15.12	0.25	6928.48	508.24
contra_DGsup	660.10	46.62	11.57	0.53	13917.17	1628.70
contra_ECT	512.50	27.28	11.96	0.29	18921.88	1845.06
contra_ECT1	606.00	37.47	11.82	0.28	20550.97	1806.88
contra_ECT3	536.50	17.22	12.02	0.26	19837.71	1872.91
contra_ECT5	476.30	29.77	11.96	0.31	17508.27	1868.62
contra_ECT6a	442.70	32.68	11.89	0.36	16556.67	1718.32
contra_ECT6b	325.30	46.58	12.17	0.44	12622.67	1965.85
contra_ENTl	478.60	21.28	11.83	0.33	17055.64	1806.84
contra_ENTl1	603.60	25.38	11.59	0.29	18669.31	2025.11
contra_ENTl3	499.00	23.79	11.94	0.30	17796.98	2066.18
contra_ENTl5	465.00	22.71	11.97	0.41	16541.05	1670.18
contra_ENTl6a	440.30	13.76	11.62	0.36	14013.17	1392.76
contra_ENTl6b	378.00	37.11	11.77	0.27	12214.01	1383.33
contra_FC	264.80	25.96	11.97	0.47	7479.49	1169.66
contra_hip	538.60	20.03	11.82	0.48	12498.46	1631.24
contra_hyp	123.20	7.63	13.89	0.05	9828.62	1112.02
contra_LA	454.20	26.44	12.03	0.33	16479.95	2137.54

contra_lay1	565.10	29.92	12.04	0.33	19846.77	2045.53
contra_lay2	297.90	30.47	12.60	0.38	12741.38	2550.48
contra_lay3	491.00	26.75	12.26	0.28	19969.51	2005.96
contra_lay4	486.70	29.86	12.01	0.26	18402.76	2165.19
contra_lay5	422.50	24.59	12.31	0.30	16894.89	2140.26
contra_lay6a	399.40	19.03	12.12	0.32	15544.63	2337.01
contra_lay6b	304.80	35.06	12.37	0.36	12237.21	2149.91
contra_MOp	483.40	31.78	12.17	0.40	18141.69	2883.78
contra_MOp1	582.20	52.52	12.08	0.45	19925.05	3288.75
contra_MOp3	512.20	39.87	12.16	0.40	19373.88	2997.05
contra_MOp5	467.70	34.71	12.24	0.38	17244.13	2817.74
contra_MOp6a	402.60	22.40	12.15	0.37	14927.54	2612.06
contra_MOp6b	303.00	36.57	12.36	0.39	12303.70	2625.08
contra_MOs	409.30	18.56	12.46	0.39	17230.71	3015.15
contra_MOs1	540.60	38.32	12.32	0.40	20547.80	3617.58
contra_MOs3	437.10	20.39	12.46	0.38	18325.53	3055.87
contra_MOs5	368.20	12.86	12.59	0.42	15415.76	2755.05
contra_MOs6a	337.90	24.01	12.40	0.41	13306.66	2656.58
contra_MOs6b	271.40	34.47	12.51	0.29	11264.70	2318.04
contra_PAA	387.70	21.19	12.28	0.18	13090.09	915.79
contra_PAA1	394.40	12.47	12.22	0.19	13072.57	1062.64
contra_PAA2	387.60	28.05	12.32	0.21	12913.77	945.03
contra_PAA3	381.40	25.71	12.33	0.17	13110.12	1007.26
contra_PERI	509.70	28.78	11.84	0.33	18119.81	1906.13
contra_PERI1	625.80	50.53	11.61	0.37	19753.32	2292.41
contra_PERI3	536.10	27.22	11.89	0.34	18749.52	1956.64
contra_PERI5	474.60	23.27	11.93	0.32	17413.03	1905.30
contra_PERI6a	454.00	29.87	11.76	0.33	15748.85	1685.66
contra_PERI6b	350.70	23.40	11.96	0.25	12248.25	1546.63
contra_PIR	435.00	30.08	11.97	0.23	14515.50	1519.27
contra_PIR1	484.90	40.64	11.92	0.23	15205.68	1217.43
contra_PIR2	390.10	32.50	11.98	0.16	13706.97	1307.72
contra_PIR3	434.70	25.05	11.99	0.25	14566.21	1693.48
contra_RSPd	353.40	13.87	12.66	0.33	16097.02	3178.33
contra_RSPd1	484.70	48.08	12.57	0.31	19808.56	4047.25
contra_RSPd3	389.00	20.03	12.62	0.28	17123.62	3359.66
contra_RSPd5	314.40	19.13	12.96	0.36	13930.67	2749.73

contra_RSPd6a	298.70	28.07	12.56	0.34	12154.33	2556.65
contra_RSPd6b	233.40	38.13	12.56	0.32	10898.82	2458.80
contra_RSPv	340.30	18.38	12.61	0.32	14550.58	2922.16
contra_RSPv1	377.70	14.66	12.73	0.37	15659.89	3153.96
contra_RSPv2	299.60	31.11	12.59	0.38	12766.19	2569.66
contra_RSPv3	383.60	16.19	12.34	0.29	15503.81	3073.68
contra_RSPv5	312.80	25.98	12.86	0.24	13763.00	2535.43
contra_RSPv6a	270.30	27.04	12.80	0.33	11752.34	2386.84
contra_RSPv6b	215.30	46.79	12.68	0.41	10844.37	2576.53
contra_SSp-bfd	440.90	34.73	12.28	0.28	17968.92	2186.84
contra_SSp-bfd1	563.60	38.19	12.07	0.29	20549.24	2069.99
contra_SSp-bfd3	482.60	38.70	12.37	0.27	20627.00	2061.30
contra_SSp-bfd4	469.80	36.87	12.05	0.27	17878.33	2180.31
contra_SSp-bfd5	408.20	28.73	12.40	0.29	16666.18	2199.85
contra_SSp-bfd6a	393.10	23.47	12.16	0.32	15482.61	2422.80
contra_SSp-bfd6b	297.40	55.06	12.42	0.39	12273.04	2338.81
contra_SSP-tr	467.80	28.81	12.18	0.32	18413.92	2541.67
contra_SSp-tr1	599.30	46.72	11.94	0.37	20844.78	2686.64
contra_SSp-tr3	517.40	31.08	12.23	0.32	20904.66	2608.89
contra_SSp-tr4	481.70	31.75	12.04	0.28	18147.72	2456.83
contra_SSp-tr5	424.40	25.54	12.39	0.30	16664.10	2413.25
contra_SSp-tr6a	404.10	17.60	12.09	0.33	15503.94	2470.58
contra_SSp-tr6b	307.50	36.50	12.34	0.40	12460.47	2370.15
contra_TEa	497.60	31.73	12.04	0.25	18817.64	1764.80
contra_TEa1	589.90	19.52	11.91	0.21	19990.52	1344.70
contra_TEa3	532.40	25.73	12.09	0.22	20120.48	1705.28
contra_TEa4	526.30	36.55	11.99	0.32	19435.70	2136.46
contra_TEa5	474.10	30.68	12.02	0.24	17860.28	1978.35
contra_TEa6a	426.80	37.72	12.05	0.29	16983.96	2350.69
contra_TEa6b	309.80	34.45	12.38	0.39	12582.87	2424.77
contra_th	317.10	25.89	11.73	0.27	9265.30	1151.64
ips_amgmed	290.00	35.34	12.68	0.16	11285.16	1806.20
ips_AUDd	474.90	30.05	12.30	0.45	18126.34	4155.08
ips_AUDd1	575.50	75.52	12.17	0.57	20249.76	4971.44

ips_AUDd3	507.60	43.17	12.39	0.47	20234.62	4733.64
ips_AUDd4	496.60	32.07	12.07	0.42	17792.93	4031.95
ips_AUDd5	436.80	18.83	12.34	0.41	16377.92	3822.66
ips_AUDd6a	415.30	19.38	12.16	0.41	15458.47	3639.75
ips_AUDd6b	299.00	37.25	12.52	0.37	12182.26	2871.52
ips_AUDp	480.40	28.54	12.25	0.41	17961.10	3877.89
ips_AUDp1	564.50	68.37	12.18	0.50	19587.58	4199.40
ips_AUDp3	510.60	43.14	12.31	0.42	19622.64	4352.63
ips_AUDp4	496.80	26.93	12.17	0.44	17778.09	3964.71
ips_AUDp5	455.50	29.33	12.24	0.39	16401.52	3681.50
ips_AUDp6a	414.20	8.09	12.19	0.39	15469.32	3611.93
ips_AUDp6b	304.40	14.44	12.49	0.33	11915.56	2730.04
ips_AUDv	489.50	31.38	12.19	0.42	17764.46	3716.13
ips_AUDv1	568.10	64.06	12.13	0.49	19336.97	3957.59
ips_AUDv3	518.30	33.09	12.22	0.40	19265.76	4075.51
ips_AUDv4	507.00	37.10	12.14	0.49	17707.19	3852.00
ips_AUDv5	464.30	32.76	12.12	0.42	16402.14	3720.51
ips_AUDv6a	419.00	23.27	12.24	0.43	15321.20	3664.50
ips_AUDv6b	291.00	39.07	12.55	0.45	11509.99	2616.48
ips_BLAa	436.50	28.37	12.17	0.50	13904.70	2545.69
ips_BLAp	447.75	16.47	12.36	0.43	15522.56	2838.90
ips_BLAv	383.90	50.49	12.23	0.28	12402.86	2459.46
ips_BMAp	346.30	44.86	12.34	0.23	11973.72	2181.43
ips_CA1slm	495.20	32.89	12.20	0.55	13125.35	2467.54
ips_CA1so	655.10	75.04	11.63	0.65	14584.36	2677.95
ips_CA1sp	154.70	40.52	12.47	0.45	9414.53	1743.45
ips_CA1sr	653.80	73.08	11.76	0.61	16248.03	2711.45
ips_CA2slm	510.20	65.18	11.65	0.72	9296.23	1789.68
ips_CA2so	464.60	66.01	11.82	0.76	9143.67	1751.28
ips_CA2sp	53.80	35.61	16.27	2.09	6777.55	1133.56
ips_CA2sr	427.60	92.65	12.20	0.89	9266.44	1856.75
ips_CA3slm	493.40	96.51	12.11	0.80	9366.07	1706.46
ips_CA3slu	254.90	37.02	15.13	0.74	11486.93	2360.34
ips_CA3so	425.40	86.39	12.43	0.92	9282.07	1609.19
ips_CA3sp	117.10	25.64	15.63	0.98	9307.75	1824.54
ips_CA3sr	474.60	89.11	12.57	0.90	10734.08	1943.02
ips_CC	10.20	5.56	13.11	0.16	7670.50	1721.07

ips_cing	55.90	24.80	13.38	0.47	8572.56	2103.79
ips_COApl	345.80	31.11	12.48	0.25	12282.83	2132.79
ips_COApl1	368.10	33.02	12.33	0.29	12681.87	2089.39
ips_COApl2	332.10	38.76	12.54	0.32	12092.36	2166.66
ips_COApl3	341.40	28.18	12.55	0.20	12229.55	2129.89
ips_cortex	461.20	29.80	12.30	0.44	17442.39	3944.19
ips_CP	377.20	19.80	12.20	0.34	13392.68	2592.20
ips_cpd	11.00	8.69	13.67	0.30	7318.46	1102.74
ips_DG	652.00	68.63	11.70	0.69	13594.19	2185.88
ips_DGinf	651.90	57.54	11.70	0.67	13319.36	2032.48
ips_DGpo	211.00	27.84	14.90	0.72	9596.04	1597.13
ips_DGsg	43.60	22.81	15.15	0.40	6763.70	771.94
ips_DGsup	652.80	74.73	11.70	0.70	13720.00	2267.09
ips_ECT	496.60	26.17	12.07	0.39	17289.60	3388.55
ips_ECT1	556.90	44.61	11.99	0.46	18276.86	3348.78
ips_ECT3	508.70	24.95	12.10	0.39	18125.17	3400.93
ips_ECT5	460.30	16.74	12.05	0.38	15829.63	3128.64
ips_ECT6a	446.70	23.11	12.03	0.40	14608.13	3177.95
ips_ECT6b	297.00	15.98	12.45	0.35	10847.47	2322.77
ips_ENTl	459.30	22.21	12.04	0.36	15490.56	2666.71
ips_ENTl1	520.10	49.29	11.89	0.42	16518.93	2304.99
ips_ENTl3	453.90	25.10	12.14	0.36	15992.78	2616.68
ips_ENTl5	454.00	21.60	12.03	0.41	14818.00	3202.04
ips_ENTl6a	413.75	15.47	11.82	0.42	12221.76	2930.17
ips_ENTl6b	342.63	36.50	12.12	0.29	10742.64	2520.15
ips_FC	242.90	57.46	11.96	0.44	7277.07	1208.83
ips_hip	519.60	64.80	11.97	0.68	12373.44	2391.73
ips_hyp	120.60	9.77	13.91	0.03	9703.72	1282.66
ips_LA	449.60	22.73	12.10	0.46	15059.52	2784.05
ips_lay1	550.80	56.06	12.19	0.52	19306.85	4109.94
ips_lay2	298.40	33.17	12.62	0.34	12720.47	2747.93
ips_lay3	487.00	37.08	12.35	0.43	19223.74	4304.56
ips_lay4	490.80	36.71	12.13	0.45	17700.30	4276.19
ips_lay5	428.10	24.05	12.36	0.41	16178.90	3928.62
ips_lay6a	398.20	27.37	12.21	0.45	15037.56	3898.90
ips_lay6b	292.80	44.62	12.47	0.45	11896.27	3156.56
ips_MOp	474.70	45.64	12.28	0.51	17752.58	4205.71

ips_MOp1	557.70	72.13	12.22	0.52	19431.40	4451.29
ips_MOp3	501.20	57.10	12.29	0.52	18827.53	4416.16
ips_MOp5	451.30	36.94	12.32	0.47	16801.68	3952.26
ips_MOp6a	395.20	45.42	12.20	0.53	14727.34	3898.38
ips_MOp6b	289.30	55.18	12.48	0.49	11803.58	3373.11
ips_MOs	381.60	31.08	12.59	0.42	16772.05	4101.74
ips_MOs1	523.60	49.97	12.44	0.38	20455.61	4149.95
ips_MOs3	411.80	28.86	12.63	0.43	17843.34	4292.56
ips_MOs5	342.30	32.19	12.63	0.43	14241.33	3583.15
ips_MOs6a	299.10	46.92	12.55	0.41	12252.94	3231.06
ips_MOs6b	231.60	47.16	12.64	0.36	10707.72	2752.04
ips_PAA	377.40	37.32	12.35	0.27	12523.60	2419.31
ips_PAA1	385.50	71.13	12.28	0.33	12394.21	2445.96
ips_PAA2	371.60	32.81	12.35	0.26	12345.83	2194.99
ips_PAA3	371.90	31.56	12.41	0.29	12568.93	2488.26
ips_PERI	484.80	24.26	12.01	0.36	16422.21	2841.99
ips_PERI1	563.40	48.94	11.80	0.38	17878.51	2733.09
ips_PERI3	487.80	24.53	12.07	0.36	17044.18	2704.07
ips_PERI5	466.40	30.43	12.09	0.39	15621.15	3046.08
ips_PERI6a	427.63	12.55	11.93	0.39	13728.93	3314.32
ips_PERI6b	327.88	10.47	12.23	0.32	10940.17	2522.37
ips_PIR	443.40	36.55	12.03	0.29	14038.19	2253.83
ips_PIR1	475.80	50.99	12.02	0.43	14524.46	2212.89
ips_PIR2	395.20	32.24	12.05	0.25	13384.60	1991.58
ips_PIR3	444.40	33.52	12.05	0.27	14106.96	2367.23
ips_RSPd	354.90	12.08	12.68	0.35	16321.90	3715.40
ips_RSPd1	481.20	44.94	12.58	0.38	20106.84	4442.74
ips_RSPd3	387.60	23.29	12.64	0.34	17043.43	4014.44
ips_RSPd5	308.60	20.75	12.98	0.38	13988.60	3540.01
ips_RSPd6a	293.70	33.51	12.62	0.39	12215.81	3146.79
ips_RSPd6b	214.60	21.33	12.53	0.21	10909.78	2530.55
ips_RSPv	336.70	27.89	12.61	0.34	14596.41	3317.41
ips_RSPv1	386.40	27.58	12.68	0.38	16087.89	3561.47
ips_RSPv2	297.60	32.96	12.63	0.34	12708.88	2743.77
ips_RSPv3	372.30	19.79	12.35	0.31	15263.44	3349.12
ips_RSPv5	295.40	29.53	12.85	0.34	13404.12	2937.61
ips_RSPv6a	268.40	25.94	12.64	0.33	11553.10	2692.05

ips_RSPv6b	191.50	33.33	12.72	0.35	10491.59	2515.48
ips_SSp-bfd	458.00	39.77	12.33	0.44	17687.44	4593.16
ips_SSp-bfd1	575.30	82.49	12.19	0.57	20497.79	5172.91
ips_SSp-bfd3	490.20	48.52	12.43	0.43	20327.13	5176.40
ips_SSp-bfd4	483.90	38.40	12.11	0.44	17552.74	4442.97
ips_SSp-bfd5	421.50	34.10	12.40	0.39	16294.29	4229.88
ips_SSp-bfd6a	401.60	33.14	12.19	0.44	15326.79	4016.52
ips_SSp-bfd6b	299.40	43.65	12.45	0.46	12239.30	3252.37
ips_SSp-tr	470.20	40.97	12.31	0.51	18083.66	4575.80
ips_SSp-tr1	579.20	77.19	12.16	0.57	20208.81	5283.17
ips_SSp-tr3	505.40	51.87	12.36	0.49	20262.00	5187.29
ips_SSp-tr4	486.00	44.70	12.13	0.50	17721.14	4597.08
ips_SSp-tr5	426.10	34.30	12.48	0.49	16492.42	4478.79
ips_SSp-tr6a	397.70	46.42	12.20	0.54	15474.80	4561.80
ips_SSp-tr6b	290.80	64.41	12.53	0.62	12487.01	3826.83
ips_TEa	496.40	29.18	12.14	0.42	17521.72	3528.21
ips_TEa1	565.00	49.46	12.05	0.50	18629.08	3735.33
ips_TEa3	516.90	31.66	12.18	0.40	18791.63	3675.59
ips_TEa4	499.50	28.23	12.17	0.38	17547.39	3526.36
ips_TEa5	477.90	23.35	12.05	0.37	16272.52	3406.42
ips_TEa6a	428.60	43.42	12.19	0.47	15307.66	3483.91
ips_TEa6b	303.60	53.00	12.41	0.60	11365.17	2895.59
ips_th	310.00	26.92	11.78	0.29	9124.41	1575.68

Table 2: SAP102 puncta parameters for naïve mice

	Density		**Size**		**Intensity**	
Region	**Average**	**SD**	**Average**	**SD**	**Average**	**SD**
contra_amgmed	249.00	24.48	14.70	0.26	72.11	102.49
contra_AUDd	403.80	27.59	14.39	0.34	111.53	169.02
contra_AUDd1	489.13	25.61	13.85	0.32	132.23	206.25
contra_AUDd3	433.90	30.68	14.62	0.41	119.90	181.60
contra_AUDd4	408.60	27.86	14.01	0.18	112.66	171.14
contra_AUDd5	368.40	26.31	14.33	0.34	102.34	153.88
contra_AUDd6a	374.10	23.01	14.28	0.26	102.91	156.78
contra_AUDd6b	278.40	48.11	14.43	0.40	85.34	112.81
contra_AUDp	417.30	26.76	14.23	0.30	114.65	174.99

contra_AUDp1	492.70	6.17	13.85	0.25	128.24	210.47
contra_AUDp3	446.40	28.29	14.44	0.34	122.37	187.34
contra_AUDp4	420.10	20.14	13.90	0.23	113.59	177.11
contra_AUDp5	386.00	36.11	14.21	0.32	109.16	160.34
contra_AUDp6a	383.50	29.51	14.16	0.22	106.85	160.06
contra_AUDp6b	286.60	53.74	14.28	0.36	88.74	115.90
contra_AUDv	425.80	26.39	14.12	0.27	116.64	178.73
contra_AUDv1	490.70	24.49	13.81	0.29	132.32	207.09
contra_AUDv3	452.90	20.13	14.30	0.30	121.91	191.24
contra_AUDv4	439.20	31.56	13.81	0.23	121.20	183.93
contra_AUDv5	406.30	32.01	14.10	0.29	113.18	169.61
contra_AUDv6a	384.70	29.60	14.15	0.24	107.17	160.57
contra_AUDv6b	273.40	47.99	14.33	0.25	83.99	110.72
contra_BLAa	433.20	30.14	13.70	0.26	119.33	181.52
contra_BLAp	448.00	29.40	13.77	0.24	122.85	188.01
contra_BLAv	345.40	45.50	13.99	0.21	101.28	141.90
contra_BMAp	315.20	44.55	14.20	0.26	93.55	128.97
contra_CA1slm	387.00	42.38	14.85	0.44	111.17	159.96
contra_CA1so	558.20	46.42	13.58	0.49	154.67	233.58
contra_CA1sp	178.40	26.38	16.45	0.57	55.45	71.58
contra_CA1sr	585.60	47.06	13.98	0.40	161.76	245.29
contra_CA2slm	518.10	16.56	13.11	0.31	137.02	220.10
contra_CA2so	525.60	19.90	12.97	0.22	139.67	222.93
contra_CA2sp	124.50	30.98	17.77	1.15	43.60	47.89
contra_CA2sr	482.30	21.48	13.47	0.22	129.37	203.91
contra_CA3slm	544.60	36.92	13.40	0.36	148.82	228.88
contra_CA3slu	209.10	20.81	19.45	0.14	62.38	85.10
contra_CA3so	461.00	21.45	13.46	0.44	124.09	194.66
contra_CA3sp	130.30	26.05	19.28	0.20	43.96	50.74
contra_CA3sr	544.00	32.53	13.72	0.43	147.67	229.10
contra_CC	26.40	11.36	15.94	0.60	13.57	9.27
contra_cing	90.30	29.14	15.21	0.54	33.80	34.15
contra_COApl	319.20	39.91	14.20	0.26	93.39	131.14
contra_COApl1	349.60	39.33	13.80	0.18	100.73	144.37
contra_COApl2	310.00	45.12	14.38	0.33	92.46	126.64
contra_COApl3	301.70	24.07	14.36	0.23	85.09	125.35
contra_cortex	394.80	32.00	14.30	0.27	110.34	164.62

contra_CP	353.00	34.12	14.19	0.32	100.41	146.33
contra_cpd	31.60	15.58	17.42	0.93	16.38	10.87
contra_DG	661.80	19.70	13.82	0.39	173.93	281.76
contra_DGinf	656.00	16.26	13.83	0.35	171.61	279.73
contra_DGpo	196.50	14.75	17.85	0.48	57.39	80.58
contra_DGsg	120.80	14.26	20.11	1.24	39.10	47.66
contra_DGsup	667.90	24.88	13.82	0.43	176.76	283.69
contra_ECT	462.80	26.07	13.83	0.23	125.73	194.82
contra_ECT1	535.50	34.53	13.49	0.20	145.93	225.25
contra_ECT3	471.80	21.17	13.94	0.16	126.77	199.35
contra_ECT5	439.50	31.97	13.79	0.30	121.39	184.00
contra_ECT6a	419.50	33.22	13.89	0.26	116.72	175.20
contra_ECT6b	306.60	45.46	14.07	0.32	91.62	125.20
contra_ENTl	468.40	22.47	13.64	0.21	126.18	197.74
contra_ENTl1	575.20	38.36	13.21	0.24	156.75	241.98
contra_ENTl3	486.70	26.13	13.73	0.26	131.71	205.16
contra_ENTl5	449.80	18.40	13.62	0.22	120.51	190.23
contra_ENTl6a	430.70	18.60	13.73	0.19	115.80	181.93
contra_ENTl6b	347.80	36.93	14.02	0.31	99.76	143.80
contra_FC	302.10	15.22	13.81	0.28	82.85	126.72
contra_hip	511.60	28.02	14.02	0.37	138.50	215.63
contra_hyp	121.30	11.35	15.77	0.20	37.16	48.91
contra_LA	423.30	26.79	13.88	0.37	116.09	177.62
contra_lay1	486.20	32.01	13.89	0.32	133.11	204.17
contra_lay2	255.40	43.61	14.97	0.33	78.58	103.27
contra_lay3	424.90	28.99	14.49	0.30	117.17	177.96
contra_lay4	404.50	29.91	14.02	0.22	112.16	169.11
contra_lay5	359.20	32.01	14.29	0.26	101.44	149.24
contra_lay6a	361.60	35.51	14.25	0.26	102.90	149.89
contra_lay6b	268.60	39.90	14.33	0.26	80.77	109.37
contra_MOp	392.80	51.61	14.26	0.45	114.78	161.60
contra_MOp1	486.00	56.55	13.89	0.54	139.25	201.26
contra_MOp3	417.80	52.18	14.43	0.50	121.23	172.27
contra_MOp5	373.30	54.43	14.18	0.46	110.59	152.97
contra_MOp6a	345.00	46.30	14.28	0.37	101.49	141.57
contra_MOp6b	256.60	43.28	14.40	0.28	78.64	103.91
contra_MOs	331.20	43.19	14.56	0.42	97.34	135.89

contra_MOs1	448.60	50.85	14.23	0.49	128.54	185.70
contra_MOs3	356.90	41.67	14.72	0.45	103.44	147.08
contra_MOs5	298.40	48.08	14.50	0.42	90.35	121.36
contra_MOs6a	287.10	45.39	14.45	0.37	86.83	116.77
contra_MOs6b	229.00	42.99	14.41	0.27	71.67	92.13
contra_PAA	359.60	24.66	13.92	0.11	99.57	150.38
contra_PAA1	361.00	11.70	13.69	0.10	96.62	152.73
contra_PAA2	363.10	28.41	14.02	0.08	101.40	151.42
contra_PAA3	356.20	30.32	13.99	0.15	100.17	148.21
contra_PERI	474.30	30.73	13.65	0.25	129.73	199.23
contra_PERI1	560.30	50.57	13.33	0.34	156.13	234.07
contra_PERI3	489.80	28.46	13.74	0.28	133.07	206.20
contra_PERI5	449.40	30.28	13.67	0.24	123.40	188.52
contra_PERI6a	435.90	29.81	13.67	0.20	119.89	182.75
contra_PERI6b	325.30	35.49	13.93	0.36	93.77	134.26
contra_PIR	436.20	25.17	13.62	0.15	118.79	183.47
contra_PIR1	490.60	30.39	13.17	0.20	133.59	206.40
contra_PIR2	401.90	31.57	14.13	0.22	111.96	167.77
contra_PIR3	426.30	22.93	13.66	0.16	115.76	179.47
contra_RSPd	285.20	42.28	14.69	0.34	85.63	116.21
contra_RSPd1	404.10	52.42	14.48	0.40	117.85	166.36
contra_RSPd3	306.30	44.49	14.74	0.38	91.48	125.04
contra_RSPd5	245.70	39.14	14.83	0.37	75.01	99.52
contra_RSPd6a	249.70	42.54	14.61	0.30	76.79	100.98
contra_RSPd6b	194.10	39.35	14.40	0.50	62.09	77.48
contra_RSPv	275.40	41.57	14.71	0.30	82.99	112.07
contra_RSPv1	313.10	40.77	14.66	0.31	92.21	128.35
contra_RSPv2	255.80	44.02	14.96	0.34	78.78	103.41
contra_RSPv3	295.40	40.94	14.45	0.35	87.79	120.75
contra_RSPv5	243.90	37.28	14.91	0.27	74.09	98.92
contra_RSPv6a	223.30	36.41	14.81	0.49	68.75	90.14
contra_RSPv6b	182.20	42.27	14.68	0.50	59.91	72.18
contra_SSp-bfd	384.60	32.03	14.49	0.32	107.86	160.17
contra_SSp-bfd1	487.60	33.12	13.97	0.28	133.74	204.63
contra_SSp-bfd3	417.60	31.38	14.73	0.37	116.02	174.46
contra_SSp-bfd4	393.80	31.87	14.09	0.23	110.00	164.24

contra_SSp-bfd5	346.00	31.04	14.52	0.33	97.97	143.61
contra_SSp-bfd6a	355.40	38.87	14.38	0.30	102.24	146.81
contra_SSp-bfd6b	264.00	49.81	14.39	0.34	82.13	106.54
contra_SSP-tr	391.40	40.49	14.35	0.30	111.64	162.16
contra_SSp-tr1	512.10	49.09	13.77	0.44	143.85	213.35
contra_SSp-tr3	437.00	42.30	14.58	0.33	123.55	181.60
contra_SSp-tr4	387.20	41.22	14.21	0.33	110.74	160.29
contra_SSp-tr5	343.00	38.65	14.34	0.24	99.06	141.51
contra_SSp-tr6a	352.80	39.44	14.29	0.26	101.70	145.65
contra_SSp-tr6b	266.40	41.07	14.36	0.24	80.52	108.32
contra_TEa	443.50	30.09	14.00	0.18	121.94	185.95
contra_TEa1	511.10	19.20	13.67	0.17	136.03	216.65
contra_TEa3	473.60	22.75	14.15	0.16	127.66	199.89
contra_TEa4	457.70	27.56	13.71	0.20	124.79	192.45
contra_TEa5	418.30	29.72	14.01	0.25	115.57	175.09
contra_TEa6a	403.00	40.75	14.08	0.23	114.51	167.19
contra_TEa6b	288.70	50.36	14.35	0.27	88.42	117.06
contra_th	305.80	12.22	13.25	0.25	82.88	128.80
ips_amgmed	243.40	32.27	14.73	0.17	72.64	99.24
ips_AUDd	396.80	71.88	14.50	0.48	120.91	161.51
ips_AUDd1	484.70	102.03	14.02	0.72	150.37	196.91
ips_AUDd3	424.30	81.43	14.67	0.56	130.24	172.50
ips_AUDd4	398.50	69.00	14.19	0.47	120.54	162.52
ips_AUDd5	358.10	63.23	14.53	0.37	109.06	145.66
ips_AUDd6a	364.70	59.78	14.42	0.45	109.84	148.77
ips_AUDd6b	262.50	44.52	14.50	0.25	80.44	106.32
ips_AUDp	404.60	66.22	14.39	0.50	121.43	165.31
ips_AUDp1	476.00	88.47	14.09	0.60	144.79	194.13
ips_AUDp3	427.00	79.05	14.61	0.57	130.30	173.83
ips_AUDp4	405.20	64.23	14.10	0.39	120.98	165.81
ips_AUDp5	376.50	62.69	14.39	0.49	113.52	153.58
ips_AUDp6a	366.20	52.02	14.33	0.35	108.23	150.14
ips_AUDp6b	263.30	36.30	14.48	0.24	78.58	107.42
ips_AUDv	418.70	61.82	14.29	0.47	123.82	171.76
ips_AUDv1	479.90	80.57	14.02	0.59	143.77	196.41

ips_AUDv3	442.50	68.64	14.44	0.49	131.52	181.34
ips_AUDv4	423.40	64.87	14.08	0.52	125.72	173.53
ips_AUDv5	391.40	68.07	14.28	0.49	118.56	159.53
ips_AUDv6a	377.10	55.29	14.24	0.39	111.76	154.52
ips_AUDv6b	264.10	45.25	14.40	0.29	81.01	106.95
ips_BLAa	421.50	38.20	13.98	0.36	118.51	175.46
ips_BLAp	435.50	24.23	13.94	0.31	118.50	183.22
ips_BLAv	349.20	57.85	14.00	0.30	105.34	142.39
ips_BMAp	308.30	61.38	14.31	0.38	96.09	124.59
ips_CA1slm	373.70	65.99	14.93	0.53	113.79	152.02
ips_CA1so	534.70	96.55	13.74	0.76	161.44	218.61
ips_CA1sp	179.30	51.62	16.10	0.46	61.87	70.29
ips_CA1sr	561.50	90.53	14.15	0.61	166.70	230.50
ips_CA2slm	514.50	55.66	13.30	0.62	146.02	213.72
ips_CA2so	497.60	30.37	13.21	0.47	135.41	209.38
ips_CA2sp	107.40	47.02	18.27	1.18	43.47	40.38
ips_CA2sr	458.40	52.14	13.76	0.62	131.23	189.84
ips_CA3slm	517.00	90.82	13.70	0.79	155.58	211.49
ips_CA3slu	193.50	47.55	19.95	0.55	65.39	75.83
ips_CA3so	430.80	71.79	13.80	0.80	129.29	176.11
ips_CA3sp	125.70	33.91	19.66	0.53	44.95	48.10
ips_CA3sr	511.00	86.64	14.06	0.89	153.15	209.17
ips_CC	27.10	13.92	15.99	0.91	14.48	9.30
ips_cing	74.20	27.15	15.51	0.75	29.40	27.50
ips_COApl	300.20	44.80	14.29	0.30	89.90	122.48
ips_COApl1	322.40	49.38	13.90	0.33	96.51	131.64
ips_COApl2	292.80	47.53	14.40	0.36	88.77	119.03
ips_COApl3	293.90	45.06	14.43	0.31	88.43	119.73
ips_cortex	379.20	73.14	14.46	0.47	116.82	153.92
ips_CP	323.00	45.57	14.33	0.26	95.79	132.20
ips_cpd	31.20	18.65	17.45	1.19	17.12	10.66
ips_DG	650.00	41.54	13.94	0.51	176.50	273.78
ips_DGinf	649.00	30.36	13.92	0.47	173.44	274.77
ips_DGpo	188.80	20.76	18.04	0.69	57.07	76.44
ips_DGsg	117.60	31.56	20.22	1.23	42.65	44.61
ips_DGsup	651.00	51.08	13.97	0.54	179.15	273.05
ips_ECT	440.30	52.26	14.03	0.45	126.76	182.02

ips_ECT1	490.60	60.42	13.82	0.52	141.34	202.87
ips_ECT3	444.60	50.88	14.11	0.46	127.51	184.00
ips_ECT5	416.50	54.41	14.10	0.47	121.37	171.54
ips_ECT6a	405.70	50.82	14.00	0.38	117.73	167.28
ips_ECT6b	266.63	18.06	14.31	0.08	74.77	110.97
ips_ENTl	447.20	30.60	13.84	0.29	122.98	187.49
ips_ENTl1	503.90	47.05	13.62	0.56	141.28	210.04
ips_ENTl3	452.70	25.31	13.87	0.22	123.03	190.54
ips_ENTl5	434.50	39.41	13.89	0.24	122.01	180.96
ips_ENTl6a	379.63	44.87	13.99	0.27	109.69	156.68
ips_ENTl6b	312.63	51.83	14.33	0.28	94.77	127.18
ips_FC	291.80	20.89	13.81	0.30	81.70	121.53
ips_hip	491.40	74.90	14.20	0.60	145.28	201.78
ips_hyp	118.60	12.88	15.82	0.24	36.89	47.54
ips_LA	406.30	45.45	13.94	0.37	116.51	168.11
ips_lay1	459.00	83.45	14.11	0.64	139.30	187.23
ips_lay2	257.80	50.90	15.05	0.42	81.04	103.69
ips_lay3	402.00	78.55	14.66	0.51	123.93	163.21
ips_lay4	386.60	78.62	14.18	0.48	119.97	156.74
ips_lay5	343.80	71.59	14.44	0.41	107.56	138.98
ips_lay6a	341.90	72.10	14.42	0.42	107.21	138.14
ips_lay6b	252.10	60.03	14.52	0.33	81.74	100.80
ips_MOp	373.10	82.77	14.41	0.65	117.73	150.68
ips_MOp1	449.90	93.02	14.14	0.74	139.45	182.67
ips_MOp3	396.90	87.92	14.63	0.72	125.04	160.42
ips_MOp5	347.60	78.10	14.31	0.57	110.14	140.18
ips_MOp6a	328.20	82.50	14.33	0.56	106.40	131.76
ips_MOp6b	244.60	67.50	14.51	0.40	81.75	97.29
ips_MOs	301.10	64.27	14.71	0.45	95.13	121.25
ips_MOs1	427.60	59.64	14.37	0.56	125.54	175.76
ips_MOs3	326.90	63.39	14.87	0.46	101.40	132.26
ips_MOs5	276.10	60.33	14.58	0.43	87.86	110.91
ips_MOs6a	246.80	63.39	14.70	0.42	81.33	98.35
ips_MOs6b	202.30	51.73	14.74	0.42	67.30	80.16
ips_PAA	335.50	52.76	14.13	0.26	100.66	136.94
ips_PAA1	337.30	80.12	13.86	0.40	107.92	135.83
ips_PAA2	332.60	42.41	14.30	0.15	97.37	136.66

ips_PAA3	334.80	46.80	14.19	0.31	99.02	137.17
ips_PERI	449.70	37.04	13.89	0.39	125.26	187.78
ips_PERI1	510.20	52.19	13.65	0.50	144.14	212.20
ips_PERI3	453.30	28.74	13.95	0.42	124.10	190.33
ips_PERI5	439.00	41.32	13.94	0.38	123.66	182.66
ips_PERI6a	394.88	41.95	14.03	0.22	112.77	163.57
ips_PERI6b	297.88	29.20	14.47	0.18	85.43	123.08
ips_PIR	434.60	36.73	13.74	0.29	121.34	181.33
ips_PIR1	475.00	46.00	13.39	0.40	133.70	197.75
ips_PIR2	406.40	26.96	14.27	0.31	111.99	170.24
ips_PIR3	428.00	35.66	13.75	0.27	119.42	178.61
ips_RSPd	281.80	50.14	14.77	0.31	86.76	114.06
ips_RSPd1	396.80	58.87	14.44	0.44	117.64	162.61
ips_RSPd3	300.40	57.66	14.82	0.35	93.31	121.41
ips_RSPd5	244.50	48.69	14.89	0.29	77.09	98.23
ips_RSPd6a	240.60	54.69	14.71	0.36	77.59	96.20
ips_RSPd6b	181.90	29.88	14.78	0.42	56.74	73.01
ips_RSPv	273.10	50.29	14.74	0.34	84.62	110.33
ips_RSPv1	316.20	51.99	14.60	0.35	95.78	128.65
ips_RSPv2	257.30	50.88	15.04	0.43	80.91	103.48
ips_RSPv3	286.10	48.21	14.51	0.36	87.29	116.09
ips_RSPv5	226.70	43.65	14.89	0.35	71.40	91.01
ips_RSPv6a	222.70	45.51	14.75	0.30	70.82	89.20
ips_RSPv6b	164.50	39.85	15.06	0.89	55.07	64.70
ips_SSp-bfd	374.00	85.51	14.61	0.48	118.65	150.91
ips_SSp-bfd1	475.80	115.14	14.15	0.77	151.47	192.40
ips_SSp-bfd3	400.80	94.85	14.84	0.52	127.75	161.69
ips_SSp-bfd4	378.50	81.89	14.17	0.44	118.75	153.10
ips_SSp-bfd5	336.60	76.69	14.61	0.43	107.09	135.58
ips_SSp-bfd6a	343.10	73.44	14.53	0.43	107.87	138.54
ips_SSp-bfd6b	259.50	61.20	14.53	0.37	83.90	103.85
ips_SSp-tr	370.10	90.14	14.56	0.57	118.84	149.01
ips_SSp-tr1	474.40	101.99	14.09	0.76	147.81	192.53
ips_SSp-tr3	404.90	95.68	14.82	0.61	129.00	163.37
ips_SSp-tr4	366.20	92.40	14.33	0.55	118.37	147.31
ips_SSp-tr5	325.20	84.82	14.51	0.48	106.25	130.39
ips_SSp-tr6a	332.90	93.34	14.53	0.51	110.32	133.29

ips_SSp-tr6b	249.40	80.16	14.58	0.47	86.15	98.93
ips_TEa	428.40	57.36	14.18	0.47	125.10	176.36
ips_TEa1	486.00	63.21	13.92	0.56	140.92	200.59
ips_TEa3	443.70	59.17	14.34	0.49	129.42	182.74
ips_TEa4	426.00	51.34	14.01	0.42	122.94	175.96
ips_TEa5	412.00	61.57	14.18	0.51	122.07	168.92
ips_TEa6a	389.00	67.92	14.19	0.57	117.92	158.52
ips_TEa6b	279.20	54.57	14.29	0.26	87.08	112.70
ips_th	302.60	9.41	13.31	0.30	81.41	127.79

Appendix 4: Raw PSD95 from LFPI experiment at 7 and 28 days

Table 1: PSD95 puncta density at 7 days

	Injury		Sham	
region	Average	SD	Average	SD
contra_amgmed	315.36	34.25	307.00	30.49
contra_AUDd	471.09	38.70	456.50	43.31
contra_AUDd1	572.36	70.12	547.50	54.92
contra_AUDd3	513.45	44.53	498.50	51.80
contra_AUDd4	493.91	41.12	478.56	39.82
contra_AUDd5	440.05	30.33	423.19	51.61
contra_AUDd6a	417.64	21.72	398.56	40.12
contra_AUDd6b	246.50	69.91	234.31	75.80
contra_AUDp	478.64	37.98	460.19	44.50
contra_AUDp1	570.32	61.37	560.81	66.55
contra_AUDp3	517.23	46.28	503.38	53.31
contra_AUDp4	504.18	36.54	487.13	43.41
contra_AUDp5	458.09	36.26	437.38	50.78
contra_AUDp6a	425.55	31.91	398.13	33.53
contra_AUDp6b	254.73	74.55	220.06	73.94
contra_AUDv	498.55	46.30	481.50	45.56
contra_AUDv1	586.86	70.94	579.19	66.39
contra_AUDv3	540.00	52.31	523.94	48.66
contra_AUDv4	527.86	43.30	510.63	57.83
contra_AUDv5	487.68	44.50	467.25	54.68
contra_AUDv6a	431.09	40.55	407.31	32.12
contra_AUDv6b	281.68	48.98	264.50	67.41
contra_BLAa	461.50	40.15	444.63	37.02
contra_BLAp	483.77	51.14	462.19	37.60
contra_BLAv	402.64	45.95	384.06	37.13
contra_BMAp	367.09	55.23	347.00	20.51
contra_CA1slm	512.77	47.19	497.63	25.07
contra_CA1so	662.05	62.26	635.81	52.60
contra_CA1sp	172.05	31.81	149.25	26.38
contra_CA1sr	694.36	62.42	671.19	49.26
contra_CA2slm	552.32	43.85	545.06	12.74
contra_CA2so	518.64	33.35	507.19	23.98

contra_CA2sp	69.18	22.23	54.75	17.25
contra_CA2sr	477.82	37.10	477.44	31.42
contra_CA3slm	575.36	50.66	558.00	23.26
contra_CA3slu	272.86	29.17	261.75	14.73
contra_CA3so	484.09	41.28	473.69	27.24
contra_CA3sp	97.00	27.04	108.06	18.97
contra_CA3sr	536.27	48.67	531.50	18.78
contra_CC	6.82	3.57	8.00	3.12
contra_cing	76.14	25.20	59.13	16.56
contra_COApl	364.50	46.12	349.31	24.73
contra_COApl1	399.00	39.33	383.06	22.89
contra_COApl2	361.09	44.73	347.50	36.72
contra_COApl3	358.59	54.35	339.38	22.03
contra_cortex	455.36	32.27	441.88	41.92
contra_CP	385.68	34.69	373.63	19.01
contra_cpd	12.36	8.15	12.25	7.57
contra_DG	698.73	64.19	669.31	46.91
contra_DGinf	699.55	60.12	670.94	47.82
contra_DGpo	229.50	26.69	226.63	16.97
contra_DGsg	53.68	21.20	48.63	10.35
contra_DGsup	699.82	68.52	669.00	46.97
contra_ECT	510.05	53.13	500.25	42.06
contra_ECT1	587.41	88.03	579.69	59.10
contra_ECT3	541.68	57.00	527.69	43.19
contra_ECT5	491.77	46.02	475.31	44.42
contra_ECT6a	443.95	40.83	423.06	34.89
contra_ECT6b	289.00	52.68	300.19	43.87
contra_ENTl	482.50	56.90	463.31	38.23
contra_ENTl1	572.55	80.11	561.56	63.75
contra_ENTl3	504.82	64.36	490.75	50.30
contra_ENTl5	466.64	55.42	443.81	36.78
contra_ENTl6a	437.27	43.47	417.63	25.20
contra_ENTl6b	325.41	59.20	334.19	48.72
contra_FC	295.41	59.40	284.88	57.10
contra_hip	564.55	47.13	544.31	29.27
contra_hyp	128.64	19.50	124.25	16.19
contra_LA	469.59	40.36	451.81	41.86

contra_lay1	549.18	47.31	544.63	58.26
contra_lay2	306.14	32.14	294.00	22.60
contra_lay3	491.64	37.90	479.38	48.80
contra_lay4	485.68	34.57	470.06	42.31
contra_lay5	431.32	30.27	417.00	43.12
contra_lay6a	400.36	24.87	387.06	32.25
contra_lay6b	264.59	47.76	271.31	42.15
contra_MOp	457.05	37.33	444.13	53.17
contra_MOp1	552.50	57.31	547.31	81.35
contra_MOp3	491.59	41.78	484.50	62.38
contra_MOp5	451.32	43.58	448.31	59.03
contra_MOp6a	391.05	40.01	385.50	41.60
contra_MOp6b	281.32	65.62	289.63	27.79
contra_MOs	388.86	25.02	379.44	46.47
contra_MOs1	515.14	51.67	504.75	78.45
contra_MOs3	416.55	31.80	421.88	52.48
contra_MOs5	356.14	28.40	348.88	36.44
contra_MOs6a	318.82	34.86	307.13	35.00
contra_MOs6b	241.64	59.54	229.13	53.63
contra_PAA	389.14	37.42	380.31	35.72
contra_PAA1	410.20	50.92	392.00	34.57
contra_PAA2	394.50	41.06	383.75	52.51
contra_PAA3	383.95	35.46	374.75	27.20
contra_PERI	504.82	54.94	489.13	44.87
contra_PERI1	582.86	85.41	581.81	69.59
contra_PERI3	526.45	62.15	512.88	45.47
contra_PERI5	490.23	49.04	468.75	44.38
contra_PERI6a	446.32	42.50	432.44	35.23
contra_PERI6b	291.36	58.04	296.38	42.14
contra_PIR	465.36	38.50	443.75	27.67
contra_PIR1	516.55	60.89	493.25	40.87
contra_PIR2	402.95	48.00	399.44	14.35
contra_PIR3	461.36	35.71	441.63	27.78
contra_RSPd	352.82	21.83	355.25	34.80
contra_RSPd1	477.77	63.20	481.69	59.92
contra_RSPd3	385.77	27.00	385.44	45.25
contra_RSPd5	310.91	23.81	315.75	26.21

contra_RSPd6a	300.50	24.29	291.63	29.96
contra_RSPd6b	221.68	56.86	237.75	49.67
contra_RSPv	339.77	21.71	335.94	22.74
contra_RSPv1	391.82	32.17	381.81	39.90
contra_RSPv2	306.59	31.51	293.38	21.67
contra_RSPv3	378.50	27.29	380.69	36.40
contra_RSPv5	316.64	27.73	324.25	26.83
contra_RSPv6a	282.45	29.94	276.56	24.72
contra_RSPv6b	232.95	48.05	216.63	50.29
contra_SSp-bfd	444.64	31.29	426.63	46.22
contra_SSp-bfd1	564.09	52.50	545.19	65.07
contra_SSp-bfd3	484.91	40.31	462.88	56.89
contra_SSp-bfd4	464.50	32.24	448.31	42.81
contra_SSp-bfd5	414.73	28.10	396.13	43.00
contra_SSp-bfd6a	397.32	22.64	381.94	33.21
contra_SSp-bfd6b	257.55	60.50	264.38	61.83
contra_SSP-tr	458.09	34.06	448.88	44.14
contra_SSp-tr1	560.59	48.67	563.94	61.32
contra_SSp-tr3	502.14	41.19	493.69	52.24
contra_SSp-tr4	475.41	37.18	461.94	46.35
contra_SSp-tr5	425.36	37.12	419.25	44.35
contra_SSp-tr6a	392.14	29.17	393.25	34.48
contra_SSp-tr6b	245.32	60.25	267.50	47.13
contra_TEa	516.23	53.70	495.50	40.56
contra_TEa1	595.95	81.37	580.56	63.29
contra_TEa3	553.18	54.20	532.31	51.80
contra_TEa4	538.77	50.17	520.00	43.75
contra_TEa5	499.73	53.40	480.19	46.53
contra_TEa6a	439.32	42.35	414.50	37.29
contra_TEa6b	281.36	46.95	306.69	37.66
contra_th	320.55	30.80	308.50	25.08
ips_amgmed	298.27	38.37	285.19	20.74
ips_AUDd	432.86	40.18	428.19	36.78
ips_AUDd1	518.41	80.29	505.44	70.26

ips_AUDd3	469.95	52.77	462.13	46.08
ips_AUDd4	454.82	39.00	452.81	35.85
ips_AUDd5	396.86	34.76	400.00	33.43
ips_AUDd6a	378.86	32.31	381.75	25.14
ips_AUDd6b	228.36	66.95	279.00	47.64
ips_AUDp	449.14	41.21	439.75	41.89
ips_AUDp1	549.59	73.78	515.50	66.92
ips_AUDp3	488.50	51.72	477.06	48.19
ips_AUDp4	475.00	45.90	462.31	45.60
ips_AUDp5	417.77	33.78	417.56	41.09
ips_AUDp6a	378.23	37.27	389.44	30.30
ips_AUDp6b	221.55	65.63	239.56	67.96
ips_AUDv	472.18	44.69	455.75	44.93
ips_AUDv1	588.00	57.44	536.56	63.03
ips_AUDv3	519.55	48.02	491.94	38.74
ips_AUDv4	485.00	47.57	463.94	36.34
ips_AUDv5	442.82	38.82	439.88	47.32
ips_AUDv6a	390.36	41.34	382.13	43.12
ips_AUDv6b	258.50	46.40	261.25	69.96
ips_BLAa	444.27	32.30	438.44	25.04
ips_BLAp	461.50	37.24	445.56	38.96
ips_BLAv	376.50	63.62	377.31	57.81
ips_BMAp	344.05	58.90	331.56	35.79
ips_CA1slm	515.68	42.99	493.06	19.66
ips_CA1so	666.86	60.91	632.06	51.30
ips_CA1sp	166.64	42.06	136.38	18.48
ips_CA1sr	704.91	61.67	670.38	57.97
ips_CA2slm	544.41	38.20	545.63	28.30
ips_CA2so	504.27	37.12	500.38	26.62
ips_CA2sp	62.00	31.94	37.00	12.03
ips_CA2sr	481.14	38.00	469.38	39.78
ips_CA3slm	547.23	44.04	539.94	43.56
ips_CA3slu	269.45	29.19	260.75	28.40
ips_CA3so	474.05	47.59	460.50	43.77
ips_CA3sp	105.45	21.89	85.25	28.76
ips_CA3sr	527.18	41.94	516.50	41.12
ips_CC	6.41	4.10	7.38	2.72

ips_cing	75.41	31.06	44.06	17.54
ips_COApl	360.45	58.72	327.00	23.44
ips_COApl1	403.86	65.60	358.06	27.55
ips_COApl2	350.91	65.06	318.69	28.82
ips_COApl3	350.14	57.56	319.63	28.22
ips_cortex	399.27	33.35	406.13	36.62
ips_CP	352.18	37.30	355.13	23.25
ips_cpd	9.82	5.33	11.75	8.21
ips_DG	703.36	57.84	663.31	48.77
ips_DGinf	697.77	54.42	665.44	47.89
ips_DGpo	227.36	27.78	218.50	24.17
ips_DGsg	60.18	19.72	43.75	15.42
ips_DGsup	707.45	60.86	663.19	49.79
ips_ECT	486.91	43.84	480.81	48.32
ips_ECT1	570.23	76.77	554.19	78.11
ips_ECT3	516.23	50.46	511.06	53.30
ips_ECT5	465.32	39.36	455.94	43.31
ips_ECT6a	417.41	40.53	405.75	47.41
ips_ECT6b	266.09	65.90	271.25	63.75
ips_ENTl	460.14	57.83	452.06	49.38
ips_ENTl1	579.27	92.58	558.31	77.28
ips_ENTl3	479.95	74.17	475.63	64.71
ips_ENTl5	435.32	49.12	437.31	40.86
ips_ENTl6a	390.00	45.92	403.31	46.85
ips_ENTl6b	297.23	53.58	334.06	64.70
ips_FC	281.64	38.34	262.44	40.11
ips_hip	559.18	39.94	543.88	29.36
ips_hyp	128.64	16.37	124.25	16.16
ips_LA	428.32	31.15	425.56	32.97
ips_lay1	477.55	59.94	485.00	59.02
ips_lay2	286.64	39.52	278.25	20.17
ips_lay3	433.86	42.60	435.75	45.41
ips_lay4	430.95	39.80	429.06	39.47
ips_lay5	378.09	29.16	387.50	32.51
ips_lay6a	345.23	40.90	355.69	32.71
ips_lay6b	229.86	52.97	240.69	50.33
ips_MOp	378.45	44.08	378.31	33.08

ips_MOp1	415.36	74.29	439.57	59.82
ips_MOp3	401.27	54.98	403.44	38.86
ips_MOp5	388.55	42.99	384.81	36.78
ips_MOp6a	336.82	49.52	322.00	54.35
ips_MOp6b	218.23	85.12	200.50	59.97
ips_MOs	327.55	36.93	334.81	24.52
ips_MOs1	404.65	64.29	429.94	52.83
ips_MOs3	357.95	44.25	369.31	32.27
ips_MOs5	310.32	38.89	314.25	27.84
ips_MOs6a	276.45	44.29	261.63	37.29
ips_MOs6b	231.18	50.66	189.94	34.18
ips_PAA	366.23	40.28	366.88	52.44
ips_PAA1	388.64	53.32	370.31	62.77
ips_PAA2	363.73	42.44	361.00	31.06
ips_PAA3	359.77	43.85	368.00	60.61
ips_PERI	484.68	47.89	476.63	53.50
ips_PERI1	601.95	74.49	560.88	79.94
ips_PERI3	514.59	54.03	490.81	50.37
ips_PERI5	454.95	43.07	460.38	53.27
ips_PERI6a	413.18	48.70	424.81	50.71
ips_PERI6b	283.59	60.03	276.13	71.03
ips_PIR	436.64	43.54	421.31	42.49
ips_PIR1	501.27	64.19	472.75	67.52
ips_PIR2	380.77	64.55	376.38	36.19
ips_PIR3	429.82	38.30	418.94	38.17
ips_RSPd	321.45	26.47	334.25	23.74
ips_RSPd1	408.95	53.37	420.06	41.21
ips_RSPd3	352.09	35.92	359.56	24.65
ips_RSPd5	289.50	30.46	299.94	35.33
ips_RSPd6a	273.86	36.60	271.38	26.51
ips_RSPd6b	237.18	51.38	214.06	40.09
ips_RSPv	321.00	26.63	322.25	22.94
ips_RSPv1	363.09	38.55	355.81	15.82
ips_RSPv2	286.59	39.38	277.19	20.87
ips_RSPv3	364.64	30.47	361.88	25.83
ips_RSPv5	302.55	22.12	310.69	32.00
ips_RSPv6a	261.50	32.01	254.25	31.05

ips_RSPv6b	235.86	55.75	204.81	32.84
ips_SSp-bfd	400.14	42.88	410.50	45.41
ips_SSp-bfd1	498.23	80.04	513.31	55.30
ips_SSp-bfd3	438.59	57.64	450.13	58.95
ips_SSp-bfd4	426.64	43.96	431.06	42.78
ips_SSp-bfd5	371.32	34.46	381.75	40.22
ips_SSp-bfd6a	352.41	39.92	368.81	33.84
ips_SSp-bfd6b	232.27	66.49	264.00	55.93
ips_SSp-tr	378.86	34.83	394.63	39.56
ips_SSp-tr1	460.91	69.96	475.19	67.78
ips_SSp-tr3	408.77	46.21	418.38	52.91
ips_SSp-tr4	397.00	36.26	406.81	39.89
ips_SSp-tr5	359.00	27.30	378.25	34.57
ips_SSp-tr6a	328.18	53.75	343.06	37.64
ips_SSp-tr6b	201.14	65.53	216.88	56.78
ips_TEa	485.91	43.03	476.00	48.08
ips_TEa1	576.68	71.69	560.25	62.17
ips_TEa3	523.91	51.86	508.81	47.18
ips_TEa4	494.95	49.53	480.88	51.17
ips_TEa5	467.77	39.46	456.75	43.85
ips_TEa6a	396.14	36.26	397.75	46.87
ips_TEa6b	253.64	47.99	260.44	71.17
ips_th	309.82	30.51	296.75	28.23

Table 2: PSD95 puncta size at 7 days

	Injury		**Sham**	
region	**Average**	**SD**	**Average**	**SD**
contra_amgmed	12.47	0.17	12.44	0.14
contra_AUDd	12.23	0.16	12.15	0.13
contra_AUDd1	12.12	0.21	12.02	0.14
contra_AUDd3	12.38	0.14	12.28	0.12
contra_AUDd4	12.06	0.20	11.95	0.16
contra_AUDd5	12.25	0.18	12.17	0.16
contra_AUDd6a	12.06	0.17	12.01	0.09
contra_AUDd6b	12.62	0.29	12.52	0.36
contra_AUDp	12.19	0.18	12.11	0.15

contra_AUDp1	12.11	0.22	11.98	0.15
contra_AUDp3	12.32	0.18	12.22	0.16
contra_AUDp4	12.04	0.15	11.93	0.13
contra_AUDp5	12.17	0.17	12.10	0.16
ontra_AUDp6a	12.06	0.22	12.01	0.12
contra_AUDp6b	12.52	0.33	12.56	0.29
contra_AUDv	12.09	0.21	11.98	0.20
contra_AUDv1	12.05	0.25	11.89	0.20
contra_AUDv3	12.19	0.18	12.06	0.24
contra_AUDv4	12.00	0.16	11.84	0.15
contra_AUDv5	12.01	0.21	11.96	0.22
contra_AUDv6a	12.07	0.28	11.99	0.15
contra_AUDv6b	12.45	0.30	12.43	0.27
contra_BLAa	11.93	0.32	11.78	0.19
contra_BLAp	11.99	0.34	11.88	0.18
contra_BLAv	12.07	0.25	11.99	0.21
contra_BMAp	12.21	0.27	12.20	0.22
contra_CA1slm	11.92	0.20	11.93	0.16
contra_CA1so	11.30	0.22	11.35	0.19
contra_CA1sp	12.43	0.24	12.47	0.25
contra_CA1sr	11.41	0.20	11.44	0.18
contra_CA2slm	11.19	0.22	11.21	0.09
contra_CA2so	11.24	0.19	11.26	0.08
contra_CA2sp	14.40	0.68	15.09	0.79
contra_CA2sr	11.50	0.23	11.53	0.15
contra_CA3slm	11.55	0.28	11.63	0.18
contra_CA3slu	14.47	0.44	14.43	0.42
contra_CA3so	11.73	0.34	11.74	0.15
contra_CA3sp	15.41	0.71	15.26	0.33
contra_CA3sr	11.92	0.38	11.92	0.18
contra_CC	13.28	0.45	13.06	0.22
contra_cing	13.26	0.26	13.12	0.23
contra_COApl	12.29	0.28	12.26	0.22
contra_COApl1	12.08	0.25	12.07	0.23
contra_COApl2	12.33	0.29	12.30	0.31
contra_COApl3	12.35	0.31	12.33	0.17
contra_cortex	12.19	0.14	12.14	0.14

contra_CP	12.02	0.25	11.98	0.15
contra_cpd	13.99	0.75	13.89	0.39
contra_DG	11.27	0.26	11.30	0.15
contra_DGinf	11.30	0.28	11.31	0.11
contra_DGpo	14.39	0.28	14.49	0.23
contra_DGsg	15.13	0.33	14.87	0.38
contra_DGsup	11.25	0.25	11.29	0.18
contra_ECT	11.99	0.22	11.87	0.17
contra_ECT1	11.96	0.25	11.77	0.20
contra_ECT3	12.03	0.19	11.92	0.17
contra_ECT5	11.91	0.25	11.82	0.17
contra_ECT6a	11.93	0.24	11.83	0.24
contra_ECT6b	12.46	0.42	12.30	0.27
contra_ENTl	11.85	0.27	11.74	0.22
contra_ENTl1	11.72	0.26	11.64	0.36
contra_ENTl3	11.91	0.26	11.79	0.23
contra_ENTl5	11.98	0.30	11.84	0.16
contra_ENTl6a	11.70	0.26	11.59	0.24
contra_ENTl6b	12.01	0.37	11.88	0.28
contra_FC	11.70	0.14	11.68	0.16
contra_hip	11.56	0.24	11.59	0.15
contra_hyp	13.92	0.11	13.88	0.18
contra_LA	11.88	0.30	11.81	0.21
contra_lay1	12.10	0.16	12.01	0.16
contra_lay2	12.50	0.11	12.60	0.15
contra_lay3	12.27	0.13	12.22	0.15
contra_lay4	12.04	0.14	11.94	0.13
contra_lay5	12.23	0.16	12.19	0.14
contra_lay6a	12.09	0.17	12.05	0.13
contra_lay6b	12.48	0.22	12.39	0.20
contra_MOp	12.10	0.14	12.15	0.19
contra_MOp1	12.03	0.19	12.08	0.27
contra_MOp3	12.09	0.14	12.14	0.20
contra_MOp5	12.14	0.15	12.15	0.17
contra_MOp6a	12.08	0.15	12.17	0.18
contra_MOp6b	12.45	0.34	12.30	0.11
contra_MOs	12.46	0.15	12.51	0.21

contra_MOs1	12.39	0.17	12.38	0.24
contra_MOs3	12.48	0.14	12.51	0.22
contra_MOs5	12.57	0.17	12.70	0.22
contra_MOs6a	12.38	0.18	12.44	0.20
contra_MOs6b	12.53	0.22	12.52	0.27
contra_PAA	12.10	0.22	12.03	0.28
contra_PAA1	11.95	0.26	11.96	0.26
contra_PAA2	12.05	0.23	12.01	0.35
contra_PAA3	12.18	0.20	12.09	0.26
contra_PERI	11.90	0.25	11.80	0.24
contra_PERI1	11.81	0.28	11.69	0.33
contra_PERI3	11.94	0.22	11.83	0.24
contra_PERI5	11.93	0.29	11.83	0.18
contra_PERI6a	11.78	0.28	11.70	0.29
contra_PERI6b	12.32	0.47	12.18	0.27
contra_PIR	11.80	0.25	11.74	0.15
contra_PIR1	11.68	0.25	11.63	0.16
contra_PIR2	11.86	0.25	11.79	0.15
contra_PIR3	11.83	0.25	11.76	0.15
contra_RSPd	12.65	0.13	12.66	0.17
contra_RSPd1	12.57	0.24	12.53	0.16
contra_RSPd3	12.59	0.11	12.56	0.19
contra_RSPd5	13.00	0.17	13.03	0.24
contra_RSPd6a	12.54	0.14	12.67	0.20
contra_RSPd6b	12.57	0.15	12.51	0.15
contra_RSPv	12.52	0.12	12.58	0.15
contra_RSPv1	12.53	0.12	12.62	0.20
contra_RSPv2	12.50	0.11	12.60	0.15
contra_RSPv3	12.26	0.12	12.31	0.13
contra_RSPv5	12.77	0.16	12.73	0.13
contra_RSPv6a	12.70	0.16	12.82	0.18
contra_RSPv6b	12.54	0.31	12.52	0.17
contra_SSp-bfd	12.27	0.15	12.22	0.16
contra_SSp-bfd1	12.12	0.18	12.05	0.17
contra_SSp-bfd3	12.40	0.15	12.38	0.20
contra_SSp-bfd4	12.06	0.18	11.95	0.14

contra_SSp-bfd5	12.31	0.18	12.30	0.13
contra_SSp-bfd6a	12.10	0.18	12.03	0.12
contra_SSp-bfd6b	12.58	0.29	12.43	0.24
contra_SSP-tr	12.19	0.11	12.13	0.13
contra_SSp-tr1	12.02	0.13	11.93	0.16
contra_SSp-tr3	12.27	0.12	12.21	0.14
contra_SSp-tr4	12.04	0.12	11.98	0.14
contra_SSp-tr5	12.30	0.17	12.24	0.13
contra_SSp-tr6a	12.09	0.15	12.05	0.13
contra_SSp-tr6b	12.53	0.26	12.42	0.17
contra_TEa	12.03	0.23	11.92	0.17
contra_TEa1	11.99	0.28	11.84	0.22
contra_TEa3	12.12	0.19	11.96	0.17
contra_TEa4	11.98	0.20	11.84	0.12
contra_TEa5	11.93	0.21	11.86	0.18
contra_TEa6a	12.05	0.31	12.00	0.17
contra_TEa6b	12.44	0.32	12.23	0.24
contra_th	11.66	0.17	11.67	0.12
ips_amgmed	12.54	0.20	12.61	0.12
ips_AUDd	12.27	0.19	12.25	0.16
ips_AUDd1	12.21	0.24	12.24	0.28
ips_AUDd3	12.37	0.23	12.29	0.21
ips_AUDd4	12.13	0.20	12.11	0.14
ips_AUDd5	12.32	0.20	12.32	0.13
ips_AUDd6a	12.07	0.19	12.09	0.14
ips_AUDd6b	12.72	0.29	12.50	0.31
ips_AUDp	12.15	0.18	12.18	0.19
ips_AUDp1	12.05	0.21	12.16	0.24
ips_AUDp3	12.18	0.18	12.19	0.27
ips_AUDp4	12.02	0.19	12.09	0.18
ips_AUDp5	12.19	0.18	12.22	0.17
ips_AUDp6a	12.11	0.24	12.10	0.17
ips_AUDp6b	12.77	0.26	12.71	0.31
ips_AUDv	11.97	0.13	12.03	0.20
ips_AUDv1	11.88	0.12	12.02	0.27

ips_AUDv3	11.95	0.11	11.98	0.23
ips_AUDv4	11.98	0.17	12.03	0.16
ips_AUDv5	11.95	0.17	12.02	0.21
ips_AUDv6a	12.03	0.24	12.11	0.19
ips_AUDv6b	12.65	0.18	12.58	0.32
ips_BLAa	11.84	0.22	11.88	0.21
ips_BLAp	11.91	0.22	11.97	0.22
ips_BLAv	12.18	0.29	12.21	0.35
ips_BMAp	12.37	0.31	12.39	0.39
ips_CA1slm	11.88	0.24	11.95	0.18
ips_CA1so	11.22	0.26	11.38	0.21
ips_CA1sp	12.47	0.24	12.55	0.22
ips_CA1sr	11.33	0.23	11.44	0.22
ips_CA2slm	11.21	0.27	11.33	0.20
ips_CA2so	11.28	0.21	11.38	0.15
ips_CA2sp	15.09	1.20	15.70	1.32
ips_CA2sr	11.53	0.31	11.70	0.26
ips_CA3slm	11.63	0.35	11.80	0.33
ips_CA3slu	14.48	0.41	14.65	0.37
ips_CA3so	11.75	0.40	11.96	0.28
ips_CA3sp	15.28	0.40	15.75	0.80
ips_CA3sr	11.91	0.41	12.11	0.28
ips_CC	13.29	0.44	13.06	0.23
ips_cing	13.18	0.25	13.09	0.35
ips_COApl	12.37	0.35	12.49	0.21
ips_COApl1	12.17	0.32	12.28	0.20
ips_COApl2	12.42	0.38	12.53	0.28
ips_COApl3	12.44	0.36	12.56	0.23
ips_cortex	12.29	0.18	12.28	0.16
ips_CP	12.10	0.23	12.12	0.18
ips_cpd	13.99	0.64	13.83	0.63
ips_DG	11.20	0.28	11.35	0.21
ips_DGinf	11.22	0.27	11.35	0.18
ips_DGpo	14.39	0.30	14.52	0.24
ips_DGsg	15.05	0.37	15.05	0.58
ips_DGsup	11.18	0.29	11.35	0.24
ips_ECT	11.88	0.15	11.92	0.19

ips_ECT1	11.88	0.24	11.87	0.18
ips_ECT3	11.91	0.16	11.94	0.18
ips_ECT5	11.77	0.14	11.82	0.16
ips_ECT6a	11.87	0.16	11.93	0.30
ips_ECT6b	12.42	0.33	12.48	0.41
ips_ENTl	11.81	0.21	11.82	0.20
ips_ENTl1	11.56	0.23	11.56	0.24
ips_ENTl3	11.81	0.25	11.83	0.22
ips_ENTl5	11.95	0.21	11.94	0.25
ips_ENTl6a	11.79	0.19	11.77	0.21
ips_ENTl6b	12.12	0.26	12.01	0.34
ips_FC	11.80	0.16	11.77	0.08
ips_hip	11.51	0.26	11.65	0.22
ips_hyp	13.92	0.10	13.88	0.20
ips_LA	11.90	0.22	11.93	0.22
ips_lay1	12.24	0.20	12.22	0.18
ips_lay2	12.56	0.16	12.61	0.13
ips_lay3	12.31	0.18	12.30	0.16
ips_lay4	12.18	0.23	12.19	0.17
ips_lay5	12.34	0.15	12.35	0.15
ips_lay6a	12.18	0.19	12.19	0.15
ips_lay6b	12.64	0.20	12.55	0.25
ips_MOp	12.31	0.26	12.41	0.19
ips_MOp1	12.41	0.39	12.44	0.24
ips_MOp3	12.35	0.33	12.48	0.20
ips_MOp5	12.26	0.24	12.35	0.16
ips_MOp6a	12.24	0.22	12.35	0.17
ips_MOp6b	12.58	0.29	12.69	0.37
ips_MOs	12.73	0.23	12.72	0.18
ips_MOs1	12.73	0.30	12.70	0.25
ips_MOs3	12.79	0.27	12.79	0.21
ips_MOs5	12.83	0.26	12.84	0.13
ips_MOs6a	12.51	0.12	12.58	0.19
ips_MOs6b	12.57	0.15	12.64	0.21
ips_PAA	12.33	0.24	12.30	0.36
ips_PAA1	12.22	0.29	12.25	0.36
ips_PAA2	12.34	0.27	12.29	0.36

ips_PAA3	12.35	0.22	12.34	0.38
ips_PERI	11.78	0.16	11.84	0.20
ips_PERI1	11.65	0.19	11.69	0.21
ips_PERI3	11.80	0.14	11.87	0.19
ips_PERI5	11.84	0.21	11.88	0.21
ips_PERI6a	11.76	0.24	11.78	0.26
ips_PERI6b	12.31	0.44	12.41	0.49
ips_PIR	11.85	0.21	11.90	0.22
ips_PIR1	11.80	0.27	11.82	0.28
ips_PIR2	11.98	0.34	12.03	0.29
ips_PIR3	11.83	0.17	11.90	0.20
ips_RSPd	12.80	0.16	12.76	0.18
ips_RSPd1	12.80	0.24	12.70	0.18
ips_RSPd3	12.75	0.17	12.71	0.19
ips_RSPd5	13.07	0.14	13.02	0.21
ips_RSPd6a	12.65	0.18	12.71	0.09
ips_RSPd6b	12.46	0.18	12.48	0.18
ips_RSPv	12.61	0.15	12.63	0.12
ips_RSPv1	12.71	0.18	12.71	0.11
ips_RSPv2	12.56	0.16	12.61	0.14
ips_RSPv3	12.33	0.16	12.35	0.14
ips_RSPv5	12.79	0.15	12.76	0.21
ips_RSPv6a	12.69	0.20	12.81	0.11
ips_RSPv6b	12.56	0.19	12.47	0.28
ips_SSp-bfd	12.36	0.24	12.27	0.19
ips_SSp-bfd1	12.24	0.26	12.12	0.24
ips_SSp-bfd3	12.45	0.28	12.30	0.22
ips_SSp-bfd4	12.25	0.28	12.18	0.18
ips_SSp-bfd5	12.45	0.19	12.44	0.21
ips_SSp-bfd6a	12.18	0.22	12.12	0.18
ips_SSp-bfd6b	12.71	0.29	12.47	0.21
ips_SSp-tr	12.38	0.19	12.37	0.18
ips_SSp-tr1	12.26	0.27	12.25	0.20
ips_SSp-tr3	12.44	0.22	12.44	0.21
ips_SSp-tr4	12.27	0.24	12.32	0.21
ips_SSp-tr5	12.47	0.15	12.46	0.15
ips_SSp-tr6a	12.24	0.25	12.22	0.16

ips_SSp-tr6b	12.80	0.35	12.62	0.28
ips_TEa	11.92	0.15	11.93	0.19
ips_TEa1	11.90	0.20	11.85	0.18
ips_TEa3	11.90	0.16	11.91	0.21
ips_TEa4	11.97	0.15	11.98	0.21
ips_TEa5	11.79	0.14	11.87	0.17
ips_TEa6a	12.03	0.22	12.07	0.27
ips_TEa6b	12.55	0.26	12.53	0.37
ips_th	11.84	0.19	11.82	0.17

Table 3: PSD95 puncta intensity at 7 days

	Injury		**Sham**	
region	**Average**	**SD**	**Average**	**SD**
contra_amgmed	12995.74	2966.05	12691.52	2394.19
contra_AUDd	19984.26	4269.30	19658.92	2756.98
contra_AUDd1	21654.19	4454.66	20812.08	2656.84
contra_AUDd3	22387.37	4674.55	21953.59	2896.94
contra_AUDd4	20134.59	4483.84	19711.07	3102.17
contra_AUDd5	18449.34	4047.57	18310.46	2945.41
contra_AUDd6a	17211.65	3883.18	16955.50	2784.05
contra_AUDd6b	12463.08	3278.44	12119.61	1909.13
contra_AUDp	19973.43	4309.67	19612.72	2894.11
contra_AUDp1	21394.86	4334.89	21085.31	3215.65
contra_AUDp3	22088.33	4672.71	21902.58	3220.05
contra_AUDp4	20301.61	4492.15	19889.97	3066.53
contra_AUDp5	18843.38	4184.86	18427.54	2972.79
ontra_AUDp6a	17376.81	4147.87	17047.40	2714.34
contra_AUDp6b	12399.45	3634.64	11902.12	1730.60
contra_AUDv	20033.72	4501.86	19617.16	2943.45
contra_AUDv1	21627.34	4831.26	21356.96	3185.38
contra_AUDv3	22075.43	4993.20	21780.14	3309.07
contra_AUDv4	20627.55	4608.29	20245.74	3403.68
contra_AUDv5	19037.84	4456.16	18561.95	3113.91
contra_AUDv6a	17513.66	4263.90	17040.50	2747.98
contra_AUDv6b	12810.86	3607.02	12513.11	2178.76
contra_BLAa	15997.54	3904.58	15416.02	2769.13
contra_BLAp	17241.96	4085.05	17101.43	2759.16

contra_BLAv	14582.16	3620.79	14149.48	2611.59
contra_BMAp	13708.62	3306.74	13249.68	2497.65
contra_CA1slm	15039.23	3156.36	13374.91	1772.15
contra_CA1so	16258.74	3192.62	14732.51	2219.87
contra_CA1sp	10776.94	2046.65	9688.88	1165.42
contra_CA1sr	18604.79	3311.09	16705.59	2530.92
contra_CA2slm	10778.78	2329.72	9929.08	1395.45
contra_CA2so	10651.33	2358.28	9835.44	1647.22
contra_CA2sp	7865.82	1296.54	7486.41	643.97
contra_CA2sr	10484.76	2247.10	9886.53	1610.64
contra_CA3slm	10704.42	2167.39	9878.58	1503.35
contra_CA3slu	13240.39	3068.84	12350.96	1756.64
contra_CA3so	10502.24	2211.63	9774.85	1575.88
contra_CA3sp	9561.69	1794.43	9118.41	669.69
contra_CA3sr	11817.58	2356.87	11005.11	1716.32
contra_CC	7996.47	1343.41	7856.79	460.58
contra_cing	9820.15	1699.90	8874.05	1160.28
contra_COApl	13926.44	3103.83	13710.61	2950.79
contra_COApl1	14544.70	3191.90	14477.10	3099.89
contra_COApl2	13788.95	3015.08	13636.78	3117.84
contra_COApl3	13908.92	3163.48	13611.18	2830.52
contra_cortex	18951.25	3746.67	18372.02	2774.57
contra_CP	15007.94	3465.22	14629.89	2436.74
contra_cpd	7666.12	1291.34	7881.45	922.36
contra_DG	15072.98	2691.06	13462.39	1758.84
contra_DGinf	14564.32	2374.37	13068.83	1801.67
contra_DGpo	10563.30	1810.84	9851.01	1177.13
contra_DGsg	7301.77	894.61	6857.01	325.79
contra_DGsup	15363.37	2898.79	13695.90	1760.28
contra_ECT	19775.04	4664.05	19371.20	2987.72
contra_ECT1	21236.38	5007.87	20791.06	3360.84
contra_ECT3	21177.16	4961.62	20791.10	3365.96
contra_ECT5	18570.10	4523.21	17964.55	2937.80
contra_ECT6a	17359.06	4389.50	16831.13	2700.59
contra_ECT6b	12807.41	3404.43	12732.70	2022.40
contra_ENTl	17350.93	4592.71	16964.02	3006.13
contra_ENTl1	18729.70	4218.80	17949.82	3045.55

contra_ENTl3	18294.20	4552.14	17786.39	3213.47
contra_ENTl5	17072.57	4617.16	16724.56	3142.67
contra_ENTl6a	14836.85	4255.32	14259.34	2284.29
contra_ENTl6b	12343.84	3253.60	12303.43	2284.65
contra_FC	8531.22	1724.34	7179.72	761.82
contra_hip	14062.48	2712.94	12585.90	1882.41
contra_hyp	10833.81	2068.31	10603.23	1793.99
contra_LA	16837.86	3981.70	16686.36	3006.12
contra_lay1	20391.18	3806.68	19851.68	3158.57
contra_lay2	14655.17	3196.52	12483.85	2112.65
contra_lay3	21038.48	4102.85	20307.55	3188.96
contra_lay4	19818.00	4163.10	19097.96	2973.23
contra_lay5	18200.91	3870.16	17558.12	2790.63
contra_lay6a	16471.83	3726.08	15806.27	2579.32
contra_lay6b	12392.50	2958.66	12032.60	1817.54
contra_MOp	18621.56	3359.68	17427.91	2958.14
contra_MOp1	19931.29	3577.65	19534.72	3769.52
contra_MOp3	19802.91	3602.14	18801.68	3488.96
contra_MOp5	18498.02	3665.28	17239.58	2970.93
contra_MOp6a	15984.73	3610.83	14376.48	2492.22
contra_MOp6b	12642.51	3052.67	11415.42	1644.91
contra_MOs	18558.38	3141.31	17159.62	3046.10
contra_MOs1	21877.06	4334.53	20628.60	3856.76
contra_MOs3	19682.62	3427.09	18711.95	3291.27
contra_MOs5	16901.53	3571.76	15525.74	2881.04
contra_MOs6a	14333.23	3244.86	12754.48	2351.87
contra_MOs6b	11974.40	2699.40	10702.77	2040.77
contra_PAA	14010.84	3147.67	14201.60	2640.32
contra_PAA1	14041.21	3437.44	14095.38	2646.14
contra_PAA2	13975.68	3194.32	14178.72	2709.21
contra_PAA3	14180.91	3162.18	14274.70	2648.24
contra_PERI	18722.54	4566.73	18371.67	2996.13
contra_PERI1	20027.27	4831.12	19746.43	3199.95
contra_PERI3	19742.87	4842.20	19419.76	3239.86
contra_PERI5	18050.39	4491.77	17503.94	3178.20
contra_PERI6a	16228.15	4328.62	15740.42	2378.86
contra_PERI6b	12440.65	3375.51	12200.93	1860.48

contra_PIR	15523.77	3541.86	15077.78	2561.45
contra_PIR1	15897.22	3496.15	15512.03	2677.42
contra_PIR2	14645.16	3499.78	14272.59	2449.51
contra_PIR3	15650.76	3556.59	15203.21	2577.16
contra_RSPd	18036.39	3448.88	16654.21	2791.83
contra_RSPd1	21633.70	4738.12	20531.89	3743.91
contra_RSPd3	18985.33	3580.46	17682.70	3155.17
contra_RSPd5	16224.51	3612.51	14810.05	2329.50
contra_RSPd6a	14048.04	2973.97	12524.85	2176.64
contra_RSPd6b	12161.13	2688.61	10955.96	2015.51
contra_RSPv	16381.21	3253.98	14340.36	2496.80
contra_RSPv1	18469.70	3737.10	16054.49	3043.32
contra_RSPv2	14657.42	3182.48	12496.62	2071.30
contra_RSPv3	17358.88	3324.98	15385.41	2840.59
contra_RSPv5	15793.06	3373.60	14267.48	2282.10
contra_RSPv6a	13383.31	2849.27	12108.43	1935.19
contra_RSPv6b	12622.55	2568.38	10951.72	2007.18
contra_SSp-bfd	19265.36	4089.16	18628.16	2916.66
contra_SSp-bfd1	21471.57	4235.56	19930.24	3429.01
contra_SSp-bfd3	21875.01	4592.29	20654.58	3243.12
contra_SSp-bfd4	19411.84	4291.02	18552.15	2892.29
contra_SSp-bfd5	18167.52	3960.16	17540.34	2761.27
contra_SSp-bfd6a	16745.82	3858.78	16337.97	2798.11
contra_SSp-bfd6b	12382.78	2791.82	12413.50	2191.05
contra_SSP-tr	19044.90	3625.69	18192.10	2728.89
contra_SSp-tr1	19933.49	3882.10	19555.59	3199.03
contra_SSp-tr3	21214.59	4195.05	20085.29	3179.75
contra_SSp-tr4	19526.48	3935.29	18379.49	2859.95
contra_SSp-tr5	18175.66	3659.12	17301.71	2638.97
contra_SSp-tr6a	16401.53	3640.51	15482.64	2662.52
contra_SSp-tr6b	12423.54	3159.15	11980.80	2122.20
contra_TEa	20211.95	4730.58	19619.59	2964.24
contra_TEa1	21628.72	4934.73	20991.24	3326.99
contra_TEa3	22009.35	5059.88	21467.90	3229.73

contra_TEa4	20824.57	4804.51	20333.61	3314.18
contra_TEa5	18948.11	4514.74	18460.16	2877.69
contra_TEa6a	17581.36	4265.14	17373.06	2823.52
contra_TEa6b	12703.70	3478.39	12905.91	2121.86
contra_th	10610.20	2182.54	9679.39	1414.98
ips_amgmed	12668.97	2131.28	11859.26	2165.96
ips_AUDd	19495.64	4150.24	17331.15	3292.57
ips_AUDd1	21199.38	4534.17	18384.96	3697.85
ips_AUDd3	21594.47	4615.12	18962.34	3585.40
ips_AUDd4	19582.83	3878.65	17572.80	3336.30
ips_AUDd5	17781.41	3722.12	15954.34	3305.54
ips_AUDd6a	16303.68	3546.50	14673.81	3356.53
ips_AUDd6b	12137.74	2828.27	11570.45	2521.64
ips_AUDp	20036.33	3902.62	17425.22	3206.04
ips_AUDp1	21973.55	4089.35	18309.35	3116.71
ips_AUDp3	22020.60	4170.89	19084.12	3397.54
ips_AUDp4	20191.79	3865.82	17757.87	3253.50
ips_AUDp5	18443.62	3753.73	16259.24	3265.66
ips_AUDp6a	16681.10	3644.88	14905.75	3367.01
ips_AUDp6b	12032.40	2653.37	10978.96	2051.35
ips_AUDv	20154.84	3799.93	17484.19	3202.56
ips_AUDv1	22572.42	3653.45	18758.76	3071.17
ips_AUDv3	22090.67	3949.40	19101.48	3400.87
ips_AUDv4	20283.07	3921.71	17741.71	3348.57
ips_AUDv5	18462.71	3675.63	16329.30	3290.29
ips_AUDv6a	16830.80	3678.25	15042.74	3423.64
ips_AUDv6b	12497.80	2715.91	11280.70	2619.34
ips_BLAa	16120.67	2824.90	14945.42	3026.37
ips_BLAp	17287.75	2826.48	16037.80	3231.75
ips_BLAv	14979.16	3227.61	13674.05	2770.48
ips_BMAp	13941.65	2627.63	12904.76	2721.63
ips_CA1slm	15054.25	3091.60	12904.33	2130.06
ips_CA1so	16307.48	3035.32	14167.89	2262.50
ips_CA1sp	10656.25	2001.05	9069.21	1270.80
ips_CA1sr	18682.10	3324.58	16300.39	2749.00
ips_CA2slm	10714.28	2023.86	9526.66	1684.91
ips_CA2so	10615.82	2038.57	9318.34	1664.21

ips_CA2sp	7648.18	1039.77	6871.13	839.21
ips_CA2sr	10406.51	1852.56	9385.08	1761.42
ips_CA3slm	10434.36	1808.78	9578.94	1589.29
ips_CA3slu	12907.10	2210.07	11613.57	2202.74
ips_CA3so	10267.89	1798.47	9270.12	1634.98
ips_CA3sp	9424.49	1361.60	8335.50	1077.48
ips_CA3sr	11564.87	1879.14	10662.61	1930.32
ips_CC	7994.56	1429.40	7397.54	777.78
ips_cing	9765.70	1774.40	8247.48	1203.72
ips_COApl	14426.59	2804.88	12773.78	2527.50
ips_COApl1	15082.42	2870.29	13195.79	2837.44
ips_COApl2	14232.22	2883.40	12534.25	2378.33
ips_COApl3	14356.08	2724.10	12831.69	2593.39
ips_cortex	17496.41	3625.73	15669.78	2880.90
ips_CP	13903.49	2573.91	12848.80	2639.64
ips_cpd	7619.60	968.40	7591.94	1069.25
ips_DG	15096.10	2550.50	13151.69	1941.37
ips_DGinf	14528.48	2323.34	12737.41	1850.85
ips_DGpo	10770.73	1732.11	9525.59	1340.51
ips_DGsg	7458.69	837.95	6728.92	552.09
ips_DGsup	15402.51	2688.19	13362.33	1990.51
ips_ECT	19950.01	3817.65	17882.82	3506.72
ips_ECT1	21420.93	4198.79	19035.15	3967.37
ips_ECT3	21309.93	4102.06	19095.27	3772.69
ips_ECT5	18155.29	3566.75	16442.67	3417.34
ips_ECT6a	16602.36	3712.20	15063.62	3607.55
ips_ECT6b	12638.59	2822.04	11812.51	2880.12
ips_ENTl	17919.08	4065.97	16614.89	3461.95
ips_ENTl1	19837.15	4470.94	17665.87	3793.34
ips_ENTl3	18904.54	4414.46	17402.32	3774.28
ips_ENTl5	16946.06	3779.10	16050.66	3504.23
ips_ENTl6a	13991.29	3330.68	13207.56	3594.19
ips_ENTl6b	11975.41	2069.65	11653.82	2723.63
ips_FC	8331.78	1447.94	7151.21	863.09
ips_hip	14049.86	2517.95	12182.30	2015.12
ips_hyp	10881.09	1710.19	10578.84	1807.96
ips_LA	16397.47	2832.49	15467.90	3103.73

ips_lay1	19270.39	3962.03	17053.47	2672.29
ips_lay2	13785.90	3460.46	11714.79	1400.62
ips_lay3	19420.08	4184.67	17358.83	3149.02
ips_lay4	18427.70	4072.84	16459.87	3338.07
ips_lay5	16789.52	3676.10	15048.85	3042.62
ips_lay6a	14858.35	3594.70	13213.63	2918.89
ips_lay6b	11723.17	2563.57	10504.45	2195.13
ips_MOp	15836.02	3597.63	14083.49	2288.04
ips_MOp1	16754.51	3497.13	15286.36	2043.26
ips_MOp3	16456.14	3750.48	14942.44	2366.13
ips_MOp5	16134.44	3787.08	14157.22	2606.20
ips_MOp6a	14224.84	3615.29	11899.84	2439.20
ips_MOp6b	11394.33	2822.97	9584.82	1865.02
ips_MOs	16200.91	3773.86	14733.47	2230.64
ips_MOs1	18417.08	3896.37	17552.56	2191.79
ips_MOs3	17193.06	4039.47	15853.40	2308.18
ips_MOs5	15547.67	3834.48	13444.39	2424.77
ips_MOs6a	13139.52	3240.88	11066.31	1968.77
ips_MOs6b	11571.21	2734.66	9322.43	1471.14
ips_PAA	14355.53	3007.83	13275.20	2664.71
ips_PAA1	14342.77	3070.86	13037.14	2760.76
ips_PAA2	14140.20	3184.67	13135.46	2469.71
ips_PAA3	14571.25	2874.89	13524.24	2787.86
ips_PERI	19210.91	3613.49	17371.30	3448.44
ips_PERI1	21433.28	4303.22	18637.37	3713.42
ips_PERI3	20319.39	4027.57	18140.03	3490.17
ips_PERI5	17800.31	3419.33	16468.01	3465.12
ips_PERI6a	15305.83	3572.09	14431.97	3652.29
ips_PERI6b	12618.14	2734.95	11547.33	2699.75
ips_PIR	16053.50	3384.04	14511.99	2808.59
ips_PIR1	16888.76	3393.57	14959.99	2882.81
ips_PIR2	15957.22	3696.61	14206.58	2846.12
ips_PIR3	15811.70	3279.66	14457.89	2811.80
ips_RSPd	16730.82	3717.33	15074.54	1989.05
ips_RSPd1	19486.60	4320.04	17923.45	1821.42
ips_RSPd3	17474.74	3938.23	15708.32	1998.47
ips_RSPd5	15359.28	3595.04	13796.31	2265.32

ips_RSPd6a	13212.45	3043.60	11392.38	1832.58
ips_RSPd6b	11805.78	2897.11	10128.47	1630.62
ips_RSPv	15681.65	3490.08	13429.94	2008.36
ips_RSPv1	17282.32	4054.31	14629.32	1916.70
ips_RSPv2	13743.45	3406.59	11719.95	1400.85
ips_RSPv3	16934.89	3546.31	14389.32	2295.48
ips_RSPv5	15173.24	3046.20	13464.08	2192.16
ips_RSPv6a	12949.62	2829.93	11005.46	1825.62
ips_RSPv6b	12084.29	2820.74	10174.55	1723.11
ips_SSp-bfd	18262.19	4205.43	16385.74	3728.01
ips_SSp-bfd1	20207.85	5069.35	18205.64	3349.26
ips_SSp-bfd3	20340.96	4915.34	18603.03	3939.73
ips_SSp-bfd4	18561.31	4132.82	16754.06	3766.31
ips_SSp-bfd5	17058.82	3816.62	15448.87	3476.21
ips_SSp-bfd6a	15434.60	3669.46	14030.27	3507.43
ips_SSp-bfd6b	11920.87	2648.22	11062.48	2752.70
ips_SSp-tr	16616.98	3621.75	14767.28	3069.98
ips_SSp-tr1	17979.62	3915.34	15830.82	2965.09
ips_SSp-tr3	17876.25	4035.35	15867.71	3359.07
ips_SSp-tr4	16970.89	3673.89	15136.89	3048.84
ips_SSp-tr5	15930.37	3557.33	14282.08	3117.46
ips_SSp-tr6a	14178.83	3609.15	12565.28	2960.22
ips_SSp-tr6b	11191.33	2588.87	10012.18	2210.18
ips_TEa	20203.56	3676.00	17916.24	3518.49
ips_TEa1	21800.00	4062.88	19398.63	3544.80
ips_TEa3	21907.93	4078.74	19385.10	3636.63
ips_TEa4	20309.29	3917.66	18113.53	3711.91
ips_TEa5	18434.48	3496.77	16629.04	3436.62
ips_TEa6a	16984.97	3491.54	15551.04	3552.84
ips_TEa6b	12472.37	2509.15	11517.49	2751.87
ips_th	10821.45	1924.80	9655.73	1695.91

Table 4: PSD95 puncta density at 28 days

	Injury		**Sham**	
region	**Average**	**SD**	**Average**	**SD**
contra_amgmed	294.25	29.77	318.00	32.54
contra_AUDd	449.35	30.87	460.70	16.26

contra_AUDd1	533.55	53.19	558.90	32.10
contra_AUDd3	481.70	37.49	492.90	26.68
contra_AUDd4	481.15	36.57	490.10	26.53
contra_AUDd5	419.05	27.26	427.40	22.36
contra_AUDd6a	396.30	24.19	403.90	13.78
contra_AUDd6b	258.40	58.12	268.75	73.29
contra_AUDp	450.40	28.90	469.65	16.78
contra_AUDp1	533.65	42.96	560.85	24.18
contra_AUDp3	479.10	33.64	503.90	22.34
contra_AUDp4	483.20	27.25	495.00	18.33
contra_AUDp5	430.20	27.47	454.15	21.31
contra_AUDp6a	402.85	22.67	414.50	16.23
contra_AUDp6b	249.90	65.49	279.80	62.04
contra_AUDv	470.75	30.00	488.80	17.63
contra_AUDv1	550.65	49.29	569.00	29.48
contra_AUDv3	508.10	34.27	523.20	21.23
contra_AUDv4	500.90	32.80	515.70	15.62
contra_AUDv5	456.35	30.39	475.60	22.99
contra_AUDv6a	402.00	27.30	422.80	18.77
contra_AUDv6b	257.75	51.14	269.05	58.08
contra_BLAa	430.20	31.85	456.10	35.83
contra_BLAp	451.80	35.18	474.05	50.76
contra_BLAv	377.35	59.43	422.83	50.79
contra_BMAp	340.20	43.17	386.67	55.64
contra_CA1slm	490.25	28.53	525.20	34.15
contra_CA1so	630.00	35.99	668.75	40.14
contra_CA1sp	167.45	18.40	163.05	23.72
contra_CA1sr	665.15	46.28	696.60	42.18
contra_CA2slm	537.25	30.28	554.50	29.65
contra_CA2so	487.50	31.05	501.70	17.95
contra_CA2sp	63.60	19.30	62.45	21.73
contra_CA2sr	464.15	37.93	474.85	25.85
contra_CA3slm	537.75	31.98	568.90	26.78
contra_CA3slu	257.40	29.16	269.00	13.28
contra_CA3so	455.75	37.20	472.45	25.12
contra_CA3sp	79.30	13.59	101.45	22.79
contra_CA3sr	511.90	35.44	534.25	25.51

contra_CC	5.85	2.33	9.00	2.49
contra_cing	64.85	14.07	80.65	27.26
contra_COApl	346.85	48.32	398.72	79.48
contra_COApl1	389.28	61.29	413.50	50.59
contra_COApl2	337.70	56.49	403.72	85.88
contra_COApl3	339.25	43.76	390.00	86.32
contra_cortex	430.20	24.46	442.60	12.18
contra_CP	368.00	17.26	372.50	10.36
contra_cpd	10.40	5.64	13.40	6.90
contra_DG	674.60	49.21	717.60	54.01
contra_DGinf	674.35	54.40	718.65	55.00
contra_DGpo	213.60	22.22	236.55	16.33
contra_DGsg	53.90	9.68	66.55	21.76
contra_DGsup	675.40	47.02	716.55	53.60
contra_ECT	487.95	37.03	500.65	27.80
contra_ECT1	564.95	62.57	578.35	45.74
contra_ECT3	514.20	39.45	522.15	35.33
contra_ECT5	467.75	31.36	483.30	28.41
contra_ECT6a	414.40	21.72	433.75	36.67
contra_ECT6b	274.61	43.54	289.60	55.39
contra_ENTl	466.20	42.93	477.50	32.53
contra_ENTl1	570.80	64.40	550.70	59.83
contra_ENTl3	487.20	44.59	496.50	47.34
contra_ENTl5	447.80	40.61	462.40	29.68
contra_ENTl6a	418.15	43.29	430.40	34.16
contra_ENTl6b	335.80	45.05	330.10	46.69
contra_FC	289.30	41.56	308.35	46.38
contra_hip	535.30	31.82	565.70	25.01
contra_hyp	116.80	15.13	126.30	10.27
contra_LA	441.60	33.47	465.45	35.23
contra_lay1	524.30	37.78	537.70	22.55
contra_lay2	287.25	23.29	298.10	19.60
contra_lay3	463.40	29.67	472.40	18.51
contra_lay4	465.60	31.36	474.20	11.66
contra_lay5	405.75	20.26	420.40	13.48
contra_lay6a	377.80	16.42	388.50	8.09
contra_lay6b	251.15	27.89	275.10	25.48

contra_MOp	437.05	37.64	451.10	31.97
contra_MOp1	540.85	59.97	555.05	52.55
contra_MOp3	471.10	49.54	490.20	38.05
contra_MOp5	431.95	32.03	443.55	37.89
contra_MOp6a	374.00	24.47	380.60	22.35
contra_MOp6b	255.60	46.93	290.80	32.52
contra_MOs	361.25	33.08	371.90	24.45
contra_MOs1	486.70	48.19	503.95	48.48
contra_MOs3	394.20	37.03	407.60	29.10
contra_MOs5	338.20	28.09	340.50	24.40
contra_MOs6a	307.90	29.99	307.65	20.10
contra_MOs6b	246.50	44.14	229.25	35.02
contra_PAA	386.50	55.33	420.50	63.54
contra_PAA1	398.20	52.82	417.83	77.83
contra_PAA2	388.70	73.17	427.00	54.93
contra_PAA3	380.60	52.06	413.89	61.28
contra_PERI	487.05	40.08	491.35	29.81
contra_PERI1	572.00	69.58	553.85	43.39
contra_PERI3	506.55	44.50	504.00	36.38
contra_PERI5	466.15	34.22	470.15	40.18
contra_PERI6a	430.60	40.61	449.20	26.71
contra_PERI6b	263.00	38.85	322.25	44.39
contra_PIR	437.00	38.28	458.25	42.67
contra_PIR1	485.05	55.04	502.50	56.49
contra_PIR2	391.50	33.56	401.00	45.82
contra_PIR3	433.00	37.28	457.95	41.98
contra_RSPd	331.55	25.37	345.45	20.50
contra_RSPd1	448.65	39.41	457.65	51.82
contra_RSPd3	358.75	25.83	382.15	31.29
contra_RSPd5	299.35	24.66	309.05	17.28
contra_RSPd6a	286.05	28.08	297.10	19.14
contra_RSPd6b	226.10	47.49	244.20	36.79
contra_RSPv	322.50	20.42	329.20	14.89
contra_RSPv1	354.20	16.77	369.05	33.45
contra_RSPv2	288.15	23.78	298.65	19.44
contra_RSPv3	356.30	15.42	366.90	22.27
contra_RSPv5	304.65	28.69	319.60	29.76

contra_RSPv6a	264.55	29.15	278.60	22.08
contra_RSPv6b	222.45	68.06	241.55	48.32
contra_SSp-bfd	420.40	26.44	422.20	14.83
contra_SSp-bfd1	544.70	54.02	532.20	33.57
contra_SSp-bfd3	452.60	34.52	452.30	22.69
contra_SSp-bfd4	450.05	37.64	449.90	18.55
contra_SSp-bfd5	388.70	19.68	394.95	16.12
contra_SSp-bfd6a	378.15	15.60	380.20	10.81
contra_SSp-bfd6b	247.05	43.80	256.95	46.04
contra_SSP-tr	435.20	29.43	449.50	18.56
contra_SSp-tr1	544.70	53.33	559.50	33.29
contra_SSp-tr3	474.90	35.23	488.90	25.86
contra_SSp-tr4	449.15	28.92	467.60	23.93
contra_SSp-tr5	402.10	21.01	423.25	19.51
contra_SSp-tr6a	377.10	18.98	388.45	17.23
contra_SSp-tr6b	231.80	39.70	272.15	26.19
contra_TEa	483.55	33.86	497.25	25.31
contra_TEa1	560.90	63.94	591.65	57.80
contra_TEa3	515.90	40.63	521.45	37.36
contra_TEa4	514.85	44.65	528.40	36.17
contra_TEa5	471.25	35.55	489.20	30.68
contra_TEa6a	403.90	28.49	425.55	27.00
contra_TEa6b	273.55	47.95	295.00	44.13
contra_th	307.00	26.35	322.90	10.82
ips_amgmed	289.80	26.69	295.70	24.53
ips_AUDd	432.60	21.64	452.75	25.90
ips_AUDd1	507.65	45.24	544.10	41.32
ips_AUDd3	457.40	25.92	489.90	24.02
ips_AUDd4	459.25	27.87	476.60	22.21
ips_AUDd5	404.25	18.57	416.70	26.14
ips_AUDd6a	394.80	22.58	398.55	16.97
ips_AUDd6b	253.00	55.37	281.60	38.14
ips_AUDp	449.50	27.72	458.45	29.71
ips_AUDp1	535.95	44.85	538.30	62.63

ips_AUDp3	480.10	30.69	496.85	38.16
ips_AUDp4	474.80	35.32	487.40	25.22
ips_AUDp5	416.40	25.84	431.85	30.86
ips_AUDp6a	391.75	28.26	394.60	13.78
ips_AUDp6b	219.80	57.70	260.75	46.70
ips_AUDv	466.65	34.94	471.30	25.63
ips_AUDv1	548.00	58.20	556.65	45.65
ips_AUDv3	501.40	41.50	507.25	29.34
ips_AUDv4	481.40	28.98	493.55	26.64
ips_AUDv5	440.30	29.00	448.40	29.59
ips_AUDv6a	381.05	30.91	392.70	12.66
ips_AUDv6b	243.15	38.59	262.70	47.36
ips_BLAa	435.95	30.21	436.70	26.51
ips_BLAp	449.05	43.53	462.55	37.36
ips_BLAv	375.25	49.31	392.75	46.46
ips_BMAp	341.10	40.22	366.95	32.62
ips_CA1slm	490.95	24.06	514.85	35.63
ips_CA1so	650.00	41.71	662.05	44.73
ips_CA1sp	165.10	20.03	155.55	36.94
ips_CA1sr	678.40	46.62	692.45	48.30
ips_CA2slm	548.15	34.55	553.25	17.22
ips_CA2so	510.75	38.49	510.65	16.69
ips_CA2sp	65.30	24.97	55.15	14.74
ips_CA2sr	474.80	33.55	476.65	26.72
ips_CA3slm	540.20	39.68	561.25	25.93
ips_CA3slu	256.65	23.44	265.85	21.87
ips_CA3so	462.80	40.01	475.95	17.06
ips_CA3sp	78.60	17.85	87.60	26.85
ips_CA3sr	510.65	26.03	530.45	28.78
ips_CC	6.20	1.69	6.50	1.65
ips_cing	65.85	17.94	62.40	24.69
ips_COApl	346.10	40.24	373.95	59.75
ips_COApl1	372.25	30.50	385.80	53.41
ips_COApl2	339.40	44.17	375.10	65.81
ips_COApl3	338.90	43.85	367.85	58.54
ips_cortex	416.60	22.49	431.30	21.14
ips_CP	358.95	25.78	368.10	24.44

ips_cpd	8.30	5.40	9.10	7.58
ips_DG	683.35	50.01	703.80	58.53
ips_DGinf	679.60	54.70	701.60	50.74
ips_DGpo	210.10	24.33	233.25	16.76
ips_DGsg	53.00	10.99	60.45	21.27
ips_DGsup	686.90	47.84	706.95	63.86
ips_ECT	471.05	26.84	487.00	16.57
ips_ECT1	515.25	39.69	563.40	25.49
ips_ECT3	489.50	28.64	507.95	17.21
ips_ECT5	449.70	20.63	466.45	19.07
ips_ECT6a	396.55	31.16	423.70	26.05
ips_ECT6b	284.90	50.11	288.20	42.42
ips_ENTl	454.05	38.22	451.00	23.02
ips_ENTl1	516.50	47.19	519.25	31.15
ips_ENTl3	469.40	51.74	459.10	21.48
ips_ENTl5	439.35	33.58	443.65	22.30
ips_ENTl6a	404.50	31.02	420.75	26.15
ips_ENTl6b	288.20	64.40	315.10	29.96
ips_FC	278.10	54.53	300.20	60.83
ips_hip	544.10	28.42	560.50	28.49
ips_hyp	115.70	17.24	123.10	11.14
ips_LA	436.45	29.38	454.35	35.49
ips_lay1	497.60	34.78	522.85	23.74
ips_lay2	279.55	21.40	289.40	19.46
ips_lay3	445.25	27.14	463.80	23.44
ips_lay4	446.70	28.85	461.20	24.84
ips_lay5	395.80	19.11	408.05	17.51
ips_lay6a	369.60	15.40	378.30	12.26
ips_lay6b	247.40	25.24	257.60	28.76
ips_MOp	422.00	27.95	418.85	17.65
ips_MOp1	502.30	48.05	515.35	31.69
ips_MOp3	451.95	32.60	445.15	24.43
ips_MOp5	420.60	31.63	412.55	19.59
ips_MOp6a	368.85	27.71	354.65	23.51
ips_MOp6b	254.20	45.54	230.95	50.37
ips_MOs	352.85	26.91	348.10	14.60
ips_MOs1	462.10	58.95	463.95	39.83

ips_MOs3	393.25	34.20	390.00	27.82
ips_MOs5	334.15	30.47	324.95	13.01
ips_MOs6a	300.30	39.98	281.60	29.88
ips_MOs6b	246.05	32.58	219.35	53.80
ips_PAA	377.35	41.62	385.95	48.88
ips_PAA1	387.90	44.49	390.90	63.93
ips_PAA2	377.95	44.77	383.50	38.32
ips_PAA3	369.90	44.47	384.95	49.76
ips_PERI	466.50	28.11	481.25	16.62
ips_PERI1	518.75	51.11	567.05	43.94
ips_PERI3	487.00	30.93	502.50	20.43
ips_PERI5	448.35	23.71	456.90	16.21
ips_PERI6a	404.35	26.26	418.35	20.66
ips_PERI6b	273.15	50.69	290.90	47.88
ips_PIR	420.40	27.48	436.50	27.86
ips_PIR1	456.90	37.70	486.85	45.37
ips_PIR2	385.80	27.22	389.10	28.42
ips_PIR3	417.75	28.60	434.20	25.11
ips_RSPd	328.55	20.58	338.10	15.58
ips_RSPd1	432.95	35.45	445.80	38.42
ips_RSPd3	359.30	23.52	369.60	22.18
ips_RSPd5	292.10	25.24	303.35	15.92
ips_RSPd6a	277.85	31.34	284.65	21.99
ips_RSPd6b	234.30	36.82	245.50	39.46
ips_RSPv	317.60	22.27	321.70	12.45
ips_RSPv1	351.15	20.44	354.35	14.95
ips_RSPv2	279.70	21.12	289.70	20.04
ips_RSPv3	356.30	19.56	366.25	14.17
ips_RSPv5	297.70	38.11	309.90	20.75
ips_RSPv6a	262.45	25.97	270.35	26.19
ips_RSPv6b	244.65	31.96	237.15	65.91
ips_SSp-bfd	412.90	26.84	431.55	24.71
ips_SSp-bfd1	501.35	41.68	547.90	31.96
ips_SSp-bfd3	440.30	33.03	471.10	29.95
ips_SSp-bfd4	440.65	30.56	456.05	27.41
ips_SSp-bfd5	385.70	21.70	402.45	18.11
ips_SSp-bfd6a	375.50	20.28	386.30	17.51

ips_SSp-bfd6b	249.45	31.62	279.10	38.89
ips_SSp-tr	411.45	25.85	430.40	26.48
ips_SSp-tr1	503.30	37.68	530.20	26.40
ips_SSp-tr3	440.75	33.51	462.20	31.42
ips_SSp-tr4	431.00	34.17	445.45	28.08
ips_SSp-tr5	390.45	22.99	404.20	23.36
ips_SSp-tr6a	368.70	16.85	375.50	14.65
ips_SSp-tr6b	224.45	47.25	216.60	60.94
ips_TEa	471.95	31.99	478.40	19.92
ips_TEa1	541.00	59.78	561.15	28.52
ips_TEa3	500.30	39.77	513.35	24.64
ips_TEa4	478.30	28.35	496.60	20.50
ips_TEa5	453.25	28.58	459.80	25.80
ips_TEa6a	384.00	30.52	402.85	18.15
ips_TEa6b	275.40	25.89	273.55	37.43
ips_th	303.60	30.65	313.50	17.08

Table 5: PSD95 puncta size at 28 days

	Injury		**Sham**	
region	**Average**	**SD**	**Average**	**SD**
contra_amgmed	12.63	0.23	12.52	0.30
contra_AUDd	12.30	0.26	12.24	0.22
contra_AUDd1	12.24	0.33	12.16	0.18
contra_AUDd3	12.43	0.28	12.40	0.20
contra_AUDd4	11.99	0.21	11.97	0.21
contra_AUDd5	12.29	0.26	12.22	0.23
contra_AUDd6a	12.13	0.24	12.09	0.27
contra_AUDd6b	12.54	0.32	12.58	0.46
contra_AUDp	12.26	0.29	12.20	0.23
contra_AUDp1	12.22	0.33	12.14	0.26
contra_AUDp3	12.40	0.31	12.36	0.23
contra_AUDp4	12.00	0.25	11.98	0.23
contra_AUDp5	12.24	0.27	12.14	0.24
contra_AUDp6a	12.12	0.26	12.05	0.22
contra_AUDp6b	12.60	0.35	12.40	0.34
contra_AUDv	12.11	0.31	12.08	0.23
contra_AUDv1	12.08	0.38	12.04	0.24

contra_AUDv3	12.17	0.33	12.19	0.22
contra_AUDv4	11.91	0.27	11.89	0.22
contra_AUDv5	12.06	0.31	12.01	0.27
contra_AUDv6a	12.12	0.27	12.02	0.24
contra_AUDv6b	12.48	0.29	12.43	0.31
contra_BLAa	12.01	0.47	11.90	0.35
contra_BLAp	12.13	0.48	11.99	0.37
contra_BLAv	12.17	0.39	12.02	0.27
contra_BMAp	12.31	0.33	12.17	0.34
contra_CA1slm	11.97	0.22	11.86	0.31
contra_CA1so	11.35	0.25	11.26	0.30
contra_CA1sp	12.25	0.21	12.52	0.23
contra_CA1sr	11.42	0.24	11.38	0.31
contra_CA2slm	11.33	0.27	11.24	0.43
contra_CA2so	11.39	0.24	11.33	0.30
contra_CA2sp	15.00	1.10	15.38	1.52
contra_CA2sr	11.64	0.32	11.54	0.40
contra_CA3slm	11.73	0.33	11.58	0.47
contra_CA3slu	14.76	0.54	14.73	0.60
contra_CA3so	11.95	0.38	11.76	0.45
contra_CA3sp	15.79	0.80	15.58	0.58
contra_CA3sr	12.07	0.39	11.87	0.51
contra_CC	13.03	0.34	13.25	0.38
contra_cing	13.13	0.30	13.24	0.25
contra_COApl	12.43	0.38	12.16	0.46
contra_COApl1	12.23	0.47	12.03	0.38
contra_COApl2	12.46	0.45	12.15	0.46
contra_COApl3	12.50	0.35	12.26	0.49
contra_cortex	12.26	0.24	12.22	0.20
contra_CP	12.09	0.29	12.03	0.24
contra_cpd	13.74	0.44	14.22	0.70
contra_DG	11.30	0.23	11.25	0.37
contra_DGinf	11.34	0.22	11.28	0.35
contra_DGpo	14.56	0.38	14.52	0.46
contra_DGsg	14.95	0.42	15.12	0.48
contra_DGsup	11.28	0.23	11.22	0.38
contra_ECT	12.04	0.38	12.00	0.24

contra_ECT1	12.05	0.44	12.00	0.24
contra_ECT3	12.09	0.39	12.06	0.24
contra_ECT5	11.95	0.38	11.87	0.21
contra_ECT6a	11.97	0.31	11.93	0.27
contra_ECT6b	12.41	0.23	12.25	0.41
contra_ENTl	11.90	0.42	11.84	0.28
contra_ENTl1	11.74	0.54	11.75	0.32
contra_ENTl3	11.97	0.43	11.91	0.31
contra_ENTl5	12.02	0.40	11.90	0.25
contra_ENTl6a	11.69	0.42	11.63	0.26
contra_ENTl6b	12.00	0.38	12.02	0.42
contra_FC	11.80	0.23	11.74	0.25
contra_hip	11.62	0.26	11.54	0.34
contra_hyp	13.96	0.18	14.01	0.19
contra_LA	12.11	0.50	11.86	0.37
contra_lay1	12.19	0.27	12.15	0.21
contra_lay2	12.61	0.18	12.63	0.20
contra_lay3	12.34	0.26	12.32	0.21
contra_lay4	12.02	0.22	11.98	0.20
contra_lay5	12.31	0.23	12.23	0.19
contra_lay6a	12.15	0.23	12.09	0.21
contra_lay6b	12.52	0.21	12.48	0.21
contra_MOp	12.15	0.24	12.19	0.23
contra_MOp1	12.07	0.28	12.13	0.27
contra_MOp3	12.15	0.25	12.18	0.25
contra_MOp5	12.20	0.23	12.22	0.23
contra_MOp6a	12.13	0.18	12.18	0.21
contra_MOp6b	12.43	0.20	12.47	0.22
contra_MOs	12.56	0.26	12.63	0.24
contra_MOs1	12.51	0.29	12.58	0.30
contra_MOs3	12.58	0.28	12.63	0.26
contra_MOs5	12.66	0.28	12.76	0.28
contra_MOs6a	12.47	0.23	12.55	0.20
contra_MOs6b	12.47	0.23	12.69	0.16
contra_PAA	12.23	0.45	12.03	0.36
contra_PAA1	12.14	0.44	11.98	0.39
contra_PAA2	12.22	0.54	11.97	0.40

contra_PAA3	12.29	0.43	12.12	0.36
contra_PERI	11.94	0.39	11.92	0.25
contra_PERI1	11.87	0.46	11.93	0.26
contra_PERI3	11.98	0.40	11.99	0.26
contra_PERI5	11.96	0.38	11.92	0.26
contra_PERI6a	11.79	0.34	11.73	0.25
contra_PERI6b	12.35	0.25	12.16	0.36
contra_PIR	12.00	0.43	11.87	0.28
contra_PIR1	11.94	0.51	11.78	0.33
contra_PIR2	12.03	0.41	11.94	0.25
contra_PIR3	12.01	0.42	11.88	0.27
contra_RSPd	12.74	0.25	12.75	0.25
contra_RSPd1	12.67	0.26	12.73	0.27
contra_RSPd3	12.69	0.25	12.65	0.28
contra_RSPd5	13.15	0.27	13.13	0.24
contra_RSPd6a	12.62	0.21	12.70	0.19
contra_RSPd6b	12.56	0.23	12.63	0.19
contra_RSPv	12.63	0.19	12.67	0.21
contra_RSPv1	12.71	0.20	12.78	0.24
contra_RSPv2	12.61	0.18	12.63	0.20
contra_RSPv3	12.34	0.19	12.36	0.23
contra_RSPv5	12.80	0.21	12.79	0.29
contra_RSPv6a	12.77	0.19	12.84	0.22
contra_RSPv6b	12.60	0.39	12.59	0.29
contra_SSp-bfd	12.32	0.24	12.30	0.21
contra_SSp-bfd1	12.18	0.27	12.18	0.22
contra_SSp-bfd3	12.45	0.26	12.46	0.21
contra_SSp-bfd4	12.03	0.23	12.01	0.19
contra_SSp-bfd5	12.39	0.21	12.35	0.21
contra_SSp-bfd6a	12.14	0.24	12.10	0.23
contra_SSp-bfd6b	12.58	0.27	12.62	0.31
contra_SSP-tr	12.23	0.22	12.19	0.20
contra_SSp-tr1	12.06	0.24	12.05	0.22
contra_SSp-tr3	12.30	0.24	12.27	0.22
contra_SSp-tr4	12.07	0.19	12.01	0.22

contra_SSp-tr5	12.36	0.22	12.28	0.17
contra_SSp-tr6a	12.12	0.20	12.09	0.20
contra_SSp-tr6b	12.60	0.25	12.50	0.19
contra_TEa	12.06	0.35	12.00	0.23
contra_TEa1	12.02	0.38	11.99	0.24
contra_TEa3	12.10	0.37	12.10	0.20
contra_TEa4	11.99	0.34	11.91	0.28
contra_TEa5	11.97	0.34	11.90	0.25
contra_TEa6a	12.13	0.34	12.00	0.30
contra_TEa6b	12.42	0.30	12.33	0.32
contra_th	11.70	0.21	11.71	0.19
ips_amgmed	12.67	0.16	12.73	0.10
ips_AUDd	12.34	0.16	12.33	0.20
ips_AUDd1	12.32	0.21	12.31	0.23
ips_AUDd3	12.44	0.16	12.42	0.21
ips_AUDd4	12.09	0.17	12.10	0.17
ips_AUDd5	12.34	0.16	12.35	0.22
ips_AUDd6a	12.20	0.17	12.19	0.21
ips_AUDd6b	12.62	0.29	12.60	0.27
ips_AUDp	12.27	0.17	12.26	0.21
ips_AUDp1	12.23	0.20	12.22	0.21
ips_AUDp3	12.32	0.16	12.31	0.24
ips_AUDp4	12.09	0.20	12.06	0.20
ips_AUDp5	12.27	0.18	12.26	0.22
ips_AUDp6a	12.23	0.18	12.22	0.22
ips_AUDp6b	12.82	0.28	12.76	0.21
ips_AUDv	12.17	0.19	12.16	0.20
ips_AUDv1	12.14	0.25	12.11	0.21
ips_AUDv3	12.17	0.19	12.18	0.22
ips_AUDv4	12.10	0.17	12.09	0.20
ips_AUDv5	12.10	0.18	12.13	0.25
ips_AUDv6a	12.29	0.22	12.21	0.21
ips_AUDv6b	12.59	0.26	12.65	0.22
ips_BLAa	12.10	0.28	12.06	0.29
ips_BLAp	12.18	0.29	12.10	0.31
ips_BLAv	12.30	0.25	12.24	0.24

ips_BMAp	12.42	0.25	12.29	0.31
ips_CA1slm	11.98	0.20	11.90	0.28
ips_CA1so	11.31	0.23	11.28	0.25
ips_CA1sp	12.27	0.23	12.53	0.24
ips_CA1sr	11.41	0.21	11.38	0.26
ips_CA2slm	11.30	0.19	11.23	0.21
ips_CA2so	11.28	0.19	11.32	0.14
ips_CA2sp	14.28	0.67	15.85	0.91
ips_CA2sr	11.59	0.20	11.61	0.22
ips_CA3slm	11.70	0.25	11.60	0.27
ips_CA3slu	14.73	0.28	14.75	0.42
ips_CA3so	11.89	0.22	11.84	0.30
ips_CA3sp	15.71	0.43	15.86	0.73
ips_CA3sr	12.05	0.23	11.97	0.36
ips_CC	13.20	0.45	13.22	0.33
ips_cing	13.11	0.32	13.23	0.31
ips_COApl	12.52	0.32	12.43	0.30
ips_COApl1	12.37	0.32	12.27	0.24
ips_COApl2	12.54	0.36	12.40	0.39
ips_COApl3	12.62	0.31	12.51	0.30
ips_cortex	12.35	0.18	12.33	0.17
ips_CP	12.14	0.17	12.12	0.25
ips_cpd	13.56	0.80	13.86	1.12
ips_DG	11.28	0.19	11.26	0.31
ips_DGinf	11.32	0.19	11.29	0.31
ips_DGpo	14.54	0.25	14.60	0.41
ips_DGsg	15.01	0.32	15.15	0.26
ips_DGsup	11.25	0.19	11.23	0.32
ips_ECT	12.13	0.18	12.05	0.23
ips_ECT1	12.15	0.18	11.95	0.26
ips_ECT3	12.16	0.19	12.09	0.24
ips_ECT5	11.99	0.18	11.98	0.18
ips_ECT6a	12.14	0.26	12.02	0.30
ips_ECT6b	12.51	0.31	12.50	0.33
ips_ENTl	12.02	0.16	11.98	0.21
ips_ENTl1	11.91	0.17	11.88	0.25
ips_ENTl3	12.08	0.14	12.07	0.19

ips_ENTl5	12.02	0.23	11.98	0.25
ips_ENTl6a	11.86	0.24	11.76	0.24
ips_ENTl6b	12.37	0.40	12.21	0.29
ips_FC	11.77	0.28	11.75	0.30
ips_hip	11.60	0.21	11.57	0.27
ips_hyp	13.97	0.18	14.02	0.19
ips_LA	12.11	0.24	12.02	0.34
ips_lay1	12.32	0.20	12.30	0.15
ips_lay2	12.67	0.23	12.70	0.20
ips_lay3	12.41	0.19	12.39	0.17
ips_lay4	12.17	0.19	12.14	0.17
ips_lay5	12.36	0.17	12.35	0.17
ips_lay6a	12.23	0.18	12.22	0.19
ips_lay6b	12.59	0.19	12.61	0.17
ips_MOp	12.35	0.26	12.39	0.22
ips_MOp1	12.42	0.34	12.41	0.28
ips_MOp3	12.40	0.28	12.44	0.25
ips_MOp5	12.31	0.23	12.34	0.20
ips_MOp6a	12.22	0.24	12.32	0.21
ips_MOp6b	12.49	0.20	12.64	0.19
ips_MOs	12.73	0.33	12.74	0.22
ips_MOs1	12.81	0.38	12.72	0.28
ips_MOs3	12.79	0.37	12.75	0.23
ips_MOs5	12.76	0.28	12.86	0.28
ips_MOs6a	12.54	0.26	12.65	0.24
ips_MOs6b	12.51	0.21	12.70	0.21
ips_PAA	12.37	0.31	12.30	0.27
ips_PAA1	12.28	0.34	12.18	0.32
ips_PAA2	12.36	0.35	12.25	0.30
ips_PAA3	12.45	0.31	12.42	0.24
ips_PERI	12.05	0.18	11.99	0.22
ips_PERI1	12.05	0.23	11.87	0.31
ips_PERI3	12.08	0.18	12.04	0.22
ips_PERI5	11.98	0.18	11.98	0.18
ips_PERI6a	11.96	0.25	11.88	0.21
ips_PERI6b	12.43	0.31	12.41	0.41
ips_PIR	12.19	0.23	12.08	0.19

ips_PIR1	12.12	0.27	11.97	0.25
ips_PIR2	12.24	0.20	12.19	0.20
ips_PIR3	12.19	0.22	12.09	0.18
ips_RSPd	12.80	0.28	12.78	0.23
ips_RSPd1	12.73	0.30	12.74	0.26
ips_RSPd3	12.76	0.29	12.69	0.24
ips_RSPd5	13.15	0.24	13.09	0.22
ips_RSPd6a	12.65	0.22	12.77	0.23
ips_RSPd6b	12.60	0.31	12.56	0.24
ips_RSPv	12.68	0.23	12.70	0.19
ips_RSPv1	12.76	0.26	12.80	0.23
ips_RSPv2	12.66	0.24	12.70	0.20
ips_RSPv3	12.35	0.22	12.38	0.20
ips_RSPv5	12.85	0.32	12.82	0.20
ips_RSPv6a	12.84	0.19	12.87	0.18
ips_RSPv6b	12.50	0.24	12.56	0.22
ips_SSp-bfd	12.37	0.17	12.34	0.16
ips_SSp-bfd1	12.31	0.19	12.25	0.18
ips_SSp-bfd3	12.47	0.17	12.44	0.16
ips_SSp-bfd4	12.14	0.19	12.13	0.17
ips_SSp-bfd5	12.42	0.17	12.40	0.17
ips_SSp-bfd6a	12.19	0.17	12.17	0.18
ips_SSp-bfd6b	12.65	0.23	12.56	0.22
ips_SSp-tr	12.39	0.22	12.37	0.19
ips_SSp-tr1	12.32	0.27	12.33	0.18
ips_SSp-tr3	12.50	0.22	12.47	0.21
ips_SSp-tr4	12.24	0.21	12.22	0.23
ips_SSp-tr5	12.44	0.19	12.41	0.20
ips_SSp-tr6a	12.19	0.19	12.19	0.21
ips_SSp-tr6b	12.59	0.22	12.72	0.22
ips_TEa	12.16	0.22	12.12	0.17
ips_TEa1	12.13	0.27	12.02	0.17
ips_TEa3	12.18	0.21	12.14	0.19
ips_TEa4	12.15	0.23	12.11	0.19
ips_TEa5	12.02	0.21	12.04	0.20
ips_TEa6a	12.30	0.29	12.21	0.21
ips_TEa6b	12.64	0.26	12.61	0.26

ips_th	11.72	0.20	11.74	0.15

Table 6: PSD95 puncta intensity at 28 days

	Injury		Sham	
region	Average	SD	Average	SD
contra_amgmed	12012.71	2499.64	13690.88	2835.38
contra_AUDd	18203.25	2833.02	20217.44	2820.59
contra_AUDd1	19381.81	2992.54	21407.20	2829.69
contra_AUDd3	20001.92	3039.45	22085.35	3121.87
contra_AUDd4	18026.81	2755.48	20249.88	2957.90
contra_AUDd5	16920.57	2671.03	18861.13	2808.15
contra_AUDd6a	15806.43	2573.68	17444.72	2603.58
contra_AUDd6b	11317.67	2435.11	12539.29	1779.66
contra_AUDp	18115.12	2922.62	20352.87	2924.34
contra_AUDp1	19506.59	3101.71	21839.46	3022.60
contra_AUDp3	20058.99	3212.36	22410.66	2974.49
contra_AUDp4	18150.74	2735.24	20556.59	2951.87
contra_AUDp5	17125.63	2841.90	19364.97	2943.69
contra_AUDp6a	16018.81	2864.39	17906.93	2808.99
contra_AUDp6b	11311.19	2694.64	13306.66	2701.49
contra_AUDv	18389.50	3231.20	20269.69	2966.34
contra_AUDv1	20048.92	3636.86	21655.29	2817.06
contra_AUDv3	20328.31	3498.00	21953.95	3117.65
contra_AUDv4	18628.56	3235.41	20703.74	3099.18
contra_AUDv5	17329.73	2955.59	19480.46	3037.99
contra_AUDv6a	16027.37	3068.28	18147.08	2912.82
contra_AUDv6b	11449.43	2463.17	13076.70	2204.35
contra_BLAa	14702.99	2877.27	16872.11	3394.74
contra_BLAp	16162.81	3536.37	18170.18	3710.21
contra_BLAv	13163.23	3762.55	16168.85	3517.22
contra_BMAp	12540.86	3158.73	15204.43	3202.05
contra_CA1slm	14262.79	1166.96	15233.53	2589.37
contra_CA1so	15323.54	1259.60	16669.41	2411.56
contra_CA1sp	10456.19	895.80	11153.64	1676.18
contra_CA1sr	17621.65	1291.15	18857.55	2653.11
contra_CA2slm	10069.19	958.70	11095.74	1572.04
contra_CA2so	9772.03	1099.08	11011.70	1668.75

contra_CA2sp	7479.43	627.82	8068.09	989.73
contra_CA2sr	9795.56	930.61	10728.87	1479.73
contra_CA3slm	10050.74	989.75	11156.37	1405.65
contra_CA3slu	12473.62	1326.59	13575.54	1734.64
contra_CA3so	9792.32	858.02	10617.97	1339.44
contra_CA3sp	8879.48	1006.70	10114.46	1391.00
contra_CA3sr	11300.68	1116.74	12113.55	1425.07
contra_CC	7414.91	907.42	8459.33	845.24
contra_cing	9233.77	990.35	9908.54	1465.49
contra_COApl	13107.97	3620.15	15854.75	3223.63
contra_COApl1	13918.22	4035.08	16146.44	3072.24
contra_COApl2	13010.80	3683.26	16008.39	3398.30
contra_COApl3	13018.75	3473.76	15697.78	3144.20
contra_cortex	17547.50	2332.69	19110.79	2709.84
contra_CP	13844.25	2427.34	15475.25	2668.29
contra_cpd	7448.26	990.61	7821.20	1141.29
contra_DG	14770.19	1252.44	15728.07	2396.92
contra_DGinf	14447.93	1410.60	15439.93	2333.38
contra_DGpo	10176.12	773.03	11166.45	1383.78
contra_DGsg	7199.59	351.17	7658.01	866.56
contra_DGsup	14910.71	1211.04	15861.24	2417.25
contra_ECT	18303.20	3544.28	19930.54	3368.68
contra_ECT1	20039.83	4364.81	21219.34	4338.25
contra_ECT3	19593.38	3944.97	20952.46	3691.95
contra_ECT5	17017.58	3297.48	18921.46	3246.21
contra_ECT6a	15906.92	3072.12	18028.53	3302.04
contra_ECT6b	11960.14	1804.75	13567.48	2636.81
contra_ENTl	16505.04	3828.18	17988.88	3451.95
contra_ENTl1	17839.79	4436.87	18632.05	3594.50
contra_ENTl3	17417.74	4126.12	18763.32	3627.89
contra_ENTl5	16085.09	3618.29	18026.93	3381.93
contra_ENTl6a	13757.64	3149.58	15611.09	3374.83
contra_ENTl6b	11828.04	2603.64	13287.92	2326.61
contra_FC	7738.57	893.72	9049.06	1917.96
contra_hip	13513.55	1170.75	14531.85	2150.11
contra_hyp	9999.20	1792.49	11053.87	2001.92
contra_LA	16012.17	3218.58	17896.20	3327.46

contra_lay1	19108.59	2527.05	20310.99	2602.30
contra_lay2	13002.31	1508.65	14079.72	2675.96
contra_lay3	19320.73	2552.09	20804.82	2855.51
contra_lay4	17819.15	2511.44	19704.19	2814.47
contra_lay5	16589.37	2299.65	18430.77	2732.22
contra_lay6a	15034.08	2204.68	16774.01	2579.56
contra_lay6b	11223.91	1676.23	12747.97	1845.61
contra_MOp	18118.48	2380.57	19151.53	3082.13
contra_MOp1	19948.42	3042.89	21035.14	3747.54
contra_MOp3	19244.47	2743.67	20400.53	3401.64
contra_MOp5	17633.07	2011.58	18762.82	2940.43
contra_MOp6a	15084.75	1712.06	16120.23	2650.05
contra_MOp6b	11883.49	1523.08	12835.13	2394.32
contra_MOs	17277.84	2251.45	18819.88	3140.98
contra_MOs1	20610.05	2790.50	22448.94	4035.03
contra_MOs3	18477.08	2488.13	20158.76	3468.49
contra_MOs5	15763.22	1840.32	17059.58	2775.46
contra_MOs6a	13169.01	1414.94	14027.60	2487.06
contra_MOs6b	11302.27	1254.92	11932.16	2142.44
contra_PAA	13593.05	4076.60	15918.10	3330.10
contra_PAA1	13487.23	3891.44	15411.71	3077.05
contra_PAA2	13514.47	4179.29	15805.61	3475.87
contra_PAA3	13663.08	4069.14	16213.98	3378.57
contra_PERI	17556.08	3837.01	18773.67	3155.21
contra_PERI1	18953.72	4581.97	19419.37	3363.90
contra_PERI3	18430.63	4073.17	19538.15	3393.65
contra_PERI5	16848.80	3398.94	18089.72	3106.91
contra_PERI6a	14877.96	3154.67	16988.01	3272.59
contra_PERI6b	11307.31	2086.01	13659.50	2604.69
contra_PIR	14632.35	3717.80	16416.23	3564.83
contra_PIR1	15167.45	3876.81	16773.99	3460.70
contra_PIR2	13916.94	3639.89	15511.97	3317.51
contra_PIR3	14684.64	3671.76	16594.97	3642.83
contra_RSPd	16726.93	1943.05	17950.26	3316.55
contra_RSPd1	20611.67	2554.61	21510.91	4004.25
contra_RSPd3	17677.07	2127.14	19034.54	3497.48
contra_RSPd5	15039.76	1714.14	16296.24	2720.27

contra_RSPd6a	12859.12	1409.05	13946.33	2469.39
contra_RSPd6b	11239.29	1384.28	12276.09	2100.08
contra_RSPv	14827.07	1621.57	15797.82	2912.19
contra_RSPv1	16622.72	1970.65	17241.86	3377.79
contra_RSPv2	13057.79	1544.87	14106.66	2707.64
contra_RSPv3	15899.43	1648.43	16882.35	2992.95
contra_RSPv5	14488.40	1803.22	15745.74	2810.39
contra_RSPv6a	12355.78	1424.47	13416.59	2368.72
contra_RSPv6b	11496.84	1521.34	12476.25	2524.77
contra_SSp-bfd	17424.68	2301.49	19090.64	2691.99
contra_SSp-bfd1	19502.02	2786.30	20410.94	2590.88
contra_SSp-bfd3	19485.27	2479.38	20883.40	2756.40
contra_SSp-bfd4	17383.50	2334.31	19093.56	2844.75
contra_SSp-bfd5	16406.68	2228.12	18173.24	2704.41
contra_SSp-bfd6a	15191.11	2338.66	16857.36	2570.71
contra_SSp-bfd6b	11085.51	1780.89	12545.68	1770.09
contra_SSP-tr	18028.54	2225.57	19276.35	2805.24
contra_SSp-tr1	19695.73	3016.10	20337.85	2568.03
contra_SSp-tr3	19854.62	2665.07	20979.00	2989.63
contra_SSp-tr4	17893.97	2110.87	19415.62	3030.82
contra_SSp-tr5	16753.40	1906.67	18515.35	2782.99
contra_SSp-tr6a	15125.07	1875.63	16639.05	2572.53
contra_SSp-tr6b	11259.10	1415.65	12704.12	1827.79
contra_TEa	18564.99	3386.20	19978.21	3287.45
contra_TEa1	20425.06	4240.90	21757.02	4313.59
contra_TEa3	20347.67	3959.29	21386.67	3677.48
contra_TEa4	18876.35	3388.41	20705.41	3530.90
contra_TEa5	17292.17	3196.20	19155.83	3159.29
contra_TEa6a	16214.70	3171.99	18149.47	3214.02
contra_TEa6b	11776.40	2354.12	13436.20	2337.96
contra_th	9634.41	1163.00	10673.47	1870.98
ips_amgmed	11562.35	2162.10	12986.71	2252.66
ips_AUDd	17014.54	2813.68	18999.33	3109.57
ips_AUDd1	18482.29	3123.29	20507.33	3513.79

ips_AUDd3	18677.50	2768.34	20910.32	3231.80
ips_AUDd4	16860.95	2798.34	18910.45	3126.94
ips_AUDd5	15890.18	2771.39	17508.11	2912.57
ips_AUDd6a	15017.27	2933.07	16263.19	2933.98
ips_AUDd6b	10922.17	2163.84	12393.59	2236.13
ips_AUDp	17427.95	3017.86	18802.60	3030.66
ips_AUDp1	19096.12	3151.45	20162.89	2980.91
ips_AUDp3	19034.95	3082.44	20626.88	3266.47
ips_AUDp4	17364.95	2969.13	19056.02	3166.95
ips_AUDp5	16186.71	2868.65	17622.25	3008.31
ips_AUDp6a	15094.73	3249.13	16207.88	2807.20
ips_AUDp6b	10623.41	2217.03	11826.00	1430.61
ips_AUDv	17420.19	3104.91	18822.26	2900.07
ips_AUDv1	18947.34	3514.04	20380.68	3287.42
ips_AUDv3	18840.86	3271.01	20555.38	3252.78
ips_AUDv4	17599.35	2863.67	19128.01	3114.61
ips_AUDv5	16255.11	2953.86	17531.76	2857.84
ips_AUDv6a	14946.60	3169.30	16272.40	2703.69
ips_AUDv6b	10806.85	2174.50	11813.12	1878.70
ips_BLAa	14480.38	2933.57	16162.12	2949.64
ips_BLAp	15697.91	3194.13	17720.72	3197.18
ips_BLAv	12964.03	3149.26	15092.39	3119.00
ips_BMAp	12389.00	2603.67	14305.13	2739.76
ips_CA1slm	14034.20	1452.16	14690.28	2660.09
ips_CA1so	15493.41	1532.03	16225.45	2510.38
ips_CA1sp	10331.24	948.08	10718.53	1815.50
ips_CA1sr	17725.08	1668.88	18416.58	2724.32
ips_CA2slm	10056.56	1374.39	10657.90	1634.98
ips_CA2so	10312.59	1828.83	10376.68	1554.44
ips_CA2sp	7358.46	998.24	7778.99	921.69
ips_CA2sr	9813.68	1467.33	10273.37	1685.82
ips_CA3slm	9952.64	1340.60	10586.43	1523.47
ips_CA3slu	12343.23	1709.41	12860.59	2103.28
ips_CA3so	9735.86	1372.32	10244.14	1453.34
ips_CA3sp	8600.04	1044.54	9463.80	1550.36
ips_CA3sr	11057.87	1355.90	11703.55	1648.19
ips_CC	7558.74	684.04	7968.09	1128.48

ips_cing	9061.67	1033.20	9486.12	1799.87
ips_COApl	12428.16	2600.27	14848.03	3201.81
ips_COApl1	12587.01	2636.85	15118.73	3177.93
ips_COApl2	12172.78	2573.53	14881.34	3303.08
ips_COApl3	12522.94	2659.72	14762.88	3099.61
ips_cortex	16629.93	2392.32	17980.89	2881.27
ips_CP	12899.73	2352.79	14061.84	2514.51
ips_cpd	7021.19	1216.74	7263.81	1365.42
ips_DG	14666.92	1662.03	15184.23	2397.73
ips_DGinf	14328.02	1730.68	14847.61	2190.73
ips_DGpo	10076.44	992.08	10800.27	1491.92
ips_DGsg	7079.02	448.89	7512.48	976.83
ips_DGsup	14866.96	1619.00	15378.73	2513.80
ips_ECT	17029.45	2781.34	18613.28	2562.34
ips_ECT1	17939.94	2976.32	19916.03	2287.94
ips_ECT3	17986.30	2865.19	19616.88	2611.62
ips_ECT5	15928.40	2760.05	17419.97	2850.35
ips_ECT6a	14499.80	2921.25	16109.95	2980.81
ips_ECT6b	11145.79	2444.30	12253.68	1981.38
ips_ENTl	15793.28	2789.54	16986.71	2722.36
ips_ENTl1	16446.48	2850.16	17788.42	2550.54
ips_ENTl3	16606.40	2991.23	17741.16	2742.18
ips_ENTl5	15317.23	2866.64	16567.41	2917.51
ips_ENTl6a	12875.22	3091.80	14310.83	3057.30
ips_ENTl6b	10919.76	2537.75	12539.47	2445.50
ips_FC	7912.76	1016.02	8753.01	1668.69
ips_hip	13517.49	1511.10	14011.37	2145.46
ips_hyp	9910.37	1740.38	10949.89	1981.41
ips_LA	15389.99	2896.13	16972.06	3168.45
ips_lay1	18008.44	2358.83	19362.30	2726.84
ips_lay2	12761.57	1266.20	13724.17	2644.23
ips_lay3	17977.17	2460.83	19587.70	3101.65
ips_lay4	16879.72	2545.61	18428.97	3100.27
ips_lay5	15734.00	2392.60	17148.96	2847.45
ips_lay6a	14086.20	2115.99	15328.96	2866.31
ips_lay6b	10774.89	1560.47	11751.59	2084.12
ips_MOp	16728.56	1902.58	17778.35	2887.65

ips_MOp1	17956.17	2118.41	19637.15	3347.33
ips_MOp3	17534.33	1939.19	18693.71	3041.10
ips_MOp5	16674.69	2020.00	17375.28	2846.74
ips_MOp6a	14126.79	1714.81	14729.23	2928.49
ips_MOp6b	11162.18	1090.31	11571.53	2277.75
ips_MOs	16481.05	2055.14	17621.01	3252.91
ips_MOs1	19379.30	3005.22	20743.15	3427.34
ips_MOs3	17768.32	2429.29	19166.28	3471.43
ips_MOs5	15259.54	2162.18	16268.48	3242.30
ips_MOs6a	12528.72	1387.36	13119.56	2662.01
ips_MOs6b	10846.45	1199.32	11441.79	2451.92
ips_PAA	12922.04	3270.93	14812.23	2915.34
ips_PAA1	12600.93	3228.42	14675.32	2986.93
ips_PAA2	12807.82	3169.50	14703.82	2737.56
ips_PAA3	13177.48	3354.61	15051.00	3114.96
ips_PERI	16406.96	2662.23	18103.20	2691.03
ips_PERI1	17354.47	2870.39	19168.62	2550.72
ips_PERI3	17254.88	2809.48	19064.80	2864.41
ips_PERI5	15552.82	2677.72	17133.92	2755.85
ips_PERI6a	13532.28	2680.78	15236.51	2910.84
ips_PERI6b	10888.05	2344.40	12072.01	2235.24
ips_PIR	14269.39	2804.54	16396.47	2764.87
ips_PIR1	14714.33	2667.06	16973.66	2723.20
ips_PIR2	14123.74	2631.48	16207.92	2873.83
ips_PIR3	14191.67	2931.16	16287.36	2791.36
ips_RSPd	16307.65	1948.56	17658.25	3480.49
ips_RSPd1	19608.35	2309.93	21180.26	3408.10
ips_RSPd3	17210.00	2008.54	18617.78	3437.07
ips_RSPd5	14495.94	1554.17	15802.12	3121.43
ips_RSPd6a	12374.50	1291.52	13463.32	2647.82
ips_RSPd6b	11103.64	1142.86	12097.46	2701.39
ips_RSPv	14522.46	1502.08	15488.53	2949.32
ips_RSPv1	16200.88	1566.43	16744.87	3202.37
ips_RSPv2	12767.35	1263.66	13705.53	2626.76
ips_RSPv3	15637.77	1619.33	16632.16	3190.73
ips_RSPv5	14131.07	1644.63	15293.92	2825.30
ips_RSPv6a	12100.08	1288.74	13107.47	2715.21

ips_RSPv6b	11258.70	1451.38	12053.20	2620.16
ips_SSp-bfd	16723.32	2708.37	18384.02	3130.92
ips_SSp-bfd1	18182.53	2487.75	20528.28	3512.13
ips_SSp-bfd3	18469.10	2847.65	20709.70	3606.19
ips_SSp-bfd4	16726.58	2671.35	18438.12	3240.09
ips_SSp-bfd5	15796.18	2660.35	17306.63	2953.45
ips_SSp-bfd6a	14550.41	2584.47	15826.67	2947.37
ips_SSp-bfd6b	10890.38	1709.09	12184.02	2364.98
ips_SSp-tr	16703.41	2151.07	17655.42	2913.31
ips_SSp-tr1	18102.49	2410.67	18755.22	2818.24
ips_SSp-tr3	18115.80	2444.86	19001.11	3250.86
ips_SSp-tr4	16802.02	2098.26	17749.88	2983.39
ips_SSp-tr5	15759.08	2105.34	16941.75	2845.55
ips_SSp-tr6a	13991.76	1909.26	15015.36	2866.09
ips_SSp-tr6b	10574.82	1266.10	11201.67	2036.15
ips_TEa	17271.34	3033.95	18914.27	2801.91
ips_TEa1	18401.13	3439.23	20387.42	2796.59
ips_TEa3	18528.66	3257.07	20383.35	2958.00
ips_TEa4	17386.43	2922.87	19102.60	2876.40
ips_TEa5	16077.38	2846.69	17566.31	2771.14
ips_TEa6a	14999.14	2833.52	16479.44	2797.27
ips_TEa6b	11070.04	1805.23	11962.40	1678.88
ips_th	9556.58	1276.56	10422.96	1841.58

Appendix 5: Raw SAP102 from LFPI experiment at 7 and 28 days

Table 1: SAP102 puncta density at 7 days

	Injury		Sham	
region	Average	SD	Average	SD
contra_amgmed	266.45	46.69	257.38	39.12
contra_AUDd	391.91	56.59	391.63	48.56
contra_AUDd1	465.41	78.75	455.81	55.20
contra_AUDd3	423.59	66.61	423.56	54.96
contra_AUDd4	395.00	56.45	391.94	44.99
contra_AUDd5	361.55	53.26	360.13	55.15
contra_AUDd6a	363.77	47.87	361.00	44.63
contra_AUDd6b	219.45	68.02	211.44	63.89
contra_AUDp	401.73	57.83	399.13	47.86
contra_AUDp1	470.68	70.24	477.00	62.55
contra_AUDp3	435.82	69.05	437.25	58.91
contra_AUDp4	406.14	55.87	407.50	48.46
contra_AUDp5	377.91	57.40	371.00	51.92
contra_AUDp6a	370.77	58.18	362.44	42.72
contra_AUDp6b	223.23	70.39	199.00	65.34
contra_AUDv	420.55	63.39	418.13	48.05
contra_AUDv1	479.55	81.95	490.06	66.09
contra_AUDv3	453.86	75.84	458.75	54.62
contra_AUDv4	428.59	60.32	427.19	55.90
contra_AUDv5	403.86	61.68	398.88	56.76
contra_AUDv6a	376.64	62.28	372.94	38.52
contra_AUDv6b	243.59	59.44	237.50	61.93
contra_BLAa	430.00	50.22	424.25	46.88
contra_BLAp	453.91	52.06	448.44	33.55
contra_BLAv	362.23	56.76	351.88	53.05
contra_BMAp	324.55	66.32	301.94	34.61
contra_CA1slm	378.95	74.82	365.00	39.87
contra_CA1so	544.50	60.21	531.56	50.48
contra_CA1sp	189.68	46.01	163.94	27.59
contra_CA1sr	598.73	62.74	580.81	52.88
contra_CA2slm	523.55	41.25	521.63	20.82
contra_CA2so	508.86	24.43	504.13	29.87

contra_CA2sp	119.32	34.29	101.56	21.27
contra_CA2sr	470.50	29.99	464.75	29.19
contra_CA3slm	554.64	53.99	550.44	34.00
contra_CA3slu	208.95	48.27	198.31	27.90
contra_CA3so	466.64	46.00	457.44	39.23
contra_CA3sp	113.77	33.77	113.50	18.41
contra_CA3sr	538.05	54.81	541.50	29.61
contra_CC	22.73	14.53	17.88	5.44
contra_cing	82.27	24.35	65.69	18.70
contra_COApl	317.59	61.75	302.63	43.63
contra_COApl1	341.36	57.11	327.00	45.28
contra_COApl2	321.00	58.78	303.50	51.39
contra_COApl3	311.05	67.34	292.06	42.24
contra_cortex	375.55	51.07	371.25	48.54
contra_CP	337.18	61.94	330.63	42.77
contra_cpd	37.00	23.52	31.13	15.32
contra_DG	667.32	40.64	656.88	27.84
contra_DGinf	659.27	37.29	651.38	25.92
contra_DGpo	197.23	23.95	192.94	14.58
contra_DGsg	120.64	29.21	116.94	12.00
contra_DGsup	672.50	43.90	661.31	31.15
contra_ECT	440.95	60.02	439.50	52.05
contra_ECT1	497.50	84.44	499.44	68.52
contra_ECT3	462.14	65.01	457.13	53.59
contra_ECT5	425.64	55.74	423.13	54.98
contra_ECT6a	395.18	59.40	393.25	50.94
contra_ECT6b	255.00	63.48	271.25	42.83
contra_ENTl	443.68	57.43	435.19	47.44
contra_ENTl1	516.23	61.13	513.81	75.89
contra_ENTl3	469.50	50.56	459.38	56.72
contra_ENTl5	431.05	56.73	421.50	48.08
contra_ENTl6a	399.95	61.40	393.69	36.66
contra_ENTl6b	299.86	72.76	306.56	52.66
contra_FC	317.23	40.74	321.25	33.40
contra_hip	515.05	50.09	503.63	36.70
contra_hyp	123.27	24.05	119.81	25.70
contra_LA	415.50	53.97	414.13	47.05

contra_lay1	444.18	54.55	448.88	59.12
contra_lay2	262.68	50.63	234.50	36.46
contra_lay3	404.27	57.09	400.44	54.62
contra_lay4	384.14	53.95	377.44	48.28
contra_lay5	347.82	49.55	343.75	50.12
contra_lay6a	344.82	49.45	338.88	43.97
contra_lay6b	228.14	50.35	232.88	39.71
contra_MOp	371.14	51.26	357.75	56.58
contra_MOp1	443.73	64.94	440.06	84.55
contra_MOp3	398.36	56.72	387.69	66.89
contra_MOp5	355.95	54.14	349.75	59.71
contra_MOp6a	331.23	53.80	319.69	51.98
contra_MOp6b	234.68	65.09	236.00	28.48
contra_MOs	309.45	44.88	291.69	57.98
contra_MOs1	409.59	64.29	399.25	79.18
contra_MOs3	330.09	52.45	324.00	61.83
contra_MOs5	274.50	45.15	257.19	55.05
contra_MOs6a	269.50	48.40	248.38	51.08
contra_MOs6b	208.27	56.34	191.50	51.05
contra_PAA	347.18	55.42	345.19	54.38
contra_PAA1	361.90	69.94	348.25	58.30
contra_PAA2	355.14	58.67	352.50	67.18
contra_PAA3	340.41	50.16	338.13	46.79
contra_PERI	449.73	54.17	442.13	56.94
contra_PERI1	501.45	77.54	505.94	72.72
contra_PERI3	468.91	55.33	454.13	61.27
contra_PERI5	442.23	44.83	427.56	58.68
contra_PERI6a	407.77	57.57	406.88	46.49
contra_PERI6b	260.32	66.50	272.50	38.97
contra_PIR	440.50	44.60	434.19	29.78
contra_PIR1	493.64	56.86	485.19	29.24
contra_PIR2	407.18	52.02	408.56	18.79
contra_PIR3	429.55	42.72	423.38	32.78
contra_RSPd	283.59	44.90	269.56	48.03
contra_RSPd1	385.41	75.73	383.00	61.24
contra_RSPd3	307.23	51.78	297.19	50.45
contra_RSPd5	239.86	42.52	223.13	47.34

contra_RSPd6a	250.41	39.71	228.81	51.61
contra_RSPd6b	190.14	54.03	193.88	51.44
contra_RSPv	273.68	46.46	253.56	42.02
contra_RSPv1	322.23	53.88	301.06	48.49
contra_RSPv2	262.91	50.07	234.50	35.54
contra_RSPv3	294.27	47.08	277.75	45.52
contra_RSPv5	241.95	45.08	230.81	38.78
contra_RSPv6a	231.23	41.08	210.13	40.58
contra_RSPv6b	195.60	45.49	180.31	52.17
contra_SSp-bfd	362.36	57.42	357.50	52.99
contra_SSp-bfd1	451.32	68.01	445.63	61.87
contra_SSp-bfd3	391.91	68.09	383.63	60.59
contra_SSp-bfd4	369.41	52.38	363.56	47.23
contra_SSp-bfd5	330.27	54.25	324.38	50.25
contra_SSp-bfd6a	340.23	52.23	335.63	44.59
contra_SSp-bfd6b	220.32	56.84	229.94	55.58
contra_SSP-tr	365.36	53.19	361.00	49.91
contra_SSp-tr1	444.91	59.47	456.31	59.19
contra_SSp-tr3	401.45	62.00	396.25	58.53
contra_SSp-tr4	364.36	58.72	356.19	50.36
contra_SSp-tr5	332.36	51.18	328.50	50.75
contra_SSp-tr6a	331.32	51.33	331.13	47.33
contra_SSp-tr6b	213.77	58.78	228.38	43.92
contra_TEa	436.32	65.68	431.56	48.99
contra_TEa1	493.41	88.11	491.75	68.09
contra_TEa3	468.36	74.18	462.88	56.40
contra_TEa4	446.95	62.72	435.13	50.39
contra_TEa5	420.00	64.74	416.44	54.06
contra_TEa6a	387.77	63.59	382.06	43.83
contra_TEa6b	248.59	56.57	271.94	42.90
contra_th	294.73	18.07	286.13	17.45
ips_amgmed	256.82	42.13	236.88	30.16
ips_AUDd	361.18	62.16	335.25	67.50
ips_AUDd1	423.68	85.10	383.75	81.63

ips_AUDd3	387.23	75.62	349.06	76.33
ips_AUDd4	372.68	55.68	357.19	48.56
ips_AUDd5	332.05	57.05	313.56	64.34
ips_AUDd6a	330.95	52.09	315.75	62.98
ips_AUDd6b	208.09	58.86	236.25	53.73
ips_AUDp	379.18	58.56	356.06	63.81
ips_AUDp1	453.55	80.52	407.31	73.82
ips_AUDp3	410.27	70.52	378.69	65.25
ips_AUDp4	395.73	50.43	365.19	52.64
ips_AUDp5	350.14	52.06	333.81	63.34
ips_AUDp6a	336.77	52.20	328.88	64.15
ips_AUDp6b	202.27	61.08	205.75	58.15
ips_AUDv	403.73	53.61	373.06	61.98
ips_AUDv1	492.68	61.32	429.38	68.41
ips_AUDv3	437.55	59.16	398.06	55.42
ips_AUDv4	409.18	49.59	372.56	51.00
ips_AUDv5	376.27	51.95	359.69	67.25
ips_AUDv6a	351.77	53.75	329.31	67.44
ips_AUDv6b	230.95	45.46	228.13	62.66
ips_BLAa	425.73	44.31	420.50	31.72
ips_BLAp	442.73	39.55	432.19	36.85
ips_BLAv	352.55	68.19	337.88	64.48
ips_BMAp	308.14	68.44	285.44	55.65
ips_CA1slm	383.45	73.57	348.06	54.70
ips_CA1so	547.55	63.41	510.81	62.97
ips_CA1sp	188.14	48.09	153.00	30.17
ips_CA1sr	607.36	62.07	567.75	67.74
ips_CA2slm	514.55	41.88	516.44	36.99
ips_CA2so	499.82	29.31	500.88	27.80
ips_CA2sp	106.95	33.21	83.50	28.91
ips_CA2sr	471.05	32.45	468.81	32.20
ips_CA3slm	530.36	55.39	524.19	53.99
ips_CA3slu	206.18	43.94	184.50	47.97
ips_CA3so	454.00	52.11	443.44	52.85
ips_CA3sp	115.86	27.43	97.13	28.65
ips_CA3sr	530.50	56.03	520.38	54.84
ips_CC	21.86	14.12	14.75	5.01

ips_cing	82.41	27.20	50.63	18.85
ips_COApl	320.27	72.34	272.00	40.72
ips_COApl1	356.36	77.84	301.44	46.70
ips_COApl2	318.18	74.51	270.56	42.14
ips_COApl3	307.64	70.36	265.50	42.37
ips_cortex	330.64	57.08	317.63	57.47
ips_CP	316.55	44.92	303.06	40.78
ips_cpd	35.14	20.34	31.13	21.34
ips_DG	664.14	40.52	643.06	43.42
ips_DGinf	656.68	36.97	637.25	39.78
ips_DGpo	192.09	22.44	187.38	19.06
ips_DGsg	126.23	28.72	110.81	19.10
ips_DGsup	670.18	45.41	648.94	45.96
ips_ECT	428.09	46.72	412.06	52.71
ips_ECT1	485.36	73.00	458.69	70.24
ips_ECT3	445.32	47.61	431.44	55.13
ips_ECT5	413.32	47.62	394.88	51.56
ips_ECT6a	381.77	48.54	361.38	64.83
ips_ECT6b	253.55	68.92	245.56	68.27
ips_ENTl	429.77	56.17	426.75	47.98
ips_ENTl1	537.18	74.13	520.56	68.50
ips_ENTl3	452.86	64.89	446.13	51.24
ips_ENTl5	408.82	51.47	413.13	43.97
ips_ENTl6a	363.68	55.59	369.81	55.91
ips_ENTl6b	279.41	58.00	306.13	68.90
ips_FC	293.32	32.72	295.88	34.05
ips_hip	510.64	48.99	493.75	48.33
ips_hyp	122.82	21.54	120.25	24.79
ips_LA	392.73	40.41	385.81	40.87
ips_lay1	385.95	68.10	379.44	61.55
ips_lay2	238.45	59.45	213.13	26.23
ips_lay3	355.18	64.36	338.44	60.91
ips_lay4	350.32	57.63	332.25	52.17
ips_lay5	311.45	53.85	298.50	58.14
ips_lay6a	298.36	60.34	287.25	59.90
ips_lay6b	205.23	49.79	203.94	49.94
ips_MOp	313.95	59.85	294.13	51.13

ips_MOp1	329.91	82.99	336.00	60.97
ips_MOp3	334.77	67.40	319.00	47.83
ips_MOp5	318.86	58.75	295.69	56.09
ips_MOp6a	287.77	63.81	259.56	63.07
ips_MOp6b	193.41	71.24	171.94	53.12
ips_MOs	262.09	57.51	246.00	45.40
ips_MOs1	311.10	71.25	325.56	52.89
ips_MOs3	284.77	61.97	274.56	46.65
ips_MOs5	245.23	56.25	225.63	41.24
ips_MOs6a	234.41	54.36	204.56	48.81
ips_MOs6b	205.00	48.73	156.38	39.59
ips_PAA	337.14	54.57	326.31	64.76
ips_PAA1	361.23	70.90	327.44	78.46
ips_PAA2	335.77	54.38	327.06	50.04
ips_PAA3	329.64	53.84	323.69	67.44
ips_PERI	440.64	44.08	428.44	51.73
ips_PERI1	529.73	63.77	490.69	65.19
ips_PERI3	459.27	45.65	437.94	45.05
ips_PERI5	418.05	43.86	419.06	56.97
ips_PERI6a	384.86	57.42	387.56	59.72
ips_PERI6b	268.00	62.64	251.75	70.42
ips_PIR	423.91	46.53	408.88	46.13
ips_PIR1	490.14	55.88	468.44	62.05
ips_PIR2	387.32	72.34	375.75	49.27
ips_PIR3	410.91	42.04	398.00	40.77
ips_RSPd	255.23	49.25	242.69	34.11
ips_RSPd1	324.41	63.07	323.13	41.28
ips_RSPd3	276.23	56.59	265.69	31.99
ips_RSPd5	219.64	43.22	207.19	43.33
ips_RSPd6a	223.36	48.39	199.25	39.92
ips_RSPd6b	197.23	57.30	162.75	37.88
ips_RSPv	253.68	50.27	234.19	35.38
ips_RSPv1	289.95	59.49	269.75	28.81
ips_RSPv2	238.59	59.07	212.94	26.38
ips_RSPv3	278.82	49.27	257.88	41.55
ips_RSPv5	228.91	43.18	212.38	40.55
ips_RSPv6a	210.77	44.73	186.81	43.11

ips_RSPv6b	195.64	59.01	157.69	37.23
ips_SSp-bfd	329.05	65.92	311.38	74.20
ips_SSp-bfd1	397.05	90.97	391.13	69.50
ips_SSp-bfd3	352.73	77.56	328.88	82.99
ips_SSp-bfd4	346.73	60.22	329.38	64.32
ips_SSp-bfd5	303.86	57.16	287.56	70.10
ips_SSp-bfd6a	303.00	63.07	295.13	70.58
ips_SSp-bfd6b	204.77	54.06	219.56	60.56
ips_SSp-tr	304.36	58.40	299.00	58.67
ips_SSp-tr1	361.27	71.88	368.44	70.02
ips_SSp-tr3	322.82	65.45	317.63	64.28
ips_SSp-tr4	316.55	54.75	307.00	51.36
ips_SSp-tr5	288.36	52.23	281.75	56.58
ips_SSp-tr6a	277.77	69.25	270.31	60.07
ips_SSp-tr6b	181.91	53.50	184.00	52.66
ips_TEa	419.27	49.50	397.13	59.49
ips_TEa1	486.86	69.70	455.13	70.55
ips_TEa3	445.95	56.67	417.94	54.71
ips_TEa4	421.14	50.50	400.69	57.48
ips_TEa5	405.36	51.25	383.88	61.79
ips_TEa6a	359.27	49.50	351.44	66.51
ips_TEa6b	232.95	46.48	232.06	63.43
ips_th	280.18	22.28	274.75	19.65

Table 2: SAP102 puncta size at 7 days

	Injury		**Sham**	
region	**Average**	**SD**	**Average**	**SD**
contra_amgmed	14.66	0.21	14.53	0.21
contra_AUDd	14.42	0.25	14.29	0.27
contra_AUDd1	13.96	0.30	13.83	0.20
contra_AUDd3	14.75	0.30	14.66	0.32
contra_AUDd4	14.08	0.29	13.88	0.20
contra_AUDd5	14.36	0.30	14.16	0.33
contra_AUDd6a	14.26	0.26	14.16	0.24
contra_AUDd6b	14.56	0.40	14.40	0.39
contra_AUDp	14.34	0.20	14.20	0.22
contra_AUDp1	14.03	0.26	13.73	0.18

contra_AUDp3	14.64	0.22	14.53	0.31
contra_AUDp4	14.08	0.30	13.80	0.12
contra_AUDp5	14.21	0.27	14.08	0.22
contra_AUDp6a	14.27	0.20	14.12	0.20
contra_AUDp6b	14.40	0.21	14.42	0.32
contra_AUDv	14.21	0.28	14.05	0.20
contra_AUDv1	13.98	0.41	13.69	0.27
contra_AUDv3	14.51	0.30	14.35	0.24
contra_AUDv4	13.95	0.28	13.76	0.15
contra_AUDv5	14.08	0.28	13.97	0.20
contra_AUDv6a	14.19	0.27	14.07	0.21
contra_AUDv6b	14.34	0.19	14.13	0.19
contra_BLAa	13.67	0.22	13.49	0.16
contra_BLAp	13.64	0.29	13.49	0.10
contra_BLAv	13.87	0.26	13.73	0.29
contra_BMAp	14.18	0.39	14.10	0.24
contra_CA1slm	14.70	0.34	14.65	0.42
contra_CA1so	13.29	0.21	13.27	0.31
contra_CA1sp	16.33	0.59	16.45	0.48
contra_CA1sr	13.74	0.24	13.76	0.40
contra_CA2slm	12.95	0.14	12.87	0.13
contra_CA2so	12.85	0.11	12.77	0.12
contra_CA2sp	18.05	1.05	18.57	0.86
contra_CA2sr	13.27	0.19	13.20	0.17
contra_CA3slm	13.20	0.23	13.11	0.16
contra_CA3slu	19.66	0.66	19.47	0.52
contra_CA3so	13.21	0.23	13.10	0.16
contra_CA3sp	20.07	0.79	19.81	0.39
contra_CA3sr	13.45	0.20	13.31	0.14
contra_CC	16.24	1.11	15.88	0.66
contra_cing	15.44	0.71	15.11	0.46
contra_COApl	14.31	0.32	14.22	0.21
contra_COApl1	13.85	0.24	13.80	0.28
contra_COApl2	14.49	0.41	14.34	0.31
contra_COApl3	14.40	0.35	14.35	0.17
contra_cortex	14.32	0.20	14.24	0.22
contra_CP	14.22	0.16	14.13	0.18

contra_cpd	17.58	1.40	17.65	1.09
contra_DG	13.72	0.27	13.78	0.37
contra_DGinf	13.78	0.29	13.80	0.27
contra_DGpo	17.44	0.34	17.47	0.29
contra_DGsg	20.56	0.64	20.59	0.78
contra_DGsup	13.69	0.30	13.78	0.45
contra_ECT	13.98	0.25	13.79	0.17
contra_ECT1	13.76	0.36	13.48	0.19
contra_ECT3	14.04	0.27	13.91	0.22
contra_ECT5	13.91	0.30	13.73	0.14
contra_ECT6a	13.99	0.30	13.82	0.23
contra_ECT6b	14.33	0.37	14.16	0.20
contra_ENTl	13.69	0.24	13.59	0.21
contra_ENTl1	13.45	0.30	13.32	0.44
contra_ENTl3	13.76	0.25	13.64	0.22
contra_ENTl5	13.68	0.25	13.59	0.21
contra_ENTl6a	13.75	0.27	13.68	0.17
contra_ENTl6b	13.94	0.21	13.91	0.31
contra_FC	13.64	0.25	13.54	0.21
contra_hip	13.83	0.23	13.84	0.34
contra_hyp	15.96	0.41	15.85	0.43
contra_LA	13.69	0.23	13.56	0.14
contra_lay1	14.00	0.19	13.84	0.18
contra_lay2	15.02	0.34	15.01	0.27
contra_lay3	14.60	0.22	14.56	0.27
contra_lay4	14.12	0.21	13.96	0.22
contra_lay5	14.21	0.24	14.10	0.24
contra_lay6a	14.23	0.23	14.16	0.26
contra_lay6b	14.40	0.28	14.26	0.27
contra_MOp	14.14	0.24	14.11	0.27
contra_MOp1	13.91	0.31	13.93	0.41
contra_MOp3	14.35	0.26	14.38	0.36
contra_MOp5	13.97	0.23	13.94	0.24
contra_MOp6a	14.09	0.26	14.09	0.29
contra_MOp6b	14.33	0.39	14.16	0.25
contra_MOs	14.56	0.23	14.53	0.28
contra_MOs1	14.33	0.18	14.27	0.37

contra_MOs3	14.77	0.22	14.73	0.26
contra_MOs5	14.44	0.35	14.43	0.36
contra_MOs6a	14.43	0.35	14.42	0.32
contra_MOs6b	14.52	0.38	14.44	0.66
contra_PAA	13.99	0.24	13.83	0.31
contra_PAA1	13.50	0.21	13.45	0.39
contra_PAA2	14.06	0.31	14.06	0.35
contra_PAA3	14.13	0.24	13.92	0.27
contra_PERI	13.77	0.24	13.66	0.24
contra_PERI1	13.59	0.31	13.44	0.49
contra_PERI3	13.83	0.26	13.70	0.26
contra_PERI5	13.72	0.26	13.67	0.18
contra_PERI6a	13.81	0.27	13.65	0.19
contra_PERI6b	14.19	0.33	14.15	0.33
contra_PIR	13.61	0.21	13.49	0.09
contra_PIR1	13.15	0.27	13.04	0.14
contra_PIR2	14.29	0.26	14.11	0.12
contra_PIR3	13.64	0.21	13.51	0.09
contra_RSPd	14.72	0.24	14.59	0.27
contra_RSPd1	14.41	0.27	14.36	0.19
contra_RSPd3	14.78	0.28	14.65	0.30
contra_RSPd5	14.86	0.33	14.71	0.38
contra_RSPd6a	14.68	0.34	14.53	0.39
contra_RSPd6b	14.64	0.43	14.41	0.39
contra_RSPv	14.69	0.26	14.61	0.24
contra_RSPv1	14.56	0.18	14.53	0.29
contra_RSPv2	15.01	0.34	15.00	0.27
contra_RSPv3	14.32	0.25	14.20	0.21
contra_RSPv5	14.86	0.35	14.66	0.27
contra_RSPv6a	14.86	0.41	14.71	0.43
contra_RSPv6b	14.89	0.65	14.65	0.51
contra_SSp-bfd	14.54	0.29	14.48	0.31
contra_SSp-bfd1	14.07	0.25	13.92	0.22
contra_SSp-bfd3	14.89	0.31	14.86	0.36
contra_SSp-bfd4	14.21	0.26	14.02	0.23

contra_SSp-bfd5	14.47	0.37	14.29	0.31
contra_SSp-bfd6a	14.38	0.28	14.32	0.32
contra_SSp-bfd6b	14.55	0.43	14.40	0.41
contra_SSP-tr	14.33	0.23	14.27	0.26
contra_SSp-tr1	13.90	0.26	13.78	0.16
contra_SSp-tr3	14.71	0.31	14.66	0.31
contra_SSp-tr4	14.20	0.24	14.15	0.31
contra_SSp-tr5	14.13	0.21	14.09	0.31
contra_SSp-tr6a	14.24	0.22	14.16	0.32
contra_SSp-tr6b	14.45	0.35	14.29	0.31
contra_TEa	14.09	0.29	13.92	0.21
contra_TEa1	13.89	0.40	13.65	0.28
contra_TEa3	14.37	0.34	14.20	0.31
contra_TEa4	13.84	0.25	13.66	0.14
contra_TEa5	13.97	0.34	13.83	0.20
contra_TEa6a	14.10	0.30	13.97	0.20
contra_TEa6b	14.36	0.31	14.10	0.22
contra_th	13.13	0.13	13.08	0.18
ips_amgmed	14.61	0.23	14.55	0.20
ips_AUDd	14.37	0.17	14.47	0.40
ips_AUDd1	13.98	0.28	14.18	0.35
ips_AUDd3	14.56	0.24	14.77	0.50
ips_AUDd4	14.01	0.17	14.01	0.24
ips_AUDd5	14.38	0.22	14.34	0.46
ips_AUDd6a	14.32	0.23	14.35	0.39
ips_AUDd6b	14.73	0.28	14.47	0.41
ips_AUDp	14.24	0.15	14.35	0.36
ips_AUDp1	13.83	0.25	14.11	0.39
ips_AUDp3	14.37	0.17	14.56	0.41
ips_AUDp4	13.89	0.20	14.00	0.25
ips_AUDp5	14.27	0.23	14.29	0.42
ips_AUDp6a	14.33	0.22	14.27	0.40
ips_AUDp6b	14.61	0.36	14.58	0.37
ips_AUDv	14.04	0.11	14.19	0.34
ips_AUDv1	13.59	0.16	13.92	0.41

ips_AUDv3	14.12	0.12	14.34	0.38
ips_AUDv4	13.87	0.13	14.02	0.26
ips_AUDv5	14.05	0.20	14.09	0.37
ips_AUDv6a	14.19	0.18	14.27	0.45
ips_AUDv6b	14.56	0.32	14.40	0.33
ips_BLAa	13.64	0.15	13.62	0.17
ips_BLAp	13.67	0.14	13.67	0.21
ips_BLAv	13.93	0.22	13.88	0.31
ips_BMAp	14.27	0.47	14.12	0.36
ips_CA1slm	14.66	0.26	14.71	0.46
ips_CA1so	13.25	0.27	13.39	0.36
ips_CA1sp	16.37	0.49	16.70	0.61
ips_CA1sr	13.64	0.26	13.83	0.44
ips_CA2slm	13.00	0.20	13.02	0.22
ips_CA2so	12.93	0.11	12.89	0.12
ips_CA2sp	18.39	1.02	19.01	1.35
ips_CA2sr	13.26	0.21	13.28	0.18
ips_CA3slm	13.26	0.34	13.32	0.28
ips_CA3slu	19.67	0.55	19.69	0.26
ips_CA3so	13.21	0.27	13.29	0.25
ips_CA3sp	19.96	0.42	20.08	0.91
ips_CA3sr	13.48	0.30	13.52	0.23
ips_CC	16.38	1.05	15.50	0.80
ips_cing	15.34	0.85	15.08	0.67
ips_COApl	14.33	0.44	14.32	0.21
ips_COApl1	13.79	0.34	13.85	0.17
ips_COApl2	14.58	0.55	14.50	0.27
ips_COApl3	14.43	0.47	14.46	0.31
ips_cortex	14.31	0.15	14.31	0.24
ips_CP	14.17	0.24	14.11	0.21
ips_cpd	17.75	1.36	17.37	1.19
ips_DG	13.68	0.29	13.91	0.59
ips_DGinf	13.73	0.29	13.95	0.56
ips_DGpo	17.56	0.38	17.44	0.34
ips_DGsg	20.53	0.62	20.60	0.83
ips_DGsup	13.64	0.30	13.88	0.62
ips_ECT	13.83	0.11	13.91	0.29

ips_ECT1	13.61	0.25	13.72	0.32
ips_ECT3	13.86	0.14	13.93	0.25
ips_ECT5	13.76	0.13	13.84	0.34
ips_ECT6a	13.88	0.19	14.06	0.49
ips_ECT6b	14.43	0.26	14.33	0.41
ips_ENTl	13.68	0.12	13.65	0.22
ips_ENTl1	13.25	0.12	13.31	0.23
ips_ENTl3	13.68	0.16	13.68	0.19
ips_ENTl5	13.72	0.15	13.61	0.25
ips_ENTl6a	13.90	0.20	13.84	0.34
ips_ENTl6b	14.29	0.32	14.03	0.35
ips_FC	13.79	0.24	13.56	0.20
ips_hip	13.78	0.24	13.91	0.41
ips_hyp	15.97	0.41	15.85	0.44
ips_LA	13.76	0.12	13.76	0.19
ips_lay1	14.08	0.28	14.08	0.17
ips_lay2	15.16	0.32	15.08	0.35
ips_lay3	14.46	0.16	14.52	0.22
ips_lay4	14.06	0.12	14.08	0.20
ips_lay5	14.26	0.17	14.21	0.26
ips_lay6a	14.25	0.19	14.23	0.30
ips_lay6b	14.58	0.30	14.38	0.31
ips_MOp	14.19	0.18	14.21	0.26
ips_MOp1	14.30	0.56	14.31	0.27
ips_MOp3	14.38	0.30	14.43	0.26
ips_MOp5	13.99	0.14	13.98	0.29
ips_MOp6a	14.01	0.17	14.07	0.28
ips_MOp6b	14.43	0.39	14.34	0.35
ips_MOs	14.64	0.20	14.56	0.27
ips_MOs1	14.64	0.33	14.57	0.35
ips_MOs3	14.80	0.21	14.73	0.24
ips_MOs5	14.53	0.22	14.46	0.31
ips_MOs6a	14.43	0.38	14.40	0.34
ips_MOs6b	14.53	0.49	14.31	0.42
ips_PAA	14.16	0.28	13.95	0.35
ips_PAA1	13.74	0.29	13.59	0.34
ips_PAA2	14.41	0.27	14.20	0.27

ips_PAA3	14.29	0.32	14.06	0.38
ips_PERI	13.65	0.08	13.72	0.25
ips_PERI1	13.33	0.16	13.45	0.26
ips_PERI3	13.68	0.09	13.76	0.24
ips_PERI5	13.68	0.16	13.71	0.30
ips_PERI6a	13.73	0.13	13.81	0.35
ips_PERI6b	14.31	0.34	14.37	0.39
ips_PIR	13.68	0.11	13.64	0.19
ips_PIR1	13.24	0.20	13.21	0.26
ips_PIR2	14.33	0.15	14.25	0.23
ips_PIR3	13.67	0.12	13.64	0.18
ips_RSPd	14.78	0.32	14.66	0.25
ips_RSPd1	14.62	0.23	14.48	0.16
ips_RSPd3	14.81	0.31	14.69	0.22
ips_RSPd5	14.92	0.43	14.77	0.38
ips_RSPd6a	14.73	0.48	14.65	0.37
ips_RSPd6b	14.62	0.51	14.39	0.53
ips_RSPv	14.75	0.30	14.63	0.29
ips_RSPv1	14.69	0.25	14.58	0.23
ips_RSPv2	15.15	0.32	15.09	0.37
ips_RSPv3	14.37	0.29	14.25	0.24
ips_RSPv5	14.88	0.40	14.67	0.36
ips_RSPv6a	14.89	0.45	14.85	0.38
ips_RSPv6b	14.65	0.73	14.87	1.03
ips_SSp-bfd	14.48	0.22	14.47	0.30
ips_SSp-bfd1	14.10	0.35	14.05	0.24
ips_SSp-bfd3	14.67	0.25	14.75	0.35
ips_SSp-bfd4	14.14	0.16	14.12	0.24
ips_SSp-bfd5	14.49	0.25	14.44	0.35
ips_SSp-bfd6a	14.38	0.24	14.34	0.31
ips_SSp-bfd6b	14.63	0.36	14.39	0.29
ips_SSp-tr	14.39	0.17	14.30	0.22
ips_SSp-tr1	14.18	0.44	14.08	0.21
ips_SSp-tr3	14.64	0.21	14.59	0.21
ips_SSp-tr4	14.15	0.18	14.12	0.23
ips_SSp-tr5	14.23	0.17	14.14	0.24
ips_SSp-tr6a	14.23	0.16	14.15	0.26

ips_SSp-tr6b	14.70	0.38	14.36	0.31
ips_TEa	13.94	0.11	14.01	0.31
ips_TEa1	13.63	0.24	13.67	0.30
ips_TEa3	14.00	0.13	14.13	0.33
ips_TEa4	13.79	0.14	13.85	0.28
ips_TEa5	13.86	0.18	13.96	0.35
ips_TEa6a	14.20	0.22	14.14	0.49
ips_TEa6b	14.50	0.35	14.44	0.40
ips_th	13.31	0.13	13.23	0.23

Table 3: SAP102 puncta intensity at 7 days

	Injury		**Sham**	
region	**Average**	**SD**	**Average**	**SD**
contra_amgmed	12678.02	2385.72	12564.75	2665.01
contra_AUDd	13287.69	2394.93	13077.69	2406.78
contra_AUDd1	13174.40	2616.21	12830.27	2581.44
contra_AUDd3	13668.30	2445.38	13477.44	2588.42
contra_AUDd4	13425.20	2461.81	13194.51	2305.14
contra_AUDd5	13053.72	2376.52	12883.25	2402.56
contra_AUDd6a	13043.67	2369.26	12952.25	2449.88
contra_AUDd6b	11205.07	2144.41	11248.86	1773.58
contra_AUDp	13459.53	2485.62	13377.10	2495.10
contra_AUDp1	13280.62	2472.81	13478.99	2743.48
contra_AUDp3	14066.69	2568.03	14025.62	2745.63
contra_AUDp4	13537.08	2527.23	13471.87	2486.13
contra_AUDp5	13237.44	2460.07	13103.07	2456.38
contra_AUDp6a	13155.79	2534.99	13030.71	2418.07
contra_AUDp6b	11293.25	2679.50	10766.03	1710.59
contra_AUDv	13650.92	2631.28	13591.15	2601.88
contra_AUDv1	13561.35	2854.22	13635.73	2838.20
contra_AUDv3	14352.27	2930.31	14280.75	2957.59
contra_AUDv4	13772.81	2596.62	13664.26	2609.10
contra_AUDv5	13487.21	2528.91	13371.64	2600.21
contra_AUDv6a	13281.41	2618.67	13200.91	2429.02
contra_AUDv6b	11608.85	2569.64	11440.69	2073.87
contra_BLAa	15729.22	3283.96	15450.63	3258.43
contra_BLAp	16086.54	3299.69	15828.50	3172.42

contra_BLAv	14364.87	2961.90	14307.77	2763.31
contra_BMAp	13863.53	2839.59	13671.58	2750.39
contra_CA1slm	12810.76	2334.43	11829.43	1441.66
contra_CA1so	14006.66	2367.25	13117.99	2161.91
contra_CA1sp	12615.81	1944.45	11756.74	1501.86
contra_CA1sr	15025.80	2493.51	13792.57	2152.51
contra_CA2slm	14731.10	2746.57	13753.75	1935.34
contra_CA2so	16958.46	2999.95	16394.05	2510.63
contra_CA2sp	12933.76	1807.28	12576.27	1406.24
contra_CA2sr	15562.37	2970.49	14725.96	2241.06
contra_CA3slm	13800.86	2470.51	12765.43	1984.66
contra_CA3slu	11748.56	2025.08	11285.93	1859.87
contra_CA3so	12140.97	2306.20	11424.22	1709.50
contra_CA3sp	11037.01	1622.98	10602.94	1282.63
contra_CA3sr	13386.66	2338.36	12745.50	1799.09
contra_CC	6959.60	448.62	7219.61	420.91
contra_cing	9009.43	1251.46	8542.38	1137.11
contra_COApl	13595.85	2510.30	13601.07	3061.59
contra_COApl1	13044.39	2426.60	13438.84	2856.76
contra_COApl2	13990.39	2574.89	13903.71	3272.47
contra_COApl3	13677.01	2589.09	13486.82	2995.18
contra_cortex	13065.55	2237.64	12800.42	2526.69
contra_CP	12058.47	2215.41	11751.20	2173.24
contra_cpd	6670.20	467.10	6752.29	622.03
contra_DG	19359.89	3187.83	17673.32	2652.56
contra_DGinf	18708.93	2894.35	17096.75	2539.29
contra_DGpo	12267.46	1919.96	11374.52	1495.48
contra_DGsg	13574.06	1729.39	12650.14	871.95
contra_DGsup	19755.46	3435.41	18063.48	2713.00
contra_ECT	14360.87	2861.12	14126.65	2863.56
contra_ECT1	14388.05	3145.61	14183.04	3025.35
contra_ECT3	14889.17	3067.48	14509.62	2977.42
contra_ECT5	14262.36	2788.99	14031.36	2834.95
contra_ECT6a	13866.55	2762.93	13650.64	2769.97
contra_ECT6b	12225.09	2572.60	12323.86	2038.01
contra_ENTl	15221.62	2785.66	15090.19	3459.46
contra_ENTl1	15145.03	2534.33	14727.77	3859.73

contra_ENTl3	15989.89	2687.19	15788.73	3811.98
contra_ENTl5	15368.08	3075.05	15255.20	3444.58
contra_ENTl6a	14154.88	2908.01	13946.31	2860.85
contra_ENTl6b	12819.44	2585.13	12963.75	2621.70
contra_FC	15237.53	2605.19	13409.40	2026.84
contra_hip	14238.54	2442.87	13292.75	1941.88
contra_hyp	10921.93	1747.21	10823.64	2127.42
contra_LA	14184.15	2839.26	14110.55	2903.55
contra_lay1	12982.01	2179.37	12920.21	2796.16
contra_lay2	12878.91	2209.44	11983.90	2248.05
contra_lay3	13484.40	2316.25	13164.05	2732.95
contra_lay4	13301.97	2348.93	13040.59	2477.76
contra_lay5	12942.91	2225.84	12695.60	2452.86
contra_lay6a	12796.04	2274.78	12537.72	2419.95
contra_lay6b	11283.25	2103.26	11218.49	1939.42
contra_MOp	12840.39	2076.98	12356.74	2745.86
contra_MOp1	12788.32	2204.78	12837.11	3546.49
contra_MOp3	13339.58	2160.66	13117.26	3215.86
contra_MOp5	12801.50	2131.94	12264.77	2606.33
contra_MOp6a	12511.30	2150.04	11774.98	2331.58
contra_MOp6b	11411.49	2076.95	10792.77	1873.18
contra_MOs	12393.20	1869.58	11900.40	2700.05
contra_MOs1	12976.24	2411.13	12713.78	3617.81
contra_MOs3	12786.78	1952.99	12555.71	3071.77
contra_MOs5	12054.93	1817.37	11562.37	2342.24
contra_MOs6a	11676.80	1984.68	10976.68	2221.55
contra_MOs6b	10616.49	1869.37	10085.18	1864.23
contra_PAA	13811.19	2719.12	14130.09	2730.93
contra_PAA1	13100.57	2797.68	13117.27	2492.34
contra_PAA2	14225.63	2978.27	14472.78	2812.61
contra_PAA3	13963.67	2687.39	14321.94	2790.26
contra_PERI	14702.83	2729.96	14483.43	3170.32
contra_PERI1	14463.63	2945.12	14127.81	3121.63
contra_PERI3	15098.91	2809.63	14981.42	3449.50
contra_PERI5	14753.32	2742.56	14602.59	3210.27
contra_PERI6a	14100.55	2719.79	13924.43	2789.36
contra_PERI6b	12567.13	2630.96	12530.58	2266.55

contra_PIR	15487.68	3026.64	15290.71	2929.69
contra_PIR1	15040.62	3091.35	14826.47	3048.05
contra_PIR2	16462.88	3213.72	16255.58	3107.79
contra_PIR3	15222.29	2983.48	15004.20	2864.05
contra_RSPd	12430.22	1967.46	12027.03	2467.65
contra_RSPd1	13195.00	2682.15	13000.18	3155.10
contra_RSPd3	12771.01	2061.85	12490.95	2699.42
contra_RSPd5	11988.31	1796.91	11499.48	2156.02
contra_RSPd6a	11743.77	1906.88	11124.24	2139.46
contra_RSPd6b	10536.93	1796.08	10082.35	1894.02
contra_RSPv	12460.11	2004.07	11641.87	2086.40
contra_RSPv1	13076.31	2432.00	12181.52	2524.97
contra_RSPv2	12879.06	2209.70	11947.32	2208.20
contra_RSPv3	12564.48	2008.12	11772.68	2126.76
contra_RSPv5	11926.04	1787.42	11265.11	1932.95
contra_RSPv6a	11589.77	1887.08	10936.91	1996.51
contra_RSPv6b	11006.45	1792.16	10246.65	1896.43
contra_SSp-bfd	12958.21	2367.14	12543.25	2411.22
contra_SSp-bfd1	12988.96	2535.48	12107.93	2536.83
contra_SSp-bfd3	13254.13	2489.02	12594.43	2490.52
contra_SSp-bfd4	13242.51	2410.62	12973.34	2371.38
contra_SSp-bfd5	12774.32	2295.27	12572.44	2330.10
contra_SSp-bfd6a	12667.20	2276.72	12576.85	2482.26
contra_SSp-bfd6b	11022.48	1900.57	11223.42	2050.28
contra_SSP-tr	12628.35	2236.15	12450.75	2626.28
contra_SSp-tr1	12410.80	2339.37	12701.31	3035.58
contra_SSp-tr3	13009.55	2427.76	12813.82	2908.99
contra_SSp-tr4	12784.02	2234.00	12507.68	2609.74
contra_SSp-tr5	12593.50	2223.76	12324.07	2508.21
contra_SSp-tr6a	12460.78	2217.10	12164.50	2440.72
contra_SSp-tr6b	11073.92	2022.73	11070.30	2063.85
contra_TEa	14062.69	2825.26	13864.77	2777.57
contra_TEa1	14012.14	3109.20	13745.74	3016.73
contra_TEa3	14623.36	3055.67	14489.61	3001.92

contra_TEa4	14264.37	2775.91	14077.51	2826.52
contra_TEa5	13913.61	2749.70	13727.12	2767.86
contra_TEa6a	13583.82	2723.92	13460.24	2623.03
contra_TEa6b	11917.30	2522.14	11970.23	1930.25
contra_th	13591.10	2555.95	12836.64	1955.72
ips_amgmed	12885.53	1908.79	11900.93	2277.18
ips_AUDd	12759.51	2293.65	11907.13	2332.46
ips_AUDd1	12722.79	2671.19	11447.84	2459.21
ips_AUDd3	13070.93	2550.26	11959.71	2424.00
ips_AUDd4	13350.00	2401.23	12422.99	2220.64
ips_AUDd5	12595.02	2180.31	11901.35	2271.82
ips_AUDd6a	12399.28	2119.17	11831.44	2405.86
ips_AUDd6b	11073.57	1940.26	10841.31	2159.53
ips_AUDp	13229.36	2244.93	12178.51	2276.81
ips_AUDp1	13390.19	2648.47	11692.07	2260.88
ips_AUDp3	13664.93	2397.73	12370.11	2323.60
ips_AUDp4	13716.87	2286.80	12599.42	2199.05
ips_AUDp5	12927.53	2233.70	12166.27	2298.72
ips_AUDp6a	12640.47	2104.57	12053.50	2496.86
ips_AUDp6b	11117.20	2146.26	10505.06	1921.40
ips_AUDv	13665.13	2214.78	12470.38	2380.37
ips_AUDv1	14084.12	2299.73	12091.27	2218.19
ips_AUDv3	14117.92	2364.62	12715.67	2360.07
ips_AUDv4	14024.37	2243.82	12765.07	2432.62
ips_AUDv5	13267.48	2195.50	12439.40	2465.47
ips_AUDv6a	12991.46	2111.14	12334.68	2685.62
ips_AUDv6b	11502.40	2017.22	11007.80	2311.83
ips_BLAa	16088.26	2490.25	15121.59	3177.61
ips_BLAp	16300.48	2644.91	15292.69	3209.57
ips_BLAv	14895.32	2655.88	13842.60	2889.92
ips_BMAp	13970.55	2413.52	13121.54	3028.86
ips_CA1slm	12887.88	2156.06	11635.35	1602.14
ips_CA1so	14195.56	2201.19	12680.41	2106.26
ips_CA1sp	12695.92	1820.86	11417.67	1517.96
ips_CA1sr	15283.09	2375.43	13659.53	2326.34
ips_CA2slm	14549.93	2363.74	13258.71	2259.86
ips_CA2so	17061.65	2471.83	15637.06	2413.80

ips_CA2sp	12959.71	1480.79	11937.43	1375.62
ips_CA2sr	15418.39	2387.04	13961.02	2486.91
ips_CA3slm	13375.81	2209.73	12437.19	2153.23
ips_CA3slu	11729.36	1700.09	10872.16	1987.06
ips_CA3so	12003.41	1987.76	11028.39	1843.88
ips_CA3sp	11124.98	1453.64	10387.16	1394.01
ips_CA3sr	13245.19	2038.39	12354.44	2034.97
ips_CC	6867.72	552.51	6944.63	439.27
ips_cing	8886.26	1345.26	7906.38	1115.39
ips_COApl	14433.84	2932.30	12425.10	2774.33
ips_COApl1	14113.94	2907.93	12161.51	3040.27
ips_COApl2	14884.48	3064.84	12609.83	2855.08
ips_COApl3	14337.71	2930.40	12456.07	2750.67
ips_cortex	12134.14	2158.23	11433.01	2150.77
ips_CP	12052.53	1693.79	11361.83	2185.18
ips_cpd	6624.89	403.90	6834.62	669.02
ips_DG	18991.39	2991.11	17276.16	2850.54
ips_DGinf	18350.92	2858.49	16604.49	2683.85
ips_DGpo	12302.75	1919.58	11118.80	1543.27
ips_DGsg	13625.96	1717.29	12404.98	1020.89
ips_DGsup	19396.55	3084.34	17698.10	2956.78
ips_ECT	14592.43	2400.13	13626.30	2887.17
ips_ECT1	14421.49	2924.00	13352.89	3154.47
ips_ECT3	15044.53	2535.93	13924.67	2887.48
ips_ECT5	14329.61	2354.89	13606.70	2871.57
ips_ECT6a	13836.81	2134.79	13176.13	2916.31
ips_ECT6b	12444.98	2081.63	12012.90	2770.21
ips_ENTI	16130.40	2820.10	15413.34	3135.23
ips_ENTI1	16893.28	3215.58	15579.83	3447.06
ips_ENTI3	17087.82	3049.03	16142.21	3280.30
ips_ENTI5	15483.09	2848.98	15204.15	3271.08
ips_ENTI6a	14047.18	2303.21	13873.20	3201.83
ips_ENTI6b	12921.32	1945.25	12902.72	2989.13
ips_FC	14645.84	2279.53	12872.05	1657.85
ips_hip	14373.42	2175.36	13020.02	2052.18
ips_hyp	11045.59	1497.21	10860.87	2046.87
ips_LA	14259.19	2090.45	13608.61	2823.74

ips_lay1	12061.05	2354.19	11202.80	2086.85
ips_lay2	12132.63	2368.24	11210.41	1682.10
ips_lay3	12400.50	2274.43	11614.89	2215.62
ips_lay4	12720.36	2336.01	11912.48	2224.54
ips_lay5	12136.82	2101.34	11518.97	2157.82
ips_lay6a	11779.54	2154.99	11144.04	2167.18
ips_lay6b	10766.55	1967.91	10278.64	1999.83
ips_MOp	11534.16	2145.48	10760.39	1854.84
ips_MOp1	10727.91	2195.81	9888.73	1976.71
ips_MOp3	11684.86	2213.63	11071.16	1876.99
ips_MOp5	11823.30	2183.35	10963.77	1841.02
ips_MOp6a	11505.42	2240.06	10430.70	1926.53
ips_MOp6b	10472.71	2115.24	9678.39	1782.01
ips_MOs	11178.55	2091.04	10558.01	1674.65
ips_MOs1	11033.78	2223.39	10562.95	1818.90
ips_MOs3	11382.49	2197.62	10906.99	1698.50
ips_MOs5	11245.43	2082.28	10492.75	1665.71
ips_MOs6a	10879.43	2029.29	9928.86	1748.51
ips_MOs6b	10336.04	1869.68	9147.67	1603.22
ips_PAA	14307.76	2855.41	13387.52	3359.85
ips_PAA1	13684.53	3059.68	12463.56	3395.77
ips_PAA2	14789.13	3261.23	13687.63	3554.90
ips_PAA3	14381.52	2673.39	13737.74	3298.51
ips_PERI	15359.94	2388.79	14376.20	2993.00
ips_PERI1	15712.26	2920.92	14284.31	3163.29
ips_PERI3	16056.52	2559.78	14805.36	3040.35
ips_PERI5	14993.24	2301.84	14404.75	3133.96
ips_PERI6a	14049.96	2235.73	13557.97	3001.08
ips_PERI6b	12921.66	2046.79	12281.40	2795.35
ips_PIR	15957.59	3003.55	14825.09	3101.71
ips_PIR1	16218.37	3225.79	14809.83	3258.86
ips_PIR2	16820.54	3405.30	15385.35	3235.26
ips_PIR3	15527.27	2753.96	14571.48	3052.19
ips_RSPd	11552.99	2082.87	11037.51	1614.15
ips_RSPd1	11613.36	2558.94	11240.29	1784.71
ips_RSPd3	11837.33	2173.27	11303.00	1590.63
ips_RSPd5	11423.04	1897.32	10869.72	1630.79

ips_RSPd6a	11137.01	1911.75	10361.43	1705.94
ips_RSPd6b	10267.53	1909.86	9435.11	1543.58
ips_RSPv	11896.26	2077.10	11019.75	1716.57
ips_RSPv1	12289.69	2663.38	11263.10	1736.27
ips_RSPv2	12131.73	2370.45	11214.18	1683.99
ips_RSPv3	12234.94	2059.88	11169.51	1710.46
ips_RSPv5	11504.66	1825.34	10746.86	1730.47
ips_RSPv6a	11067.18	1869.36	10213.88	1691.82
ips_RSPv6b	10484.15	1821.31	9429.89	1438.31
ips_SSp-bfd	12163.90	2308.76	11555.18	2391.78
ips_SSp-bfd1	12219.16	2841.08	11425.14	2406.77
ips_SSp-bfd3	12296.09	2491.12	11636.09	2457.22
ips_SSp-bfd4	12763.03	2327.06	12104.27	2315.28
ips_SSp-bfd5	12098.95	2095.26	11605.94	2311.28
ips_SSp-bfd6a	11816.57	2145.53	11349.09	2430.43
ips_SSp-bfd6b	10758.93	1922.61	10390.41	2259.80
ips_SSp-tr	11247.08	2025.07	10714.87	2182.15
ips_SSp-tr1	10964.73	2251.78	10213.45	2278.84
ips_SSp-tr3	11159.18	2097.72	10740.09	2341.76
ips_SSp-tr4	11716.01	2106.72	10971.17	1988.58
ips_SSp-tr5	11511.74	2012.12	11000.25	2198.33
ips_SSp-tr6a	11113.49	2185.57	10631.03	2133.88
ips_SSp-tr6b	10247.01	2081.57	9815.54	1984.66
ips_TEa	14024.67	2250.32	13133.55	2762.58
ips_TEa1	13998.52	2510.46	13101.88	2893.01
ips_TEa3	14397.28	2464.58	13346.95	2709.27
ips_TEa4	14584.79	2297.36	13503.71	2723.93
ips_TEa5	13760.44	2189.24	13074.28	2787.52
ips_TEa6a	13317.39	2094.77	12819.68	2873.99
ips_TEa6b	11901.11	1991.17	11414.49	2595.00
ips_th	13549.35	2342.16	12530.27	2141.95

Table 4: SAP102 puncta density at 28 days

	Injury		**Sham**	
region	**Average**	**SD**	**Average**	**SD**
contra_amgmed	237.80	37.99	270.40	45.36
contra_AUDd	364.30	45.42	384.75	40.31

contra_AUDd1	423.55	57.33	450.95	39.29
contra_AUDd3	385.15	53.11	408.05	49.25
contra_AUDd4	371.30	48.82	388.60	46.78
contra_AUDd5	337.75	42.19	354.35	45.89
contra_AUDd6a	341.00	39.05	357.15	36.59
contra_AUDd6b	218.05	57.48	229.30	62.77
contra_AUDp	369.85	45.05	397.40	37.68
contra_AUDp1	430.90	51.07	462.15	38.07
contra_AUDp3	393.95	52.10	424.95	41.54
contra_AUDp4	375.55	41.61	394.70	37.46
contra_AUDp5	347.55	43.41	377.95	40.14
contra_AUDp6a	348.90	41.55	369.30	34.37
contra_AUDp6b	211.85	63.88	251.40	60.58
contra_AUDv	384.60	51.15	410.45	40.44
contra_AUDv1	439.20	61.57	465.90	51.50
contra_AUDv3	413.55	57.75	438.40	47.00
contra_AUDv4	392.55	52.64	415.80	42.78
contra_AUDv5	368.75	51.08	393.00	44.48
contra_AUDv6a	348.40	46.99	378.55	34.40
contra_AUDv6b	219.50	53.45	240.50	52.53
contra_BLAa	398.20	47.36	428.20	40.63
contra_BLAp	420.75	51.85	441.90	55.36
contra_BLAv	328.95	74.49	383.56	55.23
contra_BMAp	291.75	58.64	346.44	61.59
contra_CA1slm	370.95	40.84	395.75	68.88
contra_CA1so	526.10	39.72	552.40	50.17
contra_CA1sp	182.70	24.75	191.00	36.63
contra_CA1sr	578.75	47.55	597.15	54.13
contra_CA2slm	512.15	37.46	532.40	37.50
contra_CA2so	488.00	33.31	498.50	17.94
contra_CA2sp	103.80	23.27	115.45	34.27
contra_CA2sr	454.50	34.39	468.50	19.07
contra_CA3slm	529.45	41.92	554.45	47.94
contra_CA3slu	186.35	32.87	207.25	36.50
contra_CA3so	434.35	37.87	455.60	36.30
contra_CA3sp	91.35	19.39	118.20	22.10
contra_CA3sr	520.70	46.61	541.10	37.48

contra_CC	14.30	6.38	25.20	10.03
contra_cing	67.70	13.03	83.80	23.26
contra_COApl	291.35	64.05	358.83	84.38
contra_COApl1	317.56	74.73	365.72	60.48
contra_COApl2	293.65	70.96	370.28	86.83
contra_COApl3	281.95	58.61	351.17	90.80
contra_cortex	347.20	39.34	365.70	38.18
contra_CP	302.65	49.48	325.90	42.45
contra_cpd	23.35	15.44	38.00	20.14
contra_DG	657.15	33.86	670.50	42.26
contra_DGinf	650.40	39.06	666.85	39.51
contra_DGpo	181.40	17.91	201.00	14.51
contra_DGsg	119.55	14.83	137.90	30.39
contra_DGsup	663.05	31.27	673.45	43.93
contra_ECT	409.50	57.26	426.35	40.76
contra_ECT1	461.60	78.45	472.85	47.18
contra_ECT3	427.35	62.47	438.65	49.67
contra_ECT5	394.85	55.27	414.35	36.94
contra_ECT6a	365.80	46.15	397.00	39.17
contra_ECT6b	238.39	41.23	258.95	58.67
contra_ENTl	428.45	53.18	439.00	37.06
contra_ENTl1	508.65	77.27	491.95	58.72
contra_ENTl3	452.95	47.03	455.75	39.25
contra_ENTl5	413.25	55.19	430.20	33.05
contra_ENTl6a	379.45	67.63	397.45	53.73
contra_ENTl6b	292.85	54.36	299.45	51.86
contra_FC	313.70	32.69	323.15	37.90
contra_hip	495.90	39.49	515.05	39.48
contra_hyp	108.40	19.69	121.40	17.27
contra_LA	388.60	58.33	415.45	45.01
contra_lay1	415.45	47.80	434.60	37.17
contra_lay2	237.95	29.99	250.50	41.94
contra_lay3	369.30	44.82	388.10	42.49
contra_lay4	355.25	42.66	371.80	41.95
contra_lay5	321.80	37.17	341.50	38.91
contra_lay6a	318.95	33.96	338.70	38.88
contra_lay6b	209.45	29.25	231.05	28.25

contra_MOp	350.10	47.73	361.10	52.05
contra_MOp1	427.75	66.61	435.95	67.32
contra_MOp3	373.70	56.75	389.05	63.83
contra_MOp5	336.65	44.04	347.55	54.93
contra_MOp6a	313.55	35.29	318.30	44.49
contra_MOp6b	210.25	42.36	236.35	42.21
contra_MOs	285.10	47.36	292.35	48.86
contra_MOs1	381.95	56.67	400.90	63.66
contra_MOs3	304.10	49.98	321.30	58.97
contra_MOs5	258.15	41.49	257.55	44.90
contra_MOs6a	248.85	35.07	249.75	41.49
contra_MOs6b	199.75	33.96	188.85	37.09
contra_PAA	335.40	74.60	383.00	68.04
contra_PAA1	340.60	74.11	376.00	82.76
contra_PAA2	340.90	88.63	393.22	67.46
contra_PAA3	330.45	69.70	377.17	66.22
contra_PERI	422.80	54.31	429.65	37.49
contra_PERI1	476.80	81.60	463.00	50.65
contra_PERI3	436.85	55.54	434.75	44.34
contra_PERI5	413.40	48.68	418.65	41.09
contra_PERI6a	381.10	58.64	410.60	39.34
contra_PERI6b	225.90	37.88	287.80	56.60
contra_PIR	411.85	51.45	434.60	44.41
contra_PIR1	463.60	60.07	480.90	52.59
contra_PIR2	389.25	48.66	400.80	45.94
contra_PIR3	398.60	51.31	426.30	45.32
contra_RSPd	255.80	37.37	272.90	48.11
contra_RSPd1	353.80	52.91	371.65	66.69
contra_RSPd3	276.30	40.76	301.70	56.55
contra_RSPd5	213.50	34.39	225.80	43.93
contra_RSPd6a	225.65	30.57	237.35	40.26
contra_RSPd6b	185.70	42.44	197.15	40.47
contra_RSPv	253.35	29.01	264.50	38.92
contra_RSPv1	292.10	31.92	299.35	49.33
contra_RSPv2	238.00	29.67	250.90	42.53
contra_RSPv3	275.70	28.46	287.30	37.82
contra_RSPv5	223.80	30.85	243.70	43.76

contra_RSPv6a	209.50	28.31	220.15	35.44
contra_RSPv6b	176.95	53.65	201.05	48.13
contra_SSp-bfd	334.10	40.72	345.95	44.61
contra_SSp-bfd1	427.65	58.14	427.15	49.76
contra_SSp-bfd3	352.80	47.67	365.60	48.02
contra_SSp-bfd4	343.80	44.23	355.00	43.42
contra_SSp-bfd5	303.85	35.14	317.20	43.46
contra_SSp-bfd6a	316.45	35.69	328.80	43.09
contra_SSp-bfd6b	203.50	37.53	217.05	38.65
contra_SSP-tr	343.15	41.68	357.80	47.58
contra_SSp-tr1	429.20	59.54	441.55	46.47
contra_SSp-tr3	371.80	47.42	389.45	53.81
contra_SSp-tr4	339.60	41.65	355.90	52.71
contra_SSp-tr5	309.85	38.01	329.25	45.36
contra_SSp-tr6a	311.45	34.89	325.90	42.38
contra_SSp-tr6b	193.70	31.22	224.50	29.20
contra_TEa	401.00	55.91	418.95	44.63
contra_TEa1	453.20	80.18	480.20	62.80
contra_TEa3	426.15	65.89	437.45	53.30
contra_TEa4	411.35	58.93	430.70	53.06
contra_TEa5	390.15	57.62	408.20	46.75
contra_TEa6a	354.20	48.82	386.20	39.91
contra_TEa6b	235.05	46.86	265.45	45.11
contra_th	289.45	17.95	295.20	7.28
ips_amgmed	230.50	35.78	240.30	37.11
ips_AUDd	354.30	49.96	376.45	46.41
ips_AUDd1	408.50	66.72	446.10	57.20
ips_AUDd3	367.40	53.08	403.05	49.65
ips_AUDd4	364.35	46.41	378.20	48.27
ips_AUDd5	331.85	47.25	344.60	40.69
ips_AUDd6a	338.25	49.68	343.95	44.08
ips_AUDd6b	217.65	49.66	239.85	33.59
ips_AUDp	368.40	53.15	381.25	47.28
ips_AUDp1	432.45	64.54	443.45	61.22

ips_AUDp3	386.70	55.92	409.05	54.47
ips_AUDp4	375.40	52.02	389.35	52.40
ips_AUDp5	341.35	53.86	358.35	50.15
ips_AUDp6a	337.20	53.69	346.15	39.56
ips_AUDp6b	192.45	49.72	217.45	23.07
ips_AUDv	377.10	62.08	391.45	47.48
ips_AUDv1	433.60	85.14	449.90	54.59
ips_AUDv3	396.85	67.56	414.40	52.22
ips_AUDv4	380.05	50.76	396.05	49.11
ips_AUDv5	363.20	58.55	374.60	54.53
ips_AUDv6a	329.75	50.83	345.15	38.69
ips_AUDv6b	208.65	37.73	224.90	31.58
ips_BLAa	405.60	44.39	409.55	36.46
ips_BLAp	420.30	48.31	434.25	40.55
ips_BLAv	324.55	67.90	355.75	54.14
ips_BMAp	288.35	59.98	321.45	47.03
ips_CA1slm	367.55	46.09	384.65	75.87
ips_CA1so	537.20	53.30	548.05	45.64
ips_CA1sp	179.80	25.10	180.20	45.03
ips_CA1sr	585.30	51.71	592.70	53.75
ips_CA2slm	524.85	40.34	526.80	31.14
ips_CA2so	507.25	32.74	502.65	17.18
ips_CA2sp	112.35	29.47	104.45	21.60
ips_CA2sr	462.65	29.26	468.25	22.24
ips_CA3slm	531.85	48.34	548.25	39.51
ips_CA3slu	185.75	34.12	200.65	36.81
ips_CA3so	440.00	44.46	456.30	26.57
ips_CA3sp	92.10	19.83	103.70	25.84
ips_CA3sr	512.95	40.35	534.90	40.99
ips_CC	14.20	6.16	20.70	11.36
ips_cing	69.65	17.14	71.55	26.13
ips_COApl	289.20	57.91	319.55	65.14
ips_COApl1	303.35	53.23	329.95	63.30
ips_COApl2	288.40	55.17	325.60	72.02
ips_COApl3	280.60	60.09	315.40	63.62
ips_cortex	336.30	44.38	354.50	42.18
ips_CP	285.00	48.91	305.55	49.82

ips_cpd	20.10	17.37	30.60	18.08
ips_DG	658.85	36.55	663.90	35.86
ips_DGinf	646.70	39.38	657.85	30.51
ips_DGpo	179.50	17.48	196.80	15.68
ips_DGsg	117.15	18.32	128.00	27.69
ips_DGsup	667.35	34.88	668.55	40.26
ips_ECT	391.20	47.76	416.85	42.25
ips_ECT1	419.00	57.24	472.75	45.82
ips_ECT3	398.80	50.21	424.05	44.88
ips_ECT5	386.75	42.87	407.20	44.08
ips_ECT6a	352.10	49.92	381.10	44.58
ips_ECT6b	246.95	49.76	250.60	42.60
ips_ENTl	410.30	45.71	417.05	29.64
ips_ENTl1	452.50	63.21	473.95	37.15
ips_ENTl3	422.70	50.79	424.35	30.05
ips_ENTl5	406.50	41.30	413.60	27.40
ips_ENTl6a	357.70	50.10	383.55	38.93
ips_ENTl6b	253.10	69.87	280.00	36.73
ips_FC	300.55	43.13	307.10	50.04
ips_hip	502.60	42.22	511.30	36.30
ips_hyp	107.50	20.13	118.90	16.96
ips_LA	378.25	43.86	396.15	55.09
ips_lay1	401.35	49.21	428.50	36.69
ips_lay2	230.00	29.79	242.60	41.24
ips_lay3	352.60	48.87	377.50	43.45
ips_lay4	347.80	48.57	363.20	48.53
ips_lay5	316.80	42.40	331.50	40.01
ips_lay6a	308.55	37.44	321.60	42.41
ips_lay6b	207.10	26.98	215.40	29.73
ips_MOp	339.85	44.79	335.50	39.18
ips_MOp1	407.75	59.57	413.05	48.26
ips_MOp3	354.45	47.23	352.85	42.19
ips_MOp5	332.85	45.41	326.80	38.49
ips_MOp6a	307.75	40.48	294.20	43.63
ips_MOp6b	207.35	36.64	192.35	43.01
ips_MOs	276.95	45.45	270.60	41.92
ips_MOs1	371.65	64.08	365.60	49.57

ips_MOs3	302.35	54.58	303.80	49.26
ips_MOs5	253.25	37.81	246.25	39.96
ips_MOs6a	243.00	41.73	229.70	42.57
ips_MOs6b	202.65	31.56	186.10	48.64
ips_PAA	325.20	68.50	344.35	56.87
ips_PAA1	329.25	74.73	351.20	73.20
ips_PAA2	329.65	69.61	345.90	49.41
ips_PAA3	316.25	66.66	340.80	52.21
ips_PERI	399.95	47.14	427.45	39.30
ips_PERI1	427.40	68.85	486.00	66.28
ips_PERI3	411.80	49.13	437.30	46.48
ips_PERI5	398.65	41.26	416.90	35.20
ips_PERI6a	362.35	42.80	384.35	37.05
ips_PERI6b	235.05	52.08	256.25	48.93
ips_PIR	383.00	38.65	408.30	30.44
ips_PIR1	429.10	41.44	456.55	40.86
ips_PIR2	356.00	37.16	370.00	33.60
ips_PIR3	376.20	39.88	401.40	29.74
ips_RSPd	251.55	36.59	265.90	48.10
ips_RSPd1	347.95	45.41	364.70	52.01
ips_RSPd3	275.05	40.32	293.30	50.42
ips_RSPd5	211.25	32.76	226.25	42.93
ips_RSPd6a	223.85	32.10	226.05	42.37
ips_RSPd6b	193.00	37.98	200.30	46.29
ips_RSPv	247.55	29.93	256.75	38.89
ips_RSPv1	287.25	29.14	288.95	36.89
ips_RSPv2	230.15	29.68	242.75	41.42
ips_RSPv3	271.75	32.03	283.80	43.17
ips_RSPv5	221.30	37.78	234.60	41.56
ips_RSPv6a	204.15	28.86	210.95	42.44
ips_RSPv6b	195.00	37.38	197.70	60.62
ips_SSp-bfd	331.70	50.48	352.55	46.51
ips_SSp-bfd1	398.25	52.80	440.95	48.23
ips_SSp-bfd3	343.60	55.70	378.55	49.79
ips_SSp-bfd4	344.30	50.86	358.35	53.62
ips_SSp-bfd5	307.70	49.53	324.80	41.46
ips_SSp-bfd6a	315.75	44.78	327.90	44.00

ips_SSp-bfd6b	208.95	28.68	233.55	35.88
ips_SSp-tr	324.70	41.68	344.90	44.70
ips_SSp-tr1	407.45	45.15	436.35	28.88
ips_SSp-tr3	342.90	49.38	369.00	47.42
ips_SSp-tr4	327.55	46.86	345.25	47.87
ips_SSp-tr5	302.25	39.04	320.20	42.50
ips_SSp-tr6a	300.70	37.72	311.30	42.67
ips_SSp-tr6b	188.15	35.30	185.05	49.30
ips_TEa	384.20	60.17	400.95	42.84
ips_TEa1	427.20	79.35	461.25	40.87
ips_TEa3	400.35	67.83	420.65	49.43
ips_TEa4	382.85	53.31	406.90	44.90
ips_TEa5	376.35	56.74	390.10	44.72
ips_TEa6a	336.95	48.60	358.65	41.76
ips_TEa6b	228.90	29.37	235.15	32.41
ips_th	287.70	19.15	289.60	7.66

Table 5: SAP102 puncta size at 28 days

	Injury		**Sham**	
region	**Average**	**SD**	**Average**	**SD**
contra_amgmed	14.67	0.22	14.64	0.19
contra_AUDd	14.40	0.24	14.45	0.34
contra_AUDd1	14.22	0.33	13.99	0.37
contra_AUDd3	14.76	0.24	14.81	0.45
contra_AUDd4	13.92	0.29	13.99	0.31
contra_AUDd5	14.24	0.26	14.30	0.33
contra_AUDd6a	14.22	0.22	14.38	0.31
contra_AUDd6b	14.32	0.27	14.60	0.37
contra_AUDp	14.34	0.25	14.36	0.32
contra_AUDp1	14.12	0.40	13.96	0.40
contra_AUDp3	14.71	0.25	14.72	0.39
contra_AUDp4	13.96	0.34	14.06	0.28
contra_AUDp5	14.17	0.26	14.15	0.32
contra_AUDp6a	14.19	0.22	14.28	0.23
contra_AUDp6b	14.30	0.24	14.33	0.25
contra_AUDv	14.22	0.30	14.26	0.35
contra_AUDv1	14.05	0.45	13.98	0.43

contra_AUDv3	14.50	0.34	14.60	0.40
contra_AUDv4	13.86	0.36	13.90	0.32
contra_AUDv5	14.08	0.32	14.04	0.43
contra_AUDv6a	14.20	0.18	14.18	0.23
contra_AUDv6b	14.23	0.24	14.35	0.19
contra_BLAa	13.79	0.49	13.67	0.31
contra_BLAp	13.80	0.47	13.67	0.26
contra_BLAv	13.96	0.36	13.78	0.32
contra_BMAp	14.11	0.36	14.09	0.39
contra_CA1slm	14.47	0.25	14.58	0.48
contra_CA1so	13.22	0.25	13.28	0.43
contra_CA1sp	15.83	0.63	16.54	0.56
contra_CA1sr	13.62	0.23	13.77	0.48
contra_CA2slm	13.00	0.23	12.98	0.53
contra_CA2so	12.94	0.20	12.92	0.24
contra_CA2sp	18.27	1.38	18.61	1.25
contra_CA2sr	13.30	0.20	13.39	0.38
contra_CA3slm	13.24	0.25	13.19	0.58
contra_CA3slu	19.83	0.71	19.74	0.86
contra_CA3so	13.31	0.29	13.20	0.52
contra_CA3sp	20.41	0.98	19.95	0.65
contra_CA3sr	13.53	0.30	13.46	0.53
contra_CC	15.62	0.92	16.25	0.91
contra_cing	14.89	0.63	15.31	0.55
contra_COApl	14.33	0.28	14.12	0.51
contra_COApl1	13.92	0.43	13.71	0.50
contra_COApl2	14.47	0.30	14.17	0.60
contra_COApl3	14.42	0.30	14.32	0.55
contra_cortex	14.28	0.17	14.40	0.28
contra_CP	14.24	0.26	14.30	0.29
contra_cpd	16.88	1.28	17.64	1.28
contra_DG	13.69	0.27	13.83	0.56
contra_DGinf	13.80	0.26	13.79	0.54
contra_DGpo	17.69	0.44	17.65	0.58
contra_DGsg	20.38	0.80	20.45	0.59
contra_DGsup	13.62	0.26	13.88	0.61
contra_ECT	14.05	0.40	14.04	0.34

contra_ECT1	13.93	0.51	13.85	0.45
contra_ECT3	14.12	0.42	14.19	0.37
contra_ECT5	13.92	0.42	13.92	0.32
contra_ECT6a	14.11	0.37	13.97	0.28
contra_ECT6b	14.19	0.33	14.26	0.25
contra_ENTl	13.78	0.33	13.73	0.33
contra_ENTl1	13.52	0.47	13.55	0.48
contra_ENTl3	13.84	0.35	13.80	0.33
contra_ENTl5	13.78	0.33	13.64	0.31
contra_ENTl6a	13.76	0.37	13.79	0.37
contra_ENTl6b	14.05	0.39	14.13	0.37
contra_FC	13.56	0.28	13.59	0.35
contra_hip	13.76	0.19	13.86	0.47
contra_hyp	15.73	0.42	15.98	0.38
contra_LA	13.83	0.41	13.72	0.33
contra_lay1	14.06	0.22	14.04	0.35
contra_lay2	14.87	0.39	15.09	0.28
contra_lay3	14.58	0.17	14.71	0.34
contra_lay4	13.96	0.23	14.11	0.27
contra_lay5	14.15	0.19	14.26	0.26
contra_lay6a	14.16	0.18	14.30	0.26
contra_lay6b	14.24	0.23	14.42	0.20
contra_MOp	14.05	0.26	14.28	0.34
contra_MOp1	13.85	0.35	13.95	0.43
contra_MOp3	14.27	0.29	14.48	0.40
contra_MOp5	13.90	0.23	14.13	0.31
contra_MOp6a	13.94	0.25	14.27	0.31
contra_MOp6b	14.19	0.31	14.41	0.27
contra_MOs	14.41	0.27	14.68	0.21
contra_MOs1	14.27	0.25	14.39	0.33
contra_MOs3	14.65	0.30	14.85	0.25
contra_MOs5	14.26	0.30	14.60	0.20
contra_MOs6a	14.22	0.33	14.64	0.32
contra_MOs6b	14.26	0.32	14.55	0.35
contra_PAA	13.99	0.38	13.87	0.41
contra_PAA1	13.63	0.50	13.53	0.44
contra_PAA2	14.19	0.40	13.98	0.38

contra_PAA3	14.12	0.36	14.01	0.43
contra_PERI	13.87	0.41	13.89	0.34
contra_PERI1	13.78	0.56	13.80	0.48
contra_PERI3	13.93	0.43	14.02	0.35
contra_PERI5	13.79	0.38	13.81	0.34
contra_PERI6a	13.84	0.37	13.77	0.28
contra_PERI6b	14.10	0.28	14.12	0.27
contra_PIR	13.77	0.35	13.66	0.26
contra_PIR1	13.36	0.56	13.19	0.35
contra_PIR2	14.33	0.24	14.31	0.28
contra_PIR3	13.77	0.33	13.68	0.25
contra_RSPd	14.59	0.31	14.76	0.19
contra_RSPd1	14.41	0.25	14.52	0.30
contra_RSPd3	14.70	0.32	14.78	0.22
contra_RSPd5	14.67	0.39	14.96	0.27
contra_RSPd6a	14.43	0.36	14.73	0.33
contra_RSPd6b	14.42	0.43	14.67	0.46
contra_RSPv	14.52	0.30	14.74	0.17
contra_RSPv1	14.51	0.25	14.65	0.24
contra_RSPv2	14.86	0.38	15.09	0.28
contra_RSPv3	14.17	0.27	14.35	0.19
contra_RSPv5	14.64	0.38	14.78	0.21
contra_RSPv6a	14.63	0.44	14.89	0.28
contra_RSPv6b	14.51	0.72	14.64	0.44
contra_SSp-bfd	14.44	0.22	14.66	0.35
contra_SSp-bfd1	14.07	0.34	14.08	0.36
contra_SSp-bfd3	14.80	0.23	15.03	0.42
contra_SSp-bfd4	13.96	0.18	14.19	0.25
contra_SSp-bfd5	14.32	0.22	14.54	0.32
contra_SSp-bfd6a	14.25	0.23	14.48	0.33
contra_SSp-bfd6b	14.36	0.26	14.60	0.30
contra_SSP-tr	14.23	0.20	14.41	0.30
contra_SSp-tr1	13.94	0.23	13.94	0.45
contra_SSp-tr3	14.60	0.26	14.77	0.37
contra_SSp-tr4	14.01	0.25	14.26	0.30

contra_SSp-tr5	14.05	0.23	14.23	0.24
contra_SSp-tr6a	14.08	0.21	14.32	0.29
contra_SSp-tr6b	14.27	0.29	14.45	0.27
contra_TEa	14.13	0.37	14.12	0.32
contra_TEa1	13.87	0.49	13.93	0.47
contra_TEa3	14.36	0.42	14.49	0.35
contra_TEa4	13.85	0.44	13.82	0.34
contra_TEa5	13.99	0.36	13.94	0.39
contra_TEa6a	14.24	0.28	14.07	0.28
contra_TEa6b	14.18	0.25	14.19	0.17
contra_th	13.14	0.20	13.19	0.23
ips_amgmed	14.59	0.18	14.79	0.17
ips_AUDd	14.28	0.23	14.35	0.24
ips_AUDd1	14.02	0.38	13.98	0.29
ips_AUDd3	14.57	0.31	14.62	0.30
ips_AUDd4	13.82	0.19	13.98	0.24
ips_AUDd5	14.18	0.23	14.28	0.25
ips_AUDd6a	14.12	0.23	14.28	0.25
ips_AUDd6b	14.32	0.29	14.41	0.17
ips_AUDp	14.23	0.24	14.27	0.25
ips_AUDp1	14.01	0.24	13.96	0.35
ips_AUDp3	14.46	0.26	14.49	0.34
ips_AUDp4	13.87	0.20	13.96	0.25
ips_AUDp5	14.17	0.26	14.24	0.23
ips_AUDp6a	14.11	0.24	14.22	0.27
ips_AUDp6b	14.42	0.45	14.40	0.12
ips_AUDv	14.16	0.24	14.20	0.30
ips_AUDv1	14.02	0.37	13.88	0.37
ips_AUDv3	14.36	0.31	14.38	0.38
ips_AUDv4	13.93	0.24	13.95	0.22
ips_AUDv5	14.07	0.26	14.21	0.36
ips_AUDv6a	14.15	0.27	14.23	0.23
ips_AUDv6b	14.28	0.43	14.41	0.18
ips_BLAa	13.71	0.26	13.77	0.29
ips_BLAp	13.81	0.25	13.78	0.29
ips_BLAv	14.01	0.25	13.93	0.25

ips_BMAp	14.19	0.26	14.06	0.33
ips_CA1slm	14.47	0.28	14.47	0.44
ips_CA1so	13.21	0.28	13.26	0.34
ips_CA1sp	15.86	0.61	16.48	0.75
ips_CA1sr	13.59	0.30	13.66	0.45
ips_CA2slm	12.98	0.20	13.00	0.26
ips_CA2so	12.84	0.14	12.90	0.13
ips_CA2sp	17.43	0.58	18.66	0.90
ips_CA2sr	13.22	0.18	13.33	0.20
ips_CA3slm	13.25	0.26	13.24	0.40
ips_CA3slu	19.62	0.63	19.63	0.73
ips_CA3so	13.25	0.20	13.23	0.30
ips_CA3sp	20.18	0.66	20.24	0.69
ips_CA3sr	13.48	0.20	13.50	0.32
ips_CC	15.70	0.98	16.05	0.89
ips_cing	14.83	0.59	15.37	0.53
ips_COApl	14.33	0.25	14.21	0.35
ips_COApl1	13.89	0.30	13.86	0.30
ips_COApl2	14.54	0.25	14.33	0.45
ips_COApl3	14.49	0.29	14.33	0.36
ips_cortex	14.26	0.24	14.33	0.17
ips_CP	14.17	0.24	14.20	0.24
ips_cpd	16.56	1.48	17.50	1.38
ips_DG	13.72	0.36	13.72	0.53
ips_DGinf	13.81	0.35	13.73	0.52
ips_DGpo	17.64	0.43	17.63	0.46
ips_DGsg	20.61	0.86	20.35	0.77
ips_DGsup	13.66	0.37	13.73	0.58
ips_ECT	14.03	0.25	13.99	0.26
ips_ECT1	13.99	0.35	13.70	0.30
ips_ECT3	14.10	0.23	14.09	0.30
ips_ECT5	13.91	0.28	13.89	0.27
ips_ECT6a	14.01	0.28	14.02	0.28
ips_ECT6b	14.18	0.47	14.30	0.21
ips_ENTl	13.80	0.21	13.79	0.22
ips_ENTl1	13.61	0.27	13.46	0.34
ips_ENTl3	13.87	0.22	13.89	0.26

ips_ENTl5	13.77	0.26	13.72	0.18
ips_ENTl6a	13.80	0.26	13.86	0.26
ips_ENTl6b	13.99	0.27	14.11	0.28
ips_FC	13.68	0.30	13.58	0.31
ips_hip	13.75	0.28	13.78	0.41
ips_hyp	15.71	0.43	15.97	0.37
ips_LA	13.83	0.22	13.85	0.31
ips_lay1	14.08	0.26	14.03	0.20
ips_lay2	14.98	0.44	15.19	0.32
ips_lay3	14.51	0.28	14.57	0.23
ips_lay4	13.92	0.20	14.03	0.17
ips_lay5	14.12	0.23	14.22	0.16
ips_lay6a	14.11	0.24	14.25	0.17
ips_lay6b	14.24	0.33	14.41	0.14
ips_MOp	14.13	0.33	14.30	0.22
ips_MOp1	14.08	0.43	14.11	0.25
ips_MOp3	14.38	0.35	14.57	0.33
ips_MOp5	13.93	0.29	14.10	0.22
ips_MOp6a	13.95	0.30	14.18	0.19
ips_MOp6b	14.16	0.36	14.45	0.29
ips_MOs	14.49	0.38	14.66	0.22
ips_MOs1	14.50	0.37	14.46	0.28
ips_MOs3	14.71	0.38	14.80	0.24
ips_MOs5	14.31	0.39	14.64	0.24
ips_MOs6a	14.27	0.39	14.59	0.26
ips_MOs6b	14.24	0.38	14.72	0.27
ips_PAA	14.12	0.25	14.09	0.28
ips_PAA1	13.69	0.34	13.65	0.35
ips_PAA2	14.37	0.25	14.32	0.24
ips_PAA3	14.29	0.23	14.23	0.29
ips_PERI	13.89	0.27	13.86	0.25
ips_PERI1	13.83	0.40	13.58	0.40
ips_PERI3	13.95	0.25	13.97	0.34
ips_PERI5	13.83	0.28	13.80	0.19
ips_PERI6a	13.85	0.26	13.83	0.16
ips_PERI6b	14.10	0.35	14.22	0.22
ips_PIR	13.88	0.18	13.80	0.22

ips_PIR1	13.46	0.23	13.33	0.29
ips_PIR2	14.36	0.30	14.42	0.28
ips_PIR3	13.89	0.18	13.82	0.19
ips_RSPd	14.61	0.33	14.72	0.17
ips_RSPd1	14.42	0.27	14.39	0.26
ips_RSPd3	14.71	0.32	14.80	0.21
ips_RSPd5	14.70	0.35	14.84	0.23
ips_RSPd6a	14.48	0.42	14.70	0.34
ips_RSPd6b	14.35	0.45	14.71	0.25
ips_RSPv	14.58	0.33	14.75	0.22
ips_RSPv1	14.52	0.27	14.66	0.25
ips_RSPv2	14.97	0.44	15.18	0.32
ips_RSPv3	14.24	0.30	14.34	0.22
ips_RSPv5	14.65	0.47	14.86	0.29
ips_RSPv6a	14.67	0.36	14.89	0.29
ips_RSPv6b	14.35	0.34	14.76	0.49
ips_SSp-bfd	14.34	0.27	14.43	0.23
ips_SSp-bfd1	14.05	0.30	13.97	0.29
ips_SSp-bfd3	14.64	0.32	14.72	0.33
ips_SSp-bfd4	13.90	0.22	14.06	0.27
ips_SSp-bfd5	14.28	0.30	14.37	0.24
ips_SSp-bfd6a	14.17	0.25	14.33	0.22
ips_SSp-bfd6b	14.31	0.34	14.35	0.17
ips_SSp-tr	14.27	0.27	14.35	0.17
ips_SSp-tr1	14.05	0.28	14.04	0.17
ips_SSp-tr3	14.66	0.30	14.70	0.27
ips_SSp-tr4	13.98	0.24	14.10	0.18
ips_SSp-tr5	14.05	0.25	14.15	0.17
ips_SSp-tr6a	14.06	0.24	14.21	0.16
ips_SSp-tr6b	14.23	0.37	14.48	0.26
ips_TEa	14.13	0.30	14.11	0.28
ips_TEa1	14.01	0.51	13.82	0.25
ips_TEa3	14.35	0.39	14.27	0.36
ips_TEa4	13.90	0.21	13.90	0.20
ips_TEa5	14.02	0.30	14.08	0.39
ips_TEa6a	14.13	0.28	14.16	0.25
ips_TEa6b	14.21	0.44	14.41	0.23

ips_th	13.14	0.21	13.19	0.17

Table 6: SAP102 puncta intensity at 28 days

	Injury		Sham	
region	Average	SD	Average	SD
contra_amgmed	11801.18	2257.54	13485.10	2669.58
contra_AUDd	12048.69	1863.23	13139.68	1838.90
contra_AUDd1	11571.48	1942.98	12780.61	1940.43
contra_AUDd3	12208.38	1941.69	13444.63	2002.76
contra_AUDd4	12193.08	1883.42	13275.66	1952.62
contra_AUDd5	11981.11	1851.47	13021.45	1816.29
contra_AUDd6a	12194.67	1822.28	12945.07	1737.57
contra_AUDd6b	10595.57	1767.22	11235.07	1256.96
contra_AUDp	12273.37	1926.37	13509.97	1970.32
contra_AUDp1	11875.85	1953.48	13282.52	2008.52
contra_AUDp3	12592.44	2045.97	13969.25	1993.31
contra_AUDp4	12263.06	1868.48	13512.51	1987.54
contra_AUDp5	12164.10	1879.12	13393.65	1997.07
contra_AUDp6a	12318.67	1892.90	13283.63	1939.00
contra_AUDp6b	10548.58	1926.23	11618.98	1787.86
contra_AUDv	12550.00	2061.49	13586.85	2065.30
contra_AUDv1	12186.53	2240.57	13272.68	2126.02
contra_AUDv3	12931.46	2149.98	13912.81	2128.29
contra_AUDv4	12590.68	2097.26	13601.77	2139.67
contra_AUDv5	12466.74	1974.51	13607.02	2095.73
contra_AUDv6a	12444.42	2042.21	13560.46	2150.35
contra_AUDv6b	10711.03	2002.56	11749.72	1929.43
contra_BLAa	14109.76	2680.33	16003.06	3287.81
contra_BLAp	14578.82	2971.45	16231.93	3524.91
contra_BLAv	13219.45	3240.98	15655.88	2955.31
contra_BMAp	12893.13	2900.65	15390.03	3043.74
contra_CA1slm	12730.88	1169.10	13302.22	1959.62
contra_CA1so	13495.87	1351.44	14141.64	1665.69
contra_CA1sp	12481.69	1136.63	12945.69	1398.68
contra_CA1sr	14648.48	1291.15	15164.49	1880.02
contra_CA2slm	13934.32	1381.78	14895.93	2036.75
contra_CA2so	16154.28	1815.46	17012.05	2368.54

contra_CA2sp	12944.95	1074.70	13227.39	1332.66
contra_CA2sr	14690.13	1395.76	15789.29	2171.88
contra_CA3slm	13080.54	1170.32	13958.23	1723.87
contra_CA3slu	11262.71	963.96	11697.16	1485.46
contra_CA3so	11569.16	933.21	12137.33	1490.97
contra_CA3sp	10917.84	860.27	11294.25	1243.67
contra_CA3sr	12939.43	1194.12	13805.41	1641.87
contra_CC	6912.07	404.47	7000.87	415.10
contra_cing	8519.63	741.17	8817.68	1079.04
contra_COApl	12719.00	3187.48	15533.27	3009.57
contra_COApl1	12674.08	3286.75	14320.49	2422.22
contra_COApl2	13070.30	3352.36	15731.78	2702.90
contra_COApl3	12682.05	3068.16	15743.94	3252.84
contra_cortex	11893.44	1715.45	12774.65	1686.07
contra_CP	11123.12	1705.92	12092.41	1798.49
contra_cpd	6829.18	487.70	7005.13	641.45
contra_DG	18991.84	1650.39	19624.50	2708.69
contra_DGinf	18815.93	1699.37	19490.36	2787.93
contra_DGpo	12119.83	846.32	12691.91	1554.26
contra_DGsg	13947.38	813.64	14374.01	1579.07
contra_DGsup	19133.62	1650.92	19740.49	2668.46
contra_ECT	13204.16	2354.14	13951.64	2553.91
contra_ECT1	13041.76	2661.29	13609.24	3277.31
contra_ECT3	13462.74	2572.72	14104.22	2630.45
contra_ECT5	13169.36	2256.95	14177.02	2504.32
contra_ECT6a	13022.13	2128.10	14017.62	2450.78
contra_ECT6b	11718.68	1403.63	12438.72	2150.66
contra_ENTl	14286.94	2958.19	15212.32	2840.44
contra_ENTl1	13983.60	3407.47	14304.06	3052.19
contra_ENTl3	14984.82	3404.94	15804.32	2969.39
contra_ENTl5	14311.37	2770.76	15645.72	2990.55
contra_ENTl6a	13303.07	2458.04	14424.82	2711.07
contra_ENTl6b	12214.28	2157.80	13077.82	2235.09
contra_FC	14352.91	1653.18	16141.66	3122.24
contra_hip	13830.61	1249.07	14489.97	1775.01
contra_hyp	10324.96	1638.56	11347.02	1966.93
contra_LA	13219.39	2511.07	14511.01	2835.91

contra_lay1	11865.62	1745.48	12532.86	1639.87
contra_lay2	11926.28	1552.70	12492.31	1949.82
contra_lay3	12106.49	1846.93	12986.02	1691.89
contra_lay4	12078.14	1798.31	12991.34	1758.48
contra_lay5	11811.84	1654.91	12805.59	1736.80
contra_lay6a	11833.61	1618.49	12716.20	1726.87
contra_lay6b	10483.50	1413.79	11291.39	1398.20
contra_MOp	11918.78	1813.32	12582.82	1991.61
contra_MOp1	12112.60	2168.21	12758.39	2392.49
contra_MOp3	12397.35	2071.13	13105.56	2201.82
contra_MOp5	11718.93	1636.56	12495.51	1908.25
contra_MOp6a	11613.53	1466.37	12215.42	1739.72
contra_MOp6b	10449.49	1185.84	11106.18	1632.44
contra_MOs	11313.53	1670.18	12071.73	1912.87
contra_MOs1	11804.73	1926.05	12681.76	2329.26
contra_MOs3	11620.45	1873.14	12574.95	2086.47
contra_MOs5	11044.39	1512.48	11709.81	1723.39
contra_MOs6a	10778.00	1285.99	11200.61	1595.36
contra_MOs6b	10019.32	1051.48	10340.80	1611.52
contra_PAA	12999.16	3567.72	15718.27	3221.14
contra_PAA1	12035.65	3398.77	14303.40	2937.71
contra_PAA2	13438.16	3934.99	16246.73	3480.68
contra_PAA3	13167.31	3474.70	15958.16	3308.40
contra_PERI	13559.74	2625.08	14072.07	2599.02
contra_PERI1	13164.92	2903.60	13102.94	2789.49
contra_PERI3	13908.18	2960.91	14218.83	2701.82
contra_PERI5	13735.53	2514.70	14352.81	2714.69
contra_PERI6a	13175.26	2206.63	14320.21	2546.16
contra_PERI6b	11606.66	1843.10	13009.83	2400.54
contra_PIR	14042.40	3277.43	15769.44	3418.41
contra_PIR1	13568.71	3423.83	15220.54	3406.49
contra_PIR2	14799.11	3667.69	16586.33	3611.29
contra_PIR3	13841.96	3069.38	15595.95	3407.50
contra_RSPd	11355.82	1585.93	12164.84	1836.48
contra_RSPd1	11998.30	1961.93	12607.33	2117.86
contra_RSPd3	11660.30	1723.27	12549.22	1982.71
contra_RSPd5	11000.78	1474.82	11809.88	1763.16

contra_RSPd6a	10821.35	1294.17	11560.84	1679.80
contra_RSPd6b	9896.74	1151.05	10546.04	1549.79
contra_RSPv	11607.72	1450.06	12185.89	1859.91
contra_RSPv1	12096.85	1651.38	12443.28	2022.02
contra_RSPv2	11936.47	1570.72	12482.73	1943.63
contra_RSPv3	11704.29	1424.65	12338.62	1825.88
contra_RSPv5	11148.74	1339.23	11862.18	1715.51
contra_RSPv6a	10792.93	1186.03	11495.24	1744.99
contra_RSPv6b	10002.12	1219.14	10763.44	1760.38
contra_SSp-bfd	11716.17	1668.33	12465.61	1625.36
contra_SSp-bfd1	11589.46	1885.30	11981.35	1685.67
contra_SSp-bfd3	11765.15	1744.80	12451.90	1607.19
contra_SSp-bfd4	12031.24	1789.14	12887.84	1748.52
contra_SSp-bfd5	11693.27	1604.52	12606.49	1681.59
contra_SSp-bfd6a	11804.92	1614.65	12544.31	1654.73
contra_SSp-bfd6b	10316.84	1416.89	11036.15	1358.53
contra_SSP-tr	11703.19	1769.98	12407.97	1593.93
contra_SSp-tr1	11822.35	2130.28	12272.86	1396.12
contra_SSp-tr3	11933.43	1979.99	12652.63	1651.29
contra_SSp-tr4	11773.70	1757.98	12443.66	1643.86
contra_SSp-tr5	11530.58	1577.20	12398.97	1659.30
contra_SSp-tr6a	11578.14	1570.27	12335.19	1601.25
contra_SSp-tr6b	10279.00	1192.66	11109.16	1421.46
contra_TEa	13000.42	2195.83	13716.53	2406.13
contra_TEa1	12863.42	2601.03	13630.60	3118.81
contra_TEa3	13415.69	2389.78	13847.85	2613.18
contra_TEa4	13184.37	2212.37	13961.78	2398.71
contra_TEa5	12863.87	2076.67	13805.13	2391.94
contra_TEa6a	12679.56	2038.74	13772.77	2333.84
contra_TEa6b	11213.72	1822.84	12381.68	1994.94
contra_th	13049.53	1554.33	13898.85	2353.80
ips_amgmed	11390.67	1842.22	12700.15	2274.92
ips_AUDd	12045.50	2161.93	12968.53	2145.85
ips_AUDd1	11757.47	2287.86	12707.29	2266.69

ips_AUDd3	12183.61	2169.11	13352.41	2271.67
ips_AUDd4	12187.17	2278.94	13082.04	2190.15
ips_AUDd5	12002.22	2172.42	12759.29	2030.79
ips_AUDd6a	12146.60	2272.38	12745.50	2057.07
ips_AUDd6b	10586.76	1816.47	11482.27	1848.00
ips_AUDp	12243.82	2129.31	13033.07	2022.69
ips_AUDp1	12097.39	2100.51	12671.33	1899.05
ips_AUDp3	12533.82	2174.38	13399.78	2196.69
ips_AUDp4	12307.18	2066.44	13183.54	2148.24
ips_AUDp5	12089.42	2080.04	12875.08	2035.81
ips_AUDp6a	12177.34	2280.13	12896.16	1983.62
ips_AUDp6b	10159.09	1865.45	11096.08	1338.63
ips_AUDv	12152.37	2083.33	13144.23	2023.20
ips_AUDv1	11791.07	2267.89	12830.11	2106.41
ips_AUDv3	12273.04	2097.80	13455.45	2122.62
ips_AUDv4	12367.28	1991.64	13327.70	2095.00
ips_AUDv5	12238.76	2043.99	13145.91	2033.47
ips_AUDv6a	12115.83	2115.66	13024.87	1989.63
ips_AUDv6b	10467.35	1822.53	11265.99	1649.48
ips_BLAa	13885.35	2519.07	15289.66	2665.71
ips_BLAp	14077.62	2582.03	15683.66	2738.33
ips_BLAv	12640.73	2603.84	14552.96	2556.44
ips_BMAp	12368.21	2520.26	14206.07	2679.19
ips_CA1slm	12621.89	1345.05	13125.58	2126.78
ips_CA1so	13653.28	1545.13	13909.25	1802.18
ips_CA1sp	12453.17	1271.49	12689.06	1650.05
ips_CA1sr	14705.78	1556.81	15049.96	2061.55
ips_CA2slm	13902.01	1903.42	14431.59	2158.30
ips_CA2so	16493.17	2700.28	16483.65	2251.63
ips_CA2sp	12626.39	1696.63	12921.78	1235.77
ips_CA2sr	14957.59	2162.26	15291.67	2156.09
ips_CA3slm	13183.40	1684.79	13540.06	1824.52
ips_CA3slu	11322.05	1374.53	11778.44	1742.73
ips_CA3so	11588.72	1474.19	12047.02	1618.20
ips_CA3sp	10871.70	1104.86	11294.32	1395.47
ips_CA3sr	12958.62	1601.34	13480.97	1811.83
ips_CC	7054.24	430.42	6826.42	423.86

ips_cing	8479.67	761.02	8486.49	1334.15
ips_COApl	11959.51	2189.62	14282.62	3083.39
ips_COApl1	11338.15	2046.12	13666.31	2805.12
ips_COApl2	12250.89	2300.61	14719.18	3342.95
ips_COApl3	12038.11	2223.85	14245.08	3136.86
ips_cortex	11633.63	1712.33	12485.90	1949.25
ips_CP	10846.04	1680.07	11699.16	1743.89
ips_cpd	6669.41	470.21	6529.83	808.26
ips_DG	18915.63	2094.70	19329.05	2904.51
ips_DGinf	18528.86	2090.66	18943.05	2706.78
ips_DGpo	11953.43	954.53	12544.66	1542.54
ips_DGsg	13675.51	883.18	14132.85	1613.45
ips_DGsup	19164.80	2088.27	19564.46	3034.79
ips_ECT	12479.77	2050.76	13767.11	1863.91
ips_ECT1	11913.34	2125.69	13412.68	1495.09
ips_ECT3	12588.14	2094.40	13984.95	1873.59
ips_ECT5	12635.67	2060.94	13898.18	2045.97
ips_ECT6a	12516.49	2193.75	13668.31	2184.81
ips_ECT6b	11199.92	2007.16	12037.01	1774.73
ips_ENTl	13463.17	2299.53	15005.12	2333.75
ips_ENTl1	13041.97	2124.65	14649.88	2133.45
ips_ENTl3	13845.60	2412.79	15678.60	2648.63
ips_ENTl5	13676.82	2437.53	14953.63	2405.91
ips_ENTl6a	12682.60	2457.87	13937.96	2417.34
ips_ENTl6b	11514.29	2179.80	12814.55	2034.91
ips_FC	14172.34	1763.70	15480.05	2720.53
ips_hip	13895.91	1537.59	14285.23	1947.32
ips_hyp	10265.28	1506.43	11255.93	1959.17
ips_LA	12631.56	2235.22	13873.35	2469.93
ips_lay1	11601.71	1653.49	12384.10	1731.29
ips_lay2	11640.25	1369.80	12410.50	2035.31
ips_lay3	11757.69	1777.56	12736.20	1966.03
ips_lay4	11933.99	1935.63	12785.83	2079.09
ips_lay5	11622.61	1686.75	12437.76	1957.14
ips_lay6a	11518.38	1660.31	12277.69	2042.38
ips_lay6b	10267.69	1382.60	10876.72	1747.61
ips_MOp	11279.17	1387.99	11920.81	1851.70

ips_MOp1	11305.89	1642.73	12055.00	2160.49
ips_MOp3	11417.97	1466.99	12122.10	1799.08
ips_MOp5	11371.35	1421.62	11984.25	1920.68
ips_MOp6a	11141.36	1273.69	11566.64	1899.04
ips_MOp6b	10184.86	1075.84	10428.47	1696.02
ips_MOs	10905.40	1388.05	11690.19	1796.23
ips_MOs1	11445.95	1744.57	11896.96	1677.93
ips_MOs3	11158.39	1617.26	12198.57	1923.66
ips_MOs5	10802.99	1289.32	11555.52	1846.82
ips_MOs6a	10565.65	1126.12	10942.93	1786.82
ips_MOs6b	9791.72	910.70	10107.86	1670.47
ips_PAA	12299.94	2798.00	14415.91	3577.51
ips_PAA1	11373.22	2859.25	13654.63	3759.98
ips_PAA2	12771.04	3049.19	14829.69	3901.29
ips_PAA3	12527.72	2644.88	14433.44	3172.07
ips_PERI	12771.99	2001.85	14328.97	2198.16
ips_PERI1	12135.89	1885.21	13986.91	2249.32
ips_PERI3	12993.59	2087.75	14745.75	2469.63
ips_PERI5	13083.95	2164.80	14517.04	2254.17
ips_PERI6a	12564.98	2156.42	13773.95	2108.58
ips_PERI6b	11241.24	2123.06	12544.61	1955.76
ips_PIR	13004.13	2341.10	14742.23	2571.46
ips_PIR1	12607.04	2257.90	14481.88	2640.71
ips_PIR2	13287.43	2235.47	15176.43	2712.13
ips_PIR3	13021.99	2433.17	14674.98	2553.06
ips_RSPd	11142.18	1419.92	12186.58	1927.44
ips_RSPd1	11580.02	1658.09	12729.99	1960.74
ips_RSPd3	11336.48	1535.28	12551.44	1943.76
ips_RSPd5	10855.76	1292.73	11726.12	1847.07
ips_RSPd6a	10715.04	1142.51	11498.24	1930.01
ips_RSPd6b	9920.94	891.74	10610.97	1903.41
ips_RSPv	11415.28	1330.08	12102.35	1929.70
ips_RSPv1	11855.72	1473.07	12305.73	1965.27
ips_RSPv2	11651.33	1378.44	12405.19	2027.65
ips_RSPv3	11542.24	1361.90	12288.94	1938.09
ips_RSPv5	10937.27	1252.76	11703.14	1785.91
ips_RSPv6a	10633.31	1151.09	11332.34	1933.90

ips_RSPv6b	9976.79	1219.63	10399.96	2037.34
ips_SSp-bfd	11671.56	2021.72	12648.20	2147.13
ips_SSp-bfd1	11241.20	1816.14	12521.66	2166.43
ips_SSp-bfd3	11674.34	2031.16	12916.76	2264.58
ips_SSp-bfd4	11997.81	2139.93	12984.71	2263.90
ips_SSp-bfd5	11757.94	2091.54	12530.90	2043.90
ips_SSp-bfd6a	11771.54	2057.31	12455.10	2088.33
ips_SSp-bfd6b	10348.51	1545.91	11071.02	1907.84
ips_SSp-tr	11294.44	1545.64	11868.45	1881.25
ips_SSp-tr1	11548.56	1570.53	11871.84	1736.79
ips_SSp-tr3	11388.06	1697.18	11977.84	1938.87
ips_SSp-tr4	11452.22	1614.89	11978.22	1964.14
ips_SSp-tr5	11289.04	1501.16	11920.61	1851.38
ips_SSp-tr6a	11180.88	1449.71	11738.44	1940.27
ips_SSp-tr6b	9933.66	1129.88	10326.82	1728.68
ips_TEa	12222.51	2118.51	13451.77	1852.11
ips_TEa1	11800.08	2218.85	13288.13	1681.21
ips_TEa3	12286.52	2209.67	13606.16	1799.78
ips_TEa4	12565.65	2077.21	13719.38	2007.95
ips_TEa5	12399.17	2065.92	13546.12	2049.44
ips_TEa6a	12253.12	2120.64	13334.19	2022.40
ips_TEa6b	10776.75	1713.99	11525.00	1708.82
ips_th	12971.74	1505.91	13665.45	2305.78